

CARBON DIOXIDE REMOVAL FROM NATURAL GAS USING AMINE SURFACE BONDED ADSORBENTS

Orlando Leal,* Carmelo Bolivar,* Cesar Ovalles,† Argelia Urbina,† Javier Revette† and Juan Jose Garcia†, *Escuela de Química, Universidad Central de Venezuela and †INTEVEP, S. A., Apdo. Postal 76343, Caracas 1070A, Venezuela.

Keywords: Carbon dioxide removal, surface-bonded, adsorbents

INTRODUCTION

The results of research on the greenhouse effect have shown, among other things, that the concentration of trace gases occurring in the atmosphere such as carbon dioxide, methane, nitrous oxide, ozone and halocarbons have grown significantly since the pre-industrial times. During this period, the CO₂ level has risen 30% to nearly 360 ppm from a pre-industrial era level of 280 ppm [1]. On the basis of a variety of evidence a consensus is emerging among researchers that humans beings, primarily through their burning of fossil fuels, are already perturbing Earth's climate [2]. All specialists agree that without drastic steps to curb greenhouse gas emissions, the average global temperature will increase 1 to 3.5 °C during the next century because effective level of carbon dioxide are expected to double sometime between the years 2050 to 2100 [3]. It may be that human-generated emissions of carbon dioxide will have to be reduced by as much as 50-80% to avoid major climate changes. Such a reduction in the CO₂ emissions rate probably cannot be accomplished without a massive switch to non-fossil energy sources. However, it has been proposed that emissions from fossil fuels can be moderated by three strategies: exploiting the fuels more efficiently, replacing coal by natural gas and by recovering and sequestering CO₂ emissions [4]. A rough analysis, based on the use of currently accepted values, shows that natural gas is preferable to other fossil fuels in consideration of the greenhouse effect [5] and improvements can be obtained if natural gas is upgrading by scrubbing the carbon dioxide out of it.

Removal of carbon dioxide from gaseous streams have been a current procedure in the chemical industry. The presence of tiny amounts of CO₂ can act as poison in catalytic processes such as ethylene polymerization or ammonia synthesis [6]. Therefore, several procedures have been devised to eliminate carbon dioxide from ammonia plants as well as natural gas and fuel gas power plants. Three different approaches have been used: adsorption on liquid amines [7], adsorption on solid materials [8], and membrane technology [9]. The former makes extensively use of alkanolamines in plants operating at low temperatures and high pressures. In this case inhibitors should be used to prevent the corrosion problem arising from the formation of highly reactive carbamates. A process commercially known as Selexol, uses a mixtures of polypropyleneglycoldimethyl ethers and CO₂ removal is based on physical adsorption in much heavier molecules [10].

The use of membranes to remove carbon dioxide and other acid gases was assessed by Bhide and Stein [9]. Aromatic polyimide separation membranes are particularly useful for CO₂ enrichment [11], because they are able to achieve high flow rates with good selectivity and relatively low temperatures. This procedure proved effective to removed carbon dioxide in concentration ranging between 5 and 40 mol %. However, membrane saturation might produce gas losses [11].

The removal of CO₂ from closed ambients, such as submarines, by solid adsorbents has been described elsewhere [12]. A solid matrix, usually an inorganic oxide, was chemically modified to obtain a material which reversibly adsorbed carbon dioxide from atmospheres containing about 1 % by volume of CO₂. The adsorbent, which had a clay component as agglomerant, showed approximately a capacity of 20 l of wet carbon dioxide per kg of adsorbent. When silica gel was used as a solid, the modification of its surface could be accomplished by reaction with aminoalkoxysilanes such as 3-aminopropyltriethoxysilane, though condensation to the hydroxyl groups present on the silica gel surface. This process might involve the reaction of one, two or three hydroxyl groups at the surface per molecule of alkoxy silane. Therefore, the nature of the bonded species will depend upon the number and distribution of the hydroxyl groups at the surface of the silica gel. Previous studies indicated that annealed and rehydroxylated silica gel has a surface hydroxyl concentration of 4.6 -OH groups per square nanometer [13], of which 1.4 hydroxyl groups/nm² are interacting non-hydrogen bonded species and the remaining 3.2 hydroxyl/nm² are interacting groups arranged in pairs. All these groups can be involved in the reaction of the surface of the silica with polyalkoxysilanes. From C, N, H microanalysis studies, Burwell [14] concluded that this reaction gives a product with an average composition corresponding to the detachment of the silane to the surface, according to reaction (1).

that it is effective in either gas. A lower capacity was found when natural gas was used due to the residual carbon dioxide contained in it which remained in the reactor as the temperature was lowered from activation to room temperature. However this decrease is limited to less than 5%. Experiments performed at different space velocities showed that the adsorbed carbon dioxide started to be liberated by temperature programmed desorption (TPD) above 40°C and the process of release was maintained until above 100°C [12, 15]. The center of the peak is shifted to lower temperatures as the space velocity increases. At a space velocity of 2.4 h⁻¹ (1.2 l/h) the adsorption band is centered at 10°C and desorption is completed at 110°C whereas at a space velocity of 0.6 h⁻¹ (0.3 l/h) the desorption band is centered at 90°C and desorption is completed at 120°C. On the other hand if the desorption temperature was held at 140°C the adsorbent is regenerated in 2 h.

The influence of space velocity on the adsorption of carbon dioxide is shown in Fig. 2 where 100% corresponds to complete stripping of CO₂ from a natural gas containing 8.3% CO₂ and activation was undertaken under nitrogen as carrier. It is clear from this that as space velocity increases from 6 to 36 h⁻¹ (28 to 170 scf/h) the breakthrough time is reduced from 14 to 2.5 h, however the elution front remains clear-cut confirming the chemical nature of the surface adduct. The process also quantitatively subtracts carbon dioxide from the natural gas stream.

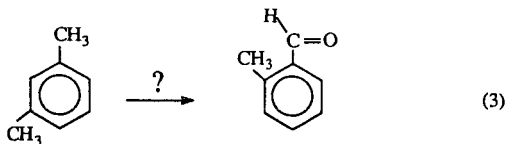
The influence of the pressure on the adsorption process is shown in Fig. 3. The capacity of the adsorbent before immediate breakthrough, when the system is operated at atmospheric pressure, is 14.0±0.7 liters of dry carbon dioxide per kilogram of adsorbent. At a pressure of 4 atm the obtained capacity is 13±2 l of CO₂/Kg taken as average value at the different space velocities tested. Whereas at a pressure of 20 atm (300 psi) the adsorptive capacity has dropped to 8.3±0.2 l of CO₂/Kg before immediate breakthrough. However a marked effect of the pressure is noticed here as the carbon dioxide seems to interact stronger with the adsorbent.

When carbon dioxide is saturated with water an increase of the capacity is observed, from 8.1 to 13.1 l of CO₂/Kg at a space velocity of 170 scf/h (Fig. 4). Carbon dioxide scrubbing by the adsorbent leads to an enrichment of the natural gas as it is presented on Table 1.

The adsorbent used in all the above experiments was a modified silica/clay aggregate described before (Adsorbent I) [12]. Two new adsorbents were obtained: a) using an extrudated silica gel as matrix (Adsorbent II), b) using a silica gel Davison 923 with a surface area of 700 m²/g (Adsorbent III). The rest of the preparation procedure remained the same.

Adsorbent II showed a lower performance than adsorbent I and only at pressures higher than atmospheric carbon dioxide was adsorbed at room temperature. Adsorbent III resulted a better scrubber for carbon dioxide and there was an enhancement of the adsorptive capacity to a maximum of 28.5 liters of wet CO₂ per Kg of adsorbent at a pressure of 60 psi (4 atm).

When these materials are exposed to water vapor after being saturated their surface with carbon dioxide, production of small amounts of a substance with odor evoking an aldehyde compound is noticed. MS analysis revealed the presence of 2-methyl benzaldehyde. On the other hand, meta-xylene was detected on the solid NMR analysis as a residue from the preparation procedure. Thus, a reaction as the one shown below (eq. 3) conceivably had occurred:



This reaction and its mechanism is under investigation.

In summary, we have prepared an adsorbent which can be used to remove carbon dioxide from natural gas at pressures higher than atmospheric pressure. This removal is selective and reversible, and carbon dioxide is released by heating the adsorbent at about 110°C using nitrogen or the same natural gas as carrier. Improvements on the capacity of the adsorbents could be done by changing the solid matrix.

REFERENCES

1. Report, United Nations Intergovernmental panel on Climate Changes, Dec 1995.
2. C. D. Keeling, T. P. Whorf, M. Wahlen and J. Van der Plicht, *Nature*, **375**, 666 (1995).
3. B. Hileman, *Chem. & Eng. News*, nov. 27, 18 (1995).
4. W. Fulkerson, R. Judkins and M. Sanghyi, *Sci. Amer.*, 83 (1990).
5. H. Rodhe, *Science*, **248**, 1217 (1990).
6. M. Buckthorp, *Nitrogen*, **113**, 34 (1978).
7. K. Volkamer and U. Wagner, *Fertilizer*, 139 (1983).
8. D. A. Boyta, U. S. Patent No. 3,847,837 (1974).
9. B. D. Bhide and S. A. Stern, *J. Membr. Sci.*, **81**, 209 (1993).
10. V. A. Shah, *Energy Prog.*, **8**, 67 (1988).
11. M. Weinberg, U. S. Patent No. 5,234,471 (1993).
12. O. Leal, C. Bolivar, G. sepulveda, G. Molleja, G. Martinez and L. Esparragoza, U. S. Patent No. 5,087,597 (1992).
13. J. H. Boer, M. E. Hermans and J. M. Vleeskins, *K. Ned. Akad. Wet.*, **B60**, 44 (1957).
14. R. L. Burwell, Jr., *Chem. Technol*, 370 (1974).
15. O. Leal, C. Bolivar, C. Ovalles, J. J. Garcia and Y. Espidel, *Inorg. Chim. Acta*, in press (1996).

Table 1. Enrichment of Natural Gas by removal of carbon dioxide.

Component ^a	Initial concentration molar % ^b	After removal molar %
CH ₄	82.9	89.1
CO ₂	7.0	-
C ₂ H ₆	9.8	10.5
C ₃ H ₈	0.24	0.26
C ₄	0.03	0.03
C ₅ ⁺	0.02	0.02

^aExperiment run at space velocity = 36 h⁻¹ and activation of adsorbent done under nitrogen.

^bMolar composition determined by GC using internal standard.

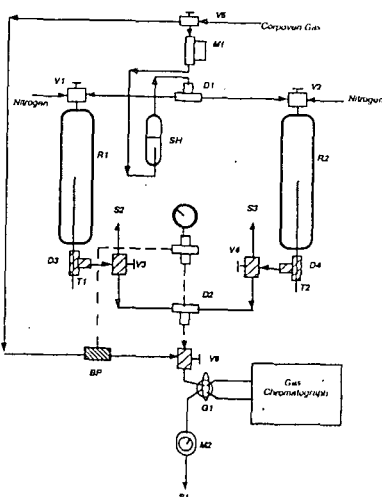


Fig. 1. Schematic diagram of flow system. D = flow splitters, R = reactors, S = gas outlet, T = thermocouple, V = three way valves, SH = water saturator, BP = back pressure valve, M1 = mass flow controller, M2 = flowmeter, M3 = manometer.

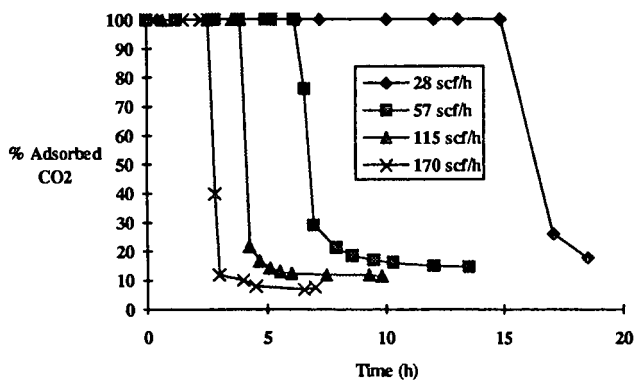


Fig. 2. Effect of space velocity on adsorption of CO₂ on adsorbent I from natural gas.

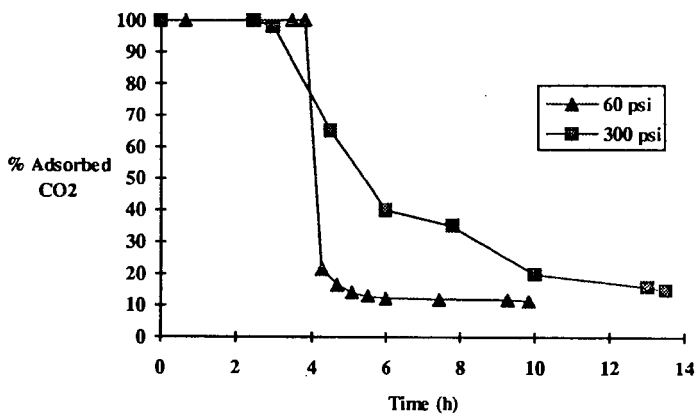


Fig. 3. Effect of pressure of operation on the removal of CO₂ on adsorbent I from natural gas.

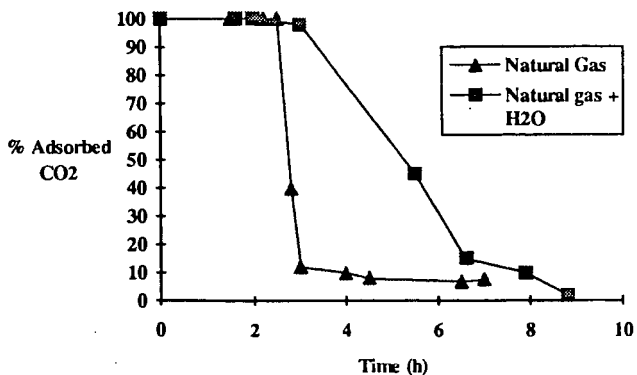


Fig. 4. Influence of water on the removal of CO₂ on adsorbent I from natural gas.

Comparison of CO_2 -Sources for Fuel Synthesis

T. WEIMER, K. SCHABER

Institut fuer Technische Thermodynamik und Kaelletechnik University of Karlsruhe, Germany;

M. SPECHT, A. BANDI

Center for Solar Energy and Hydrogen Research, Stuttgart, Germany

Keywords: CO_2 recovery, Climate neutral fuel synthesis, CO_2 sources

1 Strategies for the Substitution of Fossil Fuels

As it has been estimated in several publications, e.g. [3], the combustion of fossil fuels contribute with about 50 % to the global warming due to the increasing concentration of atmospheric CO_2 . Short term strategies for the reduction of the CO_2 -emissions are energy saving and efficient utilization. But as a successful long term strategy to stabilize the atmospheric CO_2 -content only the substitution of fossil fuels by renewable energy sources can be accepted. The potential of renewable energy sources is by several magnitudes higher than any estimated future world energy demand, [7]. Unfortunately, large renewable energy sources are almost located far away of the main energy consumption areas, e. g. in desert regions, mountains or over the oceans. If there is no realistic possibility to join an electric grid, renewable energy must be transported by energy carriers. For the intercontinental transport of energy as well as for energy storage, the generation of chemical energy carriers is the best alternative. Possible alternatives are hydrogen or liquid carbonaceous energy carriers.

On the other hand, mobile applications of carbonaceous fuels have the most dynamic growth of all energy consumption sectors. Here chemical energy carriers are again the best alternative for the storage of energy on board. Both, hydrogen and methanol generated from renewable energy sources can be applied as energy carrier in automobiles. In opposite to fossil fuels, they open the possibility to use high efficient fuel cells in transport applications. Even automobiles with high efficient combustion engines consume about the double amount of energy per mileage then fuel cell equipped cars. Therefore in mobile applications as well as for electricity the renewable generated energy carrier can substitute about the double of fossil primary energy. The most likely choice for the large scale substitution of fossil energy carriers is the generation of electricity from renewable energy or fuels for mobile applications with remote renewable energy sources.

2 Renewable Fuels for Mobile Applications

For the generation of a climate neutral fuel using renewable energy, a closed loop process without net emissions is necessary. The generation of hydrogen from water achieves the monoxide shift reaction is shown in figure 1. With the CO_2 recovery and compression to 60 bar a reduction of the energetic efficiency of the power station to 38,1 % from 43,6 % without CO_2 recovery was estimated. 88 % of the CO_2 emissions are recovered. For simplifying the further discussion pure Carbon with a heating value of 393 kJ/Mol is assumed as energy source. In the basic case without CO_2 recovery we achieve an electric output of 171 kJ(el)/Mol Carbon leading to a specific CO_2 emission of 5,85 Mol CO_2 /MJ(el). To achieve this electrical output of 171 kJ(el) in the process including a CO_2 recovery unit, 1,14 Mol of Carbon have to be fired at the new efficiency of 38,1 %. CO_2 recovery of 88 % leads to $1,14 \cdot 0,88 = 1$ Mol CO_2 /171 kJ(el) and CO_2 emissions of 0,14 Mol CO_2 /171 kJ(el) equivalent to 0,82 Mol CO_2 /MJ(el). The additional fossil energy demand E_{Carbon} for the recovery of the 1 Mol CO_2 is 0,14 Mol carbon with a heating value of 393 kJ/Mol, leading to:

$$E_{Carbon} = 55 \text{ kJ/Mol } CO_2. \quad (1)$$

A compression of CO_2 to 60 bar is included in the energy demand. The energy demand for drying and liquefaction of the compressed CO_2 is neglected.

Power plants fired with Natural Gas have lower specific emissions of CO_2 . A power plant fired with Natural Gas can achieve specific CO_2 emissions of only 2,3 Mol CO_2 /MJ(el) without any CO_2 recovery process. Because of the lower partial pressure of CO_2 in the flue gas compared to the resulting partial pressure of coal gasification a chemical absorption process with MEA Solutions leads to the lowest specific energy demand for CO_2 recovery

in natural gas fired power plants. This process was investigated by Suda et. al., [5]. Suda achieved in a pilot plant a steam demand of about 170 kJ/Mol CO_2 and an electric energy demand of 2,6 kJ/Mol CO_2 . Unfortunately, the power plant efficiency without CO_2 recovery was not published by Suda et. al. The fossil energy demand for the CO_2 recovery should be in the range of 180 kJ/Mol CO_2 assuming high efficiencies for steam and electricity generation. For the utilization in a distant located fuel synthesis, the CO_2 has to be dried, compressed and liquefied for transportation. Taking the estimated energy demand of Hendriks [1] for compression, additional 10 kJ(el)/Mol CO_2 are required, leading to a total fossil energy demand E_{NG} of

$$E_{NG} = 200 \text{ kJ/Mol } CO_2. \quad (2)$$

The drying and liquefaction are again neglected in the estimated energy demand. The CO_2 recovery process reduces the specific CO_2 emissions to the very low value of 0,3 Mol CO_2 /MJ(el).

In existing facilities of the lime and cement industry the carbon dioxide content in the flue gas is about 60 % at atmospheric pressure. A promising alternative for CO_2 recovery is flue gas compression before a physical absorption process to avoid thermal regeneration of the scrubbing liquid. The compression of the flue gas from atmospheric pressure up to 10 bar at a temperature of 330 K and of the recovered CO_2 up to 60 bar from atmospheric pressure lead to a resulting electric energy demand of about 25 kJ/Mol CO_2 . With an energetic efficiency in the range between 40 and 50 % for the generation of electricity the fossil energy demand for CO_2 recovery in the lime and cement industry is in the same range (50-60 kJ/Mol CO_2) as for the CO_2 recovery process in coal fired power plants.

The utilization of CO_2 from concentrated emissions for fuel synthesis at remote renewable energy sources leads independent of the kind of source to a long distant transport of the recovered CO_2 . For this purpose CO_2 has to be liquefied and transported. The CO_2 must be dried before liquefaction, for example by absorption with triethylene-glycol, and cooling water at temperatures below 293 K is required for the liquefaction. At least special transport facilities are necessary.

3.2 Enrichment of CO_2 from Atmosphere

A process for the recovery of CO_2 from the atmosphere can be located anywhere. Two process designs, based on absorption of CO_2 in caustic solutions, have been estimated, [7]. Taking solar energy as energy input, a process with precipitation of limestone from the scrubbing solution is more attractive than a regeneration of the scrubbing solution by electro dialysis, which is an interesting alternative if wind or hydro power are the energy sources. The basic design of the solar energy CO_2 recovery process is shown in figure 2. An electric energy demand of 70 kJ/Mol CO_2 and a heat demand of 250 kJ/Mol CO_2 was estimated, [7]. Investigations show that an electric energy demand of about 40 kJ/Mol CO_2 is achievable for the absorption process. Optimization of the precipitation can minimize the thermal energy demand for limestone decomposition to about 200 kJ/Mol CO_2 , similar to the energy demand in the limestone industry for the thermal decomposition process. Solar efficiencies of 0,2 for the generation of electricity and 0,7 for heat generation lead to a solar energy demand E_{Solar} of

$$E_{Solar} = 500 \text{ kJ/Mol } CO_2. \quad (3)$$

The recovered CO_2 can be processed directly without transportation or storage. Drying is not necessary. Additionally, because the CO_2 is produced at temperatures of about 1200 K, solar high temperature processes like a conversion to carbon monoxide with hydrogen can be attached to the recovery process. A disadvantage is the need for absorption columns with huge diameters to process the air with a low CO_2 content of 0,035 %. As the required packing height is only three to five meters and low cost concrete can be used for the column, the investment costs should be moderate. Nevertheless, additional investigations for secure uniform fluid flows in the absorption column at energy optimized conditions with low pressure drop are necessary.

3.3 Comparison of Renewable and Fossil Energy Demand

A direct comparison of the fossil energy demands (1), (2) with the renewable energy demand (3) shows a much greater energy demand for the CO_2 recovery from the atmosphere compared to concentrated emissions. But the fossil energy demand for CO_2 recovery is consumed at locations with a high energy demand and could be directly used in different

alternative manners. The renewable energy source, if used for CO_2 enrichment and fuel synthesis instead of electricity generation will be located remote.

The only alternative utilization of the renewable energy used for the CO_2 enrichment from the atmosphere is supplying the fuel synthesis. A solar efficiency for the generation of methanol (MeOH) using atmospheric CO_2 of 0,136 has been estimated [7]. Neglecting the energy demand for the CO_2 enrichment and all losses during transport of CO_2 and methanol a very high solar efficiency of 0,16 for the generation of methanol can be assumed. With the renewable energy demand (3) of 500 kJ/Mol CO_2 for the enrichment of 1 Mol CO_2 from the atmosphere an alternative synthesis of only 80 kJ MeOH is possible. Assuming application in fuel cell equipped cars, these 80 kJ MeOH can substitute the double amount of gasoline. Instead of the enrichment of 1 Mol CO_2 from the atmosphere with 500 kJ solar energy the substitution of 160 kJ gasoline with the aid of these 500 kJ renewable energy is therefore possible under optimistic assumptions.

The comparison of the possible fossil energy substitution

$$E_{subs} = 160kJ/Mol CO_2 \quad (4)$$

resulting from the solar energy demand (3) with the fossil energy demand (1), (2) leads to a more realistic energetic estimation for a decision between the different CO_2 sources for climate neutral fuel synthesis.

4 Comparison of the CO_2 Sources

The most efficient recovery processes of CO_2 from concentrated emissions achieve an optimistic energy demand of about 50 kJ/Mol CO_2 (1) obtaining gaseous CO_2 at 60 bar pressure. The costs per ton CO_2 recovered are estimated by [1] to 25 DM/t. But here the costs for drying, liquefaction, storage and transportation are not included. For the intercontinental transport tank ships will be employed. Because at ambient temperatures huge high pressure tanks at 60 bar would be required, low temperature transport at temperatures of 200 K at ambient pressure will be preferred because of lower costs. This causes investment for well isolated tank ships with cooling of the CO_2 during transport. An alternative is to cool the CO_2 by evaporation with resulting CO_2 losses.

The CO_2 recovery from the atmosphere will achieve an equivalent fossil energy demand of less than 160 kJ/Mol CO_2 (4). The only investment are for the absorption column and for the solar heated drying and thermal decomposition of limestone. No infrastructure for transport and storage of CO_2 is necessary. A combination of the CO_2 recovery from air with other solar high temperature processes is possible increasing the efficiency for the fuel generation process. This will reduce the energy demand for the methanol synthesis with atmospheric carbon dioxide as basic product. If this process is optimized, an energetic and economic comparison of the whole methanol synthesis process with renewable energy and different CO_2 sources will show the most promising CO_2 source.

Although further investigations and development are still necessary, the CO_2 recovery from air seems to be the better alternative compared to the CO_2 recovery from concentrated emissions even from today's state of investigation. The higher energy demand is supplied by remote located climate neutral energy. But the savings in investment costs compared to the utilization of concentrated CO_2 sources needing a complex infrastructure can be taken for the extension of the renewable energy plant. The more extensive use of renewable energy can supply the energy demand for the CO_2 enrichment from air.

References

- [1] C.A. Hendriks, K. Blok, and W.C. Turkenburg. *Energy*, 16:1277, 1991.
- [2] IEA. Carbon dioxide capture from power stations. Technical report, International Energy Agency, 1994.
- [3] Enquetekommission des dt. Bundestags Schutz der Erdatmosphaere. *Mehr Zukunft fuer die Erde*. Economica Verlag, Bonn, 1995.
- [4] M. Steinberg and A.S. Albanese. BNL 50877: Environmental control technology for atmospheric carbon dioxide. Technical report, Brookhaven National Laboratory, Upton NY, 1978.
- [5] T. Suda, M. Fujii, and K. Yoshida. *Energy Conv. Mgmt.*, 33:317, 1992.
- [6] Various. In *Proceedings of the 2nd International Conference on CO_2 Removal*, Kyoto, 1994.
- [7] T. Weimer, K. Schaber, and et al. *Energy Conv. Mgmt.*, 37(6-8):1351-1356, 1996.

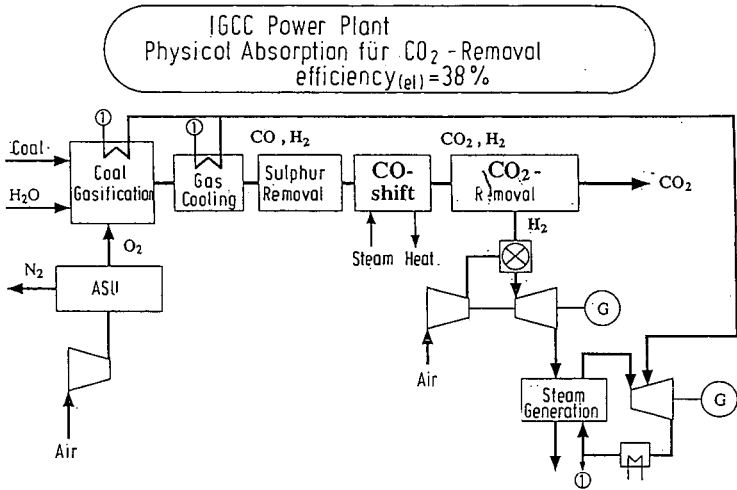


Figure 1: Coal fired Integrated Gasification Combined Cycle (IGCC) process for generation of electricity with CO_2 recovery and compression to 60 bar

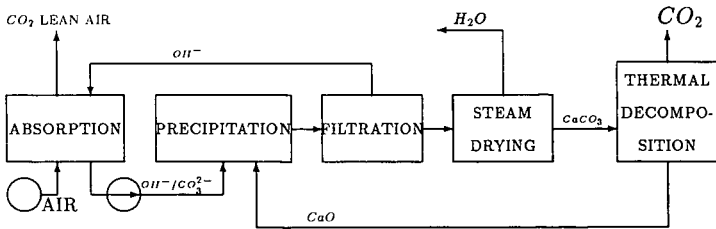


Figure 2: CO_2 -Recovery from Air with Precipitation of Limestone

CARBON DIOXIDE UTILISATION IN THE CHEMICAL INDUSTRY.

Michele Aresta, Eugenio Quaranta, Immacolata Tommasi.
Department of Chemistry,
University of Bari,
Bari, 70126 Italy.

Keywords: Carbon dioxide, mitigation, disposal, utilisation.

1. Introduction

Carbon dioxide as a raw material for the Chemical Industry is receiving growing attention because : i) if recovery of CO₂ from flue gases will be implemented, huge amounts of CO₂ will be available; ii) environmental issues urge to develop new processes/products, avoiding toxic materials. Several uses of CO₂ appear to be responding to both (i) and (ii), i.e. use as a solvent (supplanting organic solvents) use as a building blok for carboxylates/carbonates (supplanting phosgene); use as carbon-source in the synthesis of fuels (supplanting CO or coal/hydrocarbons). These options will be evaluated and their potentiality discussed.

2. Energy for human activities.

The amount of carbon based fuels used today all over the world is such to produce every year 19.6 Gt of CO₂, that are equivalent to 5 Gt of C.¹ To this amount must be added the carbon dioxide formed in autocombustion of woods or produced as the effect of deforestation (ca. 2 Gt as C) that leads to a total amount of ca. 7 Gt of C per year. The forecast is for a rapid increase of anthropogenic carbon dioxide that might reach, alone, the level of 7 Gt as C per year in ten years. To stabilize the CO₂ immission into the atmosphere would mean to "avoid" an amount of carbon dioxide sizeable at ca. 2 Gt of carbon per year. This task is not easy to be reached considering the expansion of the use of energy, and demands an integrated approach and a combination of technologies.

3. The carbon dioxide mitigation technologies.

The technologies that may contribute to reduce the carbon dioxide immission into the atmosphere can be categorized as follows.²

- * *Efficiency technologies: energy production.*
- * *Efficiency technologies: energy use.*
- * *Fuel shift.*
- * *Fixation in biomasses (plants and algae).*
- * *Carbon dioxide recovery from concentrated sources.*

The latter approach concerns the recovery from sources that contain carbon dioxide in much higher concentration than the atmosphere.

Carbon dioxide can be recovered from flue gases, using: liquid phases (monoethanolamine, MEA, by far the most used, or organic carbonates or ethers); solid phases (zeolites, oxides); or membranes.

The last approach is the most interesting and promising for coming years, while MEA is the most largely used today.

Research is needed to improve the membrane technology, mainly for ameliorating the separation of carbon dioxide from dinitrogen.

In general, the recovery technology and its cost are quite well established. Pilot and demonstration plants are available. The technology is ready for a large scale application so that in principle, if we consider only the "concentrated and continuous" sources of carbon dioxide (power plants, industrial sources), 60% of the produced carbon dioxide could be recovered.

The question is, thus: what to do with the recovered carbon dioxide?
Two options are open forwards: i) disposal; ii) utilisation and recycle.

4. Disposal of carbon dioxide: a ready technology?

Disposal of carbon dioxide in natural fields is considered with an increasing interest for the amount that could be potentially eliminated. The following options have been considered:

- i) *elimination in aquifers;*
- ii) *confination in depleted gas or oil wells;*
- iii) *ocean disposal.*

Each of these options requires a careful analysis of consequences and demands research in order to exclude possibilities of disasters to ecosystems. Limitations are: high cost, availability of sites, and capacity of available sites. Moreover, they cannot be considered of general application.

5. Utilisation of carbon dioxide.

Another approach to design the fate of recovered carbon dioxide is its utilisation.^{3,4} The use of carbon dioxide can be either technological (that does not imply its conversion) or chemical (that means to use CO₂ as a source of carbon in the synthesis of chemicals).

5.1 Technological use.

Presently, the technological use of carbon dioxide has a market of ca. 10 Mt y⁻¹.⁵ Carbon dioxide is used as: solvent, additive for beverages, water treatment, fumigant, moulding and soldering agent, propellant in place of CFC, in fire extinguishers.

The utilisation of carbon dioxide as reagent in the chemical industry can take place through the

- a) *fixation of the entire molecule;*
- b) *reduction to other C1 or Cn molecules.*

Today, most of the CO₂ used by the chemical industry is extracted from natural wells. As the extraction price is close to that for recovery from fermentation and other industrial processes, or from power plants, it may be that in the near future carbon dioxide recovered from electric energy production could find a large application in the chemical industry.

5.2 Utilisation of carbon dioxide in synthetic chemistry.

The utilisation of CO₂ as source of carbon for the synthesis of products classified as fine- or bulk-chemicals is considered with increasing interest.^{4,5} New synthetic processes using carbon dioxide have been discovered. Some of them may be developed at the industrial level if suitable economic conditions were created.

The introduction of the "carbon tax" could be the "driving force". In fact, the "environmental cost" of some currently operated processes could become a convincing issue for the innovation of industrial processes.

The development of a chemical industry based on CO₂ would have the following positive consequences:

- *avoiding the use of toxic materials in some industrial processes.*
- *Taking a step forward energy and raw materials saving through the adoption of more direct synthetic procedures.*
- *Using less drastic operative conditions.*
- *Substituting CO₂ to fossils (coal, oil, gas) as source of carbon for some industrial applications.*
- *Saving energy by recycling carbon.*
- *Boosting research for the utilisation of solar energy.*
- *Using a safe solvent.*

As the utilisation approach could contribute to solve the problem of the control of atmospheric CO₂ level, it is necessary to synthesize products with a market of several million tons per year (Mt y⁻¹) and requiring a low energy input. Products with a very long life appear quite attractive. In case of short-lived products, a very fast reaction kinetics would be required.

Species which have a market of a few thousand tons (kt) per year, cannot be considered for their contribution to the control of the emission of CO₂. Nevertheless, if they have a high added value and if the synthesis from carbon dioxide implies a simpler procedure compared to the actual synthetic methodology, the innovation could have a remarkable economic interest.

The life of a product is a very important factor. In fact, when we use a carbon based product, this is transformed again into CO₂. For example, fixing carbon dioxide in chemical substances which have a very short life wouldn't, at a glance, give a significant contribution to the problem of the control of CO₂ emission, even if large quantities were fixed. If the kinetics of formation were fast, and the methodology simple and highly effective, the application would be of industrial interest, as it would help to save resources, recycling carbon. This is the case of urea and its derivatives.

Therefore, the correct evaluation of the contribution that a synthetic procedure based on CO₂ can give to the mitigation of CO₂ or to the development of a "green industry", requires a complex analysis based on the criteria listed below.^{5,6}

- *Added value of the product.*
- *Market demand of the product.*
- *Demand of energy for the synthesis of the product.*
- *Transformation rate of CO₂ (yield and selectivity towards the product).*
- *Life of the product.*

Actually, we can separate two different approaches to carbon dioxide utilisation:

* *the first related to the opportunity of utilising CO₂ for developing a "green chemistry",*

* *the second relevant to the mitigation of the greenhouse effect.*

These two points of view may appear sometimes diverging.

5.3 *Synthesis of fuels, intermediates, and fine chemicals.*

CO₂ can be fixed in a chemical substance:

- (i) *as it is;*
- (ii) *in a reduced form.*

The species belonging to case (i) are:

carboxylates (RCOOR), carbonates (ROCOOR) and polycarbonates, carbamates (RR'NCOOR'') and polyuretanes, ureas and their derivatives.

Other C1 molecules (CO, CH₂O, CH₃OH, CH₄), or the homologous species Cn and their derivatives belong to case (ii).

These two processes can require a different energy input.

A process that could be operated in the near future is the substitution of CO₂ to phosgene, COCl₂, a toxic species (LC₅₀ 3 mg L⁻¹) currently synthesized from carbon monoxide (obtained from coal) and chlorine. Phosgene has a world market of about 6-8 Mt per year and is used in the synthesis of carbonates, polycarbonates, carbamates, polyuretanes, N-phenylureas, symmetric and asymmetric ureas, etc. As the phosgene production will not expand (no more plants can be builded), the utilisation of carbon dioxide may become a reality.

The synthesis of methanol from CO₂ also deserves attention. This product can be used as fuel or as a raw material for the synthesis of chemicals. The market might be of hundreds million tons per year.

The conversion of CO₂ into methanol requires dihydrogen. Indeed, this approach can result of great interest if a cheaper and easier conversion of water into hydrogen were found.

6. *Economics of adoption of a new synthetic procedure.*

It is obvious that the direct use of CO₂ for the synthesis of chemicals is doubly beneficial as it cuts the use of carbonaceous fossils and allows the recycling of CO₂. Processes based on CO₂ have already been developed, but not yet implemented as they are more expensive than conventional ones.

It is worth to note that often current costs of production do not include the "environmental costs": if we should consider them, the use of CO₂ as raw material for the synthesis of chemicals would become economically favourable, in a number of cases.

Considered the time necessary for R&D, it is possible that by the year 2010, more processes converting CO₂ into useful chemicals might be operated, supporting the development of a "green chemical industry".

For sure, such "know-how" will be a tool for market penetration, considering the current attitude to the assessment of the eco-compatibility of products and processes through a quantitative life cycle assessment.

7. Conclusions.

We have seen that the control of the accumulation of CO₂ in the atmosphere can be performed through different technologies based on: efficiency in energy production and use, energy saving, utilisation of alternative energies, recovery of CO₂. The latter technology, and the consequent CO₂ disposal in natural fields or utilisation, require a correct cost-benefit analysis, for assessing the application potentiality in the short-medium-long term.

Carbon based fossil fuels, liquid or gaseous, have the correct energy concentration and most probably will continue to be the main energy source in the short-medium term.

As liquid and gaseous hydrocarbons should be available for next 30 years and modern conversion methodologies and technologies allow an effective conversion of large amounts of coal into liquid fuels, a considerable part of the energy demand could be still covered by carbon based fuels in the next 50 years or so.

However, coal is estimated to be available for next two or three centuries at the proper rate of utilisation. Therefore, the CO₂-mitigation options discussed in this lecture deserve a thorough consideration.

Science and Technology open new horizons and offer solutions for political and economic evaluation.

REFERENCES.

- 1) M. Aresta, in "*Carbon Dioxide as a Source of Carbon*", M. Aresta and G. Forti eds., Reidel Publ., pp. 1-22, 1987.
- 2) IEA-OECD Expert Seminar on "*Energy technologies for reducing emission of greenhouse gases*", Paris, 12-14 April, 1989.
- 3) M. Aresta, IEA-OECD Expert Seminar on "*Energy technologies for reducing the emission of greenhouse gases*", Paris, 12-14 April 1989, IEA-OECD Publications Vol 1, p. 599-617, 1989.
- 4) M. Aresta and J.V. Schloss eds., "*Enzymatic and Model Reduction and Carboxylation Reactions for Carbon Dioxide Utilization*", Kluwer publ., 1990.
- 5) M. Aresta, E. Quaranta and I. Tommasi, in "*Energy Conversion Management*" Vol. 33, pp 495-504, 1992.
- 6) M. Aresta, in "*Energy Conversion Management*", Vol. 34, pp 745-792, 1993.

BIOMASS REACTIVITY IN GASIFICATION BY THE HYNOL PROCESS

Yuanji Dong
Acurex Environmental Corporation
4915 Prospectus Drive
Durham, NC 27709

Robert H. Borgwardt
U.S. Environmental Protection Agency
National Risk Management Research Laboratory
Air Pollution Prevention and Control Division
Research Triangle Park, NC 27711

Keywords: biomass gasification; gasification kinetics; biomass-to-methanol.

INTRODUCTION

Methanol has many advantages to be considered as an alternative fuel. About 75% of methanol production uses natural gas as feedstock. Use of biomass as feedstock to produce methanol is of current interest because it offers substantial benefits for reduction of greenhouse gas emissions. The research and development of biomass-to-methanol processes, one of which is called Hynol, are now in progress.

The Hynol process was proposed to utilize biomass as a feedstock and natural gas as a cofeedstock to increase methanol yield and reduce costs (Steinberg and Dong, 1994). The process consists of three reaction steps: (1) gasification of biomass with the H_2 -rich gas recycled from methanol synthesis, (2) steam reforming of the produced gas with an addition of natural gas feedstock, and (3) methanol synthesis from the H_2 and CO produced by the reformer. A schematic flow diagram of the process is shown in Figure 1. Since the reaction of biomass with the H_2 in the recycle gas to form CH_4 is exothermic, the heat so generated is able to offset the energy required for other endothermic reactions in a Hynol gasifier. As a result, no expensive O_2 plant or external heat source is needed for gasification. The use of natural gas as cofeedstock eases the requirement for a consistent composition of biomass feedstock. The integrated cyclical process configuration helps ensure the completion of overall conversion and increases thermal efficiency. CO shifting is not necessary and the requirement for acid gas removal is reduced, which lowers capital and operating costs.

A theoretical evaluation of the Hynol process conducted by the Air Pollution Prevention and Control Division (APPCD) of the National Risk Management Research Laboratory, U.S. Environmental Protection Agency (EPA), showed that the Hynol process represents a promising technology for maximizing fuel production inexpensively and with minimum greenhouse gas emissions (Borgwardt, 1995). Consequently, the APPCD established a laboratory to further assess the process feasibility. In the first phase of the study, a thermobalance reactor (TBR) was installed and used to evaluate biomass reactivity in gasification at the operating pressure, temperature, and feed gas composition specific for the Hynol process. The experimental work also attempted to improve understanding of the variables affecting Hynol gasification and identify needs for process development. This article summarizes the TBR results.

EXPERIMENTAL

A flow diagram of the TBR system is detailed in Figure 2. The reactor is electrically heated and consists of a 35-mm I.D. stainless steel reactor pipe, a 305-mm O.D. pressure vessel, and a topwork which accommodates a weight transducer for measurement of sample weight during reaction. A pulley assembly is used to raise and lower a sample basket between the topwork and the reaction zone.

To initiate an experimental run, a basket with known weight of biomass sample was placed into the topwork through the removable window. A constant helium flow was introduced to the topwork to protect the wood sample from contact with process gas prior to entry in the reaction zone. Mass flow controllers were used to control the flow rates of H_2 , CH_4 , CO, and CO_2 from individual gas cylinders to obtain the desired feed gas composition. Steam was added to the feed gas from a steam generator fed with distilled water by a metering pump. The gas mixture was further heated by a superheater and then entered the reactor. The reactor exit gas was cooled in a condenser to remove moisture, and then depressurized through a back-pressure regulator before it was vented to atmosphere. When pressure and temperature in the reactor system were stabilized at the desired levels, the sample basket was lowered into the reaction zone and the change in sample

weight was automatically recorded by the transducer as a function of reaction time. A computer was used to control the TBR system and log experimental data. After gasification, the basket was raised back into the topwork and the reactor was depressurized and cooled. The discharged char was then weighed to determine the final sample weight. Because changes in gas composition across the sample are negligible, the reaction can be considered to take place at constant operating conditions.

In this study, the Hynol feed gas refers to a composition -- $H_2 = 65.83\%$; $CH_4 = 11.63\%$; $CO = 8.95\%$; $CO_2 = 2.32\%$ and steam = 11.27% -- which is based on the results of a Hynol process simulation. Poplar wood, which is considered a primary candidate for large scale production as an energy crop for fossil fuel displacement (Wright, 1995), was used as a representative biomass sample. It was grown in North Carolina and cut to desired sizes and dried before its use. Composition is presented in Table 1.

KINETIC MODEL AND DATA TREATMENT

The weight transducer output was recorded as a function of reaction time during a test. The records were converted into the data of variation in sample weight with time. The biomass conversion, X , on an ash-free basis was then calculated by :

$$X = \frac{W_0 - W}{W_0 - W_0 C_A} \quad (1)$$

where W_0 is the initial sample weight, W is the sample weight at any reaction time, C_A is the weight fraction of ash obtained from the ultimate analysis of the original sample, and X is thus also a function of reaction time.

General observation of the reaction behavior revealed that biomass gasification under Hynol conditions involves two types of reactions: a rapid reaction, which may complete in a few seconds, involving devolatilization and pyrolysis reaction of the volatile matter in biomass with H_2 and steam; and a very slow reaction of residual carbon with the process gas which requires hours to finish. To quantitatively describe the rate of gasification, these two reactions are assumed to be first order with respect to the remaining solid reactants. The rate of the rapid reaction can be expressed as:

$$\frac{dX_1}{dt} = k_1 (X_C - X_1) \quad (2)$$

and the rate expression for the slow reaction is:

$$\frac{dX_2}{dt} = k_2 (1 - X_C - X_2) \quad (3)$$

where X_1 and X_2 are the conversions by the rapid and slow reactions at time t , X_C is the maximum attainable conversion by the rapid reaction, and k_1 and k_2 are the reaction rate constants for the rapid reaction and the slow reaction, respectively.

By integrating Equations (2) and (3), the total biomass conversion can be expressed by:

$$X = X_1 + X_2 = 1 - X_C \exp(-k_1 t) - (1 - X_C) \exp(-k_2 t) \quad (4)$$

The model involves three parameters: X_C , k_1 , and k_2 , which are functions of operating conditions such as biomass properties, reaction temperature, pressure, and feed gas composition. They can be determined by fitting Equation (4) to the experimental conversion data obtained from TBR tests.

RESULTS AND DISCUSSIONS

The above model was used to correlate the experimental data obtained from TBR tests. Figure 3 is a typical example of curve fitting results by the model, showing good agreement between the experimental data and the model regression over the entire reaction period.

Four different sizes of poplar particles were used to investigate the effects on gasification: 7/16-in diameter cylinders, 1/4-in diameter cylinders, 1/8-in cubes, and 20 to 30 mesh sawdust. The

rate of the rapid reaction increased significantly as a result of higher heat transfer and intraparticle diffusion rates when particle size was reduced from 7/16- to 1/8-in. Agglomeration during gasification was observed for the particles larger than 1/8-in, which inhibited gas diffusion within the particles. Sawdust heated up more quickly, and no agglomeration was observed. Experimental results showed that, at 30 atm and 800°C, about 87% of the 1/8-in poplar particles and 90% of the sawdust can be gasified by the Hynol feed gas in 60 min.

The analysis of the charred samples obtained from 7/16-in poplar particles showed that some of the volatile matter remains after gasification. However, for 1/8-in poplar particles or sawdust, nearly all of the H and O were converted into product gas in 20 min.

The agglomerates of residual chars formed in the TBR were fragile. If a fluidized bed gasifier is used, agglomeration is not likely to occur as a result of attrition; therefore, higher reaction rate and conversion than observed in TBR testing are expected in such systems.

The rapid-reaction stage of poplar gasification was found to be essentially completed in less than 0.2 to 0.3 min, contributing most of the biomass conversion. A small additional conversion is contributed by the slow reaction. To achieve high biomass conversion, sufficient gasification time must be provided. Tests showed that biomass conversion increased from 85 to 90% when gasification time extended from 20 to 150 min. The comparison between the compositions of chars after 20 and 150 min gasification indicated that there was virtually no further conversion of H and O in the char after 20 min and that the additional conversion resulted from the reaction of carbon with the process gas.

Experimental results of 60-min gasification with sawdust and 1/8-in poplar particles at different reaction temperatures showed great increase in biomass conversion and gasification rates when temperature increased from 750 to 950°C as shown in Figure 4. The rate constants for the rapid and slow reactions, k_1 and k_2 , at different reaction temperatures were determined by fitting the experimental data for gasification of 1/8-in poplar particles. The rate constants thus obtained were plotted against the reciprocal of the absolute temperature, as shown in Figure 5, and expressed as functions of reaction temperature by the Arrhenius equation:

$$k_i = k_{i0} \exp\left(-\frac{E_i}{RT}\right) \quad (5)$$

where subscript i is 1 for the rapid reaction and 2 for the slow reaction. E_i is the activation energy. The results obtained were: $k_{10} = 108.85 \text{ min}^{-1}$, $E_1 = 3.78 \text{ kcal/mol}$, $k_{20} = 22925 \text{ min}^{-1}$, and $E_2 = 34.1 \text{ kcal/mol}$. The maximum attainable conversion by the rapid reaction, X_C , was also correlated as a function of temperature for gasification of 1/8-in poplar particles by:

$$X_C = 0.9611 - 0.000149T \quad (6)$$

where T is the reaction temperature in °C. With Equations (4), (5), and (6) and the values of k_{10} , E_1 , k_{20} , and E_2 , the conversions of 1/8-in poplar particles at different temperatures and gasification times were predicted. Figure 6 compares the prediction with the conversion data obtained from the separate experimental tests at different temperatures and gasification times. The comparison covers a temperature range of 750 to 950°C and a gasification time range from 0.2 to 150 min for 1/8-in poplar particles gasified by the Hynol feed gas at 30 atm. The activation energy obtained for the rapid reaction was low, implying that heat transfer dominates the rates of devolatilization and pyrolysis of biomass in the TBR.

The effect of feed gas composition on poplar gasification was investigated by varying the flow rates of individual gas components under constant system pressure. Helium was used as an inert "make-up" gas for this purpose. At 30 atm and 800°C, the final conversion of poplar wood gasified by pure helium after 60 min was about 6% lower than that obtained under pure H_2 . If the conversion obtained after 60 min of gasification is plotted against H_2 partial pressure (P_{H_2}), a linear relationship, $\text{conversion} = 0.0017 \times P_{H_2}$, was found. When steam partial pressure in the feed gas was varied from 7 atm to zero while the partial pressures of other gas components remained constant, the conversion was proportional to steam partial pressure or $0.003 \times P_{H_2O}$. Negligible effects on the gasification conversion and reaction rate of 1/8-in poplar particles were observed as the CH_4 in the feed gas was reduced from the simulated Hynol composition, 11.63%, to zero. Replacing CO and CO_2 in the feed gas with helium did not affect the gasification rate. The conversion and reaction rates of 1/8-in poplar particles gasified by the Hynol feed gas were nearly the same as those observed by the feed gas containing no CO and CO_2 .

REFERENCES

Borgwardt, R. (1995): The Hynol Process, Presented at Symposium on Greenhouse Gas Emissions and Mitigation Research, Washington, DC. June 27-29.

Steinberg, M. and Dong, Y. (1994): Process and Apparatus for the Production of Methanol from Condensed Carbonaceous Material, U.S. Patent 5,344,848.

Wright, L. (1995): Demonstration and Commercial Production of Biomass for Energy, Proceedings, Second Biomass Conference of the Americas, NREL/CP-200-8098, National Renewable Energy Laboratory, Golden, CO, pp. 1-10.

TABLE 1. COMPOSITION OF POPLAR WOOD USED

Carbon (wt.%)	51.52	Volatile (wt.%)	91.38
Hydrogen (wt.%)	6.20	Fixed carbon (wt.%)	8.15
Oxygen (wt.%)	41.37		
Ash (wt.%)	0.47	Higher heating value	
Sulfur (wt.%)	0.02	(Btu/lb dry wood)	8768.
Nitrogen (wt.%)	0.42		

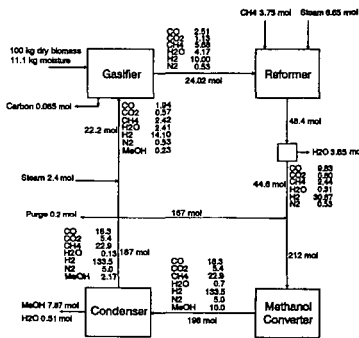


Figure 1. Schematic flow diagram of the Hynol process.

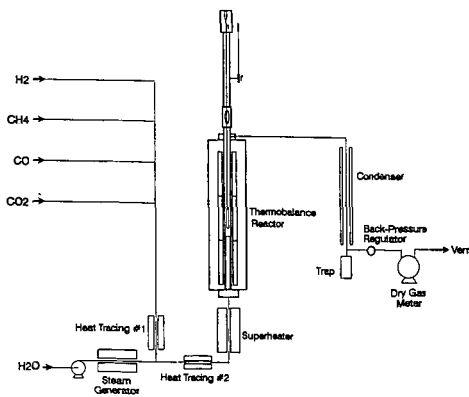


Figure 2. Flow diagram of the TBR system.

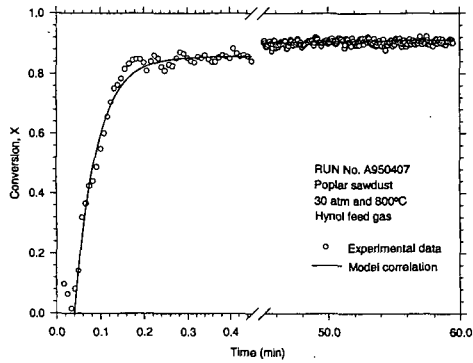


Figure 3. Example of TBR experimental data fitting by the model.

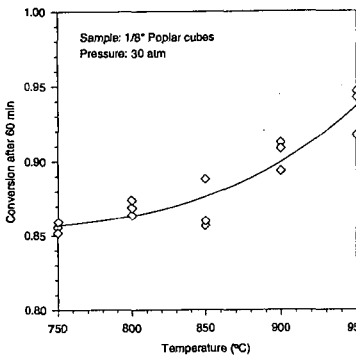


Figure 4. Effect of reaction temperature.

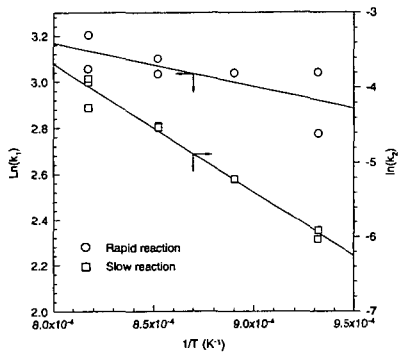


Figure 5. Arrhenius plots of the rate constants.

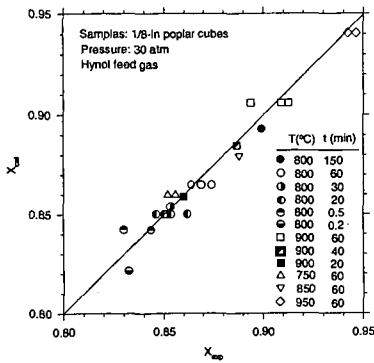


Figure 6. Comparison of the model prediction with experimental conversion data.

New Era will come with New Concept in Refinery

Masaya Kuno

1-7-13 Tsuruma, Machida-shi

Tokyo 194, Japan Member of JPI

Keywords:

Conventional crude distillation system to make crude lighter and white oil is theoretically wrong.

1) Introduction

Since the "day one", crude had been distilled at first stage, nobody except author has found out the defects of system.

Author had appealed HSP, that is, HydroStripping Process world wide since 1981. This concept was presented in Hydrocarbon Processing September 1981(1), that is, treating crude with hydrogen rich gas for the subsequent vapor phase HDS. Recently, many data have been obtained and found out the following points.

(1) Distillate are not final products, which means it is against 2nd law of entropy, that is, increasing entropy of the system.

There exists a possibility in saving energy of the system.

(2) Distillate contain S-Compounds which are able to play the important role in cracking of heavier portion in crude under hydrogen rich gas.

Therefore, distillation operation in first stage is wrong, esp., so when refiner aims to produce white oil and lighter too much.

2) What is S-Compound effect ?

S-Compounds in each fraction such Naphtha, Gasoline, Kerocene and Gas Oil must be severely reduced to meet the stringent request of environmental problem. However, such lighter fractions including S-Compounds are dispersed into crude and mixed with heavier portion, which fits the best for heavier portion cracking under hydrogen and hydrogen sulfide at lower temperature without catalyst.

S-Compounds in situ is considered to be a good electron absorber, i.e., hydrogen atom catcher which means hydrogen carrier to cracking portion where S-Compounds promote under hydrogen, radical reaction of heavier portion on the surface of metal. These phenomena is explained from following data.

For example, hydrogen sulfide was used for cracking of polypropylene under hydrogen pressure 3.0 MP at 673 K w/o cat. H₂S was added to this experiment 1.0vol%, where 97% of distillate product composed of Naphtha 53%, Kerocene 23%, Gas Oil 19% with 2% gas portion were obtained after 1hr on auto-clave test while no addition case showed only 35% distillate and 40% heavier oil and solid state 20% with 5% gas portion. From Journal of JPI Young Society.

This catalytic activity of H₂S is explained as wall effect of auto-clave metal surface, composed of 18 Cr-8Ni and Fe oxide, which was discovered by Dr. Nakamura, PhD., Fujimoto's room, Tokyo University.

H₂S is so active that it is used as a detective reagent for inorganic Compounds in chemical analysis. This result may be plausible such as sulfiding operation in HDS where H₂S or CS₂ are used for activation of catalyst surface at start-up.

The importance of this experiment is not only showing the possibility of heavier, asphaltenic and resinic portion reduction but also proposing new phase for theoretical approach of hydrocracking including actual industrial application.

H₂S may turn to HS⁻ + H⁺ or so in situ, above 403 K on the transit metals., where proton move so fast following thermal and free electron from wall, or HC that it does not always needs surface area too wide for activation.

Under rising temperature, there begin to exist the unbalanced distribution of electron on HC. H⁺ is apt to go to radical portion of HC and HS⁻ goes to aromatic portion, where they are cut to be stabilized, that is, each portion become to be the most stable state., which can be judged from the work of Bergius and Pier before World War II. Fig.1, Fig.2

Heavier portion is apt to stick the metal surface due to higher viscosity and unbalanced distribution of electron or so and ready to crack after absorbing thermal electron and hydrogen under acidic environment by H₂S or so at lower temperature.

The above can be used for explaining about lighter S-Compound effect because they are apt to proceed the metal surface and turn to hydrogen donar or that carbenium ion such HS⁻-Compounds after heated up under hydrogen, transferred from in and out cluster on the metal surface, which become radical, hydrite rich through protonation (2), while heavier HC is sticky enough to be catched on the metal surface and be enforced to react with them.

H₂S helps accelerate this transformation such as sulfiding on catalyst where Metal-Sulfur bridge is made on the surface .

H⁺ approaches to S-molecule to make H-S compounds or so while HS⁻ goes to aromatic compounds on the transit sulfided metal.

Sulfur own effect on coal liquidification reaction is well known, especially, as bronsted acid, under hydrogen at above 703 K. Some process need no catalyst on coal liquefaction except sulfur.

3) Operation condition when treated with hydrogen rich gas.

3)-1 Pressure

Too much hydrogen donor is said to stop the radical reaction which also can be explained on the above figures (3).

Hydrogen donor can not transfer electron too much, they cap the cut point and become stabilized by themselves, that is, only become aromatic compounds, which means no need of high pressure hydrogen for hydrocracking of crude. Hydrogen partial pressure is estimated from crude specification, PONA, C/H ratio and metals contents. 2 or 3 MP is enough to keep HS⁻ galvanic hydro-sulfide state.

Hydrogen donor is reduced at some rate at Desalter because Fe-Cl compounds have such ability (4). So, Desalter must be installed to reduce Cl, sea water for anti-corrosion and for hydrogen donor.

Radical reaction is also interrupted by cation so that cation should be trapped by anion, esp., Sulfur Compounds .

3)-2 Temperature

The reaction temperature is very sensitive because it depends on products spec., to be produced and on its mechanism of reactions. Hydrogenation is exothermic and thermal cracking is endothermic. Where at lower temperature, the former reaction is forwarded while heavier portion is just to be cracked under hydrogen on sulfided metals to naphtha and S Compound by H^+ , HS^- and then at higher temperature, the latter reaction is overlapped. Fig. 3

4) The meaning of mixture of heavier oil and lighter oil is as follows.

4)-1 S-Compounds around the heavier cluster become electron, hydrogen deposits when the condition of reaction reach the some level, they will start cracking reaction as catalytic, reactive points.

4)-2 The reactant are transferred through solvent around cluster. But electron rich radical is transferred to heavier unstable portion and continue cracking the remaining heavier portion at above said deposit points.

4)-3 Electronic equivalence of heavier portion seems zero at glance, is very changeable, unstable, depending on around condition so that even slight lighter portion can make better reaction condition to crack such as solvent effect which disperse heavier portion wider and make it differential parts to separate electronically and help radical approach to right points.

4)-4 Too much condensed state such carbonaceous asphaltene, resin and metals complex should be avoided because they are promoting their familiar components production when making white oil, even burning oil to meet such as CAAA in U.S.A..

4)-5 Recently, soluble metal compounds have been informed to exert much more catalytic activity in coal liquefaction (5).

Therefore, without catalyst, more preferable reactive field may be obtained in lighter crude oil which contents metal compounds.

Because only catalyst is solid and interrupt mixing effect, transfer of heat and etc. while hydrogen partial pressure, sulfur compounds, transit metal's surface and temperature are indispensable factors.

5) Conclusion

From thermodynamic, chemical reactionary and electrical equivalent points of view, existing atmospheric distillation is of problem, not economical when refiner need white oil and light oil too much.

Conventional refinery system is of try and error concerned technology, experimental technique. However, recent developed technology has begun to reveal the intrinsic quality of such intricate complex compounds.

Tubes of heat exchangers and pipe lines have enough surface to be activated by H_2S and S-Compounds with hydrogen, on alloy steel.

This new concept, treating crude with hydrogen rich gas leads to Bottomless Refinery, Jet Fuel and Naphtha Rich Refinery, therefore, Refiner should treat the crude under hydrogen at first stage if refiner want to obtain lighter and white oil too much at the lowest cost.

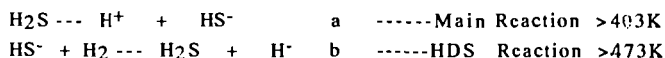
Under hydrogen treating and HDS combination, thiophene is not produced. Heavier residue Catalytic Cracking Process is not to be used any more, the same as sweating process of lighter HC.

Ironically, S-Compounds are indispensable for hydrocracking, not suitable for burning hydrocarbon, which leads us to contemplate that that mysterious, historical birth of the Earth. We are now struggling against environmental problem evoked by noble petroleum, sulfur and oxygen, aiming at sustainable economic development.

Reference only,

HS^- may become H_2S at high press H_2 . There needs some state to be maintained for reaction field where HS^- may continue to decompose the heavier hydrocarbon like sharp knife edge with H^+ and electron.

Typical reaction are as follows.



a + b



These basically reaction are proceeded through or on the S-M bridge. Each equation depends mainly on temperature and hydrogen pressure. Equation c is rarely occurred and has not detected so far.

Literature cited.

- (1) Masaya Kuno, Hydrocarbon Processing (1981)
- (2) B.W.Wojciechowski, Symposium on Hydrogen Transfer in Hydrocarbon Processing ,ACS (1994)
- (3) Junich Kubo H. Higashi, Y Ohmoto and H Arao ditto.
- (4) Johr H. Penn and Jinhai Wang ditto.
- (5) T. Kondoh, A. Matsumura, K. Okegawa, I Saitoh, Sigen and Kankyo Vo.2, No.5 (1993)

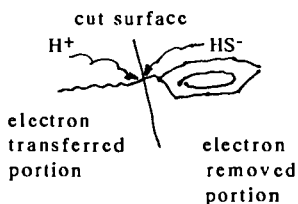
Reference

Dr. Kabe, 1983, treated Taching Crude with hydrogen, CS_2 as activator, toluene as solvent and catalyst Ni-Co-Al O at 673 K. under hydrogen pressure 100 K/G, reaction time 5 hr using autoclave. No activator case showed nothing particular.

The result was residue 40% down, while Naphtha increased 5 times that is, 30 wt% and middle increased a little, 20 to 25 wt%.

Journal of JPI, Vol 26 No3 1983.

Fig.1 shows the typical image



sulfided composition is stabilized

lighter S Compound is made.

lighter portion is produced heavier

where is cut is depends on the solvent spec, around the

(Hexane soluble) { Benzene }
(and the like) { soluble or so }

HC and on other condition such temp or so.

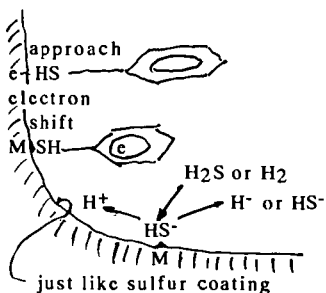
Heat of hydrogenation is enough to cut c-c bond at above 573K.

Produced heat of hydrogenation is transferred around lighter solvent and / or activate another portion to be radical.

Fig.2 shows the typical image on metal surface

on the surface of metal

Thermal electron comes from heated metal surface through Metal-Sulfur bridge

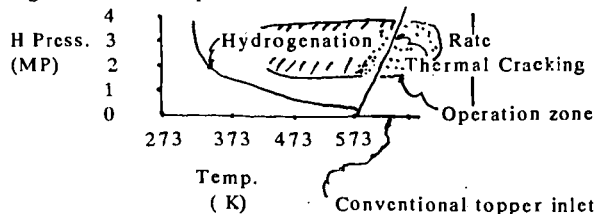


Electron proceed and move to aromatic Compounds which is under lower electron density.

When electron become rich in aromatic Compounds. H^+ can easily approach and cut the C=C bonds after hydrogenation.

M-S bridge also protect to transfer thermal electron from C=C bonds hydrocracking to metal surface, which cause not to evoke carbon making.

Fig. 3 shows the operational condition



ACID RAIN, PROMOTING THE ACCUMULATION OF CO₂ IN SURFACE WATERS ?!

Shuping Bi
Chemistry Department, Nanjing University, Nanjing,
210088, P.R.China

Keywords: acid rain, elevated concentrations of aluminum, surface waters

ABSTRACT

Acid rain and increase of CO₂ concentration in atmosphere are the important problems to the global changes. In the past, people studied them separately. Someone found that lakes are sources of atmospheric CO₂, but the mechanism is not clear. In this paper, we present our investigation on this question by using chemical equilibrium model. Theoretical calculation indicates that: in the acidic range of pH < 5, P_{CO₂} may change from 1 × 10⁻⁴ to 0.1 atm without altering pH value of waters due to the buffering actions of Al³⁺ and H⁺; Oppositely, the pH is very sensitive to the P_{CO₂} in the neutral (pH > 5) surface waters. Therefore, we come to the conclusion that acidified surface waters may hold much more CO₂ than neutral waters. Acid rain, also promotes the accumulation of CO₂ in surface waters!

INTRODUCTION

There is increased concern over the supersaturation of carbon dioxide in the surface waters of lakes^[1,2]. Processes that add and remove CO₂ occur simultaneously in the surface waters of lakes. Data on the partial pressure of carbon dioxide in the surface waters from a large number of lakes (1835) with a worldwide distribution show that only a small proportion of the 4665 samples analyzed (less than 10%) were within ± 20% of the equilibrium with the atmosphere and that most samples (87%) were supersaturated. Furthermore, lakes showed an enormous range of CO₂ concentrations from 175-fold below to 57-fold above atmospheric equilibrium at the extremes. This indicates that lakes are sources rather than sinks of atmospheric CO₂. The probable reason for this excess CO₂ may be due to the large accumulation of organic matter in the tundra and its respiration in soil or lake waters^[3,4]. Thermokarst and fluvial processes cause great erosion of peat and release of dissolved organic carbon (DOC) into lakes and rivers^[5-7], and this C may be respired to CO₂^[8,9]. There is also direct evidence that dissolved inorganic C in ground is moving from land to lakes and rivers, movement of CO₂-charged ground waters into the river can easily account for the high P_{CO₂} observed in the river. However, this explanation is not very satisfying, because it does not consider the effect of the pH of surface waters. As we know, acid rain is a very serious problem to the global changes. One of the consequences of the acidic precipitation is that H⁺ and aluminum concentrations increased in the surface waters.^[10,11] In this paper, we try to link the excess CO₂ with the acid rain by considering the effects of Al³⁺ and H⁺ buffering actions in acidified surface waters. A theoretical model based on the chemical equilibrium equations is developed for evaluating the interactions of P_{CO₂} and pH. Water quality data from the literatures for about 20 sampling stations are analyzed by our model. Interesting conclusion was obtained.

THEORY

We initially make the following assumptions:

- (1) the surface water studied is in equilibrium with the natural gibbsite. It is a dilute solution with low ionic strength^[12];
- (2) in acidic pH range, Al³⁺ and H⁺ dominate the buffering system. The chemical speciation of aluminum in acidic surface waters is complicated because Al³⁺ forms complexes with OH⁻, SO₄²⁻, F⁻ and organic compounds.^[13]

- (3) $[Al^{3+}]$ can be predicted as a function of pH using an aluminum trihydroxide solubility relation. $Al(OH)_3 + 3H^+ = Al^{3+} + 3H_2O$, $[Al^{3+}] = K_{sp}[H^+]^3$ [14];
- (4) concentrations of Fe and Mn are very low, their reactions with ligands (F^- , SO_4^{2-} , OH^- , and organic solute) are insignificant [15];
- (5) organic solutes in natural waters are presented as a triprotic acids, while two species of aluminum-organic solutes are depicted [16];
- (6) no adsorption of anions was taken into account;
- (7) for an open system, the following reactions controlling the CO_2 concentrations take place: (P_{CO_2} is the partial pressure of CO_2)

$$[H_2CO_3^*] = K_H P_{CO_2} \quad (1)$$

$$[HCO_3^-] = K_{Cl} K_H P_{CO_2} / [H^+] \quad (2)$$

$$[CO_3^{2-}] = K_{Cl} K_{Cl} K_H P_{CO_2} / [H^+]^2 \quad (3)$$

By employing the electroneutrality relationship, we can write:

$$E_N = E_{N,Al-OH} + E_{N,Al-F} + E_{N,Al-SO_4} + E_{N,Al-ORG} + E_{N,CO_2} + C_B - C_A + [NH_4^+] - [F^-] + [H^+] - [OH^-] \quad (4)$$

E_N is the discrepancy in electroneutrality, in which contributions from various components $E_{N,i}$ are:

$$E_{N,Al-OH} = 3[Al^{3+}] + 2[Al(OH)^{2+}] + [Al(OH)_2^+] - [Al(OH)_3] \quad (5)$$

$$E_{N,Al-F} = 2[AlF^{2+}] + [AlF_2^+] - [AlF_3] - 2[AlF_4^-] \quad (6)$$

$$E_{N,Al-SO_4} = [AlSO_4^+] - [Al(SO_4)_2^-] \quad (7)$$

$$E_{N,Al-ORG} = [AlHORG^+] - 3[ORG^{3-}] - 2[HORG^{2-}] - [H_2ORG^-] \quad (8)$$

$$E_{N,CO_2} = -2[CO_3^{2-}] - [HCO_3^-] \quad (9)$$

C_B is the sum of basic cation equivalence ($2[Ca^{2+}] + 2[Mg^{2+}] + [K^+] + [Na^+]$ in eq/L), C_A is the sum of acidic anion equivalence ($2[SO_4^{2-}] + [NO_3^-] + [Cl^-]$ in eq/L).

E_N is a function of $[H^+]$, $E_N = f(H^+)$. By using Newton-Raphson method, $[H^+]$ can be calculated:

$$[H^+]_{i+1} = [H^+]_i - \frac{E_N}{\left(\frac{\partial E_N}{\partial H} \right)} \quad (10)$$

$[H^+]$ is the hydrogen ion concentration at the i th iteration and $[H^+]_{i+1}$ is the hydrogen ion concentration at the $i+1$ th iteration. Equations (1-10) express the relationship of P_{CO_2} with pH in surface waters and can be used to evaluate their interactions. With fixed P_{CO_2} , pH can be given; On the other hand, P_{CO_2} can also be calculated at a fixed pH by iteration. The mass balance is:

$$C_F^- = [F^-] + [HF] + [AlF^{2+}] + 2[AlF_2^+] + 3[AlF_3] + 4[AlF_4^-] + 5[AlF_5^{2-}] \quad (11)$$

$$C_{SO_4} = [SO_4^{2-}] + [AlSO_4^+] + 2[Al(SO_4)_2^-] \quad (12)$$

$$C_{ORG} = [ORG^{3-}] + [HORG^{2-}] + [H_2ORG^-] + [H_3ORG^0] + [AlHORG^+] + [AlORG] \quad (13)$$

A GW-BASIC computer program was developed to perform the necessary calculation. All chemical reactions equilibrium constants are cited from literatures [12-14].

RESULTS AND DISCUSSION

Atmospheric deposition and processes occurring in the soil are responsible for the observed surface water chemistry in a catchment. [19] CO_2 partial pressure in soil is commonly much higher than atmospheric CO_2 partial pressure ($10^{-3.5}$ atm). When the solution is removed from

contact with the soil matrix and exposed to the atmosphere (that is when water enters the stream channel), two situations may be occurring for the CO_2 , depending on the pH value of the surface waters. Figure 1 gives the results of the theoretical calculation of pH values as the function of $C_B - C_A$ under various P_{CO_2} values for surface waters. We can use it to explain the influence of pH on the accumulation of CO_2 concentrations in surface waters.

(1) the surface water is in the acidic range of $C_B - C_A < -200 \mu\text{eq/L}$, P_{CO_2} may increase from 1×10^{-4} to 0.1 atm without change of pH. Acidic conditions restrict the dissociation of CO_2 (H_2CO_3) to H^+ and HCO_3^- due to the buffering actions of Al^{3+} and H^+ . This means that much more CO_2 concentrations can be accumulated in surface waters under acidic condition;

(2) CO_2 is not easy to accumulate in the surface water which is of $C_B - C_A > 0 \mu\text{eq/L}$. Under this condition, the water is poorly buffered and small changes in CO_2 concentration can significantly affect pH. Higher P_{CO_2} needs lower pH. Otherwise, the pH of the solution will increase, causing CO_2 lost to the atmosphere.^[20,21] This means that when water enters the neutral stream channel from soil, excess CO_2 concentrations can not be accumulated in surface waters due to the increase of pH.

Figure 2 depicts the " P_{CO_2} vs. pH" relationship for analyzing the practical sampling water quality data. The data are cited from the literatures^[22-26]. The values of P_{CO_2} are calculated from pH measured. After $\text{pH} > 5$, P_{CO_2} is not more than 20 P_0 . Conversely, P_{CO_2} increases rapidly as an exponential function at $\text{pH} < 5$. Lakes are a small but potential important conduit for carbon from terrestrial sources to the atmospheric sink. Acid rain, also promotes the accumulation of carbon dioxide in surface waters!

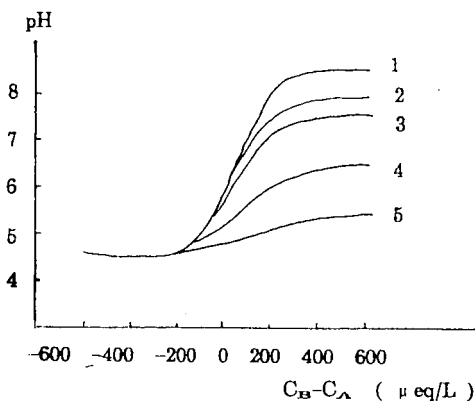


Fig.1 plot of " pH vs. $C_B - C_A$ "
 P_{CO_2} (atm):
 1 — 1×10^{-4} , 2 — 3.16×10^{-4} ,
 3 — 1×10^{-3} , 4 — 1×10^{-2} ,
 5 — 1×10^{-1}

ACKNOWLEDGEMENT

This project is financed by the National Natural Science Foundation of China, Fok Ying Tung Education Foundation of Hong Kong and State Education Committee Foundation of China. The author thanks Prof. Rongshi Cheng, Hongyuan Chen, Ying Wang and Director of Smithsonian Environmental Research Center D.L. Correll for their supports and help.

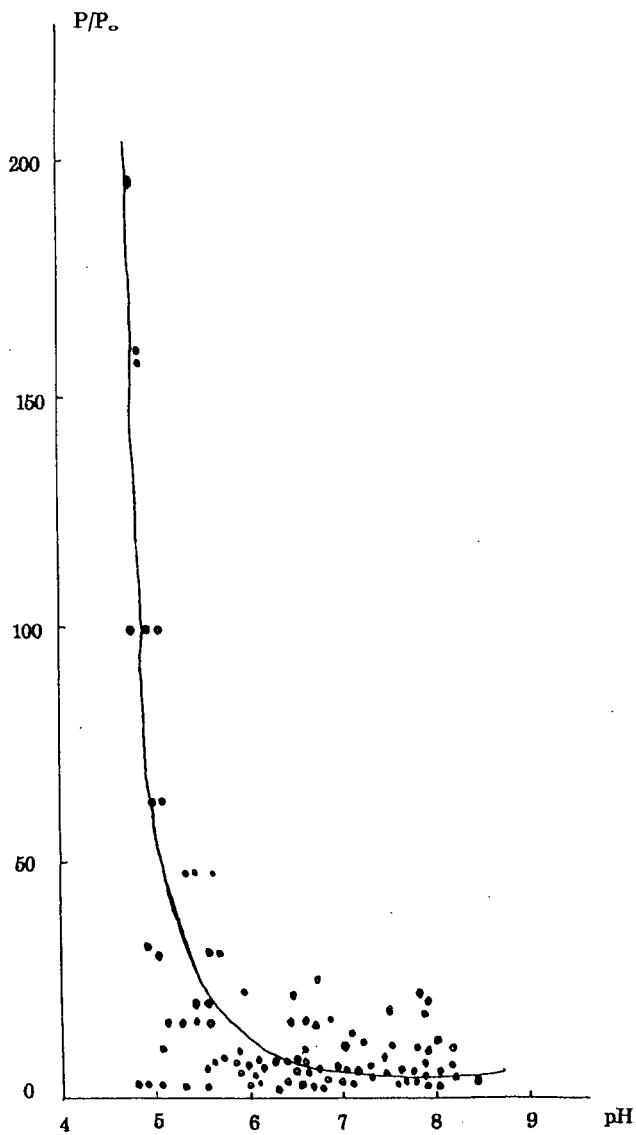


Fig.2 plot of " P_{CO_2} vs. pH "
 ($P_0 = 3.16 \times 10^{-4}$ atm)

REFERENCES

1. J.J.Cole, N.F.Caraco, G.W.Kling and T.K.Kratz, *Science.*, 265 (1994) 1568
2. G.W.Kling, G.W.Kipphut and M.C.Miller, *Science.*, 251 (1991) 298
3. G.W.Kling, G.W.Kipphut and M.C.Miller, *Hydrobiologia.*, 240 (1992) 23
4. D.W.Schindler et al, *Science.*, 177 (1972) 1192
5. D.M.Schell, *Science.*, 219 (1983) 1068
6. B.J.Peterson, J.E.Hobbie and T.L.Corliss, *Can.J.Fish.Aquat.Sci.*, 43 (1986) 1259
7. P.I.Coyne and J.J.Kelley, *Limnol.Oceanog.*, 19 (1974) 828
8. P.V.Sellmann, J.Brown, R. I. Lewellen, H. Mckim and C. Merry,
" The classification and geomorphic implications of thaw lakes of
the arctic coasta plain,Alaaka " (Rep 344, US Army Cold Regions
Research and Engineering Lab, Hanover, NH, 1975)
9. P.P.Tans, I.Y.Fung and T.Takahashi, *Science.*, 247 (1990) 1431
10. G.Sposito, *The Environmental Chemistry of Aluminum.* CRC Press,Inc.
Boca Raton, Florida, 1989.
11. W.H.Durum and J.Haffty, *Geochim Cosmochim Acta.*, 27 (1963) 1.
12. W.D.Schecher and C.T.Driscoll, *Water Resource Research.*, 23 (1987)
525.
13. Shuping Bi, *analyst.*, 120 (1995) 2033
14. W.D.Schecher, Ph.D Dissertation. Syracuse University. Syracuse,
New York, 1988.
15. E.Tipping, C.Woof and M.A.Hurley, *Water Res.*, 25(1991) 425.
16. C.T.Driscoll and W.D.Schecher, *Environ.Biochem.Health.*, 12 (1990) 28.
17. Shuping Bi, *Anal.Chimica.Acta.*, 314 (1995) 111
18. Shuping Bi and Wei Ying, *Analyst.*, 120 (1995) 2805
19. J.J.Bisogni Jr and S.L.Arroyo, *Water Res.*, 25 (1991) 185
20. B.J.Cosby, G.M.Hornberger, J.N.Galloway and R.F.Wright,
Environmental Science and Technology., 19 (1985) 1144
21. W.Stumm and J.J Morgan, *Aquatic Chemistry.*, Wiley-Interscience,
New York, 1981
22. L.A.Baker, C.D.Pollman and J.M.Eilers, *Water Resources Res.*, 24 (1988)
1069
23. J.R.Webb, B.J.Cosby, J.N.Galloway and G.M.Hornberger,
Water Resources Res., 25 (1989) 1367
24. A.T.Herlihy, P.R.Kaufmann, M.R.Church, P.J.Wigington Jr, J.R.Webb
and M.J.Sale, *Water Resources Res.*, 29 (1993) 2687
25. D.R.Dewalle and B.R.Swistock, *Water Resources Res.*, 30 (1994) 1955
26. M.B.David, G.F.Vance and J.S.Kahl, *Water Resources Res.*,
28 (1992) 389
27. K.B.Easthouse,D.E.Spyidakis and E.B.Welch, *Water, Air and Soil Pollu.*,
71 (1993) 377
28. K.E.Webster,P.L.Brezonik and B.J.Holdhusen, *Water,Air and Soil Pollu.*,
67 (1993) 397
29. R.Harriman, B.R.S.Morrism, L.A.Caines, P.Collen and A.W.Watt,
Water, Air and Soil Pollu., 32 (1987) 89
30. M.Lachance, D.Brouard and G.Walsh, *Water, Air and Soil Pollu.*,
39 (1988) 311
31. H.B.Xue and J.L.Schnoor, *Water, Air and Soil Pollu.*,
75 (1994) 61
32. S.Ikeda, J.Motonaka, T.Koizumi and T.Ishikawa, *Anal Sci.*, 7 (1991) 1077
33. R.Giovanoli, J.L.Schnoor, L.Sigg, W.Stumm and J.Zobrist,
Calyx and Caly mine., 36 (1988) 521
34. B.O.Roseland et al, *Environ Pollu.*, 76 (1992) 3
35. R.F.Wright, *Environ.Sci.*, 22 (1988) 178
36. M.Papineau and J.Haemmerli, *Water, Air and Soil Pollu.*, 61 (1992) 85

THE STABLE HIGH TEMPERATURE CO₂-ACCEPTOR. THERMOANALYTICAL STUDY

August R. Brun-Tcekhovoi¹, Sergei S. Kurdyumov¹, Leonid A. Rudnitsky²

¹Inst. of Petrochem. Synth. 117912, Leninskii pr.29, Moscow, Russia

²Inst. of Nitrogen Ind., 109815, Zemljanoi Val, 50, Moscow, Russia

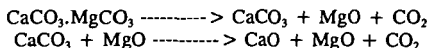
Keywords: CO₂ acceptor, thermoanalytical methods, durability

The studied high temperature CO₂-acceptor intended for the persistent removal of CO₂ from chemical reactors fits special requirements. It is characterized by the high CO₂ capacity and durability; its structure stability is held on the cyclic variation of inner stresses produced by the consequence of carbonation-decarbonation. The acceptor which consists of CaO and MgO (periclase) has been prepared from dolomite. Experimental data demonstrate CaO phase to work as CO₂-acceptor and MgO one to form a rigid framework, which provides the stability to the grains structure. The volume of CaCO₃ phase formed exceeds twice the initial volume of CaO phase. However, this effect is eliminated due to the periclase framework: acceptor grains do not demonstrate any expansion on CaCO₃ formation.

The CO₂-acceptor was developed with the properties allow using it on new effective technology of the methane steam reforming process (ASMR). The main peculiarity of this technology is continuous CO₂ remove from the reaction zone of ASMR by means of solid acceptor which continuously circulates through this zone.

The acceptor should demonstrate sufficient high activity on interaction with CO₂. Besides the acceptor must have a high attrition resistance (AR). Finally it must be stable enough to both these parameters. The most suitable materials for producing CO₂-acceptor is dolomite CaCO₃.MgCO₃.

At temperature ranges of ASMR-process dolomite is decomposed by two stages:



Formed due to stage (1) MgO is inactive because of sintering after formation. An active component of acceptor is CaO, which is formed as a result of reversible reaction (2). The direct using of dolomite as a CO₂-acceptor is impossible mainly because of phase transition which accompanied both indicated reactions.

Disordering of crystal lattice leads to lowering of AR. So the proceeding of the low temperature stage (1) induces the decrease of initial value of AR for dolomite from about 40% to zero. Stage (2) is accompanied by the transition CaCO₃ phase to CaO and vice versa.

The dolomite destruction due to phase transition made impossible a realization of prospective technology of coal-gasification known as "CO₂-acceptor process". Simultaneously an ability of dolomite to lose activity due to sintering was also found out. All these data were obtained on semi commercial plant.

According to our purposes the grain of the acceptor must include a stable and chemical inert framework, distributed in all volume of grain. Active component (CaO) is disposed in the space cells of the framework.

MgO was chosen as a matter for creating a framework because of its ability to sintering and formatting inactive and stable periclase. Further it would be expedient to choose dolomite as a MgO-containing material, which includes CaO also.

During our experiments we have developed a method of dolomite treatment which allows producing CO₂-acceptor, not having the lacks typical for dolomite.

The above discussed practical-important properties of studied solids were determined using the next methods: 1) activity A_{CO₂} was determined as CO₂ in carbonated samples; 2) the value of AR was determined in the device, simulated the air-lift at a linear velocity equaled 25-30 m/s.

The stability of samples was characterized by changing the values of A_{CO_2} , AR and by the specific surface in the long runs with intermittent cycles of decomposition (1100-1200K) and carbonation (by 900-950K). Total duration of the tests was 100h, a number of cycles was near 50.

The fresh acceptor has a high value of AR (80%), which near twice higher than for fresh dolomite. In test the AR value was lowered during 10-30h, then it remained near constant and equaled to that for fresh dolomite. The AR values for carbonated and decomposed samples differed insignificantly. It means that for the acceptor the transition of $CaCO_3$ to CaO does not affect its structure.

The A_{CO_2} value was in fact constant changed within 25 to 27 percent. This is in good agreement with the almost constant value of the specific surface, which is equal to 2.3-2.6 m^2/g for decomposed samples and to 0.4-0.8 m^2/g for carbonated samples.

For the study of formation of CO_2 -acceptor we have chosen two thermoanalytical methods: thermogravimetry and dilatometry. This permitted us firstly to register the value of mass changing and the rate of this process and secondly to register the grain-framework response to the consequence variation the volume of the active phase.

The work was carried out by microbalance "Sartorius" and dilatometer "Netzsch" adapted by us for the work in different gases flow at the temperatures from ambient to 1000°C. The same programs and conditions of experiments were used for different methods. The data on mass change and elongation are given in dimensionless form $\Delta m/m$ and $\Delta l/l$.

First of all, the behaviors of natural dolomite and acceptor in course of the cyclic $CaCO_3$ - CaO transitions were compared. In this series of experiments, the carbonate decomposition in air flow was studied only. Dilatometric curves for heating of samples are given in Fig. 1 as dependencies of temperature coefficient of linear expansion on the temperature. Dilatogram of the first decarbonation of natural dolomite (curve 1) indicates the great extent of contraction in the temperature range higher than 600°C and, especially, higher than 700°C, where decomposition of calcium carbonate takes place. At the second decarbonation (curve 2) the considerable contraction peak in the range of 400-600°C has been observed which corresponds to decomposition of magnesium carbonate. Further in the not large temperature interval (from 600 to 700°C) the grain structure is evidently supported by calcium carbonate phase, but its decomposition at temperature higher than 700°C induces endless contraction of grain which indicates to the destruction of sample.

Dilatogram of the first decarbonation of acceptor (curve 1a) shows not so significant effect of decreasing temperature coefficient in the temperature range corresponding to decomposition of magnesium carbonate and not so large contraction peak in the temperature range higher than 700°C corresponding to the decomposition of calcium carbonate.

As the cycling proceeds, the first effect disappears really, and the second decreases. On the fourth cycle (curve 2a) we obtain at almost whole temperature range the positive temperature coefficient of thermal expansion decreasing at temperature - higher 800°C only. Thus cycling the acceptor (two-phase system) leads to stabilization of the grain framework, but cycling the natural dolomite (one-phase system) induces destabilization of its structure and then destruction of the grain.

Then the comparative study of acceptor samples different in intensity of natural dolomite treatment which transforms it to CO_2 acceptor was carried out. These intensities are represented below in arbitrary units (a.u.).

In Fig. 2 the thermogravimetric curves for acceptors obtained by mild and by severe treatment of dolomite are compared (5 and 18 of a.u. correspondingly). Previously these samples were decarbonated, after that they were linearly heated and cooled in CO_2 flow. The curve for sample 5 is continuous line, the curve for sample 18 is noted by stars. It can be seen that the interaction with CO_2 begins at quite low temperature (from 300 to 400°C), but it proceeds not so quickly and follows up to relatively high temperature. The thermogravimetric curve for sample 18 is displaced to high temperatures essentially (approximately by 200K) as related to the curve for sample 5. This is connected evidently with the fact, that transforming natural dolomite into acceptor is followed by the scaling acceptor structure, - decreasing its porosity and, may be, section of transport pores and other effects inducing decrease of rate of interaction

with CO_2 . Thermogravimetric curve for sample 18 exceeds the temperature of thermodynamic equilibrium for calcium carbonate decomposition before ending the carbonation. Nevertheless it can be seen that capacities of both samples are close enough and quite large: the quantity of CO_2 uptake exceeds 30% of mass of the sample containing MgO and CaCO_3 . Decomposition of carbonate proceeds in both samples with high and close rates. The decrease of temperature returns the samples into the region of carbonate formation. Thermogravimetric curves for cooling testify the high rate of carbonation, but exceed the saturation at more low level than those for heating. This fact is induced, may be, by sintering CaO becoming real at this quite high temperature after CO_2 isolation.

Consider now the response of grain structure to calcium carbonate formation and decomposition. In Fig. 3, one from thermogravimetric curves for heating and cooling the sample 18 in CO_2 flow shown in previous figure and corresponding dilatogram, the scale for ordinate of which is increased approximately hundred times are presented. This permits us to use the common ordinate y for representation dilatogram (dotted line) and thermogravimetric curve and to compare the both curves. At heating dilatogram character corresponds to thermal expansion of the sample. The similar curve in the bottom part of the figure corresponds to thermal contraction at cooling. Thermogravimetric curve for heating demonstrates at 600°C the beginning of calcium carbonate forming. At 750°C - approximately 30% of calcium oxide transforms into carbonate. The total volume of reacting and forming phases increases approximately by 30%, however dilatogram does not indicate any expansion of sample.

On the contrary at 700°C in spite of forming the carbonate with considerable rate deceleration of thermal expansion and then contraction of sample is observed the latter finishes in the temperature region corresponding to decomposition of carbonate and isolation of CO_2 .

During the cooling of the sample at temperature about 870°C thermogravimetric curve indicates increasing the sample mass - approximately by 10% (30% of CaO forms carbonate).

There is insignificant splash in dilatogram - this effect corresponds approximately to thermal expansion of the sample at heating by 10-12 K. Thus the carbonate formation does not induce practically any expansion of acceptor. This result testifies apparently that there is some functional and space separation of two phases in acceptor. Components of these phases (CaO and MgO) constituted previously one-phase structure of dolomite. It may be thought that after segregation of phases magnesium oxide transforms into stable inert form - periclase. The latter forms grains framework keeping its stability and sitting the second phase - calcium oxide which is the acceptor really so that volume variations of the latter do not lead to the excess inner framework stresses. Suggested scheme is apparently simplified.

Consider Fig. 4 permitting to coincide thermogravimetric (top figure) and dilatometric (bottom figure) curves for heating in air the acceptors 5 and 18 subjected previously to treatment with CO_2 at high pressure, i.e. saturated completely. The dotted lines correspond to the sample 5. It can be seen that sample capacities are very high and close to one another (the calculation with regard to carbonated sample is given). Thermogravimetric curves of carbonate decomposition also coincide practically. It can be seen not large displacement (not more than 1%) in the region where decomposition of magnesium carbonate takes place - about 500°C . Analogous displacement can be observed in dilatogram for sample 18 shown in bottom figure and for some other samples. The fact that quite small quantity of decomposed magnesium carbonate can induce dilatometric effect permits us to suppose that activation of MgO can proceed on interphase boundaries where the reaction of calcium oxide can catalyze the surface layers of periclase. As thermogravimetric curves for decarbonating samples 5 and 18 practically coincide, the corresponding dilatometric effects appear to be different: sample 18 indicates more less contraction than sample 5. Evidently this is connected with larger durability and rigidity of its framework.

While during heat treatment of samples in carbon dioxide flow or in air effects of volume increase are practically absent the contraction of samples is often observed. Evidently contraction of samples is induced by a complex of reasons, which require further investigation.

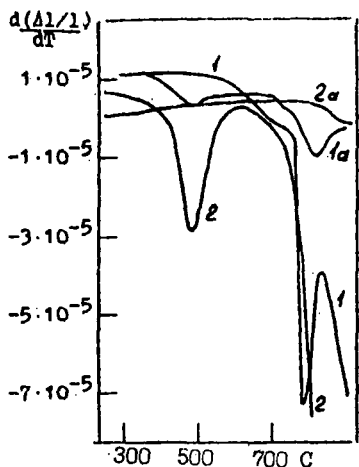


Figure 1. The dependencies of the linear expansion coefficient on temperature for cyclic heating of natural dolomite (1 and 2) and CO₂ acceptor (1a and 2a)

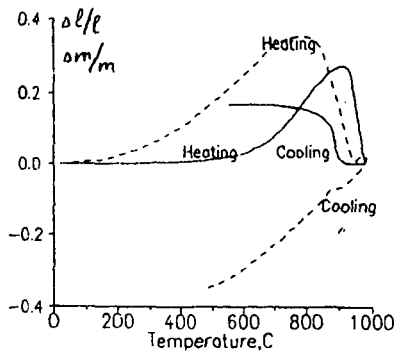


Figure 3. The comparison of the thermogravimetric and dilatometric (dotted line) curves of the heating and cooling in the CO₂ flow for acceptor 18. The y axis scale (elongation) is enlarged about 100 times.

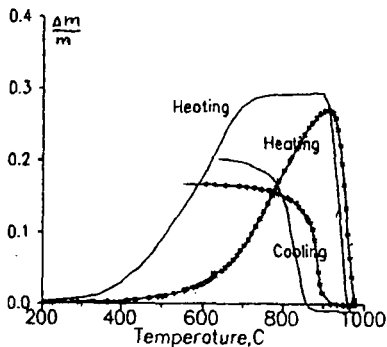


Figure 2. The thermo-weight curves of the heating and cooling in the CO₂ flow for acceptors 5 and 18 (marked with stars).

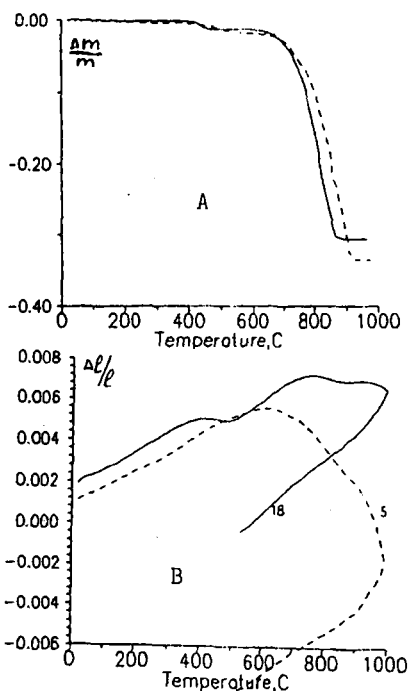


Figure 4. The comparison of the thermo weight (a) and dilatometric (b) curves of the heating and cooling in the air flow for acceptors 5 (dotted line) and 18.

FROM CARBON DIOXIDE TO C₂ ORGANIC MOLECULES

Jin K. Gong,* Chris A. Wright, Matthew Thorn, James W. McGill,
Angela Sutterer, Shannon M. Hinze, and Ryan B. Prince
Department of Chemistry
Southeast Missouri State University
Cape Girardeau, MO 63701

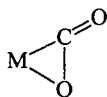
Keywords: Nickel Carbon Dioxide, Wittig Reaction, Nickel Ketene Complex

Abstract

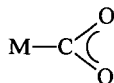
Research on the conversion of carbon dioxide into C₂ or higher organic molecules has received much attention in recent years. The key to the success of this research is carbon-carbon coupling. This paper reports the modified synthesis of a nickel carbon dioxide complex, (Cy₃P)₂NiCO₂, (Cy = cyclohexane) and the "Wittig Reaction" of this coordinated nickel carbon dioxide complex. The formed nickel ketene complex, (Cy₃P)₂Ni[η²-(C,O)-CH₂=C=O], has an unusual η²-C,O bonding mode instead of the normal η²-C,C for the later transition metals. The pathway of this "Wittig Reaction" is an unprecedented example for a transition metal carbon dioxide complex.

Carbon dioxide chemistry has been a research topic for many research groups due to its fundamental importance and practical applications. To develop efficient catalytic processes in which carbon dioxide can be used as a carbon source is one of the main objectives of this research area.¹ Carbon-carbon coupling is the key to achieve C₂ or higher organic molecules. We are reporting the first example of "Wittig Reaction" on a coordinated carbon dioxide nickel complex.

Coordination of carbon dioxide to a transition metal is one of the initial steps in the catalytic conversion of carbon dioxide into useful organic molecules. The electronic structure of carbon dioxide is perturbed by bonding to a transition metal center. Different types and degrees of altered reactivities have been observed for different coordination modes of carbon dioxide. Two coordination modes for mononuclear metal carbon dioxide complexes have been reported⁸. They are η² side-on coordination and η¹-C coordination.



η²-side-on coordination



η¹-C coordination

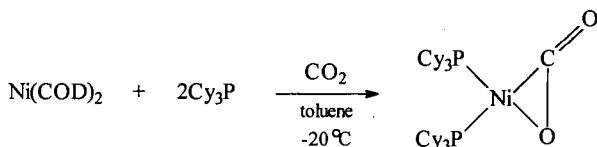


η¹-end-on coordination

The η²-side-on and η¹-C coordination modes are well established. The η¹ end-on coordination is a proposed mode as a result of calculation and has only been mentioned once as an intermediate in the literature³⁶. Theoretical studies of these coordination modes of carbon dioxide have given a better understanding of the factors governing the bonding in carbon dioxide complexes. The η² side-on mode is preferred when the metal has a dπ orbital as the HOMO and the empty dσ orbital pointing to the carbon dioxide ligand. One of the examples is Mo(0) in Cp₂MoCO₂, where Cp = cyclopentadiene. The η¹-C mode is most favored when

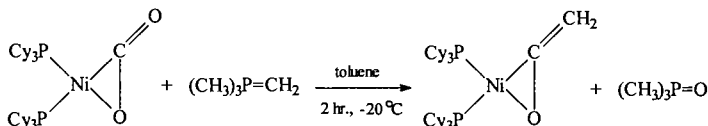
the HOMO is mainly composed of a $d\sigma$ orbital and when the metal is in a low oxidation state, as found in the d^8 complexes¹⁷.

The η^2 -coordinated nickel carbon dioxide complex, $(\text{C}_3\text{P})_2\text{NiCO}_2$, is favored as a starting complex with the ylide due to the electrophilic carbon of the coordinated CO_2 . The complex was first prepared by Michele Aresta in 1974^{1a,4}. Based on the literature procedures, the preparation was modified to a one step procedure:



where COD is 1,5-cyclooctadiene. A 50 ml Schlenk reaction flask was charged with $\text{Ni}(\text{COD})_2$, two equivalent of tricyclohexylphosphine and a minimum amount of anhydrous toluene in a nitrogen atmosphere dry box. The reaction flask was immediately brought out of the dry box and placed in an ice/salt cooling bath. bubbled the reaction solution with carbon dioxide gas via a syringe needle for about thirty minutes. During the above process, the product was precipitated out as yellow crystalline solid. The product was filtrated and washed with a small amount of ether in the dry box. The yield is around 85%. The spectral data are in agreement with the literature values. The C=O in coordinated CO_2 is characterized by a strong IR band at 1740 cm^{-1} . The $^{31}\text{P}\{^1\text{H}\}$ NMR of $(\text{C}_3\text{P})_2\text{NiCO}_2$ in C_6D_6 shows a singlet at 37.32 ppm at 298 K. The $^{31}\text{P}\{^1\text{H}\}$ NMR of $(\text{C}_3\text{P})_2\text{NiCO}_2$ in THF-d_8 at 188K shows two doublets $^2J_{\text{P-P}} = 39.6 \text{ Hz}$ at 51.7 and 20.2 ppm, respectively⁴. The estimated value for the free activation temperature of the dynamic process at the coalescence temperature (233 K) is 39.3 KJ mol^{-1} .

Trialkyl phosphorus ylides, $\text{R}_3\text{P}=\text{CH}_2$, are strong nucleophiles. They react with organic ketenes and aldehydes to form alkenes via a [2+2] cycloaddition mechanism. Such ylides can also react with bridging carbonyls in $[\eta^5\text{-CpFe}(\text{CO})_2]_2$ and $\text{Ni}_2(\mu\text{-CO})(\text{CO})_2(\text{dppm})_2$, $\text{dppm} = \text{bis}(\text{diphenylphosphino})\text{methane}$, to form μ -alkylidene complexes through the same C-C bondformation mechanism⁵. The carbon of $\eta^2\text{-CO}_2$ metal complexes has demonstrated some interesting reactivities towards nucleophiles⁶. The reaction between a metal CO_2 complex and an ylide is an unprecedented example in carbon dioxide chemistry. When $(\text{C}_3\text{P})_2\text{NiCO}_2$ is treated with excess of trimethyl phosphorus ylide at room temperature in toluene, a nickel ketene complex is formed⁷:



Free organic ketenes are very reactive molecules. They can be stabilized by transition metal complexes. Transition metal ketene complexes are important intermediates in catalysis such as in the Fischer-Tropsch process. The process involves the catalytic CO activation and carbon-carbon coupling chemistry⁸. Ketenes can be bonded to transition metal complexes in a wide variety of ways^{8a}.

The two common bonding modes for mononuclear ketene complexes are η^2 -(C, O) and η^2 -(C, C). Traditionally, the η^2 -(C, O) mode is considered to be favored by early transition metal complexes due to the electrophilic property of early transition metals. The η^2 -(C, C) mode is preferred by late transition metal complexes. Several nickel ketene complexes have been reported and characterized spectroscopically to be the η^2 -(C, C) bonding mode^{8a}. The nickel ketene complex we obtained in the above reaction is characterized to be η^2 -(C, O) bonded. A strong stretch at 1611 cm^{-1} is assigned to the C=C double bond. The first structure of an η^2 -(C, O) bonded nickel ketene complex was reported recently by Hofmann's group⁹. The nickel diphenylketene complex, (dtbpm)Ni[η^2 -(C, O)-Ph₂C₂O], has a strong band at 1643 cm^{-1} for the C=C double bond, where the chelated ligand, dtbpm, is Bis(di-tert-butylphosphino)methane.

Transition metal ketene complexes have demonstrated much interesting chemistry. The coordinated ketene can be readily converted to various organic molecules such as alcohols, aldehydes, acetones and acids⁸. The preliminary investigation shows that the nickel ketene complex we isolated has its own characteristic reactivity which is different from the η^2 -(C, C) species, (Ph₃P)₂Ni[η^2 -(C, C)-CH₂=CO], reported in the literature¹⁰. Our nickel ketene complex can react with HCl to generate acetaldehyde. Ligand effect studies are underway to understand the bonding modes of η^2 -(C, C) and η^2 -(C, O) to nickel complexes.

Acknowledgment. We acknowledge Research Corporation for the Cottrell College Science Award (C-3394) and GRFC of Southeast Missouri State Univ. C. A. Wright is grateful to the NASA JOVE scholarship.

References

1. (a) Ayers, W. M. *Catalytic Activation of Carbon Dioxide*; ACS Symposium Series 363, New York, April 13-18, 1986. (b) Palmer, D. A.; Eldik, R. V. *Chem. Rev.* **1983**, *83*, 651. (c) Darensbourg, D. J.; Kudasoski, R. A. *Adv. Organomet. Chem.* **1983**, *22*, pp 129-168. (d) Braunstein, P.; Matt, D.; Nobel, D. *J. Am. Chem. Soc.* **1988**, *110*, 3207-3212. (e) Caballol, R.; Marcos, E. S.; Barthelat, J.-C. *J. Phys. Chem.* **1987**, *91*, 1328-1333. (f) Gambarotta, S.; Arena, F.; Floriani, C.; Zanazzi, P. F. *J. Am. Chem. Soc.* **1982**, *104*, 5082-5092. (g) Jessop, P. G.; Ikarlya, T.; Noyori, R. *Nature*, **1994**, *368*, 231-233.
2. (a) Sneeden, R. P. A.; Villeurbanne, C. N. R. S. *Comprehensive Organomet. Chem.*; Wilkinson, G. Perga Press: New York, **1982**; *8*, pp 225-283. (b) Eisenberg, R.; Hendriksen, D. E. *Adv. Catal.* **1979**, *28*, 79. (c) Braunstein, P.; Matt, D.; Nobel, D. *Chem. Rev.* **1988**, *88*, pp 747-764.
3. Aresta, M.; Nobile, C. F.; Sacco, A. *Inorganica Chimica Acta*, **1975**, *12*, 167.
4. (a) Aresta, M.; Nobile, C. F.; Albano, V. G.; Forni, E.; Manassero, M. J. *Chem. Soc. Chem. Comm.* **1975**, 636. (b) Aresta, M.; Gobetto, R.; Quaranta, E.; Tommas, I., *Inorg. Chem.* **1992**, *31*, 4286
5. (a) Korswagen, R.; Alt, R.; Ziegler, M. L. *Angew Chem Int. Ed. Engl.* **1981**, *20*, 1049. (b) Gong, J. K.; Kubiak, C. *Ph.D. Thesis*, **1990**, Purdue Univ. W. Lafayette, IN.

6. (a) Aresta, M.; Nobile, C. *J. Chem. Soc., Dalton Trans.*, **1977**, 708. (b) Arce, A. J.; Deeming, A. *J. Chem. Soc., Chem. Commun.*, **1982**, 364.
7. The $^{31}\text{P}\{^1\text{H}\}$ NMR (CD_3CN , 85% H_3PO_4 external) for $(\text{C}_6\text{H}_5)_2\text{Ni}[\eta^2\text{-}(\text{C}, \text{O})\text{-CH}_2\text{=CO}]$: singlet at δ 27.15 ppm, The coupled spectrum of the byproduct, $\text{Me}_3\text{P=O}$, shows a multiplet of ten peaks centered at δ 37.98 ppm due to the coupling of phosphine to the nine protons in Me_3 . FTIR: $1611 (\text{s}) \text{cm}^{-1}$ for C=C , ^1H NMR for the CH_2 group of the coordinated ketene is at δ 2.45 (br) ppm, The yield is 52%.
8. (a) Geoffroy, G. L.; Bassner, S. L., *Adv. Organomet. Chem.*, **1988**, 28, 1. (b) Collman, J. P.; Hegedus, L. S.; Norton, J. R.; Finke, R. G. *Principles and Applications of Organotransition Metal Chemistry*, Univ. Sci. Books, **1987**, p657-659. (c) Wolczanski, P. T.; Bercaw, J. E. *Acc. Chem. Res.* **1980**, 13, 121. (d) Masters, C. *Adv. Organomet. Chem.* **1979**, 17, 61. (e) Blyholder, G.; Emmet, P. H. *J. Phys. Chem.* **1960**, 64, 470. (f) Ichikawa, M.; Sekizawa, K.; Shikakura, K.; Kawai, M. *J. Mol. Catal.* **1981**, 11, 167. (g) Takeuchi, A.; Kratzer, J. R. *J. Phys. Chem.* **1982**, 86, 2438. (h) Muetterties, E. L. *J. Chem. Rev.* **1979**, 79, 479. (i) Bell, A. T. *Catal. Rev.* **1981**, 23, 203. (j) Herrmann, W. A. *Angew. Chem., Int. Ed. Engl.* **1982**, 21, 117.
9. Hofmann, P.; Perez-Moya, L.; Steiglmann, O.; Riede, J. *Organometallics*, **1992**, 11, 1167.
10. (a) Miyashita, A.; Shitara, H.; Nohira, H. *J. Chem. Soc., Chem. Commun.* **1985**, 850. (b) Miyashita, A.; Grubbs, R. H. *Tetrahedron Lett.* **1981**, 22, 1255.

ACETYLENE-MEDIATED ALKYLATION OF MONOALKYL CARBONATES
AND CARBAMIC ACIDS WITH *TERT*-AMINE

Yoshiyuki Sasaki

National Institute for Resources and Environment,
16-3 Onogawa, Tsukuba-shi 305, Japan

Keywords: Carbon Dioxide, Dialkyl Carbonate, Acetylene

Carbonic acid diesters and carbamic acid esters are useful organic substances as intermediates for the syntheses of pharmaceutical, agricultural, and the other chemicals. They are currently synthesized in industry using the processes based on phosgene or carbon monoxide. On the other hand, since carbon dioxide is an abundant and cheap carbonyl carbon source, and is much less toxic than those raw materials, substantial efforts have been focused on its fixation into carbonyl compounds including carbonic acid diesters and carbamic acid esters.¹ However, their syntheses based on carbon dioxide reported so far require rather expensive substrates like alkyl halides, and are not competitive with the currently adopted industrial processes.

The author and his co-workers previously reported that carbamic acids derived from CO₂ and *sec*-amines reacts with alkynes to give vinyl *N,N*-dialkylcarbamates in the presence of Ru complexes.² However, a similar reaction using alcohols, which would give vinyl alkyl carbonates, failed probably because of the insufficient nucleophilicity of alcohols compared with *sec*-amines,³ save that acetylenic alcohols react with CO₂ to give cyclic carbonates, 2-oxo-propyl alkyl carbonates, 2-oxo-propyl *N,N*-dialkyl-carbamates, or 4-methyl-2-oxo-1,3-oxazolines in the presence of *tert*-amine, *sec*-amine, or *prim*-amine respectively.⁴ During the attempt of reacting monoalkyl carbonates with acetylene in the presence of *tert*-amine and Ru complexes, however, a slight formation of dialkyl carbonates was observed. Further investigation revealed that this product is formed even in the absence of ruthenium or any other transition metal complexes. This means that this reaction is totally different from the ruthenium catalyzed synthesis of vinyl *N,N*-dialkyl carbamates. Moreover, one of the alkyl groups of dialkyl carbonates was found to come from *tert*-amines originally added with the intention of increasing the nucleophilicity of alcohols while the other from alcohols. Thus, either symmetric or unsymmetric carbonic acid diesters are formed as a main product according to the alkyl groups of alcohols and *tert*-amines[eq. (1)].



Also formed are alkyl *N,N*-dialkylcarbamates, all the alkyl groups of which are originated from *tert*-amines. Therefore, this reaction may be represented as the alkylation of monoalkyl carbonates and carbamic acids with *tert*-amines; carbamic acids are considered to be formed from CO₂ and *sec*-amines resulting from the dealkylation of *tert*-amines.

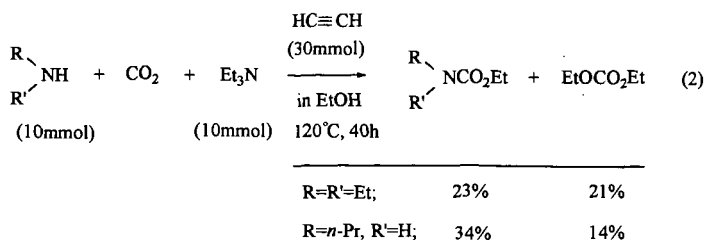
In a typical experiment, acetylene(30mmol) is introduced in a 50mL-autoclave containing *tert*-amine(30mmol) and alcohol(200mmol) at -50°C. After CO₂ is pressurized at 5MPa at ambient temperature, the autoclave is heated at a designated temperature for 16h or 40h. The products obtained are identified by spectroscopical comparison with their authentic samples either purchased or synthesized using chloroformic acid esters and analyzed by GLC. Unreacted *tert*-amines and acetylene recovered together with CO₂ through an accumulated gas-flow meter are also analyzed by GLC.

In the reaction with ethanol and triethylamine, diethyl carbonate and ethyl *N,N*-diethylcarbamate are

formed in fair yields at the reaction temperatures higher than 120°C, while practically no product is obtained at 80°C as shown in Table 1. The conversion of acetylene increases significantly with reaction temperature, while that of triethylamine levels out at about 42% with the result that the total yield of diethyl carbonate and ethyl *N, N*-diethylcarbamate based on triethylamine remains at 40% even at 180°C; but, the selectivity for these products is as high as 95%. Triethylamine is recovered unreacted in the reaction without acetylene even at 160°C. On the other hand, acetylene is mostly consumed and 33% of triethylamine is converted in the reaction without CO₂, but naturally there is no CO₂ containing product formed. This means that the presence of CO₂ rather suppresses the conversion of acetylene to some extent.

The yield of diethyl carbonate and the conversion of triethylamine increase from 32% and 45% to 78% and 83% respectively with decrease in the amount of triethylamine introduced from 30mmol to 5mmol in the reaction at 160°C for 40h as shown in Table 2. The yield of ethyl *N, N*-diethylcarbamate, on the other hand, reaches its maximum at 13% with 20mmol of triethylamine(entry 2). Neither diethyl carbonate nor ethyl *N, N*-diethylcarbamate is formed without triethylamine(entry 5). When triethylamine is used in smaller amounts, a significant formation of diethylamine is observed in the resulting reaction solution, which accounts for the formation of ethyl *N, N*-diethylcarbamate; *N, N*-diethylcarbamic acid derived from CO₂ and diethylamine formed by the preceding alkylation of monoalkyl carbonate must be alkylated in place of monoalkyl carbonate with triethylamine. It is also found that diethylamine is partially converted to triethylamine and small amounts of diethyl carbonate and ethyl *N, N*-diethylcarbamate are formed in the reaction using diethylamine instead of triethylamine(entry 6). These results, as well as the fact that the total yield(86%) of the products exceeds the conversion of triethylamine(83%) in the reaction with 5mmol of triethylamine(entry 4), suggest that more than one ethyl group in triethylamine can be used for alkylation but most probably at the expense of higher consumption in acetylene under certain conditions.

The results of the reactions with several alcohols and *tert*-amines are summarized in Table 3. When *n*-propanol is used instead of ethanol, ethyl *n*-propyl carbonate is formed in the yield of 22% together with ethyl *N, N*-diethylcarbamate(7%) and di-*n*-propyl carbonate(1%). This result clearly shows that one of the ethyl group of diethyl carbonate formed in the reaction with ethanol mostly comes from triethylamine. The slight formation of di-*n*-propyl carbonate, however, suggests that the ester exchange reaction of dialkyl carbonate occurs to some extent in excess alcohols. This reaction becomes rather significant when allyl alcohol is used probably because of its high nucleophilicity; 19% of ethyl allyl carbonate is formed together with diallyl carbonate(8%) and ethyl *N, N*-diethylcarbamate(14%). It is not yet clear why the carbamate is obtained in such a high yield in this reaction compared with the other saturated alcohols. Tri-*n*-propylamine can be also used in place of triethylamine for the reactions of these alcohols, although it shows a little lower reactivity; 12-21% yields of the corresponding *n*-propyl carbonates are formed together with small amounts of symmetric carbonates and *n*-propyl *N, N*-di-*n*-propylcarbamate. All the reaction solutions are homogeneous but colored in brown when the reaction has proceeded, while the use of either methanol or trimethylamine results in the formation of polymers probably because of their excessive reactivity toward acetylene.



chloride⁶ to acetylene giving trialkylvinylammonium salt, $R_3N-CH=CH_2^+ X^-$. The following step, the attack of monoalkylcarbonate to trialkylvinylammonium giving dialkyl carbonate, is analogous to the esterification of carboxylic acids with large steric hindrances by forming tetramethylammonium salts and their thermal decomposition.⁷

The present reaction not only provides a new synthetic method of carbonic and carbamic acid esters involving only industrially available starting materials, but also shows a new type of CO_2 fixation without catalyst.

References

- (1) (a) McGhee, W. D.; Riley, D. P.; Christ, M. E.; Christ, K. M. *Organometallics*, **1993**, *12*, 1429. (b) Oi, S.; Kuroda, Y.; Matsuno, S.; Inoue, Y. *Nippon Kagaku Kaishi*, **1993**, 985.
- (2) (a) Sasaki, Y.; Dixneuf, P. H. *J. Chem. Soc., Chem. Commun.*, **1986**, 790. (b) Sasaki, Y.; Dixneuf, P. H. *J. Org. Chem.*, **1987**, *52*, 314. (c) Mahé, R.; Sasaki, Y.; Bruneau, C.; Dixneuf, P. H. *J. Org. Chem.*, **1989**, *54*, 1518.
- (3) Unpublished result.
- (4) (a) Sasaki, Y. *Tetrahedron Lett.*, **1986**, 1573. (b) Sasaki, Y. *Bull. Natl. Res. Inst. Poll. Resour.*, **1987**, *16*(4), 13. (c) Sasaki, Y.; Dixneuf, P. H. *J. Org. Chem.*, **1987**, *52*, 4389.
- (5) Gardner, C.; Kerrigan, V.; Rose, J. D.; Weedon, b. C. I. *J. Chem. Soc.*, **1949**, 780.
- (6) Reppe, W. et al. *Annalen der Chemie*, **1956**, *601*, 81.
- (7) Prelog, V.; Piantanida, M. *Z. Physiol. Chem.*, **1936**, *244*, 56.

Table 1. Effect of the Reaction Temperature^{a)}

No.	Temp. (°C)	— Yield(%) ^{b)} —		— Conv.(%) —	
		EtOCO ₂ Et	Et ₂ NCO ₂ Et	Et ₃ N	HC≡CH
1	180	32	8	42	85
2	160	30	9	41	74
3	140	28	9	39	66
4	120	19	5	28	44
5	100	4	0	10	34
6	80	0	0	6	18
7 ^{c)}	160	0	0	3	-
8 ^{d)}	160	0	0	33	97

^{a)} CO_2 (5MPa), Et_3N (30mmol), $EtOH$ (200mmol), Acetylene(30mmol), 16h.

^{b)} based on triethylamine. ^{c)} without acetylene. ^{d)} Ar(5MPa).

Table 2. Effect of the Amount of Et₃N^{a)}

No.	Et ₃ N (mmol)	— Yield(%) ^{b)} —		— Conv.(%) —	
		EtOCO ₂ Et	Et ₂ NCO ₂ Et	Et ₃ N	HC≡CH
1	30	32	11	45	96
2	20	42	13	56	86
3	10	65	12	77	80
4	5	78	8	83	83
5	0	-	-	-	21
6 ^{c)}	0	4	1	-9	81

^{a)}CO₂(5MPa), EtOH(200mmol), Acetylene(30mmol), 160°C, 40h.

^{b)}based on amine. ^{c)}Et₂NH(5mmol).

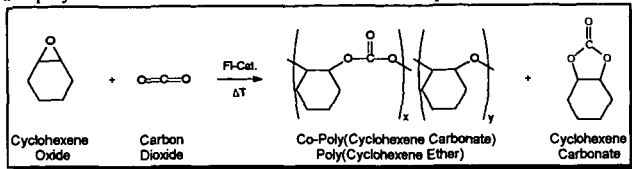
Table 3. Effect of the Alcohols and *tert*-Amines^{a)}

R ₃ N	R'OH	— yield(%) ^{b)} —			— conv.(%) —	
		R'OCO ₂ R	R'OCO ₂ R'	R ₂ NCO ₂ R	R ₃ N	HC≡CH
Et ₃ N	EtOH	30	-	9	41	74
Et ₃ N	<i>n</i> -PrOH	22	1	7	35	68
Et ₃ N	CH ₂ =CHCH ₂ OH	19	8	14	42	89
<i>n</i> -Pr ₃ N	EtOH	17	3	2	26	46
<i>n</i> -Pr ₃ N	<i>n</i> -PrOH	12	-	1	16	38
<i>n</i> -Pr ₃ N	CH ₂ =CHCH ₂ OH	21	6	4	32	56

^{a)}R₃N(ca. 30mmol), R'OH(200mmol), acetylene(30mmol), CO₂(5MPa), 160°C, 16h,

^{b)}based on amine.

This work will explore the copolymerization of CO₂ and cyclohexene oxide (CHO) to synthesize polycyclohexene carbonate (PCHC), without using organic solvents. The reaction studied (Scheme 2) forms a copolymer which includes a small amount of ether repeat units and the 1:1 adduct, 1,2-



Scheme 2: Polycyclohexene Carbonate from CO₂ and Cyclohexene Oxide

cyclohexene carbonate (CHC). The effects of running this reaction at various pressures, temperatures, and mole fractions of the epoxide on the yield and nature of the polycyclohexene carbonate formed will be discussed.

EXPERIMENTAL

Materials: Cyclohexene Oxide (Aldrich Chemicals, Milwaukee, WI) was distilled under reduced pressure over CaH₂. The purified CHO monomer was then transferred under N₂ to flasks equipped with stopcocks, and stored under N₂ until used. Methylene chloride (99.9% assay) and anhydrous methyl alcohol (99.9% assay) were used to separate and precipitate the reactor products (Malinkrodt Specialty Chemicals Co.; Paris, KY)

Research Grade CO₂ (Aircro Special Gases; Riverton, NJ) and Supercritical Grade CO₂ (Liquid Carbonic; Chicago, IL) were used after passing through a series 62, high pressure purifier, which removes oil and water from gas and liquid systems (Liquid Carbonic). Nitrogen with 99.99% purity (Liquid Carbonic) was passed through the high-pressure purifier and then into the reactor without further purification.

Synthesis of Zn-perfluoroalkyl Catalyst: A flask was charged with 8.56 g (87.3 mmoles) of maleic anhydride, then flushed with N₂. The maleic anhydride was heated at 55°C and melted. Tridecafluorooctanol, 31.8 g (87.3 mmoles), was flushed with N₂ and transferred via a Teflon needle to the melted maleic anhydride. A solution of 0.73 ml (5.24 mmoles) of triethyl amine in 15 ml of toluene was next transferred to the mixture. [Note: both the amine and toluene were distilled from calcium hydride.] The mixture was stirred and heated at 55°C overnight. Upon cooling, the perfluoroalkyl monoester that formed was isolated by vacuum filtration and vacuum dried at 50°C overnight to recover 34 g (84% yield). The perfluoroalkyl monoester was purified by recrystallizing it 5 times in hexane or 2 times in benzene. Purified perfluoroalkyl monoester, 12 g (27.26 mmoles) and zinc oxide, 2.22 g (27.26 mmoles) was added to a 250 ml three necked flask, equipped with condenser, mechanical stirrer and N₂ inert gas. Both solids were flushed with N₂, then 100 ml anhydrous 1,1,2-trichlorotrifluoroethane was transferred over the solids. The mixture was refluxed at 50°C for 24 hours. The synthesized Zn-perfluoroalkyl catalyst was recovered by filtration with a pressure funnel. The filtrate was stripped to dryness and vacuum dried at room temperature overnight. The Zn-perfluoroalkyl catalyst collected was 13.4 g (90.6% yield).

Polymerization of Polycyclohexene Carbonate: All reactions were performed in 50 ml heated reactors (Pressure Products Industries; Warminster, PA) capable of 6000 psig maximum working pressure at 340°C, and equipped with magnetically driven mixers. An air driven, gas booster compressor (Haskel Inc; Burbank, CA) was used to generate CO₂ pressure.

In a typical polymerization, the catalyst was weighed and placed into the reactor body under a natural atmosphere. The reactor was then sealed and flushed with flowing nitrogen at an inlet pressure of 100 psig and atmospheric outlet pressure for ½ - 2 hours. During this time, a measured amount of CHO was added to an addition piping under N₂ atmosphere using a graduated, glass syringe. The addition piping was then attached vertically to the reactor inlet. CO₂ at its' vapor pressure (≈850 psi at 25°C), was then used to 'push' the CHO into the reactor. After the injection of monomer, the reactor was isolated and heated to the reaction temperature. Once the reaction temperature was reached, pressurized CO₂ was added slowly (~200 psi increase in reactor pressure, letting temperature reach within 1°C of the reaction temperature each time) until the destination pressure and temperature were reached, a process which lasted 30-45 minutes. After the reaction was completed, the reactor was cooled to below 30°C and the gaseous reactor contents slowly bubbled through methylene chloride. The liquid and solid reactor contents were collected using methylene chloride to dissolve them from the reactor body and head. The reactor body and head were again rinsed with methylene chloride and this rinse was combined with the products obtained from the first reactor wash to make-up the total reaction products.

Purification of Products: The reactor rinse, the solvent used for collecting gaseous reactor contents, and reactor wash were combined and filtered. The solvent was removed under vacuum and the solid or viscous liquid reactor products were then dried in vacuo and weighed to determine the "Crude" yield. A concentrated solution was then made by dissolving the dried reactor products in a small amount of methylene chloride; this solution was then added to a large volume of methanol

from which a white, solid product precipitates. The precipitate was filtered and both the solid precipitate and the filtered solution were retained. The solid was re-dissolved in methylene chloride, concentrated and re-precipitated in fresh methanol two additional times. The solid was dried under vacuum at $\sim 50^{\circ}\text{C}$, and then weighed to determine the methanol-insoluble fraction of the product. The three methanol solutions collected from the precipitations were combined and the methanol removed under vacuum at $50\text{-}70^{\circ}\text{C}$. Residual solids were dried under vacuum at $\sim 50^{\circ}\text{C}$ to recover the methanol-soluble fraction of the product.

Characterization of Polymers: Polymer molecular weights were measured using gel permeation chromatography (GPC, Waters 150CV) and polystyrene standards. The fraction of polycarbonate repeat units was determined using a Bruker MSL 300 NMR.

RESULTS AND DISCUSSION

Poly(cyclohexene carbonate) was synthesized at different polymerization temperatures, while keeping the pressure constant, to determine the effects on the polymer product. Each reaction was run for 24 hours and the catalyst to monomer ratio of {moles of Zn} to {moles of cyclohexene oxide (C.O.)} was also kept constant. The reactor volume is unchanging, though, and the same volume of C.O. and weight of catalyst were used throughout this series. Therefore, the number of moles of CO_2 that are loaded into the reactor at constant pressure decreases as the temperature is increased throughout the temperature series. Another way to say this is that the mole fraction of C.O. increases as the temperature increases. This relationship is shown by following the mole fraction of C.O. on Table 1.

Table 1 also shows other results of the varying temperature reaction series. In Table 1 the polymer yield is presented in another form, g Polymer/g Zn, to indicate the catalysts' activity at different conditions. For comparison purposes, previous Zinc-based catalysts for the formation of polycarbonate from epoxides generally give 10-40 g Polymer/g Zinc. At higher temperatures the catalyst selectivity towards polymer decreases favoring the formation of MeOH-soluble products.

Changing the reaction pressure also has an effect on the reaction products. In a separate series of reactions the pressure was changed while the temperature remained constant at $109\text{-}110^{\circ}\text{C}$ and the polymerization was allowed to react for 24 hours. And while the catalyst to monomer ratio of {moles of Zinc} to {moles of C.O.} was kept the same as the other series, this set of experiments was done with half of the reactants as the variable temperature experiments. This means that there was more CO_2 present in the reaction mixture or that the reactions were run at lower mole fractions of C.O.. Again the same volume of C.O. and weight of catalyst were used over the entire range of pressures, therefore more CO_2 was present as the reaction pressure increased. This relationship is represented by a decrease in the mole fraction of C.O. with increasing pressures as shown in Table 2. The effect of this variation is not clear, but it seems that at these mole fractions the percentage of by-products formed is independent of pressure.

Table 2 also shows the yield results as a function of the changing pressure. The depression in yields at 4000 psig can not be attributed to the phase behavior in this set of experiments. Although, the yield depression shown at 4000 psig though can not be explained from what we know about the phase behavior of this system, the general trend of decreasing yields for the experiments run at 3000, 4000 and 5000 psig can be partially explained by the fact that the product yields decrease as the mole fraction of C.O. decreases. In the changing pressure experiments, the number of moles of CO_2 introduced at constant temperature increase as the pressure is increased. Therefore, the mole fraction of C.O. decreases and this results in decreasing yields.

A series of five reactions were run at varying mole fractions of C.O. to study the effect on the reaction products. These reactions were run for 24 hours at a constant pressure of 2000 psig and a constant temperature of $109\text{-}110^{\circ}\text{C}$. The catalyst to monomer ratio of {moles of Zinc} to {moles of C.O.} was again kept constant. Table 3 shows the characterization results of the polymer product from this series. In this series of reactions, *only* the mole fraction of C.O. was varied.

The product yields show a decreasing trend at lower mole fractions of C.O. This could be attributed to lower solvating properties at low mole fractions of C.O. The $\text{CO}_2\text{-C.O.}$ system could require certain co-solvent properties (a large enough solvating power for reactants and products) in order for good yields to be achieved. When the required co-solvent properties are not met, due to a large excess of CO_2 , the reaction system might prefer to produce MeOH-soluble products rather than the desired polycarbonate polymer.

CONCLUSIONS

A system for synthesizing polycarbonate from epoxides, which uses a CO_2 -soluble catalyst and CO_2 as a reactant and the only solvent can produce high polymer at high turnover rates. Polycarbonates containing $>90\%$ polycarbonate linkages with weight average molecular weights of 50,000-150,000 are obtained. Although the effects of pressure seem to point to 2000 psig and 110°C as the best conditions for this polymerization, further studies operating in other regimes of the phase diagram might prove enlightening. The Zinc-based, CO_2 -soluble catalyst system shows an order of magnitude higher turnovers than previously reported and the catalyst has high selectivity towards polymer under certain conditions. More work needs to be done to fully understand this system,

especially in the area of phase behavior. In a system where CO₂ is both reactant and solvent the phase behavior of the system can influence the results, and this influence needs to be completely understood to determine to best operating conditions for this synthesis.

ACKNOWLEDGMENTS

We are especially grateful to Bayer, DOE and Exxon for supporting this work financially. Special thanks goes to Brett Hyndman and Tonya Slavic for assistance with the lab work and to Exxon's Joe Sissano for help during the initial stages of this work.

REFERENCES

1. M. McHugh, V. Krukonic, *Supercritical Fluid Extraction. Principles and Practice*, Butterworths: Boston. (1986)
2. T.A. Hoefling, R. M. Enick, E.J. Beckman, *J. Phys. Chem.*, **95**, 7127. (1991)
3. J.M. DeSimone, Z. Guan, C.S. Elsbernd, *Science*, **257**, 945. (1992)
4. T.A. Hoefling, R.R. Beitle, R. M. Enick, E.J. Beckman, *Fluid Phase Equilibria*, **83**, 203. (1993)
5. D.A. Newman, T.A. Hoefling, R.R. Beitle, E.J. Beckman, R.M. Enick, *J. Supercrit. Fluids*, **6**, 205-210. (1993)
6. S. Inoue, H. Koinuma and T. Tsuruta, *Polymer Letters*, **7**, 287-292. (1969)
7. S. Inoue, H. Koinuma and T. Tsuruta, *Polymer Journal*, **2**, No. 2, 220-224. (1971)
8. S. Inoue, H. Koinuma, Y. Yokoo and T. Tsuruta, *Die Makromolekulare Chemie*, **143**, 97-104. (1971)
9. S. Inoue, M. Kobayashi, H. Koinuma and T. Tsuruta, *Die Makromolekulare Chemie*, **155**, 61-73. (1972)
10. M. Kobayashi, S. Inoue and T. Tsuruta, *Journal of Polymer Science: Polymer Chemistry Edition*, **11**, 2383-2385. (1973)
11. R.J. De Pasquale, *J.C.S. Chem. Commun.*, 157-158. (1973)
12. S. Inoue, T. Tsuruta, T. Takada, N. Miyazaki, M. Kambe and T. Takaoka, *Applied Polymer Symposium*, **26**, 257-267. (1975)
13. S. Inoue, *CHEMTECH*, Sept., 588-594. (1976)
14. T. Tsuda, Y. Chujo and T. Saegusa, *Chem. Commun.*, 415-416. (1976)
15. W. Kuran, S. Pasynkiewicz, J. Skupińska and A. Rokicki, *Die Makromolekulare Chemie*, **177**, 11-20. (1976)
16. W. Kuran, S. Pasynkiewicz and J. Skupińska, *Makromol. Chem.*, **177**, 1283-1292. (1976)
17. T. Hirano, S. Inoue and T. Tsuruta, *Makromol. Chem.*, **177**, 3245-3253. (1976)
18. W. Kuran, S. Pasynkiewicz and J. Skupińska, *Makromol. Chem.*, **178**, 47-54. (1977)
19. K. Soga, K. Uenishi, S. Hosoda and S. Ikeda, *Makromol. Chem.*, **178**, 893-897. (1977)
20. W. Kuran, S. Pasynkiewicz and J. Skupińska, *Makromol. Chem.*, **178**, 2149-2158. (1977)
21. K. Soga, K. Hyakkoku, K. Izumi and S. Ikeda, *Journal of Polymer Science: Polymer Chemistry Edition*, **16**, 2383-2392. (1978)
22. K. Soga, K. Hyakkoku and S. Ikeda, *Makromol. Chem.*, **179**, 2837-2843. (1978)
23. K. Soga, K. Uenishi and S. Ikeda, *Journal of Polymer Science: Polymer Chemistry Edition*, **17**, 415-423. (1979)
24. K. Soga, et al., *Polymer J.*, **13**(4), 407-410. (1981)
25. G. Rokicki, W. Kuran and B. Pogorzelska-Marciniak, *Monatshefte für Chemie*, **115**, 205-214. (1984)
26. U.S. Pat 4,783,445, H.-N. Sun (to Arco Chemical Co.). (Nov. 8, 1988)
27. U.S. Pat. 5,026,676, S. Motika, T. Pickering, A. Rokicki, K. Stein (to Air Products and Chemicals, Inc., Arco Chemical Co., Mitsui Petrochemical Industries Ltd.). (June 25, 1991)
28. L.-B. Chen, *Macromol. Chem., Macromol. Symp.*, **59**, 75-82. (1992)
29. W. Kuran and T. Listo, *Macromol. Chem. Phys.*, **195**, 977-984. (1994)
30. (a) D.J. Darensbourg, *Abstract and presentation from the "Third International Conference on Carbon Dioxide Utilization (ICCDU III)"*, U. of Oklahoma, April 30-May 4, 1995. (b) D.J. Darensbourg and M.W. Holtcamp, *Macromolecules*, **28**, 7577-7579, 1995.
31. F. A. Adamsky, E.J. Beckman, *Macromolecules*, **27**, 312. (1994)

TABLE 1: EFFECT OF TEMP. ON POLYCYCLOHEXENE CARBONATE FORMATION

 Conditions: P=2000 psig, t=24 hours, $N_z/N_{C_0} = 3.3 \times 10^3$

T (°C)	CONV.	SEL.	% CAR. (NMR)	X_{C_0}	g POLY g Zn	M_w ($\times 10^{-3}$)	M_w/M_n
60	5.7%	0.2%	58%	0.11	1.30	—	—
70	11%	6.3%	92%	0.12	41.1	120	27
80	28%	22%	81%	0.15	146	232	11
80	30%	17%	89%	0.13	116	109	5.8
90	—	9.1%	87%	0.15	61.5	114	6.6
90	11%	0.08%	80%	0.16	0.53	104	5.0
100	57%	30%	95%	0.16	203	174	14
100	79%	68%	93%	0.16	457	109	6.4
110	65%	50%	97%	0.18	328	195	12
110	84%	69%	96%	0.16	440	68.1	4.2
120	75%	61%	94%	0.20	406	56.2	3.6
130	60%	45%	87%	0.21	307	43.4	3.0
172	50%	2.4%	29%	0.24	15.8	9.8	2.4

TABLE 2: EFFECT OF PRES. ON POLYCYCLOHEXENE CARBONATE FORMATION

 Conditions: t=24 hours; T=110°C; $N_z/N_{C_0} = 3.3 \times 10^3$

P (psig)	CONV.	SEL.	% CAR. (NMR)	X_{C_0}	g POLY g Zn	M_w ($\times 10^{-3}$)	M_w/M_n
1000	70%	50%	86%	0.20	329	59.1	3.7
2000	75%	57%	91%	0.10	408	60.4	5.4
3000	63%	45%	83%	0.061	297	74.1	4.4
3000	57%	37%	92%	0.062	254	66.2	4.9
4000	32%	17%	89%	0.049	114	89.6	5.6
4000	28%	14%	96%	0.050	115	60.8	4.1
5000	49%	32%	87%	0.047	229	55.8	3.0
5000	30%	7%		0.040	40.2	38.5	2.7

TABLE 3: EFFECT OF X_{C_0} ON POLYCYCLOHEXENE CARBONATE FORMATION

 Conditions: 2000 psig, t=24 hours; T=110°C; $N_z/N_{C_0} = 3.3 \times 10^3$

X_{C_0}	CONV.	SEL.	% CARB. (NMR)	M_w ($\times 10^{-3}$)	M_w/M_n	g POLY g Zn
0.28	82%	65%	96%	106	3.3	421
0.18	65%	50%	97%	195	12	328
0.16	84%	69%	96%	68.1	4.2	440
0.10	75%	57%	91%	68.7	5.1	408
0.023	59%	4.8%	65%	23.8	1.8	35.0

PHOTOELECTROCHEMICAL REDUCTION OF CO₂ USING SILICATE
ROCK POWDER SUSPENDED IN WATER

Kiyohisa Ohta, Youko Ohguchi, Satoshi Kaneco, and Takayuki Mizuno
Dept. of Chem. for Materials, Fac. of Eng.,
Mie Univ., Mie, Tsu, 514, JAPAN

Keywords: Photoelectrochemical reduction of CO₂, andesite powder, methanol and formic acid.

INTRODUCTION

Until now, numerous investigators have reported chemical fixation of carbon dioxide, such as electrochemical, photochemical and photoelectrochemical reductions (1-5). In these methods, relatively, a few studies on the photoelectrochemical conversion of CO₂ have been reported.

We have recently presented a photochemical reduction of carbon dioxide and hydrogen formation by using andesite sands as a photocatalyst under sunlight irradiation (6). At ambient temperature and atmospheric pressure, 6.5x10⁻² ml g⁻¹ methane and 7.0x10⁻² ml g⁻¹ of hydrogen were formed from carbon dioxide and water on the andesite.

This report presents the photoelectrochemical reduction of CO₂ using silicate rock (andesite) powder suspended in water.

EXPERIMENTAL

For photoelectrochemical reduction of CO₂, a home-made cell (Figure 1) with a platinum anode (30 mm x 10 mm i.d., 99.95% purity) and a copper cathode (30 mm x 10 mm i.d., 99.95% purity) was used. The cathode compartment was separated from the anode compartment with a Nafion 115 membrane. 0.1 M KHCO₃ solution as an electrolyte was placed in the cell. After andesite rock powder was added to the catholyte, carbon dioxide was bubbled into the catholyte for 5 min at a rate of 40 ml min⁻¹. Carbon dioxide in the cell was reduced at a constant potential, which was controlled by a potentiogalvanostats (Model HA-501, Hokuto Denko, Japan), as irradiating light. During the reduction, andesite rock powder was dispersed by stirring. A Xe lamp (Ushio Tech. Xebex Xe-ARC 160, 1kW) was used for the illumination. The electrochemical reduction of CO₂ was investigated at -1.0 to -2.5 V vs.SCE and at 0 to 60°C. The Faradaic efficiency of products was calculated from 50 C charge-passed at each potential. Products were analyzed by gas and liquid chromatography. Andesite rocks was shattered in an iron mortar and then the powder was sieved by stainless sieves to get 31.8-24.5 mm size. After washing with 1M-nitric acid and distilled-deionized water, the rock powder was dried by heating at 150 °C for 8 h in an oven. Trace contaminants (hydrocarbon, carbon monoxide, hydrogen, etc.) in carbon dioxide gas used in this study were checked.

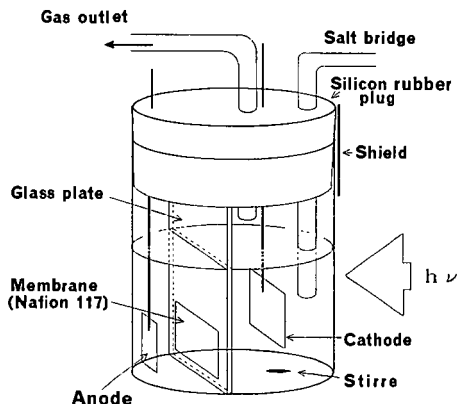


Figure 1. Cell for photoelectrochemical reduction.

RESULTS AND DISCUSSION

In previous study (6), it was found that under sunlight irradiation methane and hydrogen were formed from carbon dioxide and water on andesite sands at ambient temperature and atmospheric pressure. However, it needed the time of >10 h to obtain these products by the photochemical reduction. It was too long to obtain an adequate quantity of the products. Therefore, a photo-electrochemical reduction of CO_2 using andesite powder suspended in water was performed. First, the cyclic voltammograms in the electrolyte suspended andesite powder were measured with and without the irradiation. From the voltammograms, it was found that the electrochemical reduction of CO_2 occurred at -1.0 to -2.5 V vs.SCE and by the irradiation the current density increased about 1.5 times that obtained under no illumination.

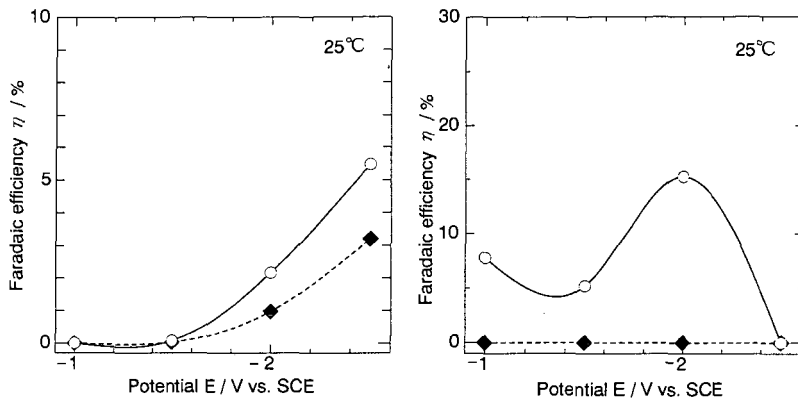


Figure 2. Faradaic efficiencies of CH_2 formation at Cu electrode saturated with CO_2 in 0.1 M KHCO_3 . \circ : Andesite suspension and illumination, \blacklozenge : No andesite
 Figure 3. Faradaic efficiencies of CH_3OH formation at Cu electrode saturated with CO_2 in 0.1 M KHCO_3 . \circ : Andesite suspension and illumination, \blacklozenge : No andesite

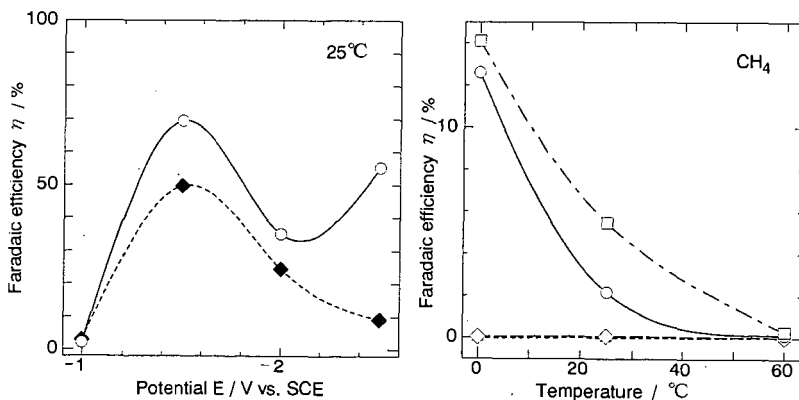


Figure 4. Faradaic efficiencies of H_2 formation at Cu electrode saturated with CO_2 in 0.1 M KHCO_3 . \circ : Andesite suspension and illumination, \blacklozenge : No andesite
 Figure 5. Effect of temperature on the efficiency at Cu electrode saturated with CO_2 in 0.1 M KHCO_3 (Andesite suspension and illumination).

\triangle : -1.0 V, \diamond : -1.5 V, \circ : -2.0 V, \square : -2.5 V,

Effects of illumination and potential.

The effects of illumination and potential on Faradaic efficiency of products were investigated at 25°C. The products were

hydrogen, methane, methanol, ethylene, carbon monoxide and formic acid. By illumination, the amounts of methane, methanol and hydrogen formed were larger than those of these products obtained without andesite, as shown in Figure 2-4. Furthermore, the Faradaic efficiencies for these products under irradiation were large, compared with the efficiencies obtained in the case of andesite addition and no illumination. These facts prove the large effect of andesite addition and illumination.

However, by the addition of andesite and the illumination the formations of ethylene, carbon monoxide and formic acid decreased. The Faradaic efficiency of methane increased as the potential became negative. The outstanding effect of andesite and illumination was observed in the case of methanol formation. The maximum was obtained at -2.0 V. The maximum hydrogen generated at -1.5 V.

At 0°C , the illumination and andesite affected on the formations of hydrogen, carbon monoxide and formic acid. Especially, the effect was outstanding for the formation of formic acid at -2.0 V. At 60°C , the effect by the addition of andesite and the illumination was not observed the formation of those products except for hydrogen formation.

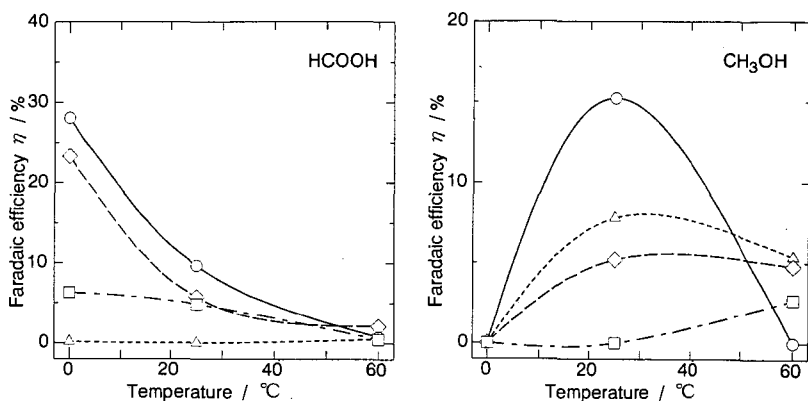


Figure 6. Effect of temperature on the efficiency at Cu electrode saturated with CO_2 in 0.1 M KHCO_3 (Andesite suspension and illumination).

Δ : -1.0 V, \diamond : -1.5 V, \circ : -2.0 V, \square : -2.5 V,

Figure 7. Effect of temperature on the efficiency at Cu electrode saturated with CO_2 in 0.1 M KHCO_3 (Andesite suspension and illumination).

Δ : -1.0 V, \diamond : -1.5 V, \circ : -2.0 V, \square : -2.5 V,

Effects of temperature

The effect of temperature on Faradaic efficiency of products was investigated at -1.0 , -1.5 , -2.0 and -2.5 V. The results for methane, methanol, and formic acid are shown in Figure 5-7. The Faradaic efficiencies of methane, ethylene and formic acid decreased with temperature. The maximum formation of methanol was obtained at 25°C . In the case of monoxide formation, the maximum efficiency was observed at 0°C and -2.0 V and the formation was almost independent of temperature. Hydrogen formation increased with temperature. The efficiency of hydrogen formation was beyond 100% at 60°C .

Under optimal experimental conditions, the Faradaic efficiencies of hydrogen, methane, methanol, ethylene, carbon monoxide, and formic acid were 120% at -2.5 V and 60°C , 14% at -2.5 V and 0°C , 15% at -2.0 V and 25°C , 2.7% at -2.5 V and 0°C , 0.88% at -2.0 V and 0°C , and 28% at -2.0 V and 0°C , respectively.

In described above, the effects of light irradiation and the addition of andesite are evident. Accordingly, X-ray diffraction signal of the andesite was measured for getting a key of the mechanism. The components of the andesite were multiple oxides consisting of SiO_2 , TiO_2 , Al_2O_3 , Fe_2O_3 , FeO , MnO , MgO , CaO , Na_2O , K_2O , H_2O , P_2O_5 , etc. Therefore, the reducing power may be due to an active site such as TiO_2 on the andesite and the semiconductivity. Something like free electron generated on

andesite probably gives desirable electrochemical reduction of CO₂. However, the detail mechanism could not be made clear.

Consequently, it was found that this method with andesite had effect on formic acid and methanol formation and hydrogen formation by the catalyzed photoelectric dissociation of water. Since silicate rock catalyst such as andesite is easy and cheap to get, the carbon dioxide reduction system developed may be able to have the economic feasibility in large scale hydrogen, methane, formic acid and methanol productions.

ACKNOWLEDGMENTS: This work was supported financially by the Ministry of Education of Japan and the Research Foundation for the Electrotechnology of Chubu.

REFERENCES

- (1) Collin, J.P.; Sauvage, J.P. *Coordination chem. rev.* **1989**, *93*, 245.
- (2) Ayers, W.M., Editor, *Catalytic activation of carbon dioxide*, ACS *Sym. ser.*, **363**, pp.1-204, ACS, Washington, DC, 1988; Rethwisch, D.G.; Dumesic, J.A. *ibid.*, Chap.8.
- (3) Inoue, T.; Fujishima, A.; Konishi, S.; Honda, K. *Nature*, **1979**, *227*, 637.
- (4) Taniguchi, I. in *Modern aspects of electrochemistry*, Plenum: New York, 1989; Vol 20, pp. 327-400.
- (5) (a) Halmann, M. In "Energy resources through photochemistry and catalysis"; Gratzel, M., Ed.; Academic Press: New York, 1983; Chap.15. (b) Halmann, M.; Aurian-Blajeni, B. *Proc. of the 2nd European Commun. Photovolt. Sol. Energ. Conf.*, **1979**, 682.
- (6) Ohta, K.; Kawamura, T.; Kuroda, S.; Mizuno, T. *Proc. Electrochem. Soc.* **1994**, *93-18*, 85.

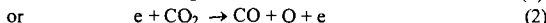
CO₂ UTILIZATION BY GAS DISCHARGES

Kamel H. Fotouh and Changjun Liu
Department of Chemical Engineering, Prairie View A&M University
Texas A&M University System, Prairie View, TX 77446

Keywords: CO₂ Utilization Gas Discharge Methane Conversion

INTRODUCTION

Carbon dioxide is the end product to complete combustion of all fossil fuels. The generation of carbon dioxide is the primary cause for the greenhouse effect. However, carbon dioxide is a potential carbon source. To utilize such a plentiful carbon source, it has been considered carbon dioxide as a feedstock for organic synthesis of carbonyl- and carboxyl-containing compounds or as an oxidant for oxidative synthesis of more valuable organics (Krylov and Mamedov, 1995; Xu and Moulijn, 1996). The heterogeneous catalysis has been extensively thought to be the desirable technique for CO₂ utilization. Especially, for the oxidative synthesis, the radical reactions have been demonstrated (Nishiyama and Aika, 1990). But, a difficulty faced in the regular catalytic conversion of carbon dioxide to usable chemicals is the industrial CO₂ emissions containing "poisonous" gases, e.g., SO_x. Although gas "scrubbing" is usually conducted first to eliminate the poisonous gases from flue gases, trace SO_x can still remain in the gases. Regarding this, some alternative technology should be investigated. The previous researches on the oxidative conversion of methane have indicated that the plasma radical reactions are quite similar to the heterogeneous catalytic radical reactions (Oumghar *et al.*, 1995), but the plasma way has a higher efficiency in initiating radicals. Reduction of CO₂ from flue gases using a corona discharge at the same time with reduction of SO_x and NO_x has also been performed by Higashi *et al.* (1985) and Xie *et al.* (1991). Maezono and Chang (1990) tried to produce the commercial CO by reduction of CO₂ from combustion gases using dc corona torches. The plasma promoted catalytic reduction of CO₂ from flue gases has also been reported (Jogan *et al.*, 1993). The oxidative synthesis of aldehydes from methane and carbon dioxide by gas discharges has been reported as early as 1930s (Finlayson, 1935). A gas mixture containing 58% methane and about 33.3% carbon dioxide was used for such a synthesis in the temperature range of 25°C to 500°C. No further mechanism analysis was reported. Exactly, carbon dioxide can contribute one of its two oxygen atoms for oxidative synthesis by electronic dissociative attachment reactions:



The O⁻ and some metastable states of O have been well-known as active oxygen species for oxidative synthesis of organics (Oumghar, *et al.*, 1995). Gas discharge (glow, corona, arc and silence discharges) is an abundant resource of free radicals. The potential to develop a technique, in which oxidative synthesis of high-valued hydrocarbons together with removal of CO₂, NO_x and SO_x is very economically attractive. The by-product of such a technique is carbon monoxide, which can be also applied for organic synthesis, e.g., F-T synthesis. In this paper, the results of oxidative methane conversion to ethane and ethylene using CO₂ as an oxidant by streamer corona discharge is reported.

EXPERIMENTAL APPARATUS AND PROCEDURE

The quartz tube reactor (with an I.D. of 6 mm and a tube length of 600 mm) for the streamer corona discharge synthesis consists of two electrodes. The top wire electrode and the lower cylindrical hollow electrode with a diameter 1 mm less than the inner diameter of the quartz tube is shown in figure 1. The gap between the two stainless steel electrodes is 12 mm. The feed gas flow enters the upstream wire electrode and exits at the downstream one. The streamer corona discharge is generated between these two electrodes by an AC generator, with which a high voltage transformer is applied. The AC voltage provides an easy way to generate the streamer discharges, which takes place only when the voltage reaches a sufficiently high level during each half cycle, as shown in figure 2. In the discharge volume, the interaction between accelerated charged particles (i.e., electrons and ions) and other chemical species (i.e., molecules and radicals) takes place. This interaction leads to the formation of new chemical species, like ethane, ethylene and carbon monoxide.

(Figures 1 and 2)

The feed gases CO₂, CH₄ and the dilution gas Helium are adjusted by controlling the flow rate. The effluent product gases run through a condenser to eliminate the moisture from the gas mixture. This gas mixture from condenser is then analyzed by an on line gas chromatography (HP5890) using a TCD detector. The gas pressure inside the reactor is slightly above the atmospheric pressure. All the experiments are initiated at room temperature (around 25°C). No attempt has been made to heat or cool the reactor externally. The gases from the gas cylinders

are mixed and then fed into the quartz reactor where a streamer corona discharge is generated. The input power to the high-voltage transformer is measured by recording the current and voltage.

With such an experimental device, the methane and carbon dioxide conversions are defined as:

Methane conversion = (moles of methane consumed/moles of methane introduced) * 100%

CO₂ conversion = (moles of CO₂ consumed/moles of CO₂ introduced) * 100%

The yield of C₂ hydrocarbons is as following:

Yield of ethane = 2 * (moles of ethane formed)/(moles of methane consumed) * 100%

Yield of ethylene = 2 * (moles of ethylene formed)/(moles of methane consumed) * 100%

RESULTS

All the corona discharge reactions are started at room temperature. The gas temperature reaches 200°C to 500°C depending on the different reaction conditions. The reaction temperature is measured by an insulated copper-constantan thermal couple situated upstream or downstream of reaction zone. The detail of such temperature measurements with plasma or electric field has been discussed elsewhere (Kingston and Jassie, 1988; Oumghar *et al.*, 1994).

The experimental results are shown in figure 3 to 6. Figure 3 shows the effect of applied voltage. When the applied voltage reaches 3.75kV, the gas discharge is initiated. The discharge reactions lead to the change in compositions. From figure 3, the reaction rate of methane and carbon dioxide have significant variations above 4.4 kV of the applied voltage. The composition of ethane increases with increasing in the applied voltage at the very beginning and then decreases, while the composition of ethylene increases slightly with increasing in the applied voltage. Figure 3 shows a significant increase in the composition of carbon monoxide. This suggests that part of C₂ products are destroyed to form CO by the increasing voltage. According to figure 3, it is not suggested that high voltage should be applied if the favorable C₂ products can not be moved out of the discharge reactor quickly.

(Figures 3, 4, 5 and 6)

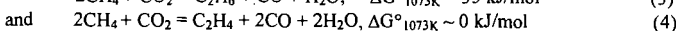
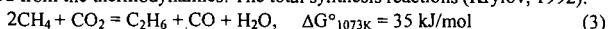
The effect of CO₂/CH₄ ratio is shown in figure 4. From reactions (1) and (2), more CO₂ in the feed will generate more active oxygen species for methane conversion. This has been demonstrated in figure 4. The conversion of CO₂ and CH₄ monotonically increase with increasing amount of carbon dioxide when the partial pressure of methane is kept constant. The yield of ethane decreases with increasing CO₂/CH₄ ratio. This means ethane has been converted to form some different species. The yield of ethylene shows a maximum when the CO₂/CH₄ ratio is equal to 2. The decrease in yield of ethylene suggests that an increase in the amount of the oxidant, CO₂, leads to the complete oxidation of hydrocarbons.

Figure 5 shows the effect of flowrate on the discharge reactions. The high flowrate results into a short residence time. The experimental results demonstrate that a higher yield of ethylene occurs at the lower flowrate or longer residence time. The conversion of CO₂ and CH₄ and the yield of ethylene decrease with the increase in the flowrate, but the yield of ethane increases. This suggests that ethane is a primary product and ethylene is the secondary product, which is formed by the oxidative of dehydrogenation of ethane. The same conclusion has also been drawn from figures 3 and 4, and can be further confirmed by the effect of frequency.

The streamer corona discharge generated by AC electric field is characterized with the temporary DC corona discharge, established within each half-cycle, as shown in figure 2. The effect of frequency is thought to be on the duration of each temporary DC corona discharge. Experimental results shown in figure 6 shows that the long duration (low frequency) is disfavorable for the yield of ethane and ethylene. The yield of ethane decreases with decreasing the frequency, but the yield of ethylene shows a maximum at frequency of 70Hz. This suggests that ethane is converted to ethylene at the lower frequencies, while at too low frequencies (less than 70 Hz) ethylene is also converted and complete oxidation occurs. The largest change in conversion of CO₂ and CH₄ is observed at the frequency of 70 Hz.

DISCUSSION

Here, we have experimentally confirmed that the streamer corona discharge oxidative coupling of methane using CO₂ as an oxidant is much more effective than the heterogeneous way, by which the yield of C₂ hydrocarbons was limited to less than 9% because of the difficulty in activation of catalysts (Nishiyama and Aika, 1990; Xu and Mouljin, 1996). This can be explained from the thermodynamics. The total synthesis reactions (Krylov, 1992):



Both these reactions are a little thermodynamically unfavorable, especially the first one. A high reaction temperature is expected for these two reactions with limited C₂ yield, if the regular catalytic way is employed. Other thermodynamically favorable reactions of CO₂ and CH₄, e.g., syngas (CO + H₂) formation, will compete with these C₂ formation reactions such regular catalytic techniques at sufficiently high temperatures. Considering this, the plasma can be

applied for enhancing the competitiveness of reactions (3) and (4). Also, from the thermodynamic point of view, the plasma will be useful for two classes of systems (Veprek, 1972): systems in which the reaction is allowed thermodynamically but hindered kinetically, and systems with which the reaction does not proceed due to an extreme chemical equilibrium constant in the absence of plasma. Reactions (3) and (4) would be covered by the first system. For this kind of reactions, a weak discharge, e.g., streamer discharge, can promote greatly the reactions. Such weak discharge promoted reactions are characterized themselves with low gaseous temperature and high electronic temperature. And, as the reaction temperature was experimentally measured to be less than 500°C, and according to researches on methane pyrolysis (Holmen *et al.*, 1995), no direct methane conversion was generated under 1000°C, therefore we may exclude the possibility of methane pyrolysis to higher hydrocarbons during our experiments. Basically, in our discharge system, a streamer corona discharge is applied to initiate the reactions. The streamer discharge, as mentioned before, has been known to produce electrons with electron energy of about 6eV (Eliasson and Kogelschatz, 1991), and such a low energy is insufficient to activate the kinetically inert methane molecule which possesses an appearance potentials of ions of around 12eV (Sorensen, 1995) although methane was passed directly through the discharge. The initiation reactions are thought to be the streamer corona-induced plasma decomposition of CO₂ as described in reactions (1) and (2). Such formed oxygen species, O[•] or O with some excited state or metastable state is very active for the coupling reactions and can lead to the products observed. The main reactions responsible for ethane, ethylene and carbon monoxide are as follow:

a. Methane Radical Formation:



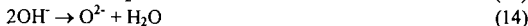
b. Ethane Formation:



c. Ethylene Formation:



d. H₂O Formation:



e. CO Formation:



CONCLUSION

CO₂ formation is a significant cause of greenhouse effect. Methane contributes also to the greenhouse effect. The combination of conversion of methane and carbon dioxide to more useful chemicals has potential industrial applications. Regarding these, we presented a streamer discharge system to oxidatively convert methane to ethylene using CO₂ as an oxidant. The results achieved right now shows the following:

(1) Conversions of methane and carbon dioxide and yield of ethylene increase with increasing input voltage and increasing CO₂ amount in the feed. The increasing CO₂ composition, however, will reduce the yield of C₂ hydrocarbons.

(2) The low flowrate leads to large conversions of methane and carbon dioxide and high yield of ethylene.

(3) The low frequency results in large conversions of methane and carbon dioxide but the maximum yield of ethylene occurs at the frequency of 70 Hz.

(4) All the experiments right now come to an end that ethylene is a second product.

REFERENCES

- Eliasson B. and Kogelschatz U. Nonequilibrium volume plasma chemical processing. *IEEE Trans. on Plasma Sci.*, 19, 1063., 1991
- Finlayson D. Manufacture of aliphatic aldehydes. US Patent 1,986,885
- Higashi M., Sugaya M., Ueki K. and Fujii K. Plasma processing of exhaust gas from a diesel engine vehicle, in *Proc. Int. Conf. on Plasma Chem.*, 2, 366., 1985.
- Holmen A., Olsvik O. and Rokstad O.A. Pyrolysis of natural gas: chemistry and process concepts. *Fuel Processing Tech.* 42, 249.,1995
- Jogan K., Mizuno A., Yamamoto T. and Chang J.-S. The effect of residence time on the CO₂ reduction from combustion flue gases by an AC ferroelectric packed bed reactor. *IEEE Trans. on Industry Applications*, 29(5), 876., 1993.

Kingston H.M. and Jassie L.B. Monitoring and predicting parameters in microwave dissolution. In: *Introduction to Microwave Sample Preparation*. Kingston H.M. and Jassie L.B., ed., ACS, Washington, DC, 1988.

Krylov, O.V. Methods for increasing the efficiency of catalysts for the oxidative condensation of methane. *Russian Chem. Rev.*, 61, 851.,1992.

Krylov O.V. and Mamedov A.Kh. Heterogeneous catalytic reactions of carbon dioxide. *Russian Chemical Reviews*, 64(9), 877., 1995.

Lee J. and Grabowski J.J. Reactions of the atomic oxygen radical anion and the synthesis of organic reactive intermediates. *Chem. Rev.*, 92, 1611.,1992

Maezono I. and Chang J.-S. Reduction of CO₂ from combustion gases by dc corona torches. *IEEE Trans. on Industry Applications*, 26(4), 651., 1990.

Nishiyama T. and Aika K.-I. Mechanism of the oxidative coupling of methane using CO₂ as an oxidant over PbO-MgO. *J. of Catalysis*, 122, 346., 1990.

Oumghar A., Legrand J.C., Diamy A.M. and Turillon N. Methane conversion by an air microwave plasma. *Plasma Chemistry and Plasma Processing*, 15(1), 87., 1995.

Oumghar A., Legrand J.C., Diamy A.M., Turillon N. and Ben-Aim R.I. A kinetic study of methane conversion by a dinitrogen microwave plasma. *Plasma Chemistry and Plasma Processing*, 14, 229., 1994.

Sorensen S.L., Karawajczyk A., Stromholm C. and Kirm M. Dissociative Photoexcitation of CH₄ and CD₄. *Chem. Phys. Letter*, 232, 554.,1995

Veprek, S. Chemical Evaporation and Deposition of Solids in a non-Isothermal Plasma. *J. of Crystal Growth*, 17, 101., 1972

Xie Z., Jogan K. and Chang J.S. The effect of residential time on the reduction of CO₂ in combustion flue gases by a corona torch. in *Conf. Rec. of IEEE-IAS Meeting*, 814., 1991.

Xu X.-D. and Moulijn J.A. Mitigation of CO₂ by chemical conversion: Plausible chemical reactions products. *Energy & Fuels*, 10, 305., 1996.

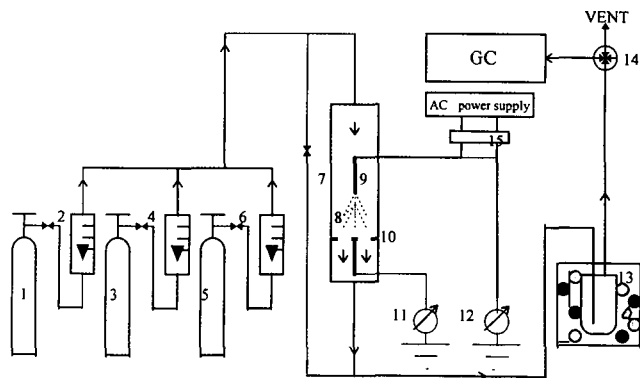


FIGURE 1 SCHEMATIC OF EXPERIMENTAL SETUP

- | | | | |
|----------------------------|--------------------------|--------------------|----------------------|
| 1,3,5 Gas Cylinders | 2,4,6 Flow Meter | 7 Reactor | 8 Streamer Discharge |
| 9 Wire Electrode | 10 Cylindrical Electrode | 11 Current Meter | 12 Voltage Meter |
| 13 Condenser(with dry ice) | 14 Multiway Value | 15 H.V.Transformer | |

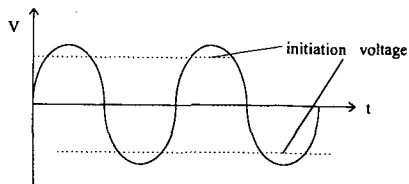


Figure 2 The AC Voltage

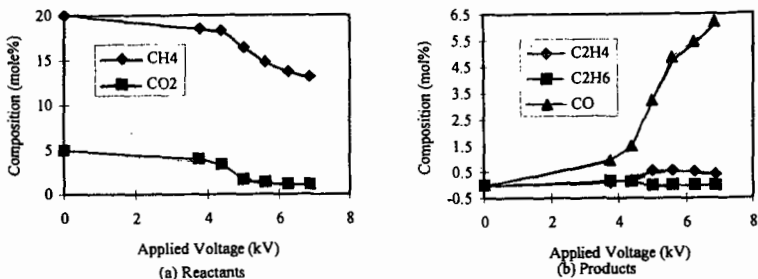


Figure 3 The effect of applied voltage

Flowrate : 100 ml/s Frequency : 60 Hz CO₂/CH₄: 4 (0.2 atm./0.05 atm.) Total Pressure: 1 atm

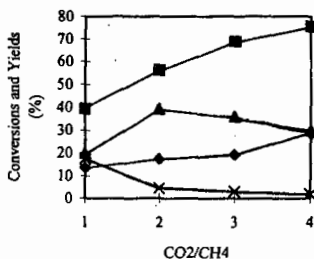
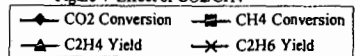


Figure 4 Effect of CO₂/CH₄



Flowrate : 100 ml/s Frequency : 60 Hz
 CH₄ Partial Pressure: 0.05 atm Total Pressure: 1 atm
 Applied Voltage: 5.6kV

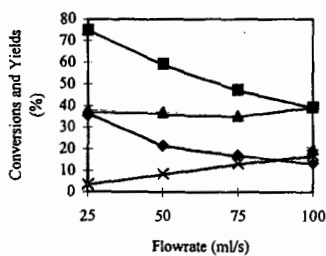
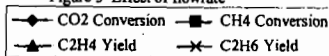


Figure 5 Effect of flowrate



Frequency: 60 Hz Applied Voltage: 5.6kV
 CO₂/CH₄: 4 (0.2 atm./0.05 atm.) Total Pressure: 1 atm

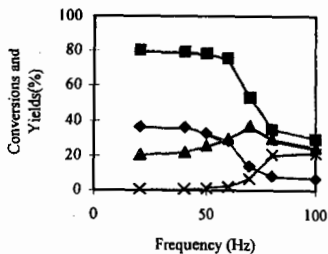
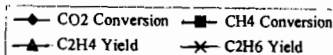


Figure 6 Effect of frequency



Flowrate : 100 ml/s Applied Voltage: 5.6kV
 CO₂/CH₄: 4 (0.2 atm./0.05 atm.) Total Pressure: 1 atm

ACTIVATION OF CARBON DIOXIDE AS AN OXIDANT OVER ZSM-5 ZEOLITE-SUPPORTED METAL OXIDE CATALYSTS

Sang-Eon Park, Jong-San Chang, and Min Seok Park
Industrial Catalysis Research Lab., Korea Research Institute of Chemical
Technology (KRICT), P.O.Box 107, Daeduck Danji, Taejeon 305-606, Korea

Keyword: carbon dioxide as an oxidant, oxygen-deficient spinel oxides, ZSM-5 zeolite support

INTRODUCTION

Chemical fixation of carbon dioxide has been concentrated on the conversion of CO₂ with various kinds of reductants into the usable chemicals in mass(1). These are mainly based on the reduction of CO₂. As a different way, CO₂ can be considered as an oxidant. Bartholomew(2) reported that oxidizability in the gasification of coke was the following order: O₂[105] > H₂O[3] > CO₂[1] > H₂[0.003], which numbers in parenthesis indicated the relative ratios of the gasification with oxidants. CO₂ has been called as nontraditional, unusual or mild oxidant and oxygen transfer agent. In this sense, carbon dioxide could be proposed as an oxidant in the oxidative conversions of hydrocarbons.

There have been some examples of utilization of carbon dioxide as an oxidant(3-5). Krylov and Mamedov(3) have studied on the oxidative conversions of alkanes, alkenes, and alcohols with carbon dioxide over Mn oxide-based catalysts and reported that oxygen generated during CO₂ reduction might participate in both partial oxidation and dehydrogenation. Yoo *et al.*(4) showed that Fe/Mo/borosilicate catalyst could activate CO₂ which could be functioning as a promoter and co-oxidant for the gas-phase oxidation of alkylaromatics with oxygen as well. Sugino *et al.*(5) reported that considerable increase in the conversion of ethylbenzene was observed with an iron-loaded catalyst in the presence of carbon dioxide, which revealed that the reaction proceeded via an oxidative dehydrogenation mechanism by CO₂.

Even though ZSM-5 zeolite has favorable adsorption property for various gases, micropore structure, high surface area, and highest thermal stability among zeolites, it has been rarely applied for supporting metal oxides. However, recently a few trials for utilizing ZSM-5 zeolite as a support for metal oxides have been appeared(6). In our previous study, it was shown that ZSM-5 zeolite could play an important role as a support for the reduced KNiCa oxide in CO₂ reforming of methane(7).

Ferrite-type oxides are known as materials exhibiting ferri- or ferromagnetism as spinel oxides and oxygen deficiency in structure(8). However, catalytic application of these ferromagnetic oxides are not so much. As an example of catalyst, ferrite was reported to be active for the selective oxidative dehydrogenation of hydrocarbons(9). Recently, it was shown that oxygen-deficient ferrites or magnetite was very reactive in the decomposition of CO₂ to carbon at 300°C(10).

In this study, the oxidative transformation of hydrocarbons such as propane and ethylbenzene was investigated by using CO₂ as an oxidant over zeolite-supported spinel oxide catalysts such as ferrites or magnetite having oxygen deficiency.

EXPERIMENTAL

Zeolite-supported magnetite (Fe₃O_{4.8}) and metal-containing ferrites (MFe₂O_{4.8}, M = Ni²⁺, Mg²⁺) were prepared by air oxidation of aqueous suspensions of Fe(II) and M(II) mixed hydroxides in slightly alkaline solution(11). These catalysts were dried *in vacuo* at 80°C and calcined under N₂ flow at 400°C for 3h. Zeolites used as supports were NaZSM-5 (Zeocat PZ-2, Si/Al = 980) and NaY (Zeocat Z6-01-01, Si/Al = 2.4). Loading of metal oxide on all the catalysts was 1.5 or 5.0 wt.%. Zeolite-supported KNiCa oxide (0.8 wt.% K-5 wt.% Ni-12 wt.% Ca), prepared by the solid-reaction method(7), was tested in the propane conversion for comparison.

All the catalytic measurements were carried out in a fixed-bed quartz reactor (i.d., 10 mm) at atmospheric pressure. In the case of oxidative dehydrogenation of ethylbenzene with CO₂, the reaction was performed by feeding ethylbenzene into the reactor by passing CO₂ through the ethylbenzene saturator thermostated at 25°C. The condensed effluent was analyzed by FID-GC. And effluent gases were analyzed by on-lined TCD-GC. The propane conversion with CO₂ were carried out at 800°C. The reactant gas mixture consisted of carbon dioxide and propane (CO₂/C₃H₈ = 3) diluted with nitrogen was co-fed into the reactor. The gaseous compositions of reactants and products were analyzed by on-lined TCD-GC.

RESULTS AND DISCUSSION

Reactions of propane with carbon dioxide

Four types of reactions could be occurring during propane conversion with CO_2 . Each of them to a different extent on different catalysis; propane dehydrogenation by CO_2 into propylene, selective decomposition into ethylene, non-selective decomposition into methane, and deep conversion into CO and H_2 , so-called reforming. The conversion of propane with carbon dioxide over zeolite-supported metal oxide catalysts was found to be conducted in an oxidative manner by looking at the products such as propylene, ethylene, methane, and CO with H_2 and water (as shown in Table 1). Two-types of activity patterns depending on the catalysts were obtained. One was catalyst system giving the oxidative dehydrogenation activity which produced olefins such as propylene and ethylene. The other was the reforming activity which produced syngas together with methane.

Even though magnetite and ferrites catalysts produced carbon directly from carbon dioxide(8), zeolite-supported catalysts were found to be effective not only for the propane dehydrogenation into olefins, but also for CO_2 activation into CO. These activities were very much dependent on metallic components in spinel oxide as well as their loadings. For example, 1.5 wt.% NiFe_2O_4 /ZSM-5 showed higher conversions of propane and CO_2 than those of 1.5 wt.% Fe_3O_4 /ZSM-5 due to the high activity on the reforming of propane and non-selective CH_4 production instead of the oxidative dehydrogenation activity on ferrite-loaded catalyst. The activities of ZSM-5-supported spinel oxides such as magnetite and ferrite were strong in the formation of olefins comparing with the reduced $\text{KNiCa}/\text{ZSM-5}$, which was known as a good catalyst in the formation of syngas(6). This result indicated that active sites for the oxidative conversion into olefins and the reforming seemed to be different. It suggested that an active site of spinel supported catalysts was not metallic Ni, but rather oxygen defects or oxygen deficiency. Higher loading of ferrite oxides resulted in the increased propane conversion with the decreased propylene selectivity and large increase in ethylene selectivity, and attributed to rather decrease in the CO_2 conversion. In propane conversion with CO_2 , carbon dioxide was considered to be dissociatively cleaved on the oxygen-deficient sites into carbon monoxide and surface oxygen species, which could be functioning as an oxidant for the conversion of propane into olefins and syngas in an oxidative manner.

Effect of CO_2 in the dehydrogenation of ethylbenzene

The results of catalytic activities in the dehydrogenation of ethylbenzene with supported ferrite catalysts are shown in Table 2. The catalysts were used after reduction at 500°C for 1h, prior to using in the reaction. Specific activity in Table 2 indicates moles of styrene produced per mole of metal oxide in an hour. The dehydrogenation of ethylbenzene with CO_2 over hydrogen-treated ferrite catalysts produced styrene and hydrogen. Considerable activities for the reaction were observed with zeolite-supported ferrite catalysts. When the reaction was conducted under an excess of CO_2 stream, higher catalytic activity over NiFe_2O_4 /ZSM-5 was obtained than in the case of a N_2 stream. Moreover, the dehydrogenation reaction over the catalyst using a N_2 stream exhibited considerable carbon deposition on the catalyst as compared to using a CO_2 stream. In addition, small amount of carbon monoxide during the reaction in a CO_2 stream was detected together with small amount of water. The zeolite-type as support had also influence on the activity in production of styrene. Comparing with dehydrogenation activity, ZSM-5 zeolite for supported ferrite catalysts appeared to be more suitable to support than Y zeolite. These results showed that zeolite-supported ferrite catalysts were to be active in the dehydrogenation of ethylbenzene to styrene and their activities were enhanced due to the presence of CO_2 . This indicated that the dehydrogenation reaction was enhanced by the oxidative manner due to the presence of CO_2 .

Evidence of oxygen deficiency by looking at the CO_2 dissociation

The activity of CO_2 decomposition into C over H_2 -treated ferrite or magnetite was found to be closely related with their oxygen deficiency(8). In order to confirm the role of oxygen deficiency of the supported spinel catalysts, the CO_2 dissociation into CO after reducing the catalysts with 5% H_2 at 500°C for 1h before putting into CO_2 pulse at 400°C . Supported-ferrite and magnetite catalysts showed significant activity of CO_2 dissociation even at lower temperature of 400°C , as presented in Table 3. In all cases, the amount of CO formed decreased greatly at initial stage and gradually at later stage with increase of the pulse numbers.

It was found that specific activities of CO formation over supported-ferrite or magnetite catalysts was much higher than those of unsupported nickel ferrite and reduced KNiCa/ZSM-5 as a reforming catalyst which was supposed to have a small oxygen deficiency. As above mentioned, the zeolite-type as support had also influence on the activity of CO formation. The activity of $\text{Fe}_3\text{O}_4\cdot 8/\text{ZSM-5}$ was almost two times higher than that of $\text{Fe}_3\text{O}_4\cdot 8/\text{Y}$ with same loading of $\text{Fe}_3\text{O}_4\cdot 8$. Moreover, the lower loadings of metal oxide gave the higher specific activities. It means that dispersion of oxygen deficient sites or oxygen defects was more efficient for the CO_2 dissociation.

It was known that ferrites and magnetite materials treated with H_2 at high temperature produced oxygen deficiency(12). It was considered that their ferromagnetism were partially related with their oxygen deficiency. In this sense, ferromagnetism of zeolite-supported ferrite or magnetite catalysts and CO_2 interaction with their ferromagnetism were examined by EPR (electron paramagnetic resonance) analysis. For example, very intensive FMR (ferromagnetic resonance) signal in EPR spectrum of 5 wt.% $\text{Fe}_3\text{O}_4\cdot 8/\text{ZSM-5}$ catalyst appeared only after evacuation at 500°C for 1h. This FMR signal gave a g value of 1.9 with $\Delta H_{pp} = 1140$ G (data not shown). After treatment with CO_2 at 600°C for 30 min, FMR intensities were significantly decreased. This supports that oxygen produced from CO_2 dissociation over the catalyst filled up the oxygen defect sites and resulted in the diminution of ferromagnetism.

In summary, not only oxygen from CO_2 molecule could be utilized as an oxidant but also surface design for chemisorptive CO_2 activation would be important in the heterogeneous activation of CO_2 as an oxidant. It was demonstrated that not only oxygen-deficient oxides such as ferrite and magnetite were active in the simultaneous activation of carbon dioxide and hydrocarbons, but also ZSM-5 zeolite could be suggested as a good support for the high dispersion of these spinels.

ACKNOWLEDGEMENTS

We acknowledge the financial support by the Ministry of Environment and Ministry of Science and Technology.

LITERATURE CITED

- (1) Halmann, M.M., Chemical Fixation of Carbon Dioxide, CRC, Boca Raton (1993).
- (2) Bartholomew, C.H., Chem. Eng., Nov. 12, 96 (1984).
- (3) Krylov, O.V. and Mamedov, A. Kh., Ind. Eng. Chem. Res., 34, 474 (1995).
- (4) Yoo, J.S., Lin, P.S. and Elfline, S.D. Appl. Catal., 106, 259 (1993).
- (5) Sugino, M., Shimada, H., Turuda, T., Miura, H., Ikenaga, N. and Suzuki, T., Appl. Catal., 121, 125 (1995).
- (6) Simard, F., Sedran, Sepulveda, Figoli, N.S. and de Lasa, H.I., Appl. Catal. A: General, 125, 81 (1995).
- (7) Chang, J.-S., Park, S.-E, Lee, K.W. and Choi, M.J., Stud. Surf. Sci. Catal. 84, 1587 (1994); Chang, J.-S., Park, S.-E and Chon, H., Appl. Catal., in press (1996).
- (8) Wohlfarth, E.P., Ferromagnetic Materials, Vol. 3, North-Holland Publishing Co., Netherlands (1982).
- (9) Stobbe, D.E., van Buren, F.R., Hoogenraad, M.S., van Dillen, A.J. and Geus, J.W., J. Chem. Soc., Faraday Soc., 87(10), 1639 (1991).
- (10) Tamaura, Y. and Tabata, M., Nature, 346, 255 (1990).
- (11) Kanzaki, T., Nakajima, J., Tamaura, Y. and Katsura, T., Bull. Chem. Soc. Jpn., 54, 135 (1981).
- (12) Togawa, T., Wada, Y., Yoshida, T. Tsuji, M. and Tamaura, Y., Mat. Res. Soc. Symp. Proc., 344, 51 (1994).

Table 1. Conversion of Propane with CO₂ over Zeolite-Supported Metal Oxide Catalysts at 800°C^{a)}

Catalyst	Conversion, %		Yield, %		Olefin Yield, %	Olefin/CH ₄	CO/Olefin
	C ₃ H ₈	CO ₂	C ₃ H ₆	C ₂ H ₄			
1.5% Fe ₃ O ₄ /ZSM-5	66.1	18.5	31.0	15.1	46.1	2.77	1.7
5% Fe ₃ O ₄ /ZSM-5	97.3	8.7	7.7	41.0	48.7	0.23	0.9
1.5% NiFe ₂ O ₄ /ZSM-5	98.4	57.8	-	14.0	14.0	0.11	17.3
5% MgFe ₂ O ₄ /ZSM-5	94.0	21.8	6.0	36.5	42.5	0.30	2.0
KNiCa/ZSM-5 ^{b)}	68.2	91.6	4.8	-	4.8	0.05	38.2

^{a)} Reaction Condition : 800°C, P(C₃H₈) = 10 kPa, CO₂/C₃H₈ = 3, GHSV = 2 × 10⁴h⁻¹.

^{b)} Same as Condition (a) except CO₂/C₃H₈ = 2; used in reaction after reduction 700°C for 1h.

Table 2. Dehydrogenation of Ethylbenzene with CO₂ over Zeolite-Supported Ferrite Catalysts at 600°C^{a)}

Catalyst	Styrene Yield (%)	Specific Activity ^{d)}
NiFe ₂ O ₄ /ZSM-5	38.3	100.8
NiFe ₂ O ₄ /ZSM-5 ^{b)}	33.9	89.2
NiFe ₂ O ₄ /Y ^{c)}	22.2	58.4
MgFe ₂ O ₄ /Y	19.2	43.3

^{a)} Loading of ferrites = 1.5 wt.%; W/F = 60 g-cat/h/mol; CO₂/EB = 30 : 1 (mol/mol); Catalyst pretreatment: reduction at 500°C for 1h. ^{b)} under N₂ flow without CO₂. ^{c)} reaction at 500°C.

^{d)} mol of styrene/metal oxide-mol h.

Table 3. The Dissociation of CO₂ over Zeolite-Supported Metal Oxide Catalysts at 400°C^{a)}

Catalyst	Amount of CO formed ^{b)} (μ mol)	Specific Activity ^{d)}
NiFe ₂ O ₄	1.18	2.7
1.5% NiFe ₂ O ₄ /ZSM-5	0.75	117.2
1.5% Fe ₃ O ₄ /ZSM-5	0.46	70.9
5% Fe ₃ O ₄ /ZSM-5	0.62	28.7
5% MgFe ₂ O ₄ /ZSM-5	0.49	19.6
1.5% Fe ₃ O ₄ /Y	0.24	37.0
1.5% NiFe ₂ O ₄ /Y	0.22	34.4
KNiCa/ZSM-5 ^{b)}	1.63	19.1

^{a)} after reduction at 500°C for 1h. ^{b)} measured at 600°C after reduction at 700°C for 1h.

^{c)} One pulse contained 30.2 μ mol of CO₂. ^{d)} mmol of CO/mol of metal oxide.

^{e)} mmol of CO/ mol of metallic Ni.

EFFECTS OF SIMULATED FLUE GAS ON GROWTH OF MICROALGAE

JOHN T. HAUCK¹, GREGORY J. OLSON²,
STEPHANIE J. SCIERKA, MILDRED B. PERRY, AND MOHAMMAD M. ATAAP³

U.S. Department of Energy
Pittsburgh Energy Technology Center
P.O. Box 10940
Pittsburgh, PA 15236

¹Carnegie Mellon Research Institute, 4400 Fifth Avenue, Pittsburgh, PA 15213

²Little Bear Laboratories, Inc., P.O. Box 1434, Red Lodge, MT 59068

³Chemical Engineering Department, University of Pittsburgh, Pittsburgh, PA 15261

Keywords: carbon dioxide, microalgae, fossil fuel combustion, SO₂, NO_x.

INTRODUCTION

Studies have demonstrated that the atmospheric carbon dioxide level is increasing on a global scale due to the emissions from increased combustion of fossil fuels. Current CO₂ emissions due to combustion of fossil fuels are estimated to be 2×10^{10} tons/yr (1). These emissions are implicated as a major contributor to the 1-2 ppm annual increase in atmospheric CO₂ concentration; the present level of atmospheric CO₂ is 360 ppm. Efforts are now under way to develop possible methods to minimize CO₂ emissions.

One method proposed for minimizing the CO₂ emissions from power plants is to grow microalgae in flue gas streams (1-7), converting CO₂ to algal biomass which could then be converted to fuels, chemicals, and foods. Algae can utilize CO₂ efficiently, yielding three to five times more biomass per land area than typical crops and terrestrial plants. Flue gas contains not only CO₂ but also oxides of sulfur and nitrogen that may be toxic to algal growth either by lowering the pH of solutions or by direct inhibition. High levels of CO₂ (10-15%) found in flue gas could also be inhibitory to algal growth.

For this work two strains of microalgae were obtained and cultured to measure their ability to fix CO₂ under realistic flue gas conditions. The selection of *Chlorella vulgaris* was based on previous work with various *Chlorella* species of microalgae for removal of CO₂ from flue gas streams (1,3). *Cyanidium caldarium* was selected because of its ability to thrive in an acidic environment and at slightly elevated temperatures.

Several studies of CO₂ removal using microalgae have been reported in literature (1-4), but the toxicity of the flue gas components has not been well-documented. This study identifies SO₂ as an inhibitory component of flue gas and highlights the inhibition of algal growth in the presence of SO₂ by using cultivation conditions which accelerate the rate of SO₂ absorption in cultures.

MATERIALS AND METHODS

Algal Strains and Culture Conditions

C. vulgaris strain 30581 was obtained from the American Type Culture Collection, Rockville, Maryland. The *C. caldarium* culture was obtained from an acidic seep in the vicinity of Frying Pan Creek north of the Norris Geyser Basin in Yellowstone National Park, Wyoming.

The *C. vulgaris* strain was grown on liquid algal proteose medium (8), containing 1.0 g bacto peptone (Difco) and one drop of a 1.0% FeCl₃ solution in 940.0 ml deionized water. In addition, the medium contained (g/L): NaNO₃ (0.250); CaCl₂ 2H₂O (0.033); MgSO₄ 7H₂O (0.075); K₂HPO₄ (0.075); KH₂PO₄ (0.175); NaCl (0.025). Prior to inoculation this solution was autoclaved at 121°C for 30 minutes. The pH of the final medium was adjusted to approximately 7.5 with sterile 1N NaOH.

The *C. caldarium* strain was grown on Allen's medium (9), which contains (g/L): (NH₄)₂SO₄ (1.3); KH₂PO₄ (0.28); MgSO₄ 7H₂O (0.25); CaCl₂ 2H₂O (0.07); and FeCl₃ 6H₂O (0.02). The pH was adjusted to 1.8 with 10N H₂SO₄. To this sterile autoclaved solution was added 1.0 ml of a 0.2 um filter-sterilized trace metals solution. The trace metals solution contained (g/L): Na₂EDTA (1.5); FeCl₃ 6H₂O (0.194); MnCl₂ 4H₂O (0.082); ZnCl₂ (0.01); CoCl₂ (0.004); Na₂MoO₄ (0.008).

Stock cultures of *C. vulgaris* were grown in 250-ml Erlenmeyer flasks under constant fluorescent illumination and static incubation at 20-25°C. Stock cultures of *C. caldarium* were grown at 45°C in 250-ml metal-capped baffled shake flasks under constant fluorescent illumination with shaking at 180 rpm.

Growth of the algae was monitored by measurement of change in optical density at 750 nm with time (Perkin-Elmer Lambda 3B UV/Vis spectrophotometer). The spectrophotometric absorbance measurements of cultures were related to biomass concentration by drying cell samples, collected on preweighed membrane filters, to constant weight at 105°C. A linear

relationship between culture absorbance at 750 nm and dry weight concentration for both *C. vulgaris* and *C. caldarium* was observed. For example, an absorbance of 0.3 corresponds to dry weight concentrations of 78 mg/L and 58 mg/L for *C. vulgaris* and *C. caldarium*, respectively. Absorbance values greater than approximately 0.3 were diluted appropriately to allow for accurate spectrophotometric measurement. In addition, small samples of the cultures were withdrawn regularly and observed by phase contrast and fluorescence microscopy employing UV (365 nm) illumination to determine cell concentration and viability. Culture pH was also monitored but was not controlled.

Experimental Reactor Setup

Growth of the two strains of microalgae, when aerated with various gases, was conducted in a small bioreactor setup. These growth tests were conducted in a five-gallon aquarium maintained at either 25°C or 45°C, depending on the alga being tested. The 45°C temperature was maintained using a 300 W laboratory immersion heater. The lower temperature was maintained by the room temperature and fluorescent lighting. The water in the aquarium was circulated using a laboratory stirrer to maintain uniform temperature.

Glass bubbler tubes (40-ml, Ace Glass Company, Vineland, NJ) were used as the algal growth vessels. Five separate tubes containing 30 ml of culture solution inoculated with the various microalgae were run in most experiments. A five-port gang valve was used to split the incoming gas from the cylinder so that five bubbler tubes could be used concurrently to determine reproducibility of algal growth in each experiment. The bubbler tubes were suspended in the aquarium and illuminated continuously with fluorescent lights mounted outside two sides of the aquarium. The light intensity was measured with a digital light meter (Model D-2000, Sylvania Light Company, West Seneca, NY) and found to be approximately 6000 lux. This light intensity was not chosen based on optimum light considerations but rather was the resultant intensity achieved using standard fluorescent lights in the reactor setup.

The various gases were bubbled through the inlet tube in each bubbler, which was submerged to the bottom of the cultures. A side-arm exit port on the bubbler tubes allowed the gas to escape. The exit gas was then vented into a hood. The flow rate of the gas mixtures through each bubbler tube was measured with either a soap-film flow tube (Supelco Inc., Bellefonte, PA) or a digital flowmeter (Humonics Optiflow 520, Fairfield, CA). A flow rate of approximately 15 ml/min through each bubbler tube was used in all experiments. Several gas mixtures (Matheson Gas Products, Inc., Secaucus, NJ) were used to evaluate their effects on both algal strains.

RESULTS AND DISCUSSION

Algal Growth in Experimental Reactor Setup

Growth of both algal strains, when aerated with compressed air and a 5% CO₂-in-compressed air mixture, was investigated. The results from the 5% CO₂ exposure are shown in Figure 1. It should be noted that the biomass concentration of *C. vulgaris* using the 5% CO₂-in-air mixture (0.57 g cells/L) was about threefold higher than that with compressed air (0.20 g cells/L) in each bubbler tube and for *C. caldarium* the 5% CO₂-in-air mixture the cell concentration showed a twentyfold increase in biomass to 3.0 g cells/L when compared with that in the presence of ambient air in shake flasks.

To determine the influence of elevated CO₂ levels found in flue gas, growth of the algal strains were monitored when aerated with a gas mixture composed of 15% CO₂, 3% O₂, balance N₂ (Figure 1). This gas composition was selected because it approximates the levels of CO₂ and O₂ in a typical flue gas stream from a coal-fired power plant. Both *C. vulgaris* and *C. caldarium* grown in 15% CO₂ exhibited a significant increase in biomass as compared to that with air aeration. The growth rate and cell yields were approximately equivalent to that obtained using the 5% CO₂ gas mixture. The ability for growth of this strain of *C. caldarium* using elevated CO₂ levels supports previous findings by Brock indicating enhanced growth of this alga in high CO₂ environments (10).

The ability of each alga to grow with aeration from SO₂-containing simulated flue gas mixtures was also examined (Figure 2). In a simulated flue gas consisting of 200 ppm SO₂, 15% CO₂, 3% O₂, balance N₂, the growth of *C. vulgaris* was completely inhibited as indicated by the steady decrease in culture absorbance from time zero. In addition, microscopic examination of samples of the cultures from the replicate bubbler tubes showed a declining cell concentration. Reduction in the number of viable algal cells was also suggested first by a decrease, and finally an absence, of UV-induced fluorescence. In contrast to *C. vulgaris*, *C. caldarium* initially exhibited some growth in the simulated flue gas containing SO₂ (Figure 2). It should be noted that this growth was approximately ca. 130 times less than that observed in an enriched CO₂ atmosphere. The different patterns of inhibition for the two algae depends to some extent on the values of optimum pH for their growth relative to the final culture pH.

The change in pH of five replicate bubbler tubes as a function of gas exposure time in Figure 3. A significant decrease in pH from 7.3 to 2.3 was observed for *C. vulgaris*. The

effect of the simulated flue gas on the pH was less pronounced for *C. caldarium* cultures. Upon introduction of the simulated flue gas, the pH was lowered to ca. 1.3 which is within the optimal range for growth of *C. caldarium*. Thus, the lowering of the pH by the flue gas does not inhibit growth of this alga but rather can provide the acidic environment needed for its growth. The growth inhibition of *C. caldarium* may have resulted from exposure to the SO₂ or some hydrolysis product.

The drop in pH, caused by the solubility of SO₂ in aqueous solutions, was particularly evident in the initially neutral pH cultures of *C. vulgaris*. Thus, inhibition of *C. vulgaris* appears to have resulted from the low pH created relative to the optimal value of about pH 7, since the growth medium was not effectively buffered to prevent acidification. The SO₂ in the simulated flue gas almost certainly had a negative effect on the growth of this alga just as was shown for *C. caldarium*. However, this was not proven in this study and further experiments using buffered media are needed to determine if the SO₂ itself is toxic to *C. vulgaris*.

Determination of Possible Growth Inhibitors

FTIR spectrophotometric analysis of the simulated flue gas indicated that no measurable amounts of contaminants, in particular the presence of SO₂ or CO. This indicates that SO₂ or an aqueous reaction product of SO₂ is the toxic agent responsible for inhibition. This is particularly evident with *C. caldarium*; growth occurs initially, but is inhibited after 20 hours. This pattern would be consistent with the accumulation of dissolved SO₂ or an aqueous oxidation product which occurs due to the high solubility of SO₂ in water (11).

To test this hypothesis one of the replicate bubbler tubes inoculated with *C. caldarium* was equipped with a "pre-bubbler" tube filled with deionized water. This pre-bubbler served as a scrubber for the flue gas prior to the gas being bubbled through the experimental culture tube. Initially, good growth occurred, similar to that when aerated with the 15% CO₂ gas mixture lacking SO₂, but inhibition prevailed at about two days (Figure 4). Apparently, the SO₂ is accumulated initially in the pre-bubbler solution, decreasing the concentration of SO₂ entering the experimental growth tube. The pre-bubbler tube delayed inhibition of the culture from 20 h to approximately 50 h but could not prevent it.

Figure 4 may also explain results of short-term studies in which operating conditions, such as flow rate (v/v. min), may delay the inhibitory effect of SO₂ containing flue gas (5). Since our experiments were designed for rapid saturation of SO₂ by using high flow rates, the inhibitory effect is clearly noticeable even with short exposure times.

Growth of *C. caldarium* on a NO_x-only flue gas consisting of approximately 50 ppm NO_x, 15% CO₂, 3% O₂, in balance N₂ was also tested. The growth of *C. caldarium* did not appear to be significantly inhibited by the NO_x flue gas which was tested only on this alga (Figure 5). This is an important finding since NO_x is a potentially harmful agent to growth of biological systems. Thus, *C. caldarium* may have considerable advantages for its use as an agent for CO₂ removal from flue gas. The apparent tolerance of this alga to nitrogen oxides and low pH environments make it a logical candidate for further studies of growth in flue gas streams.

CONCLUSIONS

A major problem in the large-scale farming of unicellular algae is the control of competing organisms. *C. caldarium* has the advantage, although not unique, of having the ability to grow in highly acidic media and at elevated temperature, where competitors are not viable. It has been shown that this alga is capable of growth in an environment with temperatures up to 57°C and as acidic as 1N H₂SO₄ (10). Because of this tolerance to acidity and elevated temperatures that may accompany flue gas streams, further investigation of *C. caldarium* for the removal of CO₂ from flue gas appears to be warranted. These studies should include assessing the possibility of adaptation of cultures to SO₂-containing flue gas to obtain further insight to the nature of inhibition for development of SO₂-resistant strains.

ACKNOWLEDGEMENTS

One of the authors (J.T.H.) held an appointment as a Graduate Student Research Participant at the Pittsburgh Energy Technology Center. In addition, another author (M.M.A.) held an appointment as a visiting faculty member at the facility. These programs are administered for the U.S. Department of Energy by Oak Ridge Institute for Science and Education, Oak Ridge, Tenn.

DISCLAIMER

Reference in this report to any specific commercial product, process, or service is made to facilitate understanding and does not necessarily imply its endorsement or favoring by the U.S. Department of Energy.

REFERENCES

1. Negoro, M., Shioji, N., Miyamoto, K., Miura, Y. (1991), *Appl. Biochem. Biotech.* **28/29**, 877-886.
2. Brown, L.M., "Biological Capture of CO₂ from Flue Gas," extended abstract presented at the Eighth Annual Coal Preparation, Utilization, and Environmental Control Contractors Conference, Pittsburgh, PA (July 1992). Contact US DOE/PETC Center for Conference Management, P.O. Box 18209, Pgh., PA 15236. 1-800-441-0875 (in PA) or 1-800-441-9927 (outside PA).
3. Watanabe, Y., Ohmura, N., Saiki, H. (1992), *Energy Convers. Mgmt.* **33**, 545-552.
4. Laws, E.A., Berning, J.L. (1992), *Biotech. Bioeng.* **37**, 936-947.
5. Woodward, C.A., MacInnis, J.M., Lewis, S.N., Greenbaum, E. (1992), *Appl. Biochem. Biotech.* **34/35**, 819-826.
6. Nishikawa, N., Hon-Nami, K., Hirano, A., Ikuta, Y., Hukuda, Y., Negoro, M., Kaneko, M., Hada, M. (1992), *Energy Convers. Mgmt.* **33**, 553-560.
7. Laws, E.A., Berning, J.L. (1991), *Bioresource Tech.* **37**, 25-33.
8. Nerad, T.A., ed. (1991), *ATCC Catalogue of Protists*, 17th ed., American Type Culture Collection, Rockville, MD.
9. Allen, M.B. (1959), *Arch. Mikrobiol.* **32**, 270-277.
10. Brock, T.D. (1978), *Thermophilic Microorganisms and Life at High Temperatures*, Springer-Verlag, New York.
11. Meites, L., ed. (1963), *Handbook of Analytical Chemistry*, McGraw-Hill, New York.

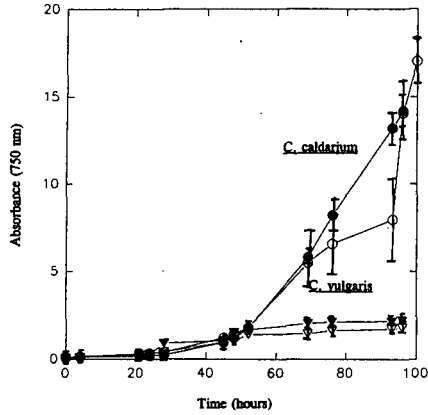


Figure 1. Growth of the strains, *C. caldarium* and *C. vulgaris*, exposed to 5% CO₂/air (●, ▽) and 15% CO₂, 3% O₂, balance N₂ (○, ▴).

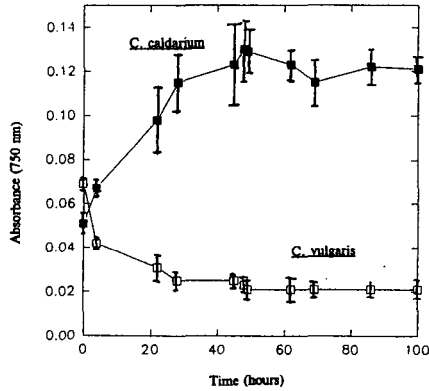


Figure 2. Growth of *C. caldarium* and *C. vulgaris* exposed to 200 ppm SO₂, 15% CO₂, 3% O₂, balance N₂.

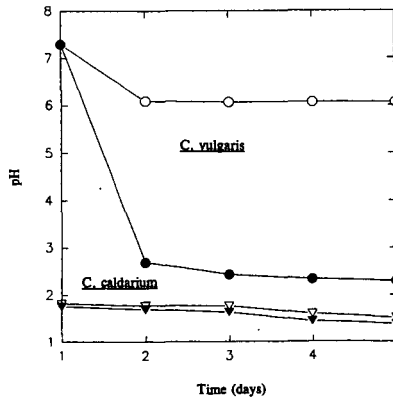


Figure 3. Change in *C. caldarium* and *C. vulgaris* culture pH as a function of simulated flue gas exposure. Cultures were aerated with 15% CO₂, 3% O₂, balance N₂ (●, ▴) and 200 ppm SO₂, 3% O₂, balance N₂ (○, ▽).

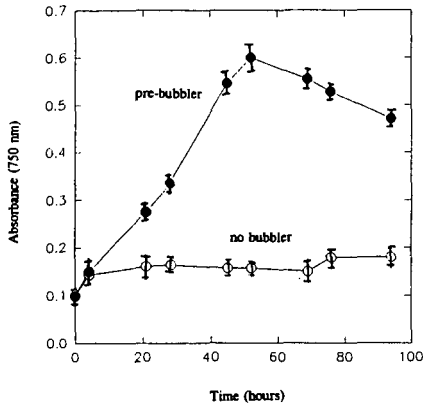


Figure 4. The effect of an SO₂ scrubber (prebubbler) on the growth of *C. caldarium* exposed to 200 ppm SO₂, 15% CO₂, 3% O₂ balance N₂.

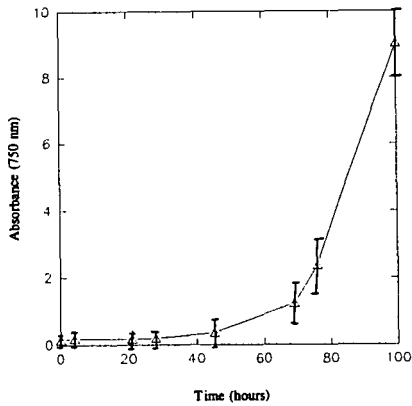


Figure 5. Growth of *C. caldarium* exposed to NO_x-only flue gas.

CURRENT ASPECTS OF CARBON DIOXIDE FIXATION BY MICROALGAE IN KOREA

J.S. Lee, K.D. Sung, M.S. Kim, S.C. Park and K.W. Lee*

Biomass Team, Alternative Energy Research Dept., KIER

71-2 Jang-dong, Yuseong-ku, Taejeon, Korea

* Catalysis Division, KRICT, 100 Jang-dong, Yuseong-ku, Taejeon, Korea

Key words: CO₂ fixation, flue gas from power plants, CO₂ tolerant microalgae.

ABSTRACT

The carbon dioxide fixation by microalgae has several merits such as the CO₂ recovery and the production of useful chemicals. Since the flue gas from a industry has some unfavorable conditions such as high CO₂ concentration and toxic chemicals like SO_x, NO_x contained in flue gas for the cultivation of most microalgae, it is important to apply a suitable strain of microalgae for the fixation of carbon dioxide emitted from various industrial sources. The current status for carbon dioxide emission from thermal power plants, which are major in Korea, is going to be described. Some research work has been done in KIER to get a suitable microalgae. Among the various microalgae tested in our laboratory, *Chlorella* sp., HA-1 and *Chlorococcum littorale* showed the satisfactory performance. The experimental results for culturing of the two microalgae will be presented.

INTRODUCTION

Global warming due to increased carbon dioxide concentration in the atmosphere is a threat causing widespread concern. CO₂ is a green house gas, as are methane, chlorofluorocarbons and water vapor. The CO₂ concentration in the atmosphere is reported to be risen by about 25% since industrial revolution(1,2). In the same time, the temperature of the northern hemisphere has also increased by 0.5°C. A prudent response is to reduce emissions of greenhouse gases while the science underlying global warming is resolved.

Various physicochemical methods such as wet and dry absorption, adsorption, and membrane separation technologies have been developed and the absorption method has been put into practice for the elimination of carbon dioxide(3) but further disposal of the trapped CO₂ is a costly process.

Biological methods, in particular using microalgal photosynthesis, have several merits such as no requirements for the pretreatment of flue gas and the further disposal of trapped CO₂ and mild conditions for CO₂ fixation. Carbon fixed by microalgae is incorporated into carbohydrates, lipids, so energy, chemicals, or foods can be produced from algal biomass.

The flue gas from power plants and steel mills contain about 10-20% of CO₂. If the CO₂ gas is once condensed by chemical or physical means to remove toxic chemicals, the gas fed for microalgal cultivation may contain higher concentration of CO₂. It has been reported, however, that high concentrations of CO₂ inhibits the rate of algal photosynthesis. Silva and Pirt reported that *Chlorella vulgaris* 211/8k strain, which is tolerant to high CO₂ concentration, showed a maximum growth rate at 7% CO₂ concentration(4). Practical growth studies with high concentrations of CO₂ have been initiated(5,6). Negoro et al. examined several strains of marine microalgae on their tolerance to 5 or 15% CO₂ and reported that some of them could grow without pH adjustment(7). Strains preferring low pH values can cut operation costs considerably by eliminating pH control. If the microalgae can be grown at high densities, the size of culturing facilities may be reduced. Desirable properties of microalgae, for the direct biological utilization of CO₂ from flue gas, are summarized in Table 1.

Many works have been carried out to find some microalgae to fit the requirements described above(8-10). Various microalgae, which may be used for CO₂ fixation work, have been obtained from several culture collections and tested in our laboratory for their feasibility for CO₂ fixation in Korea.

At first, in this paper, current aspects for the CO₂ emission in Korea is going to be described, and subsequently some preliminary works for the development of the biological fixation process of CO₂ from flue gas in KIER will be presented.

CURRENT ASPECTS OF CARBON DIOXIDE EMISSION IN KOREA

As Korea is getting developed, the amount of CO₂ emitted has been increased rapidly. Recently global warming by CO₂ have been emerged as a major environmental problem threatening global ecosystem and a concern over it is increasing gradually in Korea like in many other nations. On account of this, Korean government assisted national R&D program for CO₂ by energy conservation and renewable energy utilization, CO₂ fixation by various methods and conversion or utilization of CO₂ for various uses. Among these projects, the biological fixation of CO₂ is considered to be the most environmentally friendly technology, and hence it is started to be investigated in several universities, government institutes such as Korea Research Institute of Chemical Technology(KRICT) as well as Korea Institute of Energy Research(KIER).

Total CO₂ emission in the world was reported to be 5,696 million tons of carbon in 1988(11). Korea is responsible to a 0.88% of the total emission. It corresponds to 49.89 million tons of

carbon. The power generation shares 15.9% of total Korean CO₂ emission. Industry shares 34.1%, transportation 14.9%, others 35.1%. Among the major CO₂ emitters, only the industry and power generation sectors can take the measures to reduce or recover the CO₂ from exhausted gases.

The capacity of fossil-fuel burning power plants in Korea today is about 14,300 megawatts(MW), about 50% of it is driven by heavy oil burning plants. Coal burning power plants shares 31%, LNG burning power plants 18%. As shown in Figure 2, the contribution of several fuels for electricity generation and hence for CO₂ emission is predicted to be changed significantly in the future. According to the national plan, the number of coal-burning power plants will be remarkably increased; the capacity of coal-burning power plants is planned to be 67% of total thermal power capacity 2010 (Figure 2).

The flue gas composition is greatly dependent on the type of fuel used as shown in Table 2. The flue gas from coal-burning power plants generally has the highest concentrations of SO_x, NO_x which are toxic compounds against the microalgal growth. Unless some pretreatments to reduce the SO_x, NO_x concentrations is made, the gas can not be directly purged into microalgal culture. On the other hand, flue gas from LNG and diesel oil burning power plants is believed to have acceptable concentrations of SO_x, NO_x concerning literature. Carbon dioxide in the flue gas can be directly fixed by microalgae. The growth rate of microalgae is greatly dependent on the cultivation temperature and most microalgae exhibit the maximum growth rate between 25°C and 35°C. Since CO₂ fixation process by microalgae requires a large area for light absorption, it is believed to be installed outdoors for large scale application. Thus the control of cultivation temperature become normally very difficult.

In case of power plant application of the process, cooling water discharge temperature might determine the cultivation temperature of microalgae. Average temperature of cooling water from typical fossil-fuel burning power plant in Korea is shown in Table 3. The table shows that the minimum temperature recorded in February is 13.4°C. The lowest temperature is apparently too low for the proper cultivation of normal microalgae. However, the problem is believed to be overcome by thermal insulation or solar energy technologies such as a green house in winter.

BIOLOGICAL CARBON DIOXIDE FIXATION WORK IN KIER

Recently several applied studies aimed at the direct biological fixation of CO₂ out of the flue gases from thermal power plants have been carried out(11-13). Although the direct use of discharged gases reduces the cost of pretreatment, it imposes extreme conditions on microalgae such as high concentrations of CO₂ and the presence of toxic chemicals like SO_x, NO_x to microalgae. The best suited microalgal strain for this purpose should be selected in terms of tolerance to environmental stresses.

Materials and methods

Strain

A marine microalga *Chlorococcum littorale* and a fresh-water microalga *Chlorella* sp. HA-1 were used in this work. Each strain was obtained from Marine Biotechnology Institute(Japan) and National Institute of Environmental Studies(Japan), respectively. These strains were selected on the basis of high growth rate at high CO₂ level. The medium used for culturing *C. littorale* has following composition: (in g/l) KNO₃ 1.25, KH₂PO₄ 1.25, MgSO₄·7H₂O 1.25, NaCl 15, 1 ml of Fe solution, and 1 ml of A₅ solution. Fe solution consists of 1l water, FeSO₄·7H₂O 2, and 1 ml of concentrated H₂SO₄. MBM media(7) used for culturing of *Chlorella* sp. HA-1 has the following composition: (in mg/l), KNO₃ 250, MgSO₄·7H₂O 75, K₂HPO₄ 75, KH₂PO₄ 175, NaCl 25, CaCl₂·2H₂O 10, FeSO₄·7H₂O 2, H₃BO₃ 2.86, MnSO₄·7H₂O 2.5, ZnSO₄·7H₂O 0.222, CuSO₄·5H₂O 0.079, Na₂MoO₄ 0.021. The initial pH was 6.

Batch culture

The microalgal culture experiments were conducted to investigate the growth characteristics of the microalgae under various culture conditions. The culture equipment is shown in Figure 3. The system consists of 1l Erlenmeyer flasks as culture vessel, water bath, fluorescent lamp, CO₂ enriched air supplier. The maximum average light intensity at the surface of the culture vessel was 8 Klux. CO₂ enriched air was prepared by mixing pure CO₂ from a cylinder and air from an air pump, and filter sterilized. The temperature of the culture vessel was maintained in the water vessel equipped with a temperature controller(Jeo Tech Co., Korea). pH was not regulated. Light intensities, CO₂ concentrations, and temperature were varied in accordance with experimental conditions specified.

Assay

Light intensities were measured by a light sensor (Licor Inc, USA). Cell growth was determined either by the optical density at 660 nm using UV-spectrophotometer (HP8452A, Hewlett-Packard Inc., USA) or by dry-cell weight after filtration on cellulose acetate filter(0.45µm, Millipore Co., USA), followed by drying at 105°C overnight.

Results and discussion

The effects of light intensities and CO₂ concentrations on the cultivation of microalgae were investigated for CO₂ fixation from concentrated sources such as a power plant. *C. littorale* and *Chlorella* sp. HA-1 were selected for further experiments after screening by their performance.

The effects of 3, 6, 8 Klux light intensities on the growth of *C. littorale* at 26°C and 10% CO₂ concentration were investigated. As shown in Figure 4, the growth rates of *C. littorale* were almost the same at 6 and 8 Klux with 0.19g cell/day-1 growth. However, the growth rate at 3 Klux was 0.12g cell/day-1. This corresponds to only 60% of the growth rate at sufficient light. Figure 5 shows the growth of *Chlorella* sp. at various light intensities. Higher than 8 Klux light intensities is believed to inhibit the growth and the growth rate at 3 Klux was 0.15g cell/day-1, about 70% of its maximum at 6 Klux.

It is concluded that the light intensities around 6 Klux are sufficient for the proper growth of them, higher light intensities are of no effect with *C. littorale* and even harmful for the case of *Chlorella* sp. HA-1.

The industrial CO₂ sources are of relatively high concentration with concentration range from 10 to 20% CO₂ than natural sources. Therefore, the concentrated CO₂ resistance of the microalgae was experimented with 10, 20, 30% of CO₂ concentrations. The growth of *C. littorale* was not inhibited at 10 and 20% concentrations as shown in Figure 6., hence considering only CO₂ concentration, there might be no problem with the *C. littorale* for the CO₂ fixation application from power plant exhaust gas. However, the growth rate was declined to about half at 30% CO₂ concentration.

Figure 7 shows the CO₂ resistance of fresh water microalga *Chlorella* HA-1. This species exhibits the growth inhibition at the CO₂ concentration higher than 10%. In consequence, the CO₂ resistance of the *Chlorella* HA-1 was believed to be lower than that of marine alga *C. littorale*. Combined cycle power plants located in-land in Korea are burning LNG as fuel, and using fresh water as cooling water. Since these LNG power plants discharge the emissions containing only 9-10% CO₂, the *Chlorella* HA-1 could be applied for the CO₂ fixation in the case of in-land LNG power plants.

The effects of cultivation temperatures on the growth of microalgae were also considered. The two species showed maximum growth in the temperature range from 26°C to 30°C. The minimum average temperature of cooling water in a typical thermal power plant was 13.4°C in February, however, the problem is believed to be overcome by thermal insulation or solar energy technologies such as green house in winter.

ACKNOWLEDGEMENT

This project was supported by Korean Ministry of Environment and Ministry of Science and Technology.

REFERENCES

- (1) Barnola, J.M., Raynaud, D., Korotkevich, and Lorius, C., *Nature*, 329, 408 (1987).
- (2) Neftel, A., Oeschger, H., Schwander, J., Stouffer, B., and Zumbunn, R., *Nature*, 295, 220 (1982).
- (3) Yokoyama, T., "Japanese R&D on CO₂ Removal", Coal for Development Conference Proceedings, London, UK, 23-26th March (1993).
- (4) Silva, H.J. and Pirt, S.J., *J.Gen.Microbiol.*, 130, 2833 (1984).
- (5) Pirt, M.W. and Pirt, S.J., *J.Gen.Microbiol.*, 119, 321 (1980).
- (6) Lee, Y. and Hing, H.K., *Appl.Microb.Biotech.*, 31, 298 (1989).
- (7) Negorc, M., Shioji, N., Miyamoto, K., and Miura, Y., *Appl.Biochem.Biotechnol.*, 28/29, 877 (1991).
- (8) Watanabe, Y., Ohmura, N., and Saiki, H., *Energy Conv.& Management*, 33(5-8), 545 (1992).
- (9) Kodama, Y., Ikemoto, H., and Miyachi, S., *J.Marine Biotechnol.*, 1, 21 (1993).
- (10) Takeuchi, T., Utsunomiya, K., Kobayashi, K., Owada, M. and Karube, I., *J.Biotechnol.*, 25, 261 (1992).
- (11) Saiki, H., "Measures for CO₂ reduction by Japanese electric power industry", 1st CO₂ workshop at KRICT, Taejeon, Korea, 20-21 June (1993)
- (12) Laws, E.A., *Biores.Technol.*, 37, 25 (1991).
- (13) EPRI Project 2612-11, Electric Power Research Institute, Palo Alto, CA (1990).
- (14) Hamasaki, A., Shioji, N., Ikuta, Y., Hukuda, Y., Makita, T., Hirayama, K., Matsuzaki, H., Tsukamoto, T., and Sasaki, S., *Appl.Biochem.Biotechnol.*, 45/46, 799 (1994).

Table 1. Desirable properties of microalgae for CO₂ fixation

High CO ₂ tolerance
Low pH tolerance
Stable and high growth rate in the linear phase
Capability of growing at high cell densities
SO _x , NO _x tolerance
Thermotolerance

Table 2. Flue gas composition of thermal power plants using various fuels

Components	CO ₂ , %	SO _x , ppm	NO _x , ppm
Fuel			
Coal			
Anthracite*	15 - 16	860	200
Bituminous**	15 - 16	360	240
LNG	9 - 10	negligible	140
Diesel oil	15 - 16	180	negligible

* : Produced in Korea

** : imported low sulfur coal

Table 3. Temperature (°C) of the cooling water from fossil-fuel burning power plants in Korea.

	Jan.	Feb.	Mar.	Apr.	May	Jun.	Jul.	Aug.	Sep.	Oct.	Nov.	Dec.
Intake water	5.6	4.6	8.4	11.8	17.3	22.2	24.6	25.5	26.2	20.3	15.7	8.0
Cooling water	15.6	13.4	20.2	22.6	28.6	33.0	34.0	33.0	33.3	29.7	26.2	18.5

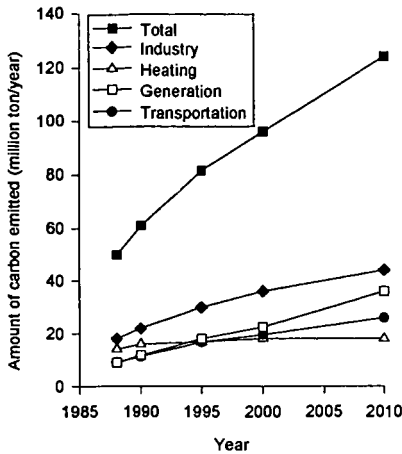


Figure 1. Domestic CO₂ emissions by sector of energy use in Korea.

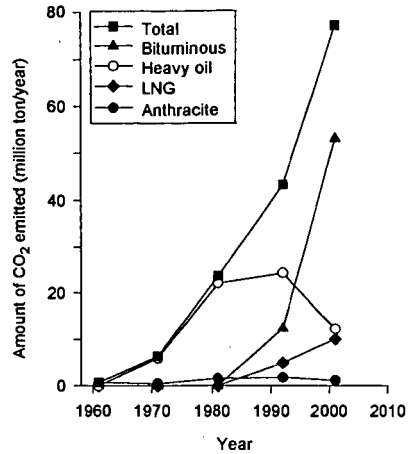
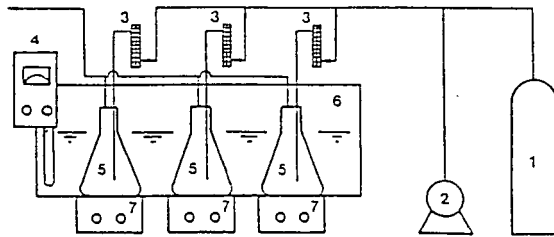


Figure 2. CO₂ emission from fossil-fuel burning power plants in Korea.



1. CO₂ cylinder 2. Air pump 3. Flow meter 4. Water circulator
5. 1L flask 6. Water bath 7. Stirrer

Figure 3. Schematic diagram of microalgal CO₂ fixation equipment.

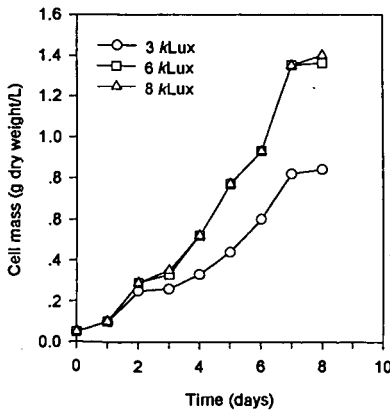


Figure 4. The effect of light intensities on the growth rate of *Clitorale*. The CO₂ concentration and the temperature were 10% and 26°C respectively.

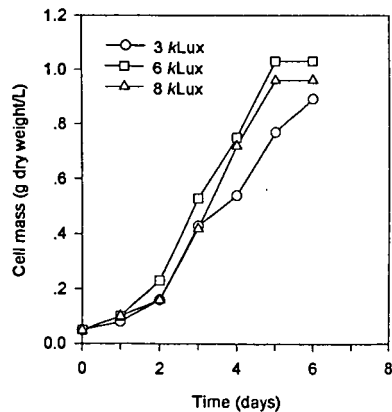


Figure 5. The effect of light intensities on the growth rate of *Chlorella* sp., HA-1. The CO₂ concentration and the temperature were 10% and 26°C respectively.

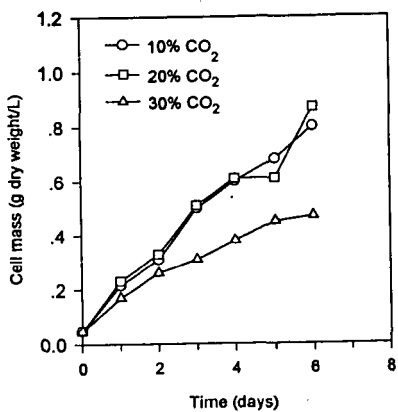


Figure 6. The effect of CO₂ concentrations on the growth rate of *Clitorale*. The experiment was carried out at 30°C and at light intensity of 6kLux.

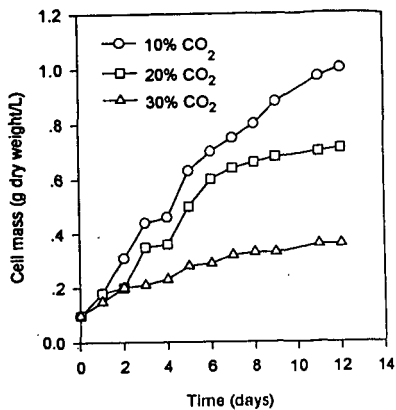


Figure 7. The effect of CO₂ concentrations on the growth rate of *Chlorella sp., HA-1*. The experiment was carried out at 30°C and at a light intensity of 6kLux.

BIOCONVERSION OF CO₂ TO ETHANOL AND OTHER COMPOUNDS

Thomas M. Wahlund, Tyrrell Conway, and F. Robert Tabita
Department of Microbiology, The Ohio State University,
484 West 12th Avenue, Columbus, Ohio 43210-1292

Keywords: Microbial CO₂ fixation, recombinant DNA, ethanol

INTRODUCTION

The light-driven process of CO₂ fixation and its conversion into a myriad of larger organic molecules is a remarkably successful strategy employed by all plants. Likewise, there are numerous types of bacteria that are capable of extremely efficient CO₂ fixation, including those that use light-driven processes, as well as several species that are capable of using the energy obtained from chemical oxidations to fuel CO₂ reduction in the dark. However, nowhere in nature can an organism be found that has coupled CO₂ fixation to significant ethanol production. With the realization that fully one-third of the corn starch used for biological ethanol formation is lost through the production of CO₂ gas, it would be desirable to discover some way to use this CO₂ for the production of value-added chemicals or other products of interest. In this paper, we discuss recent experiments to couple the metabolism of CO₂ to the synthesis of ethanol using recombinant DNA technology. A chimeric bacterium was constructed so that CO₂ may be metabolized to ethanol.

RATIONALE AND EXPERIMENTAL APPROACHES

A logical strategy for genetically engineering microorganisms with the capacity for efficient ethanol production became possible when the genes that encode the key enzymes of ethanol biosynthesis from pyruvate were cloned from the bacterium *Zymomonas mobilis* (Conway *et al.*, 1987a; Conway *et al.*, 1987b). Indeed the *Z. mobilis* pyruvate decarboxylase (*pdh*) and alcohol dehydrogenase (*adh*) genes, when expressed in *Escherichia coli*, were found to enable this host to divert a significant amount of its normal metabolic profile to ethanol synthesis (Ingram and Conway, 1988). Since a common metabolic intermediate of virtually all central metabolic pathways is pyruvate, there is considerable interest to couple pyruvate formation to ethanol synthesis. Many autotrophic bacteria use the reductive pentose phosphate or Calvin-Benson-Bassham (CBB) pathway to convert CO₂ to organic matter. Since pyruvate is a key intermediate here as well, we considered the possibility that some of this pyruvate might be converted to ethanol in a CO₂-fixing chimeric bacterium overexpressing the *Z. mobilis pdh* and *adh* genes.

Much has been learned of the molecular biology and biochemistry of CO₂ fixation in microorganisms (Tabita, 1988; Tabita, 1995) and recently the potential for the regulated expression of foreign genes under autotrophic growth conditions in phototrophic bacteria has become established (Falcone and Tabita, 1991). Although much still needs to be learned about promoter structure and other aspects of gene expression in autotrophic bacteria, it was considered well worth the effort to determine whether it would be feasible to use existing technology to convert CO₂ into ethanol. The basic idea behind this approach is illustrated in Figure 1, where it is envisioned that recombinant *Rhodobacter* species would reduce CO₂ to ethanol under purely autotrophic (organic carbon-free) growth conditions. In this scheme, hydrogen is used as the ultimate reductant in the absence of oxygen under photosynthetic growth conditions and pyruvate (a product of the CBB pathway) is reduced to ethanol through the mediation of plasmid-encoded *pdh* and *adh* genes (Figure 2). Alternatively, one may take advantage of the ability of these organisms to fix CO₂ in the dark in the presence of oxygen, again in the absence of organic carbon. The versatility of these bacteria is further underlined by their ability to also use various organic compounds, instead of hydrogen, as electron donors.

RESULTS

The feasibility of using *Rhodobacter* and related organisms for foreign gene expression was first determined by constructing a promoter-plasmid vector capable of directing the synthesis of an easily assayed indicator enzyme, β -galactosidase (encoded by the *lacZ* gene of *E. coli*). A variety of growth conditions, known to influence CO₂ fixation-related gene expression, was assessed in both *R. sphaeroides* and the related organism *R. capsulatus*. These conditions included anoxygenic growth under photoautotrophic (PA) conditions in a CO₂/H₂ atmosphere, aerobic chemoautotrophic (CLA) growth conditions in the dark in a CO₂/H₂/O₂ atmosphere, anoxygenic photoheterotrophic (PH) growth conditions in the light using organic carbon as an electron donor, and aerobic chemoheterotrophic (CH) growth conditions in the dark in the presence of organic carbon. In *R. sphaeroides*, maximum β -galactosidase activity was obtained

in PA-grown cells, which reflected the high level of RubisCO (the major CO₂ fixation enzyme of the CBB pathway) associated with these growth conditions in this organism (Tabita, 1988; Tabita, 1995; Falcone and Tabita, 1996). The lowest level of β-galactosidase was found in PH-grown cells, which also was reflected by the lower levels of RubisCO. Intermediate levels were obtained in CLA-cultured *R. sphaeroides* and to our surprise CH-dependent growth yielded fairly high levels of β-galactosidase, while the level of RubisCO was at its expected lowest point. In *R. capsulatus*, the same promoter-*lacZ* construct showed a definitive and pronounced enhancement of β-galactosidase activity under CLA-growth conditions, with much lower activity in PA-grown cells, and basically background levels in PH and CH-cultured *R. capsulatus*.

The results with the promoter-*lacZ* fusion-indicator constructs generally yielded much lower levels of β-galactosidase than we might have expected based on previous studies with the same promoter directing transcription of foreign RubisCO genes (Falcone and Tabita, 1993). There are several reasons why *lacZ* may not have been as highly expressed as the genes encoding RubisCO with this vector, including factors related to the posttranscriptional processing of the message. Despite these results, we determined if it might be possible to use this vector to express the *pdc* and *adh* genes in *R. sphaeroides* and *R. capsulatus*, under the various growth conditions reported above. Basically, the same pattern of *adh* gene expression was obtained as above, namely the highest levels of alcohol dehydrogenase activity were obtained under PA and CLA growth conditions with *R. sphaeroides* and *R. capsulatus*, respectively. Again, with this vector the level of *adh* expression was not nearly as great as we had hoped based on prior RubisCO gene expression studies. The regulated expression of *adh* (and also *pdc*) did, however, encourage us to examine whether genetically engineered *R. sphaeroides* and *R. capsulatus* were capable of synthesizing ethanol under CO₂-fixation conditions. Both strains produced between 0.07 and 0.08 percent (w/v) ethanol in culture filtrates of photoautotrophic-grown cells. Furthermore, both alcohol dehydrogenase activity and the amount of ethanol synthesized could be significantly enhanced by the addition of xylose to the growth medium under PH growth conditions. Up to 0.023 percent ethanol (w/v) was obtained in *R. sphaeroides* and about 0.014 percent ethanol was produced by *R. capsulatus* cultures, with maximum levels reached at a considerably faster rate for *R. capsulatus*.

Another factor to be considered in any microbial process to produce ethanol is the tolerance of the host organism to ethanol. Each strain of *R. sphaeroides* and *R. capsulatus* employed in our study was sensitive to fairly low concentrations of ethanol. In Figure 3, the specific growth rate and the maximum extent of growth of each organism in a xylose-mineral salts medium under PH growth conditions was determined. As shown in this figure, higher concentrations of ethanol most affected the extent of growth and not the rate of growth. However, the data do show that in terms of the specific growth rate, *R. capsulatus* was considerably more resistant to ethanol. It must be kept in mind, however, that both strains of *R. capsulatus* and *R. sphaeroides* are laboratory strains that have not been otherwise altered. Thus, it may be possible to modify the existing strains, and select for higher alcohol tolerance, as we have for temperature tolerance (Weaver and Tabita, 1983). Another alternative would be to isolate new strains.

DISCUSSION

These studies conclusively show that CO₂ may be converted to ethanol by two species of *Rhodobacter* under anoxygenic conditions in the light or under dark aerobic growth conditions. A promoter-vector molecule, which had been previously shown to be maximally effective under growth conditions which favored active CO₂ fixation, was adapted for these studies; e.g. in the absence of organic carbon. Although the overall level of *pdc* and *adh* gene expression was not as great as we had expected, the fact remains that CO₂ was converted to ethanol, both in the light and in the dark. Current studies are devoted to optimizing the position of the relevant genes within this vector and to stabilizing the *pdc* and *adh* transcript. In addition, other potential vectors have been developed which might prove even more suitable. Surprisingly, the use of xylose in photoheterotrophic cultures substantially enhanced ethanol production with our original vector, perhaps precluding the need for hydrogen as an electron donor for metabolism. Since xylose is a major constituent of corn starch, its use to stimulate plasmid-directed ethanol production in an organism with a highly active reductive pentose phosphate pathway may lead to a novel source of biologically synthesized ethanol. In this vein, it will be important to determine the total amount of ethanol derived from CO₂ and/or xylose carbon since these bacteria are known to oxidize organic carbon sources to CO₂ and refix and use this CO₂ as an electron acceptor (Tabita, 1995).

ACKNOWLEDGMENTS

This work was supported by a grant from the Consortium for Plant Biotechnology Research.

REFERENCES

1. Conway, T. Osman, Y.A., Konnan, J.I., Hoffman, E., and Ingram, L.O. (1987a) Promoter and nucleotide sequences of *Zymomonas mobilis* pyruvate decarboxylase. *J. Bacteriol.* 169, 949-954.
2. Conway, T., Sewall, G.W., Osman, Y.A., and Ingram, L.O. (1987b) Cloning and sequencing of the alcohol dehydrogenase II gene from *Zymomonas mobilis*. *J. Bacteriol.* 169, 2591-2597.
3. Ingram, L.O., and Conway, T. (1988) Expression of different levels of ethanologenic enzymes from *Zymomonas mobilis* in recombinant strains of *Escherichia coli*. *Appl. Env. Microbiol.* 54, 397-404.
4. Tabita, F.R. (1988) Molecular and cellular regulation of autotrophic carbon fixation in microorganisms. *Microbiol. Rev.* 53, 155-189.
5. Tabita, F.R. (1995) The biochemistry and metabolic regulation of carbon metabolism and CO₂ fixation in purple bacteria. *In*, Anoxygenic Photosynthetic Bacteria (R.E. Blankenship, M.T. Madigan, and C.E. Bauer, eds.) pp. 885-914, Kluwer Acad. Publ. The Netherlands.
6. Falcone, D.L., and Tabita, F.R. (1991) Expression of endogenous and foreign ribulose 1,5-bisphosphate carboxylase/oxygenase (RubisCO) genes in a RubisCO deletion mutant of *Rhodobacter sphaeroides*. *J. Bacteriol.* 173, 2099-2108.
7. Falcone, D.L., and Tabita, F.R. (1993) Complementation analysis and regulation of CO₂ fixation gene expression in a ribulose 1,5-bisphosphate carboxylase-oxygenase deletion strain of *Rhodospirillum rubrum*. *J. Bacteriol.* 175, 5066-5077.
8. Weaver, K.E., and Tabita, F.R. (1983) Isolation and partial characterization of *Rhodopseudomonas sphaeroides* mutants defective in the regulation of ribulose bisphosphate carboxylase/oxygenase. *J. Bacteriol.* 156, 507-515.

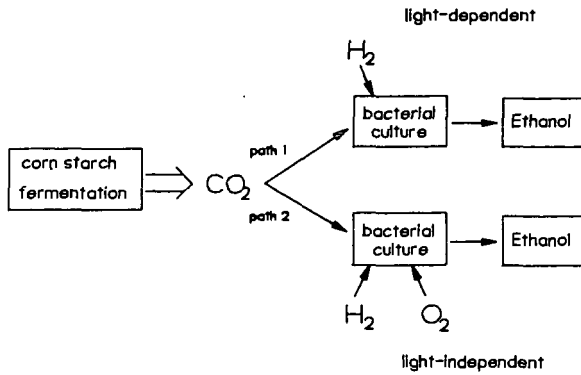
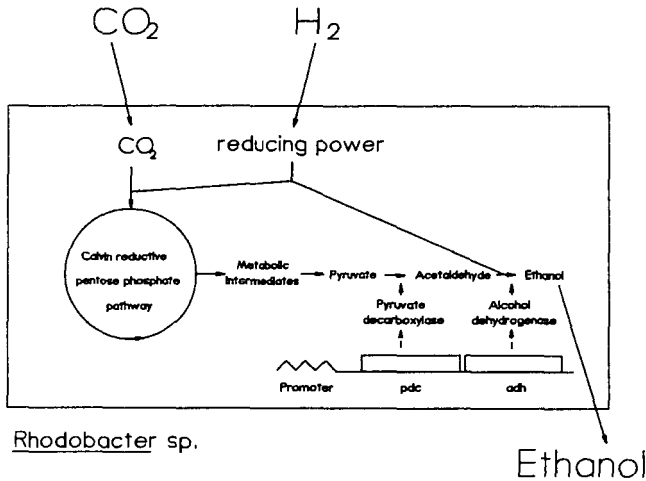


Figure 1. A general scheme to couple light-dependent and light-independent CO₂ fixation to ethanol production.



Rhodobacter sp.

Ethanol

Figure 2. Ethanol synthesis using metabolic intermediates and pyruvate produced through the CBB reductive pentose phosphate pathway of CO₂ fixation.

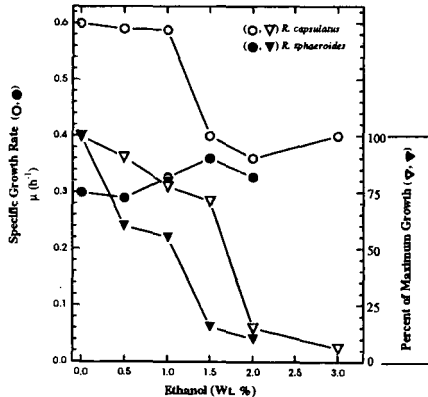


Figure 3. Specific growth rate (μ) and maximum extent (%) of growth in batch cultures of *R. sphaeroides* and *R. capsulatus* grown in a mineral salts-xylose medium containing different initial concentrations of ethanol. Cultures were bubbled with 1.5% CO₂/98.5% H₂ in the light.

METHANOL SYNTHESIS FROM CO₂ AND H₂ OVER Cu/ZnO-BASED MULTICOMPONENT CATALYSTS

Masahiro SAITO¹⁾*, Masami TAKEUCHI²⁾, Tadahiro FUJITANI¹⁾,
Jamil Toyir³⁾, Shengcheng Luo³⁾, Jingang Wu³⁾,
Taiki WATANABE²⁾ and Yuki KANAI²⁾

- 1) National Institute for Resources and Environment (NIRE), 16-3 Onogawa, Tsukuba-shi, Ibaraki 305, Japan
- 2) Research Institute for Innovative Technology for the Earth (RITE), 9-2 kizukawadai, kizu-cho, Soraku-gun, Kyoto 619-02, Japan
- 3) RITE (NEDO Industrial Technology Researcher), 16-3 Onogawa, Tsukuba-shi, Ibaraki 305, Japan

Keywords: CO₂ hydrogenation, methanol synthesis, Cu/ZnO-based multicomponent catalyst

INTRODUCTION

The greenhouse effect of carbon dioxide has been recognized to be one of the most serious problems in the world, and a number of countermeasures have been proposed so far. Catalytic hydrogenation of CO₂ to produce various kinds of chemicals and fuels has received much attention as one of the most promising mitigation options. In particular, methanol synthesis by CO₂ hydrogenation has been considered to play an important role in the transportation of hydrogen energy produced from natural energy such as solar energy, hydropower and so on, as shown in Fig. 1[1]. According to some estimations[2], an electric power of 300 MWh could be obtained from a methanol fired power plant in Japan, if methanol synthesized from CO₂ and H₂ produced by a electrolysis of water using an electric power of 1000 MWh is transported to Japan through the system shown in Fig. 1.

A practical methanol synthesis process greatly requires a high performance catalyst, which must be highly active and selective for methanol synthesis and also stable for a long period in a continuous operation. NIRE and RITE have been doing a joint research on methanol synthesis by catalytic hydrogenation of carbon dioxide. The authors have elucidated the role of metal oxides contained in Cu/ZnO-based ternary catalysts, and then developed Cu/ZnO-based multicomponent catalysts containing two or three metal oxides [3]. Furthermore, we have examined the change in the activity of the multicomponent catalysts during a long term methanol synthesis test, and investigated the methanol synthesis over the multicomponent catalysts by using a reactor with a recycling equipment for unreacted gases.

EXPERIMENTAL

All of the Cu/ZnO-based catalysts were prepared by a coprecipitation method, which was described in detail elsewhere [4]. Two kinds of Cu/ZnO-based multicomponent catalysts named MCA (Cu/ZnO/ZrO₂/Al₂O₃) and MCB (Cu/ZnO/ZrO₂/Al₂O₃/Ga₂O₃) were prepared by selecting metal oxides on the basis of the role of metal oxide. A commercial catalyst (Cu/ZnO/Al₂O₃) for methanol synthesis from syngas was used for comparison. A conventional fixed bed flow reactor was used both for short-term methanol synthesis tests and for long-term tests. Furthermore, a recycle reactor equipped with a compressor for recycling unreacted gases was used for investigating practical methanol synthesis operations. The catalyst fixed in a reactor was reduced in a gas mixture of H₂ (10%) and He (90%) at 523 K with a total pressure 5 MPa. The hydrogenation of CO₂ was then carried out at 523 K with a total pressure of 5 MPa in a fixed bed flow reactor by feeding a gas mixture of H₂ and CO₂ with a mole ratio of H₂/CO₂=3. The reaction products were analyzed by means of gas chromatographs directly connected to the reactor. The catalyst activity was measured 2h after supplying the feed gas to the reactor except for a long term methanol synthesis test. The total copper surface area of each catalyst after the reaction (Cu_{total}) was determined by the technique of N₂O reactive frontal chromatography (RFC) after re-reducing the post-reaction catalyst with H₂ at 523 K [5].

RESULTS AND DISCUSSION

The main products of CO₂ hydrogenation over Cu/ZnO-based catalysts were methanol, CO and water. Methane, dimethyl ether and methyl formate were also detected in the reaction products, but the selectivities for the by-products were less than 0.1%.

The methanol synthesis activities which were expressed by mass-time yields of methanol (MTY), Cu_{total} and the specific activities, i.e. MTY/Cu_{total}, of Cu/ZnO-based ternary catalysts (Cu/ZnO/M_xO_y) containing various metal oxides were examined. Table 1 shows the activities of a Cu/ZnO catalyst and the ternary catalysts containing the optimum amounts of Ga₂O₃, Al₂O₃, ZrO₂ and Cr₂O₃, which were higher than that of a Cu/ZnO catalyst by factor of 43%, 40%, 30% and 17%, respectively.

Fig. 2 shows the methanol synthesis activity of Cu/ZnO-based ternary catalysts containing Ga₂O₃, Al₂O₃, ZrO₂ and Cr₂O₃ on varying the content from 5 to 40 wt% as a function of total Cu surface area (Cu_{total}). For each metal oxide contained in the Cu/ZnO-based catalysts, a linear relationship between MTY and Cu_{total} was seen, indicating that the specific activity is identical for each metal oxide even if the content of a metal oxide in a Cu/ZnO-based catalyst is varied. The specific activities for the Cu/ZnO-based catalysts containing Ga₂O₃ and Cr₂O₃ were greater than that of a Cu/ZnO catalyst by factor of 40% and 30%, respectively. On the other hand, the specific activity was not altered by the addition of Al₂O₃ or ZrO₂, though these metal oxides play a role in increasing Cu surface area. This indicates that the addition of Al₂O₃ or ZrO₂ improves the dispersion of Cu particles without changing the specific activity of a Cu/ZnO catalyst, while Ga₂O₃ and Cr₂O₃ are not effective for improving the dispersion of Cu, but are effective for increasing the specific activity of a Cu/ZnO catalyst.

Table 2 shows the methanol synthesis activities of the multicomponent catalysts. The activities of the multicomponent catalysts were higher than those of the ternary catalysts, and MCB exhibited the highest activity. The total Cu surface area of MCA was higher than that of Cu/ZnO/Al₂O₃, but the specific activity of MCA was the same as that of Cu/ZnO/Al₂O₃. On the other hand, the specific activity of MCB was higher than that of Cu/ZnO/Al₂O₃, though the total Cu surface area of MCB was a little smaller than that of Cu/ZnO/Al₂O₃. These findings indicate that the promoting effect of metal oxides is exerted on the multicomponent catalysts as well as on the ternary catalysts.

Fig. 3 shows the activities of the multicomponent catalysts, Cu(50)/ZnO(45)/Al₂O₃(5) and Cu(50)/ZnO(50) as a function of the temperature on pretreatment in H₂ ranging from 523 K to 723 K. The activities of all the catalysts decreased with increasing pretreatment temperature mainly due to the decrease in Cu surface area by the sintering of Cu particles. However, the activities of MCB and MCA decreased only 10% and 15% even in pretreatment at 723 K, respectively, while the activities of the ternary catalyst and the binary catalyst decreased 30% and 85%, respectively. This suggests that the sintering of Cu particles can be suppressed by the addition of Al₂O₃, ZrO₂ and/or Ga₂O₃ to Cu/ZnO.

A methanol synthesis catalyst for a practical process is highly required to have a stable activity for a long period in a continuous operation. A long-term methanol synthesis test was performed at 523 K with a total pressure of 5 MPa by using a gas mixture of CO₂, CO and H₂, because unreacted gases and CO must be recycled to the reactor in a practical process. Fig. 4 shows the change in the activity with time on stream of MCB, which was the best catalyst among all the catalysts tested, including a commercial catalyst used for methanol synthesis from syngas. The activity of MCB decreased only by 17% in 1000 h during the test, but unchanged from 1000 h to 3400h. On the other hand, the activity of the commercial catalyst decreased by 20% in 1000 hr, and still decreased to 75% of the initial activity in 2100hr. These findings clearly indicate that the multicomponent catalyst developed in the present work is very stable for a long period in a continuous methanol synthesis operation.

Practical methanol synthesis must be performed by using a reactor with recycling equipments for unreacted gases, because the conversion of CO₂ to methanol at reaction equilibrium is very low under ordinary reaction conditions, for example, 17% at 523 K and 5 MPa. Therefore, methanol synthesis using a recycle reactor was also investigated. The products of CO₂ hydrogenation at 473 K to 548 K with a total pressure of 5 MPa in the recycle reactor were methanol, CO, water, methane, ethane, dimethyl ether, methyl formate, ethanol, propanol and butanol, but the yields of the products other than methanol, CO and water were very small. The selectivity for methanol in the products except CO and water was more than 99.8%. The reaction products were cooled to 270 K in a gas-liquid separator connected to the reactor. Liquid products collected in the gas-liquid separator were taken out of the reactor, and unreacted gases as well as gaseous products such as CO, methane, ethane and dimethyl ether were recycled back to the reactor. The concentrations of methane, ethane and dimethyl ether in a recycled gas mixture remained constant after some initial period in CO₂ hydrogenation without purging unreacted gases. Table 2 shows the composition of liquid products except H₂O taken out of the recycle reactor. The purity of methanol was 99.96 wt%, and higher than that obtained in a commercial methanol synthesis from syngas. This finding suggests that the lower CO concentration in the feed gas should result in the lower yield of by-products and thus the higher methanol purity.

CONCLUSIONS

The role of metal oxides such as Ga₂O₃, Al₂O₃, ZrO₂ and Cr₂O₃ contained in Cu/ZnO-based ternary catalysts for methanol synthesis from CO₂ and H₂ was classified into two categories: to improve the Cu dispersion and to increase the specific activity.

The Cu/ZnO-based multicomponent catalysts developed on the basis of the role of metal oxides were highly active and stable for a long period in a continuous methanol synthesis operation.

The conversion of CO₂ in a make-up gas to methanol at 473 K to 523 K with a total pressure of 5 MPa was more than 99.9% during the methanol synthesis over the multicomponent catalyst using a reactor with a recycling equipment for unreacted gases because the yields of by-products were less than 0.1%.

In conclusion, the presented results clearly show that the Cu/ZnO-based multicomponent catalysts developed in the joint research are highly effective for a practical methanol synthesis via CO₂ hydrogenation.

ACKNOWLEDGMENT

The present work was partly supported by New Energy and Industrial Technology Development Organization (NEDO).

REFERENCES

- [1] H. Sano, Proc. Int. Symp. on CO₂ Fixation & Efficient Utilization of Energy, Tokyo, Japan, p. 117(1993).
- [2] S. Kubo, private communication
- [3] M. Saito, T. Fujitani, I. Takahara, T. Watanabe, M. Takeuchi, Y. Kanai, K. Moriya, T. Kakumoto, Energy Convers. Mgmt, **36**, 577 (1995).
- [4] T. Fujitani, M. Saito, Y. Kanai, M. Takeuchi, K. Moriya, T. Watanabe, M. Kawai, and T. Kakumoto, Chem. Lett., **1993**, 1079.
- [5] G. C. Chinchin, K. C. Waugh, and D. A. Whan, Appl. Catal., **25**, 101(1986).

Table 1 Activities of Cu/ZnO and Cu/ZnO-based ternary catalysts containing the optimum amount of metal oxides

Catalyst	Composition (wt%)	Cu surface area ^{a)} (m ² /g-cat)	Methanol synthesis activity ^{b)} (g-CH ₃ OH/kg-cat·h)	Specific activity (mg-CH ₃ OH/m ² ·h)
Cu/ZnO	50/50	36.5	516	14.1
Cu/ZnO/Ga ₂ O ₃	50/25/25	37.6	738	19.6
Cu/ZnO/Al ₂ O ₃	50/45/5	47.1	721	15.3
Cu/ZnO/ZrO ₂	50/40/10	46.0	665	14.5
Cu/ZnO/Cr ₂ O ₃	50/45/5	32.8	602	18.4

a) Total Cu surface (Cu_{total}) of the catalysts re-reduced at 523 K after CO₂ hydrogenation were measured by N₂O reactive frontal chromatography.

b) Reaction conditions : weight of catalyst=1 g, H₂/CO₂ ratio in the feed=3, feed gas rate =300 ml/min, temperature=523 K, total pressure=5 MPa.

Table 2 Activities of Cu/ZnO-based multicomponent catalysts

Catalyst	Cu surface area ^{a)} (m ² /g-cat)	Methanol synthesis activity ^{b)} (g-CH ₃ OH/kg-cat·h)	Specific activity (mg-CH ₃ OH/m ² ·h)
Cu(50)/ZnO(45)/Al ₂ O ₃ (5)	47.1	721	15.3
MCA(Cu/ZnO/ZrO ₂ /Al ₂ O ₃)	49.9	767	15.3
MCB(Cu/ZnO/ZrO ₂ /Al ₂ O ₃ /Ga ₂ O ₃)	44.5	785	17.6

a) Total Cu surface areas of the catalysts re-reduced at 523 K after CO₂ hydrogenation were measured by N₂O reactive frontal chromatography.

b) Reaction conditions : weight of catalyst=1 g, H₂/CO₂ ratio in the feed=3, feed gas rate =300 ml/min, temperature=523 K, total pressure=5 MPa.

Table 3 The composition of liquid products (except water) from a recycle reactor in this work^{a)}, compared with that from a commercial plant for methanol synthesis from syngas^{b)}

Compound	Composition		
	This work	A commercial plant	
Methanol	CH ₃ OH	99.96 wt%	99.59 wt%
Methyl formate	HCOOCH ₃	330 ppm	700 ppm
Higher alcohols (C ₂ -C ₄)	ROH	30 ppm	530 ppm
Hydrocarbons (C ₆ -C ₁₀)	C _n H _m	-	50 ppm
Dimethyl ether	(CH ₃) ₂ O	-	230 ppm

a) Reaction conditions : catalyst=Cu/ZnO/ZrO₂/Al₂O₃/Ga₂O₃, H₂/CO₂ ratio in the make-up gas=3, temperature=517 K, total pressure=5 MPa.

b) cited from a booklet on ICI methanol synthesis catalysts.

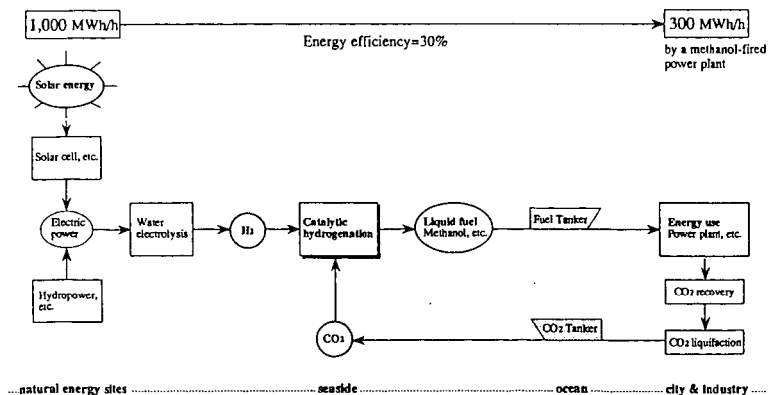


Fig. 1 Global energy network combined with catalytic hydrogenation of CO₂

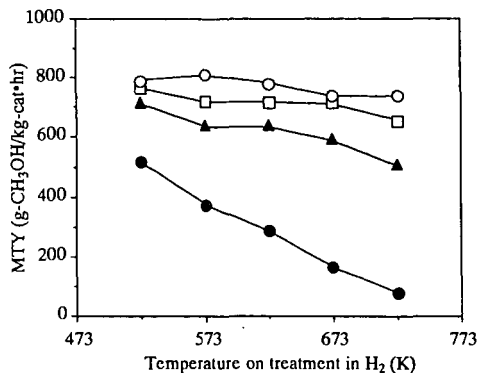


Fig. 3 Activities of various Cu/ZnO-based catalysts as a function of temperature on treatment in a stream of H₂. Reaction conditions were the same as shown in Table 1. O:MCB(Cu/ZnO/ZrO₂/Al₂O₃/Ga₂O₃), □:MCA(Cu/ZnO/ZrO₂/Al₂O₃), ▲:Cu(50)/ZnO(45)/Al₂O₃(5), ●:Cu(50)/ZnO(50)

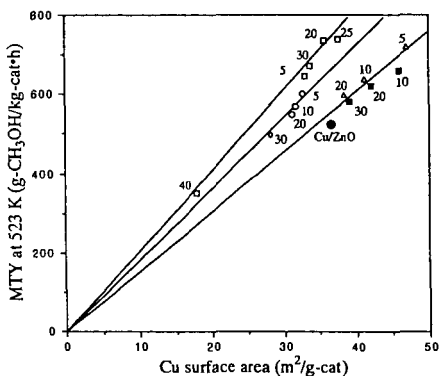


Fig.2 Methanol synthesis activity (MTY) at 523 K as a function of Cu surface area. Reaction conditions were the same as shown in Table 1. The contents (wt%) of metal oxides in the Cu/ZnO-based catalysts are indicated in the figure. Cu content of the catalysts was 50 wt%. □:Cu/ZnO/Ga₂O₃, O:Cu/ZnO/Cr₂O₃, Δ:Cu/ZnO/Al₂O₃, ■:Cu/ZnO/ZrO₂, ●:Cu/ZnO (50/50).

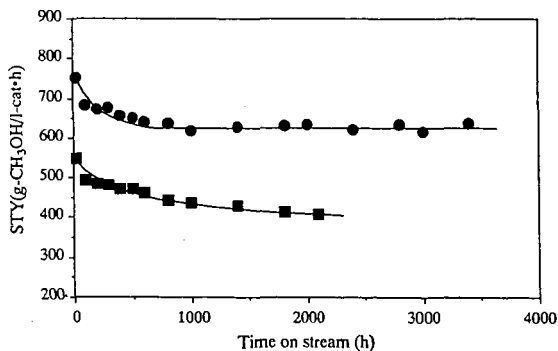


Fig. 4 Change in the activities of a multicomponent catalyst (Cu/ZnO/ZrO₂/Al₂O₃/Ga₂O₃, ●) and a commercial catalyst used for methanol synthesis from syngas (Cu/ZnO/Al₂O₃, ■) during a long-term test of methanol synthesis. The reaction conditions: temperature=523 K, pressure=5 MPa, SV=10,000, feed gas composition=CO₂(22)/CO(3)/H₂(75).

CATALYTIC HYDROGENATION OF CO₂ INTO HYDROCARBONS:
SUPPORT EFFECTS ON Fe AND Fe-K CATALYSTS.

Ki-Won Jun, Soo-Jae Lee, Myuon-Jae Choi and Kyu-Wan Lee
Catalysis Division
Korea Research Institute of Chemical Technology
Taejon 305-600, Korea

Keywords: CO₂ hydrogenation, Hydrocarbons, Support effects

INTRODUCTION

Since accumulation of carbon dioxide in the atmosphere is now regarded as one of the major reasons of the Global Warming, interest in the reutilization of carbon dioxide is on the increase [1-10]. It is desirable for the reutilization of carbon dioxide to develop the technology for the hydrogenation of carbon dioxide to valuable materials such as light olefins or liquid hydrocarbons.

However, relatively little attention has been paid so far to the catalytic hydrogenation of carbon dioxide while carbon monoxide hydrogenation has been extensively investigated with the purpose of utilization of coal as a carbon source. In previous studies [11-16], iron-based catalysts, which are originally used in the Fischer-Tropsch (F-T) reaction, have been applied to the hydrogenation of carbon dioxide to hydrocarbons. According to the results, however, it seems that those catalysts are not satisfactory because they give only small yield of C₂ hydrocarbons with the significant production of carbon monoxide and methane. It seems that the different catalytic properties are required for the hydrogenation of carbon dioxide because the chemical properties of carbon dioxide is different from carbon monoxide. Therefore, more systematic work is necessitated in order to develop suitable catalysts for the production of light olefins or liquid hydrocarbons from carbon dioxide hydrogenation.

While varying potassium content in the alumina-supported Fe-K catalysts, we found that the catalysts having high K content (K/Fe atomic ratio = 0.5-1.0) give considerably high conversion and selectivity to C₂ hydrocarbons and light olefins [17]. In the present work, we have investigated the support effects on Fe and Fe-K catalysts with the hydrogenation of CO₂.

EXPERIMENTAL

Silica gel, γ -alumina and titania (anatase) were used as the support materials. The BET surface areas, pore volumes and average pore diameters of support materials were determined by N₂ adsorption at -196°C adsorption using a volumetric apparatus (Micromeritics ASAP 2400). Characteristics of support materials are listed in Table 1.

Supported iron oxide catalysts with an iron loading of 20%(w/w) were prepared by impregnating silica gel, γ -alumina (Strem, 157m²/g) and titania (anatase) with an aqueous solution of Fe(NO₃)₃·9H₂O. To prepare supported iron-potassium catalysts with K/Fe molar ratio = 0.5), an adequate amount of K₂CO₃ was added into the aqueous solution of Fe(NO₃)₃·9H₂O before impregnation. After the impregnation, the catalyst samples were dried at 383 K for 24 hr and calcined in air at 773 K overnight.

The temperature programmed decarburization was performed with the catalysts reacted with a mixture gas of carbon dioxide and hydrogen at 573 K and 1 atm for 30 min followed by cooling down to room temperature with purging helium. The gas was changed to hydrogen and the temperature of catalyst bed was increased to 923 K with the ramp of 5 K/min. The evolved product was mainly methane and it was analyzed continuously by a flame ionization detector, which gave the temperature programmed decarburization profile.

The catalytic hydrogenation of carbon dioxide was performed in a

continuous fixed bed reactor. The catalyst was reduced in a flow of hydrogen at 723 K for 20-24 hr. After the reduction, the catalyst was brought to the reaction temperature and then the feed changed to the mixture gas of carbon dioxide and hydrogen. Space velocity was 1900 ml/g-cat.h. The products were analyzed by a gas chromatograph (Chrompack CP 9001) equipped with thermal conductivity and flame ionization detectors. Carbon monoxide, carbon dioxide and water were analyzed on a Porapak Q column and the hydrocarbons on a Poraplot Q capillary column. The experimental data were taken after 24 hr of the reaction.

RESULTS AND DISCUSSION

In the temperature programmed decarburization, the surface carbides are investigated by the temperature programmed decarburization, which shows the relative amount and stability of surface carbon species formed during the reaction.

Figure 1 shows the decarburization profile of the supported iron catalysts after treatment at the reaction condition for 30 min. The decarburization profile of the Fe/silica catalyst shows a single peak with a maximum peak temperature of 690 K. However, with the γ -alumina supported catalyst, the profile shows two peaks (685 K and 725 K), which indicates the presence of two types of carbides. The peak appearing at higher temperature (725 K) represents that more stabilized carbide is formed during the reaction on Fe/ γ -alumina. With the titania (anatase) supported catalyst, the profile shows two peaks also, but high temperature shift. The result of the high temperature shift reveals that supporting on titania (anatase) increases the stability of surface carbides on the catalyst. It seems that interaction between iron and supports exists with Fe/ γ -Al₂O₃ and Fe/TiO₂, as compared to the silica supported catalyst. It is likely that the enhancement of carbide stabilization is due to the metal-support interaction.

The hydrogenation of carbon dioxide over supported iron catalysts produces both carbon monoxide and hydrocarbons, and the influence of support on the activity and selectivity of the reaction was examined.

Table 2 shows the results of CO₂ hydrogenation on supported Fe catalysts at 573 K and 10 atm. The conversion data reflect that activities for CO₂ hydrogenation decrease in order Fe/TiO₂, Fe/ γ -Al₂O₃, Fe/SiO₂. This apparently indicates that the catalytic activity is not dependent on the surface area of support material. From the selectivity data, it will be seen that the catalysts Fe/TiO₂ and Fe/ γ -Al₂O₃ show much higher selectivity for hydrocarbons than Fe/SiO₂. Furthermore, Fe/TiO₂ and Fe/ γ -Al₂O₃ give higher selectivity for C₂ hydrocarbons as compared to the silica supported catalyst. Especially, Fe/TiO₂ shows the highest selectivity for C₂ hydrocarbons. These results also indicate that the metal-support interaction exists with Fe/ γ -Al₂O₃ and Fe/TiO₂. The high product selectivity for long-chain hydrocarbons with Fe/TiO₂ might be correlated with the results of decarburization which show that the carbides formed during the reaction are more stabilized by titania (anatase) support. It is reported that iron carbides are responsible for the formation of long-chain hydrocarbons in CO₂ hydrogenation [16].

We found that the promotion of Fe/Al₂O₃ with high K content gives the improvement in the catalytic performance for CO₂ hydrogenation to hydrocarbons [17]. The influence of support on the catalytic performance of Fe-K (K/Fe = 0.5) was examined also. Table 3 shows the results of CO₂ hydrogenation on supported Fe-K catalysts at 573 K and 10 atm. With silica and titania supports the addition of potassium decreases the catalytic activity and selectivity for hydrocarbons. In contrast, with γ -alumina support, the addition of potassium increases the catalytic activity. However, with all catalysts, the addition of potassium increases the selectivity for C₂ hydrocarbons and light olefins. It should

be noted that the combination of Fe, K and γ -alumina makes the catalyst bearing considerably high activity and selectivity. It seems that γ -alumina is not only a support but a kind of promotor in Fe-K/ γ -Al₂O₃.

SUMMARY

The effects of support on CO₂ hydrogenation into hydrocarbons over Fe and Fe-K catalysts have been investigated. The catalysts were prepared by impregnation using silica gel, γ -alumina and titania (anatase) as supports. The results of temperature programmed decarburization showed that weak interaction between iron and support exists with Fe/ γ -Al₂O₃ and strong interaction with Fe/TiO₂. The titania-supported iron catalyst gave much higher conversion and selectivity towards C₂ hydrocarbons than silica-supported iron catalysts. It is likely that the high catalytic activity and selectivity of Fe/TiO₂ are due to metal-support interaction. While potassium was being introduced into the catalysts as a promotor, it was found that potassium increased the selectivity for C₂ hydrocarbons and olefins on all supports, but increased the catalytic activity on only γ -alumina. The combination of Fe, K and γ -Al₂O₃ makes the catalyst highly active and selective for CO₂ hydrogenation to C₂ hydrocarbons and light olefins. It seems that γ -alumina functions as a promotor in Fe-K/ γ -Al₂O₃.

ACKNOWLEDGEMENT

This research being one of the National G7 projects is supported by the Ministry of Science and Technology and the Ministry of the Environment in Korea.

REFERENCES

1. B. Delmon, Appl. Catal. B 1 (1992) 139.
2. J.H. Edwards, Catal. Today 23 (1995) 59.
3. G.C. Chinchon, P.J. Denny, D.G. Parker, M.D. Spencer and D.A. Whan, Appl. Catal. 30 (1987) 333.
4. Y. Amenomiya, Appl. Catal, 30 (1987) 57.
5. K.G. Chanchlani, R.R. Hudgins and P.L. Silveston, J. Catal. 136 (1992) 59.
6. R.A. Koeppe, A. Baiker and A. Wokaun, Appl. Catal. A 84 (1992) 77.
7. S.G. Neophytides, A.J. Marchi and G.F. Froment, Appl. Catal. A 86 (1992) 45.
8. K. Fujimoto and T. Shikada, Appl. Catal. 31 (1987) 13.
9. T. Inui, K. Kitagawa, T. Takeguchi, T. Hagiwara and Y. Makino, Appl. Catal. A 94 (1993) 31.
10. M. Fujiwara, R. Kieffer, H. Ando and Y. Souma, Appl. Catal. A 121 (1995) 113.
11. D.J. Dwyer and G.A. Somorjai, J. Catal. 52 (1978) 291.
12. G.D. Weatherbee and C.H. Bartholomew, J. Catal. 87 (1984) 352.
13. T. Suzuki, K. Saeki, Y. Mayama, T. Hirai and S. Hayashi, React. Kinet. Catal. Lett. 44 (1991) 489.
14. M.-D. Lee, J.-F. Lee, C.-S. Chang and T.-Y. Dong, Appl. Catal. 72 (1991) 267.
15. J.-F. Lee, W.-S. Chern, M.-D. Lee and T.-Y. Dong, Can. J. Chem. Eng., 70 (1992) 511.
16. M.-D. Lee, J.-F. Lee and C.-S. Chang, Bull. Chem. Soc. Jpn., 62 (1989) 2756.
17. P.H. Choi, K.-W. Jun, S.-J. Lee, M.-J. Choi and K.-W. Lee, Catal. Lett., accepted.

Table 1. Characteristics of supports

Support material	BET surface area (m ² /g)	Pore volume (cc/g)	Average pore diameter (Å)
SiO ₂	462	0.731	63
Al ₂ O ₃	157	0.407	104
TiO ₂	10	0.030	118

Table 2. Effects of support on CO₂ hydrogenation performance of Fe catalysts^a

Catalyst	Conv. (%)	Selectivity (C %)		Distribution of HC (C %)			O/P ratio in C ₂₋₄
		CO	HC	C ₁	C ₂₋₄	C ₅₊	
Fe/SiO ₂	22.1	61.6	38.4	59.7	34.2	6.1	0.02
Fe/Al ₂ O ₃	43.9	4.7	95.3	27.1	54.2	18.7	0.01
Fe/TiO ₂	51.3	5.2	94.8	25.2	54.3	20.5	0.05

^aCO₂ hydrogenation at 1900 ml/g/h, 573 K and 10 atm

Table 3. Effects of support on CO₂ hydrogenation performance of Fe-K (K/Fe = 0.5 atom ratio) catalysts^a

Catalyst	Conv. (%)	Selectivity (C %)		Distribution of HC (C %)			O/P ratio in C ₂₋₄
		CO	HC	C ₁	C ₂₋₄	C ₅₊	
Fe-K/SiO ₂	14.2	62.6	37.4	14.1	59.0	26.9	3.20
Fe-K/Al ₂ O ₃	57.7	12.7	87.4	7.1	48.2	44.7	7.11
Fe-K/TiO ₂	8.4	58.1	41.9	16.6	54.3	30.4	1.01

^aCO₂ hydrogenation at 1900 ml/g/h, 573 K and 10 atm

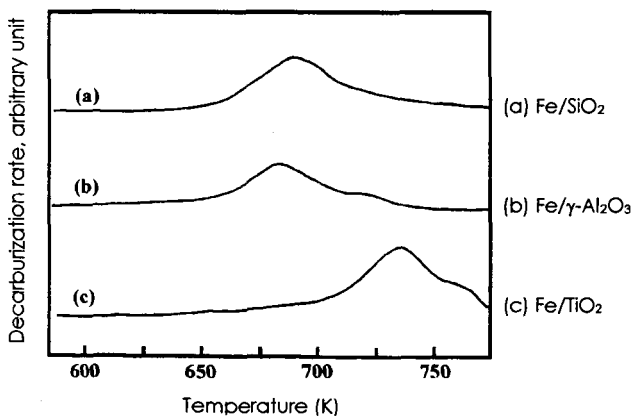


Figure 1. Temperature programmed decarburization of carbides on the catalyst surface.

HYDROGENATION OF CARBON DIOXIDE OVER Fe-ZnO/HY COMPOSITE CATALYST

Masahiro Fujiwara, Roger Kieffer[†], Hisanori Ando, Qiang Xu, Yoshie Souma
Osaka National Research Institute, AIST-MITI, 1 Midorigaoka, Ikeda, Osaka 563, Japan
[†]LERCSI, ECPM Strasbourg, 1, rue Blaise Pascal, 67008 Strasbourg Cedex, France

Keywords: Hydrogenation of carbon dioxide; Composite catalyst; Fe-ZnO catalyst

INTRODUCTION

Fe-based catalysts are often used for various fields of catalytic reactions. F-T (Fischer-Tropsch) reaction is a representative example. It is well known that the Schulz-Anderson-Flory law determines the distribution of hydrocarbons in F-T reaction. To overcome this limitation, the composite catalysts comprised of Fe-based catalyst and zeolite have been examined (1). Although these composite catalysts produced branched hydrocarbons and improved the selectivity of hydrocarbons, the distribution was essentially restricted by the Schulz-Anderson-Flory law in almost cases.

We have already reported (2,3) that hydrocarbons were obtained efficiently from carbon dioxide and hydrogen over another type of the composite catalysts which are prepared by the physical mixing of Cu-based catalysts and zeolite (4). This catalytic system combining methanol synthesis and MTG (Methanol-to-Gasoline) reaction presents a novel method for hydrocarbon synthesis which is free from the Schulz-Anderson-Flory law. We recently found (5) that, in the hydrogenation of carbon dioxide, Fe-ZnO/HY composite catalyst produced hydrocarbons with a similar distribution to the composite catalysts comprised of Cu-Zn-chromate and zeolite (3), while Fe-ZnO catalyst (6) acted as a typical F-T catalyst to afford hydrocarbons with the Schulz-Anderson-Flory distribution. This presentation describes the entire studies of the hydrogenation of carbon dioxide over Fe-ZnO/HY.

EXPERIMENTAL

Fe-based catalysts were prepared by the coprecipitation of the corresponding nitrates using sodium hydroxide. The precipitate was washed five times, dried at 120°C for 6 h and calcined at 350°C for 3 h. The composite catalysts were obtained by the physical mixing of equal amounts of Fe-based catalyst and zeolite. HY [JRC-Z-HY4.8(2)] and NaY [JRC-Z-Y4.8] were provided from the Reference Catalyst of the Catalysis Society of Japan.

The hydrogenation of carbon dioxide was carried out using a pressurized flow-type fixed-bed reactor (2). The two stage reactor reaction was carried out using two separate stainless-steel reactors in series with the same diameter which were heated at the same temperature by the respective furnaces. The carbon monoxide adsorption and dissociation were carried out on a pulse reactor. TPR (Temperature-programmed reduction) measurement was carried out as follows; the catalyst (0.5 g) was heated (temperature increase rate: 10°C/min) in a glass tube reactor under a 10% H₂/He gas flow (31 ml/min). The consumption of the mass number 2 was monitored by an on-line quadrupole mass spectrometer. As the composite catalyst used for the hydrogenation of carbon dioxide was not suitable for this measurement because of carbon remained on the catalyst, Fe-ZnO(4:1)/HY pretreated by pure hydrogen at 350°C for 6 h, calcined at 350°C in air to re-oxidize was employed as a model used composite catalyst.

RESULTS AND DISCUSSION

The drastic differences of the catalytic behaviors of Fe-based catalysts were observed between sole catalysts and the corresponding composite catalysts with HY as shown in Table 1. Especially, the difference between Fe-ZnO(4:1) and Fe-ZnO(4:1)/HY is remarkable. From the hydrocarbon distribution shown in Fig. 1, it seems that Fe-ZnO(4:1) worked as a F-T catalyst and Fe-ZnO(4:1)/HY acted as the composite catalyst which was made of methanol synthesis catalyst and zeolite. The high selectivity of the branched hydrocarbons (For example: iso-C₄/n-C₄=5.5) in the case of this composite catalyst also suggested that these hydrocarbons cannot be produced by F-T reaction and that MTG reaction over zeolite was responsible for this formation. It is also noteworthy that ethylene and propylene were yielded in good selectivities. Most of studies on the composite catalysts for the hydrogenation of carbon oxides were unsatisfactory in the olefin formation so far (1,2). It is also paid attention that the yield of hydrocarbons decreased (from 9.8 to 0.7 C-mol%) over Fe catalyst by the mixing of HY. Fe/HY produced carbon monoxide exclusively, although the decrease of the total conversion of carbon dioxide was not serious (from 18.6 to 15.3%). In other cases such as Fe-Cr₂O₃ and Fe-Al₂O₃, the yields of hydrocarbons were very low. Cobalt catalyst was also studied because it is well known as an active F-T catalyst. In the absence of HY, Co-ZnO (4:1) produced methanol, and hydrocarbons obtained were only methane. Carbon monoxide was formed exclusively over the corresponding composite catalyst. Methanation was decisively inhibited and the hydrocarbon formation by the combination of methanol synthesis and MTG reaction was not observed in this case. Therefore, the noticeable change of the catalytic behaviors of Fe-based catalyst from F-T reaction to methanol synthesis was observed only in Fe-ZnO.

Different composite catalysts such as Fe-ZnO/NaY and Fe-ZnO/SiO₂ were also examined. Although the composite catalyst with NaY produced methanol and dimethylether in high selectivities, the yields of hydrocarbons were poor. The acidity of NaY is not enough to the conversion of methanol into hydrocarbons. However, the formation of dimethylether showed that methanol is obtained in considerable yield and is able to be transformed by acidic mechanism. In the case of Fe-ZnO/SiO₂, hydrocarbons were obtained in the Schulz-Anderson-Flory

distribution, indicating that F-T reaction took place. The acidic HY was required for this change of the catalytic behaviors of Fe-ZnO. In addition, two reactor reaction in series (Fe-ZnO and HY were packed in the first or the second reactor, respectively.) gave methane with high selectivity, and the distribution of hydrocarbons was completely different from the reaction over Fe-ZnO/HY. Therefore, it is evident that the function of Fe-ZnO/HY was not to combine F-T reaction over Fe-ZnO and the reforming reaction of hydrocarbons over zeolite.

Table 1. Hydrogenation of Carbon Dioxide over Fe-Based Catalyst^{a)}

Catalyst ^{b,c)}	Conv. of CO ₂ (%)	Convert to (C-mol%)			
		C ₁	C ₂₊	Oxy ^{d)}	CO
Fe	18.6	1.4	8.4	0.0	8.8
Fe/HY	15.3	0.3	0.4	0.0	14.6
Fe-ZnO	17.2	7.6	3.1	0.5	6.0
Fe-ZnO/HY	13.3	0.4	4.5	0.2	8.2
Fe-Cr ₂ O ₃	28.1	0.5	0.1	0.3	27.2
Fe-Cr ₂ O ₃ /HY	24.9	1.1	0.6	0.0	23.2
Fe-Al ₂ O ₃	19.5	3.2	1.6	0.5	14.2
Fe-Al ₂ O ₃ /HY	15.9	0.3	0.3	0.0	15.3
Fe-ZnO/NaY	6.0	0.1	0.6	3.0	2.3
Fe-ZnO/SiO ₂	11.6	3.9	1.1	1.1	5.5
Fe-ZnO+HY ^{e)}	11.2	2.1	2.0	0.0	7.1
Co-ZnO	7.3	1.0	0.0	2.1	4.2
Co-ZnO/HY	10.2	0.0	0.0	0.0	10.2

a) 350°C, 5 MPa, SV=3000 ml/g-cat./h, H₂/CO₂=3, results after 6 h. b) Fe/Metal=4 (atomic ratio). c) Equal amount of Fe-based catalyst and HY was physically mixed for the composite catalysts. d) MeOH+MeOMe. e) Reaction using two reactors in series; Fe-ZnO in the first reactor and HY in the second reactor, SV=6000 ml/g-cat./h.

The effect of the zinc content on the catalytic behaviors was next examined as shown in Fig. 2. In the case of composite catalysts, Fe/HY and Zn/HY gave hydrocarbons in very poor yields. However, Fe-ZnO/HY with various zinc contents produced hydrocarbons in up to 5% yields, and the selectivities of C₂₊ hydrocarbons in all hydrocarbons were high [Fig. 2.(A)]. Although the zinc content was not a crucial factor in the hydrocarbon synthesis, the best yield of hydrocarbons was observed in Fe-ZnO(4:1)/HY. Fe-ZnO of which zinc content was higher than 33% can be considered as methanol synthesis catalyst, because methanol was obtained in up to 3% yield and the formation of hydrocarbons including methane was very low. It is understandable that hydrocarbons were obtained via MTG reaction in the case of the corresponding composite catalysts. However, the catalytic behaviors of Fe-ZnO(4:1)/HY were not expectable. Fe-ZnO(4:1) was a typical F-T catalyst because of the distribution of hydrocarbons approximately following the Schulz-Anderson-Flory law. On the contrary, in the case of the corresponding composite catalyst, Fe-ZnO acted as a methanol synthesis catalyst rather than a F-T catalyst [Fig. 1.(A)]. It seems that only the solid-solid interaction between Fe-ZnO and HY we noticed before (2) can explain this modification of the catalytic behaviors.

According to XRD measurement, Fe-ZnO with a zinc content lower than 33% prior to the reaction consisted of α -Fe₂O₃ and ZnFe₂O₄. In the catalyst used, the diffraction patterns of α -Fe₂O₃ disappeared completely and those of ZnFe₂O₄ remained. This suggested that α -Fe₂O₃ transformed to other iron species. As the active species for F-T reaction are generally obtained by the reduction of α -Fe₂O₃ via Fe₃O₄, the iron species derived from α -Fe₂O₃ seem to be the catalytic sites for F-T reaction. On the other hand, the diffraction patterns of ZnO and ZnFe₂O₄ were detected in Fe-ZnO with zinc contents higher than 33%. After the reaction, all peaks still remained only to become sharper. The catalytic activity for methanol synthesis of Fe-ZnO(1:2) was higher than that of ZnO as shown in Fig. 2. (A), indicating that not only ZnO (7) but also ZnFe₂O₄ are responsible for methanol synthesis. Fe-ZnO(2:1) can be regarded as pure ZnFe₂O₄, because its content of zinc and iron is similar to ZnFe₂O₄ and only the peaks of ZnFe₂O₄ were observed before the reaction by XRD measurement. However, ZnO as well as ZnFe₂O₄ were detected in the catalyst used. The spinel structure of ZnFe₂O₄ was destroyed during the reaction. Although evaluating the catalytic activity of pure ZnFe₂O₄ was unsuccessful, ZnFe₂O₄ is thought to be a significant component of Fe-ZnO to produce methanol. Moreover, in the case of the composite catalyst, it seems that some iron species from α -Fe₂O₃, which are deactivated not to be active for F-T reaction, promote this methanol synthesis, because the best yield of C₂₊ hydrocarbons was observed in Fe-ZnO(4:1) which is composed of α -Fe₂O₃ and ZnFe₂O₄.

The reaction of carbon monoxide, which is an important intermediate of F-T reaction, is also significant to reveal the influence of zeolite on the catalytic activity of Fe-ZnO. Carbon monoxide adsorption and dissociation experiments also show the change of the catalytic behavior of Fe-ZnO(4:1). The amount of adsorbed carbon monoxide can be related to the number of metallic sites active for F-T reaction. Furthermore, the amount of dissociated carbon monoxide was found to be correlated with the formation of C_{2+} species (8). Especially, this dissociation experiments at 300°C is advantageous so as to know the ability of the catalyst for F-T reaction, because the dissociation of carbon-oxygen bond in carbon monoxide is the first step of hydrocarbon formation in the conventional mechanism of F-T reaction. Table 2 shows the clear differences of the reaction manner of carbon monoxide between on Fe-ZnO and on Fe-ZnO/HY. In the case of Fe-ZnO, the adsorption of carbon monoxide was approximately the same as the reported one of α -Fe₂O₃ (9). The conversion of carbon monoxide at 300°C was very high, whereas only a limited part of carbon monoxide was involved in the Boudouart reaction, and the major part of converted carbon monoxide remained on the catalyst as surface carbon evidenced by carbon analysis. Thus, Fe-ZnO was very active for the dissociation of carbon monoxide to be an effective F-T catalyst. On the contrary, the ability of adsorbing carbon monoxide on Fe-ZnO/HY was extremely low, and the conversion of carbon monoxide at 300°C was lower than Fe-ZnO. From these results, it is obvious that the catalytic activity of Fe-ZnO for F-T reaction was diminished in the composite catalyst by the solid-solid interaction with HY.

Table 2. Adsorption and Reaction of Carbon Monoxide on Catalysts

Catalyst ^{a)}	Fe-ZnO (4:1)	Fe-ZnO (4:1)/HY
CO adsorption (μ mol) ^{b)}	15.4	1.2
CO reaction (%) ^{c)}	Total conv. of CO	78 (29) ^{d)}
	Carbon content (wt-%) ^{e)}	2 (<0.1) ^{f)}
		<0.1 (3.8) ^{f)}

a) Catalyst was pretreated by 20% H₂/N₂ for 5 h at 370°C. b) Measured by the pulse reaction of carbon monoxide (0.5 ml) at room temperature. Per 1 g of Fe-ZnO. c) Measured by the pulse reaction of carbon monoxide (0.5ml) at 300°C. d) Boudouart reaction determined by the amount of carbon dioxide detected by TCD. e) After the nine pulses of carbon monoxide. f) Catalyst used for the hydrogenation of carbon dioxide.

The solid-solid interaction was confirmed by TPR (Temperature-programmed reduction) measurement as well. The first hydrogen consumption which is thought to be caused by the reduction of α -Fe₂O₃ to Fe₃O₄, was observed at 313°C in Fe-ZnO (4:1) and also in Fe-ZnO(4:1)/HY without pretreatment. However, the temperature of the first hydrogen consumption was detected at 337°C in Fe-ZnO/HY pretreated at 350°C. Furthermore, this temperature was shifted to 376°C in Fe-ZnO/HY pretreated at 400°C. The solid-solid interaction between Fe-ZnO and HY changed the reducibility of the Fe-ZnO. These results also show that zeolite crucially affects the characteristics of Fe-ZnO.

From all results discussed here, it is obvious that hydrocarbons are produced by F-T reaction over Fe-ZnO(4:1), and by the combination of methanol synthesis and MTG reaction over Fe-ZnO(4:1)/HY, respectively. Fe-ZnO(4:1) consists of α -Fe₂O₃ and ZnFe₂O₄ in XRD measurement before reaction, and α -Fe₂O₃ produces the active species for F-T reaction by the reduction. F-T reaction works mainly in the presence of carbon monoxide formed by the reversed water-gas-shift reaction or by the decomposition of the methanol. However, in the presence of zeolite, the active sites for F-T reaction are inhibited by the solid-solid interaction with zeolite during the catalytic reaction. This effect was ascertained by the results of the carbon monoxide pulse experiments. The serious deactivation of Fe catalyst for F-T reaction also supports this phenomenon. On the other hand, the methanol formation can be attributed to Fe-promoted ZnFe₂O₄ or the related species. It seems that the influence of zeolite on this methanol synthesis is of minor importance. Therefore, hydrocarbons are produced via methanol over Fe-ZnO/HY. In other Fe-based catalysts such as Fe-Cr₂O₃ and Fe-Al₂O₃, no active species for methanol synthesis was included to result in the extremely poor yields of hydrocarbons over the corresponding composite catalysts. Co-ZnO includes no effective sites for methanol synthesis working with zeolite. The active species for F-T reaction was deactivated completely and, consequently, only carbon monoxide was obtained by the reversed water-gas-shift reaction.

The plausible reaction scheme is illustrated in Fig. 3. Fe-ZnO(4:1) has two kinds of reaction sites, that is, 1) metallic iron or other iron species active for F-T reaction derived from α -Fe₂O₃, and 2) Fe-promoted ZnFe₂O₄ or the related species for methanol synthesis. In the absence of zeolite, the F-T reaction sites exert their activity to produce hydrocarbons with the Schulz-Anderson-Flory distribution, whereas methanol formed is decomposed into carbon monoxide to promote F-T reaction. In the case of the composite catalyst, the F-T reaction sites are deactivated by zeolite while the catalytic activity for methanol synthesis is mostly maintained. Methanol formed which is not decomposed into carbon monoxide reacts over HY to form hydrocarbons with non-Schulz-Anderson-Flory distribution by MTG reaction. As carbon monoxide yielded

from methanol does not take place F-T reaction, the selectivity of carbon monoxide was very high in the case of the composite catalysts.

CONCLUSIONS

Fe-ZnO/HY composite catalyst is an original system which is able to produce olefins with a particular non-Schulz-Anderson-Flory distribution. The Fe-ZnO shows two kinds of catalytic sites, that is, iron species effective for F-T reaction formed from α -Fe₂O₃, and Fe-promoted ZnFe₂O₄ effective for methanol synthesis. In the absence of zeolite, the F-T reaction sites are very active to produce hydrocarbons with the Schulz-Anderson-Flory distribution. On the other hand, the sites for F-T reaction are deactivated and the sites for methanol synthesis promoted by iron species exhibit the catalytic activity in the case of the composite catalyst. Therefore, hydrocarbons were obtained by MTG reaction with a non-Schulz-Anderson-Flory distribution over Fe-ZnO/HY. The mechanism of the deactivation of the active sites for F-T reaction by zeolite is under investigation.

REFERENCES

1. P. D. Caesar, J. A. Brennan, W. E. Garwood and J. Ciric, *J. Catal.*, **1979**, *56*, 274; L. A. Bruce, G. J. Hope and J. F. Mathews, *Appl. Catal.*, **1984**, *9*, 351; Y. G. Shul, T. Sugiura, T. Tatsumi and H. Tominaga, *Appl. Catal.*, **1986**, *24*, 131; F. Nozaki, T. Sodesawa, S. Satoh and K. Kimura, *J. Catal.*, **1987**, *104*, 339; R. J. Gormley, V. U. S. Rao, R. R. Anderson, R. R. Schehl and R. D. H. Chi, *J. Catal.*, **1988**, *113*, 193; K. Fujimoto and K. Yokota, *Chem. Lett.*, **1991**, 559; C.-K. Kuei and M.-D. Lee, *Can. J. Chem. Eng.*, **1991**, *69*, 347; F. A. P. Cavalcanti, A. Yu. Stakheev and W. M. H. Sachtler, *J. Catal.*, **1992**, *134*, 226; Y.-M. Huang, X.-B. Meng, Z.-Y. Dang, S.-Z. Weng and C.-N. Zhang, *J. Chem. Soc., Chem. Commun.*, **1995**, 1025.
2. M. Fujiwara and Y. Souma, *J. Chem. Soc., Chem. Commun.*, **1992**, 767; M. Fujiwara, R. Kieffer, H. Ando and Y. Souma, *Appl. Catal. A*, **1995**, *121*, 113.
3. M. Fujiwara, H. Ando M. Tanaka and Y. Souma, *Appl. Catal. A*, **1995**, *130*, 105.
4. C. D. Chang, W. H. Lang and A. J. Silvestri, *J. Catal.*, **1976**, *56*, 268; T. Inui, T. Hagiwara, O. Yamase, K. Kitagawa, H. Yamaguchi and Y. Takegami, *J. Jpn. Pet. Inst.*, **1985**, *28*, 225; K. Fujimoto, H. Saima and H. Tominaga, *J. Catal.*, **1985**, *94*, 16; K. Fujimoto and T. Shikada, *Appl. Catal.*, **1987**, *31*, 13; K. Fujimoto, H. Saima and H. Tominaga, *Ind. Eng. Chem. Res.*, **1988**, *27*, 920; K. Fujimoto, H. Saima and H. Tominaga, *Bull. Chem. Soc. Jpn.*, **1988**, *61*, 2547; T. Inui and T. Takeguchi, *Catal. Today*, **1991**, *10*, 95; T. Inui, T. Takeguchi and K. Kitagawa, *Proc. 10th Intern. Congr. Catal.*, Budapest, 1992, Elsevier, Amsterdam, 1993, p.1453; T. Inui, K. Kitagawa, T. Takeguchi, T. Hagiwara and Y. Makino, *Appl. Catal. A*, **1993**, *94*, 31.
5. M. Fujiwara, H. Ando, M. Matsumoto, Y. Matsumura, M. Tanaka and Y. Souma, *Chem. Lett.*, **1995**, 839; M. Fujiwara, R. Kieffer, H. Ando, Q. Xu and Y. Souma, submitted.
6. S. L. Soled, E. Iglesia, S. Miseo, B. A. DeRites and R. A. Fiato, *Topics in Catal.*, **1995**, *2*, 193.
7. K. Klier, *Adv. Catal.*, **1982**, *31*, 243.
8. P. Chaumette, Ph. Courty, A. Kiennemann and B. Ernst., *Topics in Catal.*, **1995**, *2*, 117.
9. J. P. Reymond, B. Pommier, P. Meriaudeau and S. J. Teichner, *Bull. Soc. Chim. Fr.*, **1981**, 173.

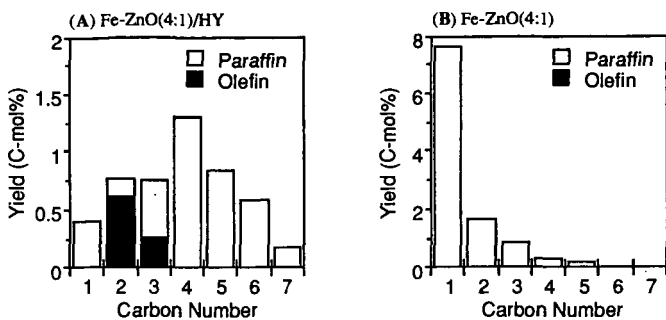


Figure 1. Hydrocarbon Distribution over (A) Fe-ZnO(4:1)/HY and (B) Fe-ZnO(4:1).

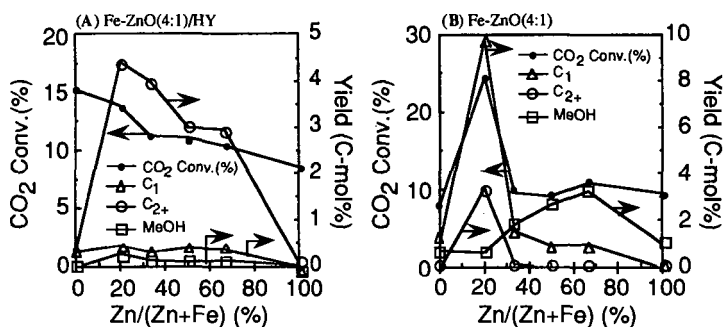


Figure 2. Effect of Zinc Content in (A) Fe-ZnO(4:1)/HY and (B) Fe-ZnO(4:1).

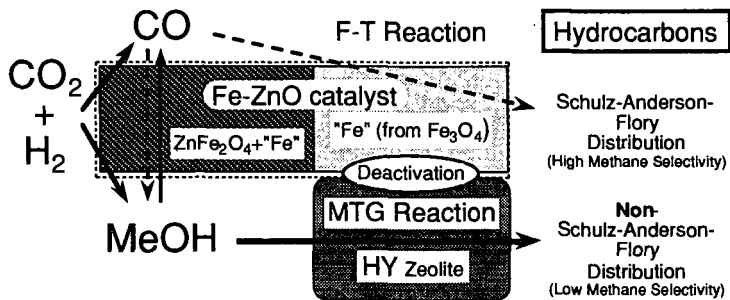


Figure 3. Reaction Scheme of Hydrocarbon Synthesis over Fe-ZnO/HY.

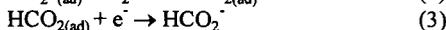
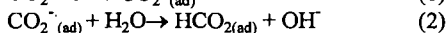
ELECTROREDUCTION OF CARBON DIOXIDE IN AQUEOUS SOLUTIONS AT METAL ELECTRODES

Jan Augustynski, Beat Jermann and Piotr Kedzierzawski
Department of Chemistry, University of Geneva
1211 Geneva 4, Switzerland

Keywords : CO₂ reduction, electrolysis, electrode activation

INTRODUCTION

The quantities of carbon stored in the form of atmospheric carbon dioxide, CO₂ in the hydrosphere and carbonates in the terrestrial environment substantially exceed those of fossil fuels. In spite of this the industrial use of carbon dioxide as a source of chemical carbon is presently limited to preparation of urea and certain carboxylic acids as well as organic carbonates and polycarbonates. However, the situation is expected to change in the future, if effective catalytic systems allowing to activate carbon dioxide will become available. In this connection, the electrochemical reduction of CO₂, requiring only an additional input of water and electrical energy, appears as an attractive possibility. For more than 100 years formic acid and formates of alkali metals were considered as the only significant products of the electroreduction of carbon dioxide in aqueous solutions. The highest current efficiencies, exceeding 90%, were obtained either with mercury or with amalgam electrodes [1-5]. The only comprehensive study regarding kinetics of CO₂ reduction in aqueous solution has been performed by Eyring et al. [6,7] using a mercury cathode. The proposed mechanism includes two charge transfer steps, eq. 1 and 3, separated by a rapid chemical reaction, eq. 2.



The involvement of the radical anion CO₂^{·-} as the intermediate of the reduction at the mercury electrode has also been confirmed by the photoemission measurements [8]. Small amounts of CO₂^{·-} radical anions have as well been identified at a lead cathode using modulated reflectance spectroscopy [9]. It is important to mention, in this connection, that both these cathodes exhibit high overvoltages for the CO₂ reduction (for the mercury electrode, for example, it exceeds 1V at a current density of 1mA/cm²). This is consistent with a strangely negative value of the half-wave potential of the reaction



close to -2V versus standard hydrogen electrode (SHE). Other "soft" metal cathodes, particularly indium and tin allow still to obtain formates with high current efficiencies but at lower overvoltages [10,11]. As all these metals (i.e., Hg, Pb, In and Sn) exhibit high overvoltages for the reduction of water (hydrogen evolution), it was believed for the long time that this must be the necessary characteristic of every efficient electrocatalyst of CO₂ reduction. It was the observation by Hori et al. [12,13] that medium hydrogen overvoltage cathodes, gold, silver and copper are able to promote formation of gaseous products of CO₂ electroreduction which has led to a marked regain of interest in this process. These authors have in fact demonstrated that the electrolysis of slightly alkaline solutions containing alkali metal hydrogen carbonates and CO₂, when conducted at gold and silver leads to the formation of carbon monoxide with faradaic yields attaining 100%. On the other hand, in the case of a copper cathode, the CO₂ reduction continues further to form hydrocarbons-methane and ethylene as well as ethanol. The next paragraphs are devoted to the discussion of the most important features of the CO₂ reduction at these three cathodes (Au, Ag, Cu).

EXPERIMENTAL

All the electrolysis experiments related in the next paragraph were carried out in a two-compartment, tight Teflon® cell. The cathodic compartment contained ca. 30 cm³ of electrolyte and was separated from the anodic one by a Nafion® membrane. The cell was equipped with a cyclic gas flow system. Before each electrolysis run, CO₂ supplied from a gas cylinder was passing through catholyte and gas circuit during 2 h to saturate the solution and to fill the system with CO₂. The total volume of the gas enclosed in the system was 185 cm³ and its circulation rate 12 cm³ min⁻¹. High purity metals rods (7 mm in diameter, 99,999%) served as cathodes. Solutions were prepared from reagent grade, chemicals and twice distilled water. In order to eliminate heavy metal contaminants, a constant current preelectrolysis (25 μA/cm²) was usually conducted for a least 48 h, under nitrogen atmosphere, between two platinum electrodes separated by a Nafion® membrane. 99.99% CO₂ was further purified by passing through an activated charcoal filter before being introduced to the cathodic compartment of the cell and to the gas flow system. Analyses of the gaseous as well as solution products of the reaction were carried out on a Hewlett Packard 5890 Model gas chromatograph. The gas was sampled periodically with a gas syringe during the electrolysis, but products in the electrolyte were analysed once electrolysis run was completed. The chromatographic column Porapak HayeSepQ was employed to determine hydrocarbons and the reaction products in the solution, whereas analyses of CO were performed with the Carbosieve S-II column.

RESULTS AND DISCUSSION

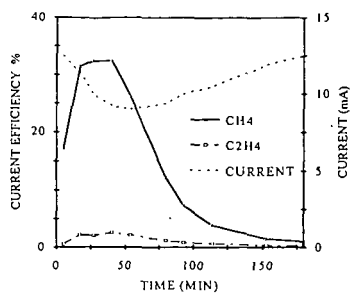
The common feature of the gold, silver and copper cathodes is the occurrence of poisoning during electroreduction of CO₂ [15-18]. This poisoning is less severe for gold, where it results in a decay of the current (at constant controlled potential) without affecting faradaic efficiency of CO formation [17], than in the case of silver for which η (CO) tends to decrease as a function of time [16,20]. The heaviest deactivation is observed for the copper electrode, where CO₂ reduction is virtually stopped after 20-40 min of continuous electrolysis being replaced by hydrogen evolution [18,19]. This problem being mentioned only in few among many papers devoted to this subject [19] it renders difficult any systematic comparison of the results obtained by different authors. In fact, in most cases the described experiments were conducted for very short periods of time corresponding to the passage of about 10C/cm² of the cathode surface. This is just less than the electrolysis duration after which, for example, a severe deactivation of the copper electrode usually starts. This phenomenon is illustrated by a series of curves in Fig. 1. Importantly, the copper electrode behaved in a similar way whether the electrolyte was pre-electrolysed or not. Moreover, XPS (X-ray induced photoelectron spectroscopic) analysis of the copper samples polarized for 2h at -1.72V in both kinds of 0.5M KHCO₃/CO₂ solutions (ie, with and without preelectrolysis) revealed only the presence of Cu, O and C signals. In particular, none of the metal elements present in trace amounts in KHCO₃, such as, for example, Fe, Zn, Cr, Pb or Cd was detected. The time associated with the deactivation of the cathode was no more affected by the degree of purity of the copper metal (99.999% vs. 99.9%). It is to be pointed out that the observed poisoning of the Cu electrode affects selectively the CO₂ reduction while, at the same time, the rate of hydrogen evolution tends to increase (cf. variation of the electrolysis current vs. time in Fig. 1. This kind of behaviour can be expected in the case of formation of the elemental carbon [19] or of a layer of organic products [20,21] at the Cu surface. An in situ electrochemical activation method has been demonstrated to act very efficiently against the inhibition of the copper cathode versus the CO₂ reduction. Such a treatment involves a periodic anodic stripping of the nascent poisoning species from the electrode surface by means of a series of 2-3 rapid voltammetric sweeps, repeated each 5-10 min. over the entire electrolysis run. The electrode activation requires less than

1 percent of the total electrolysis time (i.e., 2-3 s each 5 or 10 min.) and consumes a negligible extra amount of electrical charge (Fig. 2). Application of such a potential program allows high faradaic efficiencies of CH_4 , C_2H_4 and $\text{C}_2\text{H}_5\text{OH}$ to be maintained over long electrolysis runs. As shown in Fig. 3, no electrode deactivation was observed during a 8-days long continuous electrolysis experiment. While the total rate of hydrocarbon formation remained remarkably constant as electrolyses progressed, an increase of the amount of ethylene accompanied by a decrease of the amount of methane were in general observed. These variations in the product distributions are probably associated with the structural changes occurring at the electrode surface.

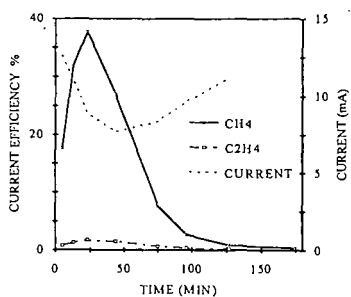
REFERENCES

- [1] M.E. Royer, *C.R. Acad. Sci. Paris* 70 (1870) 73.
- [2] A. Cohen, S. Jahn, *Ber. Dtsch. Chem. Ges.* 37 (1904) 2836.
- [3] R. Ehrenfeld, *Ber. Dtsch. Chem. Ges.* 38 (1905) 4138.
- [4] F. Fischer, O. Prziza, *Ber. Dtsch. Chem. Ges.* 47 (1914) 256.
- [5] M. Rabinovich, A. Mashovets, *Z. Elektrochem.* 36 (1930) 846.
- [6] W. Paik, T.N. Andersen, H. Eyring, *Electrochim. Acta* 14 (1969) 1217.
- [7] J. Ryu, T.N. Andersen, H. Eyring, *J. Phys. Chem.* 76 (1972) 3278.
- [8] D.J. Schiffrin, *Faraday Discuss. Chem. Soc.* 56 (1973) 75.
- [9] A.-W.B. Aylmer-Kelly, A. Bewick, P.R. Cantril, and A.M. Tuxford, *Faraday Discuss. Chem. Soc.* 56 (1974) 96.
- [10] K. Ito, T. Murata, S. Ikeda, *Bull. Nagoya Inst. Technol.* 27 (1975) 369.
- [11] Yu.B. Vassiliev, V.S. Bagotzki, N.V. Osetrova, O.A. Khazova, N.A. Mayorova, *J. Electroanal. Chem.* 189 (1985) 271.
- [12] Y. Hori, K. Kikuchi, and S. Suzuki, *Chem. Lett.* (1985) 1695.
- [13] Y. Hori, A. Murata, K. Kikuchi, and S. Suzuki, *J. Chem. Soc. Chem. Commun.* (1987) 728.
- [14] Y. Hori, K. Kikuchi, A. Murata, and S. Suzuki, *Chem. Lett.* (1986) 897.
- [15] J. Augustynski, A. Carroy, A.S. Feiner, B. Jermann, J. Link, P. Kedzierzawski, and R. Kostecki, Proceedings of the International Conference on Carbon Dioxide Utilisation, pp. 331-338, Bari, 26-30 September 1993.
- [16] R. Kostecki and J. Augustynski, *J. Appl. Electrochem.* 23 (1993) 567.
- [17] P. Kedzierzawski and J. Augustynski, *J. Electrochem. Soc.* 141 (1994) 58.
- [18] B. Jermann and J. Augustynski, *Electrochim. Acta* 39 (1994) 1891
- [19] D.W. De Wulf, T. Jin, and A.J. Bard, *J. Electrochem. Soc.* 136 (1989) 1686
- [20] R. Kostecki and J. Augustynski, *Ber. Bunsenges. Phys. Chem.* 98 (1994) 1510.
- [21] S. Kapusta and N. Hackerman, *J. Electroanal. Chem.* 134 (1982) 197.
- [22] Y. Hori, A. Murata, and R. Takahashi, *J. Chem. Soc. Faraday Trans. 1* 85 (1989) 2309.

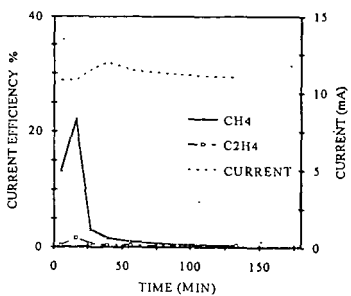
Fig. 1 Changes in the current efficiency of methane and ethylene occurring during first 2 hours of the electroreduction of CO_2 in 0.5M KHCO_3 solution at a copper electrode maintained at a constant potential of -1.72 V (vs. SHE). Temperature 22°C . All copper electrodes etched in a HCl solution [18].



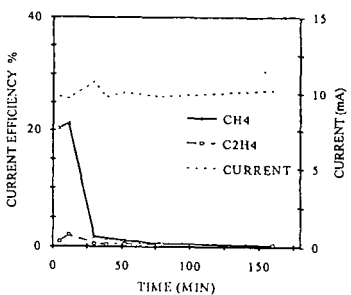
a) 99.9% copper cathode, non-pretreated KHCO_3 solution



b) 99.99% copper cathode, non-pretreated KHCO_3 solution



c) 99.9% copper cathode, pretreated KHCO_3 solution



d) 99.99% copper cathode, pretreated KHCO_3 solution

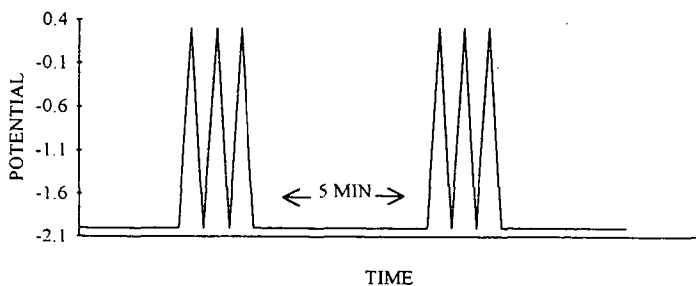


Fig. 2 Schematic representation of the anodic activation treatment (3 successive potential scans at 5 V/s into anodic region) applied to the copper electrode in the course of CO_2 electrolysis.

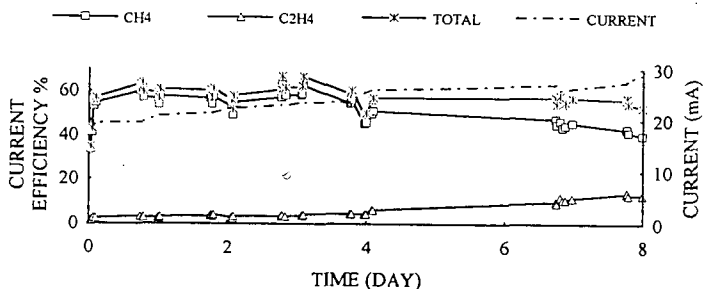


Fig. 3 Results of the 8-days long continuous electrolysis of CO_2 sat. $0.5\text{M K}_2\text{SO}_4$ solution performed at an activated copper electrode (0.28 cm^2) at 22°C . Potential -1.72 V

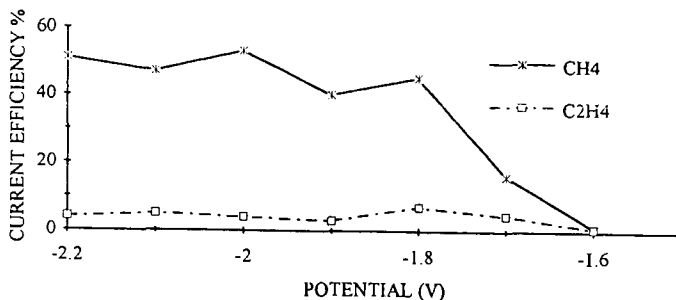


Fig. 4 Steady-state distribution of the CO_2 electrolysis products at the copper electrode as a function of the potential

CO₂ reduction reactions in heterogeneous oxidation
and catalytic cracking processes

Ag.Kh .Mamedov ,Institute Petrochemical Processes ,
30 Telnov st., 370025 , Baku ,Azerbaijan ,(8922) 66-61-50

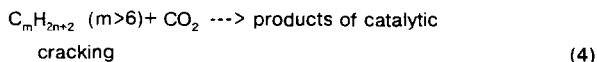
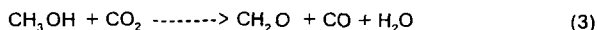
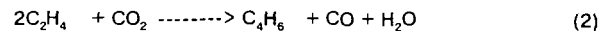
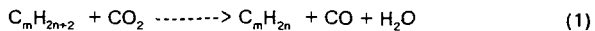
Abstract - The paper contains the results of heterogeneous catalytic activation of CO₂ by various organic substances, generalizes main scientific aspects of the new direction - "Oxidative Catalysis by Carbon Dioxide " ,and develop the petrochemical oxidative processes using carbon dioxide as an oxidant.

I.INTRODUCTION

Catalytic processes of oxidation of organic substances are realized mainly in the presence of oxygen. Low selectivity is characteristic of them due to partial conversion of crude product into CO₂.

In this connection the elaboration of new classes of oxidative processes, based on the nontraditional oxidant -carbon dioxide, is of great importance both to theory and practice and to environmental protection.

We aim to reduce CO₂ by hydrogen evolved from organic compounds IN SITU reaction,i.e. to realize the reduction of carbon dioxide with simultaneous selective oxidation of organic compounds. The reduction of carbon dioxide with alkanes, olefins, alcohols and highmolecular parafins were studied as examples of these reactions:



2.EXPERIMENTAL

Experiments were carried out in a flow vibro-fluidized catalyst bed reactor atatmosphere pressure.Catalysts were prepared by usual impregnation method on SiO₂ and Al₂O₃ usingappropriate metal salts.As metal salts Mn,Cr,Fe,K,Mo,V,W,Ca and Ni were used.These catalysts were dried at 120 °C and calcined at 700-800 °C for 5 hours.

3.RESULTS AND DISCUSSION

Model example of the specified reactions is the oxidation of methane by carbon dioxide. Investigation of CH₄ interaction with CO₂ showed that the traditional regularities of this reaction, known for nickel catalysts, are not valid in the case of manganese system, where there is no formation of carbon even during the reaction of CO₂ in equimolar mixture with CH₄. At 930 °C full conversion of CO₂ and CH₄ was observed, yielding the equimolar mixture of CO+H₂ [1].

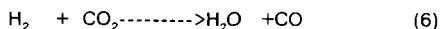
In the reaction of ethane with CO₂ the regularities of alkane oxidation with CO₂ change a little. The reduction of C-H bond energy in the case of ethane leads to the decrease of CO₂ activation temperature.

Reaction of C₂H₆ takes place at 800-830 °C. For simultaneous activation of CO₂ and dehydrogenation of ethane the catalyst has to combine reduction-oxidation and basic functions. K-Cr-Mn-O/SiO₂ system meets these requirements, in its presence the conversion of CO₂ satisfies to 52,3%, that of ethane was -82,6% with ethylene selectivity of 76,8 % [2]. Contents of ethylene and carbon monoxide in the reaction mixture are similar, thus making it possible to use this mixture without separation for carbonylation of ethylene.

The main tendency of propane oxidation with CO₂ is similar to those observed one in ethane conversion. During oxidation of propane by carbon dioxide the products are C₃H₆, C₂H₄, CO. In the presence of K-Cr-Mn-O/SiO₂ catalyst at 830°C olefins yield was 73% with the olefins selectivity of 78%. [3].

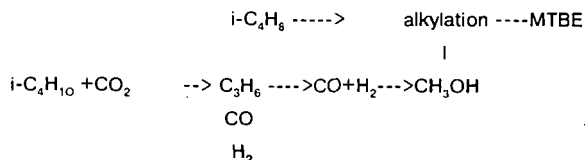
Another regularity is characteristic for isobutane rehydrogenation. The reaction of isobutane with carbon dioxide proceeds mostly by dehydrogenation mechanism followed by hydrogen oxidation. Apparently this is the result of quick decreasing of C-H bond energy in the row from methane to isobutane.

Stoichiometric equations of isobutane conversion can be represented as follows:



The yield of isobutylene in this reaction amounts to 45%, and its concentration was 20% in gas volume. The ratio of CO to H₂ is close to 1 with the high isobutylene selectivity (82 %).

Propylene in this case is by-product. The gas composition allows to recommend the new alternative process of isobutane oxidation by carbon dioxide with production of MTBE:



Combination of endothermic reaction of isobutane dehydrogenation with exothermic one of methanol production from CO+H₂ makes it possible to decrease twice energy consumption of the process and carry it out partially by thermoneutral scheme.

One of the new reactions with CO_2 participation is ethylene oxidation, which is characterized by ethylene dehydrodimerization into butadiene. Cleavage of the C-H bond in ethylene with formation and dimerization of vinyl radicals in the presence of mild oxidant - carbon dioxide, unlike molecular oxygen, proceeds selectively. Conversion of C_2H_4 in this process is not yet high, butadiene yield is 8-10% [4].

During CO_2 reaction with methanol takes place the partial oxidation reaction. On Mo-Mn-O/ SiO_2 catalyst high selectivity of CH_2O formation (90%) takes place [5].

Mechanism of CO_2 reduction during oxidation of organic substances have been established and showed that the properties and reactivity of surface oxygen, generated by carbon dioxide is different essentially from the properties of oxygen, generated from molecular oxygen.

The surface oxygen, generated by carbon dioxide, is homogeneous, but the content of the oxygen, generated by CO_2 in catalyst, is 5-6 times lower, than in the case of reoxidation by molecular oxygen.

The study of the conversion of various organic substances under the condition of stages separation showed that the rate of CO formation during CO_2 reduction in catalyst reoxidation stage is much lower, than the rate of CO formation under stationary conditions. Besides CO_2 reduction and catalyst reoxidation proceed with high rate only at higher temperatures than 700°C . At the same time under stationary conditions CO_2 reduction up to CO occurs mainly from 620°C . In order to elucidate this phenomenon, we carried out experiments with addition of 1-2% H_2 into CO_2 . It has been established, that the addition of 1% H_2 into CO_2 leads to abnormally sharp increase of CO_2 reduction rate to CO.

The observed phenomenon and the initiating effect of H_2 is probably connected with CO_2 reduction proceeding in the presence of hydrogen by new chain mechanism.

This mechanism of CO_2 activation allows to carry out in its presence not only the reactions of reduction-oxidation type, but also of acidic basic ones. Such possibility has been discovered in new reactions of oxidative cracking. Thus, destructive conversion of heptane, which was chosen as a cracking model hydrocarbon in the presence of CO_2 proceeds more efficiently than in its absence [6].

REFERENCES

1. Mamedov Ag. Kh., Mirzabekova S. R., Shirayev P. A., Shashkin D. P., Neftekhimiya., 1, 30 (1990)
2. Mamedov Ag. Kh., Mirzabekova S. R., Neftekhimiya., 3, 250 (1992)
3. Mamedov Ag. Kh., Mirzabekova., Aliev V. S., Neftekhimiya., 3, 335 (1991)
4. Mirzabekova S. R., Mamedov Ag. Kh., Aliev V. S., Neftekhimiya., 2, 114 (1993)
5. Mirzabekova S. R., Mamedov Ag. Kh., Neftekhimiya., 1, 30 (1993)
6. Mirzabekova S. R., Mamedov Ag. Kh., Krylov O. V., Kinetika i kataliz., 1, 184 (1993)

THE SERENDIPITOUS ASSOCIATION OF SEDIMENTARY BASINS AND GREENHOUSE GASES

Brian Hitchon
(Hitchon Geochemical Services Ltd., Box 79088, 1020 Sherwood Drive,
Sherwood Park, Alberta T8A 5S3, Canada)

W.D. Gunter and Thomas Gentzis
(Alberta Research Council, PO Box 8330, Edmonton, Alberta T6H 5X2, Canada)

Keywords: greenhouse gases—aquifer disposal; coalbed methane; carbon dioxide—disposal

INTRODUCTION

Sedimentary basins are the major world repository of fossil fuels—these include petroleum and natural gas, and coal. Industry has grown up over some of the sedimentary basins and in many cases is the source of major greenhouse gas emissions, the most important of which is CO₂. This is a relationship which might be expected. The realization that greenhouse gas emissions may be contributing to global warming has led to research into the mitigation of the effects of these emissions by natural processes, by use in manufacture of chemicals, and by disposal into oceans or sedimentary basins.

One of the more promising avenues of research has been into the disposal of CO₂ into aquifers deep in sedimentary basins. Of the various methods that have been suggested for the disposal of CO₂ in sedimentary basins (in geological structures such as salt domes, in depleted oil and gas reservoirs, in coalbeds, or in aquifers), only that in aquifers involving mineral trapping renders the CO₂ harmless. There is an additional advantage because the volume of pore space available in deep aquifers far exceeds that of salt domes, depleted hydrocarbon reservoirs, or enhanced oil recovery projects. Further, aquifers are widely distributed and, very important, they underlie most point sources of CO₂ emission. Carbon dioxide is an ideal candidate for aquifer disposal because of its high density and high solubility in water at the relatively high pressures that exist in deeper aquifers. This technology is economically viable and is in active development in areas as widely separated as the North Sea and Indonesia. Recently, a suggestion has been made that in addition to disposing of CO₂ into aquifers, it may also be used to remove methane from deep coalbeds. The methane-CO₂ mixture would be separated at the surface and the methane used as fuel, in the normal way. While this would produce more CO₂, the solution to that problem is clear. The CO₂ fraction of the gas that is returned to the surface could be re-used for more methane recovery or disposed of in deep aquifers. This recycling of gases is possible because there is a close association of the fossil fuel resources of sedimentary basins and the greenhouse gas emitting industry that is based on those fuels. We regard this as a serendipitous association.

SEDIMENTARY BASINS AND FOSSIL FUELS

There is a natural association of sedimentary basins (which are accumulations of sedimentary rocks) and fossil fuels through the processes of (1) accumulation of organic matter in the original sediments, (2) its burial to depths where temperatures can change (mature) the character of the organic matter, and (3) in the case of petroleum and natural gas, which are fluids, create structures into which they can migrate and accumulate. These processes result in the development of fossil fuel deposits in the sedimentary basins, and the association is a natural one. Therefore, we should expect a relation between the sedimentary basin, the exploitation of its fossil fuels, and the resulting greenhouse gas emissions.

Despite the wide range of processes that may act on basins, the relation is strong. Any specific basin may be a prolific hydrocarbon producer or not, depending on its geological history. The age of the rocks will also play a part in determining the probability of oil, natural gas, or coal being present. Despite these variables, all sedimentary basins have a common feature in the nature of the fluid that effectively fills all the pore spaces—formation water—for oil and gas are rare fluids in terms of their volume in sedimentary basins, despite their dominant economic importance. The next part of this note deals with the processes that control the movement of formation water in sedimentary basins, because it is this fluid (and the space it occupies), and not oil and gas, that is important for aquifer disposal of CO₂.

HYDROGEOLOGY OF SEDIMENTARY BASINS

It is important to understand that most sedimentary rocks contain pore space between the mineral particles, and the pores are filled with fluid, mostly formation water but occasionally hydrocarbons. Any joints, fractures or faults are also filled with formation water. The original pore space is reduced due to compaction by overlying sediments, but seldom does it disappear altogether even in the most deeply buried rocks. The pore space can also be reduced by the deposition of minerals from the formation water during diagenesis. Conversely, the formation water may be of such a composition as to dissolve minerals from the rock, perhaps even creating more pore space than in the original deposit. There is a chemical balance between the formation water and the rock, through water-rock interaction processes. This balance will be disturbed if CO₂ is injected into the sedimentary rock.

Formation water and other fluids in sedimentary basins are in constant motion, though the rate of movement is generally slow; in the Alberta Basin it is of the order of 1–10 cm/year. Fluids move through the pore spaces of the rocks basically under two forces. In the early history of sedimentary basins the driving mechanism is compaction, with the direction of movement upward and toward the existing shoreline. Once the sedimentary rocks are uplifted, the fluids in the rocks come under the influence of the meteoric water system, and fluid movement in the rocks is controlled by the local topographic elevation. This means that, as

a general rule, major upland areas are regions of recharge and major lowlands are discharge areas. The internal flow system in sedimentary basins is governed by (1) differences in the ability of the different rock types to transmit water, (2) processes due to uplift and erosion that may counter the normal topographically controlled forces, and (3) buoyancy effects due to salinity contrast between formation waters. For our purposes, however, the important thing to remember is that all formation water is in motion, however slow.

Equally important is the fact that different sedimentary rocks transmit water to different degrees. The attribute that describes this ability to transmit water is called permeability. It is unrelated to the absolute porosity (or void space) of the rock, and reflects the degree to which the pores are interconnected; an isolated pore, no matter how large, cannot transmit water. Sedimentary rocks are therefore of three types, with respect to their ability to transmit water—aquifers, aquitards and aquicludes. Aquifers are rocks from which water can be pumped or into which water can be injected; examples include most sandstones and limestones. Aquitards allow movement of water through them over geological periods of time, but pumping and injection are not feasible; examples include shales. Aquicludes are barriers to water movement, and the best example is a salt bed. Note that these definitions are for any rock, so a highly fractured shale or granite can be a good aquifer, depending on the interconnectedness of the fractures. When any fluid is injected into an aquifer it will move out from the injection well under the influence of the imposed pressure. It is important to determine the rate of movement of the injected material and the path that it may be expected to follow. It is the task of the hydrogeologist to determine the natural, undisturbed hydrogeological regime, and then see how the injected material will perturb the natural system. In conjunction with the geochemist, it is possible to predict the effects resulting from the injection of CO₂ into deep aquifers in a sedimentary basin.

AQUIFER DISPOSAL OF CO₂

The most comprehensive evaluation of the aquifer disposal of CO₂ is that carried out by the Alberta Research Council in the Alberta Basin—summarized in Hitchon (1996 and references therein). There are two ways in which CO₂ can be trapped in aquifers: (1) hydrodynamic trapping and (2) mineral trapping. At their most fundamental, these concepts refer to the injection of liquid CO₂ into aquifers, at least 800 m deep, in sedimentary basins, and into situations that either (1) trap the CO₂ into flow systems for geological periods of time (hydrodynamic trapping) or (2) convert the CO₂ to carbonate minerals and thus render it immobile (mineral trapping).

Aquifers suitable for injection of CO₂ must satisfy the following general conditions: (1) the top of the aquifer must be > 800 m deep (at this depth the CO₂ will be in a supercritical state); (2) the aquifer should be capped by a regional aquitard (sealing unit); (3) the aquifer should have enough porosity and adequate permeability; the near-well permeability should be high to allow good injection capability, but the regional permeability should be low so that the residence time of the CO₂ is high; (4) the injection site should be close to the CO₂-emitting source.

The strategy is therefore: (1) to identify the point sources of CO₂ emission; (2) to carry out a detailed, regional-scale hydrogeological analysis of the basin to identify suitable disposal aquifers that satisfy the conditions of depth, capping, permeability and storage capacity; and (3) to carry out detailed hydrogeological, injectivity and geochemical studies for the identified aquifers in the immediate vicinity of the CO₂ sources.

Hydrodynamic Trapping

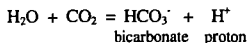
When CO₂, or any fluid, is injected into an aquifer at an appropriate pressure below the fracture pressure, it moves out from the injection well and flows with the natural flow regime. For the Alberta Basin, simple calculations show that times of the order of millions of years will still find the CO₂ within tens of kilometers of the injection site. This geological time-scale trapping of CO₂ in deep regional aquifers as a result of very low flow velocity is called hydrodynamic trapping because it depends on the hydrodynamic regime of the formation waters. Some CO₂ will dissolve in the formation water and travel as a dissolved phase; this allows the processes of diffusion, dispersion and convection to be brought into play. In the Alberta Basin the main transport mechanisms for dissolved CO₂ are molecular diffusion and dispersion; this means that the dissolved CO₂ will spread laterally over a larger mass of rock than if convection was the main transport mechanism, leading to an increased sweep efficiency.

In contrast with CO₂ injection in depleted oil and gas reservoirs, injection into deep aquifers in sedimentary basins has the advantage that it is not limited by reservoir location, size and properties. Thus there are many aquifers in the Alberta Basin suitable for CO₂ disposal; some thin, isolated aquifers in the Cretaceous and post-Cretaceous sedimentary succession in the southwestern part of the basin have the additional significant property that the flow of formation water is downdip, basin-inward, toward hydraulic sinks created by shale elastic rebound as a result of Tertiary-to-Recent erosion. Thus disposal of CO₂—and of any other liquid wastes—in these aquifers in this area will lead to the permanent capture and retention of CO₂ and other wastes (on a geological time scale).

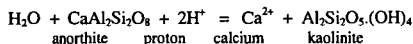
Mineral Trapping

The chemistry of formation water and rock mineralogy play an important part in determining the potential for CO₂ capture through geochemical reactions. Most important, these reactions sequester the CO₂ in immobile form as carbonate minerals.

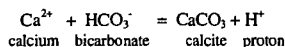
The dominant volatile components that affect mineral dissolution/precipitation reactions are CO₂, H₂S, SO₂ and O₂. These gases dissolve in the aqueous phase and alter the pH through reactions coupled to the dissociation of water. Reactions of the following type occur when CO₂ dissolves in water:



So, initially, some of the CO₂ is held in the aqueous phase as bicarbonate. Only minor amounts of bicarbonate ion and the proton will be produced, no matter how high the pressure of CO₂. This is the reason that formation waters alone are not acceptable sinks for CO₂. However, the proton results in acid conditions in the water and, therefore, the possibility of attack on the silicate minerals present in the aquifer. The attack results in free ions of elements such as Ca, Mg, and Fe being released:



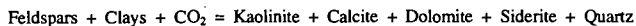
One of the fastest geochemical reactions is the precipitation of calcium carbonate, which occurs when free Ca ions exist in the presence of bicarbonate ions. The reaction produces calcite, and it is this reaction that forms the theoretical basis for the sequestering of the CO₂ as the mineral calcite.



The overall result is just the sum of these three reactions:



There are similar reactions for the formation of calcium-magnesium carbonate (dolomite) and iron carbonate (siderite). For the more complex minerals commonly found in aquifers, the reaction is of the form:



where the CO₂ is permanently fixed as the carbonate minerals calcite, dolomite and siderite. Mineral traps of CO₂ are most effective when the aquifer contains minerals that are proton sinks—that is, the basic silicate minerals such as the feldspars and clay minerals. Consequently, mineral trapping of CO₂ is favoured in sandstone aquifers over carbonate aquifers.

In the Glauconitic Sandstone aquifer of the Alberta Basin, the process of mineral trapping was examined using a water-rock reaction computer model, PATHARC.94. Based on aquifer mineralogy and estimated grain size, and using a formation water from the same aquifer, injection of CO₂ into the Glauconitic Sandstone aquifer was modelled under reservoir conditions. The times for reacting out for the various minerals are: kaolinite 80 years; biotite (as an analogue for glauconite) 100 years; albite (Na-feldspar) 540 years; and K-feldspar 820 years. The resulting mineral assemblage will consist of quartz, and significant amounts of muscovite and siderite. Calculations show that there will be complete equilibrium in 820 years, resulting in the trapping of 6.2 moles of CO₂ relative to each kilogram of formation water in the aquifer.

In summary, in the Alberta Basin, suitably located injection sites far from the basin edge and injection at depths > 800 m result in geologically long times before breakout to the surface occurs—if at all. By that time, if mineral trapping has not occurred, the pressure of CO₂ will have been reduced to such an extent (from the original injection pressure) due to solution, diffusion and dispersion that the breakout will be a harmless event, occurring over a much longer period than the original injection period.

CARBON DIOXIDE, AQUIFERS AND SEDIMENTARY BASINS

Carbon dioxide disposal into low permeability, deep aquifers in sedimentary basins has been shown to be technically feasible and perhaps offers the largest potential for the landlocked areas of the world. A preliminary economic assessment indicated that significant costs will be incurred due mainly to CO₂ capture, purification and compression, and secondarily due to the field facilities required. Despite these expenses, a recent report on the Sleipner Vest Field in the North Sea indicates that the 9.5% CO₂ will be reduced to 2.5% in the sales gas, with about 1 million tonnes per year of the waste CO₂ being injected into Tertiary sandstones; injection is scheduled to start 1996-10-01. An even larger project is the proposed removal of the 71% CO₂ in the natural gas of the Natuna Field in Indonesia—one of the largest gas fields in the world with reported 1270 billion m³ of recoverable hydrocarbon reserves. It is proposed to inject the waste gas into two carbonate aquifers near the field; construction of the facilities is scheduled to last eight years.

The work reported for the Alberta Basin has demonstrated the concepts of hydrodynamic and mineral trapping of CO₂ injected into deep aquifers using information based on a real situation. The capacity of the Alberta Basin aquifers for storage of CO₂ exceeds 20 gigatonnes. The procedures and method of conducting a hydrogeological evaluation of a potential injection site can be emulated world-wide, as can the geochemical modelling. The numerical modelling resulted in nomograms specific to the Alberta Basin, but these nomograms are also viable in other world basins where the basin and reservoir data are similar. Not all sedimentary basins are suitable for injection of CO₂—some because their basin architecture is not suitable, others because they are remote with respect to both distance and appropriate point concentrations of CO₂ emissions. Nevertheless, the results can be used in many world sedimentary basins which are in areas with

fossil fuel exploitation. The Sleipner Vest and Natuna examples cited above indicate that injection of CO₂ into aquifers is now a practical process in the petroleum industry and economically viable. The conclusion of the Final Report of the Joule II Project, *The Underground Disposal of Carbon Dioxide*, is that underground disposal is a perfectly feasible method of disposing of very large quantities of CO₂, such as are produced by fossil fuel fired power plants and most other large point sources of CO₂ (Holloway *et al.*, 1996). The same authors conclude that the next major step in implementing CO₂ storage from power plants should be the demonstration of the storage process. The Sleipner Vest and Natuna projects are essentially large-scale demonstrations of the practicality of the underground disposal of CO₂. It is in this context that the Alberta study (Hitchon, 1996) is offered for world-wide application as an example of the methodology developed to prove the concept of hydrodynamic and mineral trapping of CO₂ in aquifers.

COALBED DISPOSAL OF CO₂

Water and gases are generated during the conversion of plant material to coal, and they are either adsorbed onto the coal or are dissolved into the pore spaces. Methane is the dominant gas (about 95%), with the remaining gases including ethane, CO₂, N₂, He and H₂; H₂S is found only in trace amounts, even in high-S coals, a factor that is related to the nature of the S in coals. The amount of methane formed can be related to the maturity of the coal. The methane associated with coalbeds is termed coalbed methane (CBM).

The attraction of disposing of CO₂ in coalbeds is that it can be coupled directly with the production of methane, a fossil fuel (Gunter *et al.*, 1996). Unlike aquifer disposal of CO₂, the status of research on the recovery of methane from coalbeds using CO₂ is at an embryonic stage. It has been known for two decades that CO₂ is very effective in displacing methane from crushed coal under laboratory conditions; initially, this work was mainly aimed at improving the safety of coal mining. In the late 1980s, through a series of patents, Amoco Corporation demonstrated the potential use of CO₂ and other gases to produce methane from deep coalbeds that are considered unmineable for technological or economic reasons. The injected CO₂ is trapped by sorbing to the coal, thereby displacing the methane which flows to the production well. In 1995, Amoco started their first of a series of three nitrogen pilots, with an additional CO₂-pilot to be tested in the field in 1996.

Conventional or primary CBM recovery has been a practical operation in several coal-fields around the world, most notably in the USA. The process effectively involves the depressuring of the coalbed, which releases the adsorbed methane, as well as methane dissolved in the formation water. Although the method is conceptually simple, there are problems with recovering the methane at the imposed reduced pressure. This results in a delay in methane production and there are large amounts of formation water produced—that must be disposed to the subsurface. The disposal of CO₂ in these methane-rich coalbeds partially solves these problems by (1) increasing the drive pressure, (2) sorbing the CO₂ onto the coal and thereby driving off the methane, hence increasing the rate and the amount of methane produced, and (3) decreasing the relative rate of water production. Consequently, it is expected that this new technology will considerably increase the CBM reserves available for exploitation in North America. The fact that the coalbeds retain most of the CO₂ injected is an additional environmental benefit.

The bulk of the CBM in Canada lies in the Alberta Basin. There is CBM production from many different coal basins in the USA, but around 96% comes from just two—the San Juan Basin, located in southwestern Colorado and northwestern New Mexico, and the Black Warrior Basin in Alabama. Estimates of the CBM resource in North America vary greatly, but by all reasonable estimates, a huge amount exists. In the USA, estimates of CBM resources range from 275 to 649 TCF; in Canada there is considerable more uncertainty, and estimates range over an order of magnitude, from 200 to 3000 TCF.

Experimentally, measured adsorption isotherms for binary and ternary mixtures of CO₂, methane and N₂ show that the equilibrium gas and adsorbate phase compositions differ considerably, and that the total amount of gas mixture adsorbed is strongly dependent on composition and system. Carbon dioxide is the most strongly adsorbed gas, then methane, with N₂ being the least adsorbed. The approximate adsorption ratios are 4:2:1; that is, 4 molecules of CO₂ are adsorbed compared to 2 molecules of methane and 1 molecule of N₂, when comparing pure gases at the same temperature and pressure. Using a very conservative estimate of 150 TCF for the methane resource of the Alberta Basin, the total capacity for sorption by the deep coals of the Alberta Basin is approximately 10 gigatonnes of CO₂—very similar to that estimated for the aquifers of the Alberta Basin.

There is no reported field evaluation such as was carried out by the Alberta Research Council for aquifer injection of CO₂ in the Alberta Basin. However, what work has been done suggests that the concept of disposing of CO₂ or flue gas (a mixture of N₂ and CO₂) from the waste stream of power plants into coalbeds has considerable merit. An evaluation similar to that for aquifer CO₂ disposal is currently being carried out for the Alberta Basin.

CONCLUSIONS

Sedimentary basins, fossil fuel resources, and deleterious greenhouse gas emissions are all closely associated. To exploit the fossil fuels is to produce the greenhouse gases. This does not have to be so. The main greenhouse gas produced by the burning of fossil fuels is CO₂. Rather than discharge CO₂ to the atmosphere, it has been suggested that it be either disposed of in deep aquifers in the same sedimentary basins from which the fuel was extracted, or it be injected into deep coalbeds in the same basins to release the adsorbed methane. The former concept has been evaluated by the Alberta Research Council using field data from the Alberta Basin. Similar methodology is proposed for the Sleipner Vest Field in the North Sea,

and for the Natuna Field, Indonesia. Unlike aquifer disposal of CO₂, injection into coalbeds is not as technologically advanced. However, the concept appears viable, and a proof of concept study is being carried out for the Alberta Basin.

This note has been concerned with two of the five methodologies available for the mitigation of CO₂ emissions from the burning of fossil fuels by disposal in sedimentary basins. These two processes have much in common, and it is pertinent to close with a cartoon (Figure 1) that outlines their main features. Compared to the other three technologies, the two discussed at length in this note potentially can trap much larger volumes of CO₂. The association of sedimentary basins, fossil fuel resources and the mitigation of greenhouse gas emissions from the burning of the fuels is indeed serendipitous.

REFERENCES

Gunter W.D., T. Gentzis, B. Rottenfusser and R. Richardson (1996) *Deep Coalbed Methane in Alberta, Canada: A Fossil Fuel Resource with the Potential of Zero Greenhouse Gas Emissions*. Paper to be presented at the Third International Conference on Carbon Dioxide Removal, Massachusetts Institute of Technology, September 9-11, 1996.

Hitchon B. (editor) (1996) *Aquifer Disposal of Carbon Dioxide: hydrodynamic and mineral trapping—proof of concept*. Geoscience Publishing Ltd. (Box 79088, 1020 Sherwood Drive, Sherwood Park, Alberta T8A 5S3, Canada).

Holloway S., J.P. Heederik, L.G.H. van der Meer, I. Czernichowski-Lauriol, R. Harrison, E. Lindeberg, I.R. Summerfield, C. Rochelle, T. Schwarzkopf, O. Kaarstad and B. Berger (1996) Conclusions and recommendations. In *The Underground Disposal of Carbon Dioxide*. Contract No. JOU2 CT92 0031, Final Report. Chapter 9, p. 320–322. British Geological Survey.

CO₂ Disposal in Aquifers and Coalbeds

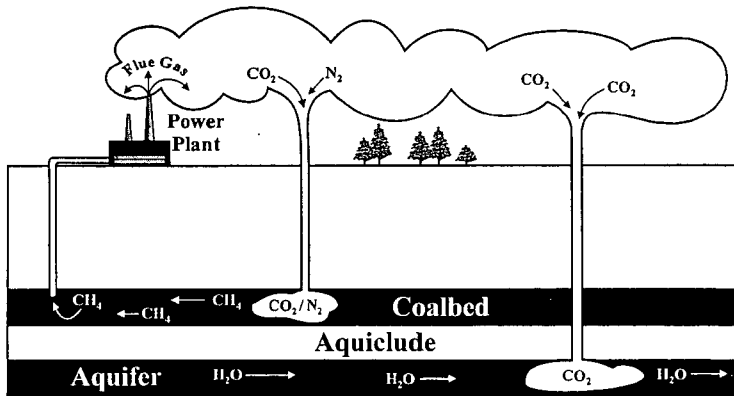


Figure 1. Cartoon showing the relation among sedimentary basins, fossil fuel resources, and the mitigation of CO₂ emissions from the burning of fossil fuels by injection into deep aquifers and the recovery of methane from coalbeds.

IS CO₂ DISPOSAL POSSIBLE?

W.S. Fyfe, R. L veill , W. Zang, Y. Chen
Dept. Of Earth Sciences,
University of Western Ontario
London, Ontario, Canada

Keywords: deep CO₂ fixation, deep biosphere

INTRODUCTION

Recently, Moore and Braswell¹ have reviewed the present state of knowledge of the carbon cycle. As they state: "the carbon cycle is still not adequately understood or quantified globally. Using averages for the 1980's, sources of atmospheric CO₂ exceed identified sinks by 1.8 - 1.2 PgC per year". It is interesting to examine their diagram of the global carbon cycle, and to note that there is essentially no attention given to processes deep in the earth's crust. One of the most interesting recent observations on the nature of the biosphere has been the discovery of thriving colonies of microorganisms at depth². While workers on the alteration of seafloor basalts had suggested the actions of deep organisms, problems related to possible deep bio-corrosion of nuclear waste containers have stimulated more careful observations. Pedersen³ has reviewed the present state of knowledge, and reported the present record of microorganisms at depths of 4.2 km below the surface, at temperatures up to 110°C.

CO₂ AND THE THREAT OF GLOBAL WARMING

Emissions of greenhouse gases, including CO₂, are on the rise. In developing countries, emissions are increasing the fastest and may soon equal those of developed countries. In countries like India and China, coal and other fossil fuels will continue to be a major source of energy for the next few decades. Thus emissions will continue to rise. Although programmes for reductions in greenhouse gas emissions are needed and encouraged, the inadequate actions by governments may soon make it necessary to develop alternative and more direct strategies to reduce the amount of greenhouse gases being emitted to the atmosphere. Currently, research on such strategies revolves primarily around three main ideas: disposal of CO₂ in the oceans, in deep aquifers, and in oil or gas reservoirs (IEA³). Another strategy involves the disposal of CO₂ in the form of carbonate minerals (Seifritz⁴; Dunsmore⁵; Lackner et al.⁶; Fyfe et al.⁷). In nature, such a process occurs on a global scale during the weathering of silicate minerals. Typical of such reactions are:



Anthorite Kaolinite Calcite/Aragonite



Forsterite Serpentine Magnesite



Fayalite Siderite Silica

This natural sink of CO₂ accounts for nearly 80% of the sum of all carbon sinks. These reactions are exothermic. It has also been shown that these reactions can be catalyzed by microorganisms, such as cyanobacteria (Ferris et al.⁸; Tazaki et al.⁹). Thus, it is possible to enhance this 'natural' process to remove significant amounts of CO₂ from fossil fuel plants and from the atmosphere? Could CO₂ be pumped underground in suitable rock formations where microbial populations are plentiful? Can we enhance the growth of these microorganisms in situ to make the whole process feasible, a sort of bioremediation of the atmosphere? The exothermic nature of the reactions is an added bonus as geothermal energy could be used to partially 'fuel' the operation, make it more economically feasible, and produce useful warm water.

CO₂ DISPOSAL

Seifritz⁴ was one of the first to point out that the natural weathering of silicates resulting in carbonate mineral formation could potentially be enhanced as a way of permanently disposing of

CO₂. Two problems were initially acknowledged: a sufficiently large source of Ca (and Mg-Fe) and the kinetics of the silicate-to-carbonate reaction. Dunsmore⁵ suggested the evaporitic salts and brines of the Alberta Sedimentary Basin would provide an ample source of Ca and Mg, which could be transformed into carbonates. The advantage of using this basin is that it is in the heart of the fossil-fuel industry in Canada where existing infrastructures could potentially be modified for CO₂ transport and disposal. Lackner et al.⁶ equally showed that common silicate minerals like olivine and plagioclase in rocks could also act as sources of Ca and Mg. As for the kinetics of reactions, microorganisms can enhance the rate of silicate weathering by producing organic acids (Hiebert and Bennett)¹⁰ and catalyze carbonate precipitation by acting as nucleation sites for mineral growth (Ferris et al.⁷; Tazaki et al.⁹). Storage of CO₂ in carbonate minerals has also been briefly discussed in relation to aquifer disposal (IEA³; Bachu¹¹) and ocean dumping (Harrison et al.¹²).

MICROBES, EXTREME ENVIRONMENTS, AND BIOMINERALIZATION

Microorganisms are able to survive in a wide variety of harsh environments, ranging from low to high temperatures, highly acidic to highly alkaline, saline, and dry conditions (Edwards¹³). The upper limit for thermophilic bacteria appears to be ~ 110°C, with some species showing optimum growth at temperatures as high as 105°C (Edwards¹³). However, many workers believe this upper limit could in fact be as high as 150°C, providing that the pressure is sufficiently high to increase the boiling point of water (Edwards¹³; Gold¹⁴). At deep sea hydrothermal vents, barothermophilic bacteria can also withstand immense pressures in addition to the elevated temperatures. Also bacteria can survive in very high concentrations of CO₂ at these vents (Childress et al.¹⁵).

Bacteria are not only ubiquitous at the Earth's surface and at deep-sea vents, but within the lithosphere as well. Bacterial populations have been found at over 4000 m deep in boreholes drilled into crystalline rocks in Sweden, in deep thermal groundwaters, in oil bearing sedimentary rocks, and over 1000 m deep in a basaltic aquifer (Pedersen²; Szewzyk et al.¹⁶; L'Haridon et al.¹⁷). In the latter case, the bacteria appear to derive their energy solely from hydrogen produced by geochemical reactions.

Microorganisms are known to influence carbonate mineral formation in a variety of environments from cold waters on lava plains in Iceland (Ferris et al.⁷; Tazaki et al.⁹) to hot springs in Kenya and New Zealand with water temperatures well above 90°C (Jones and Renault¹⁸). Biomineralization of Fe-Mn oxides and sulphides at high temperatures and pressures has also been reported from deep sea hydrothermal vents (Juniper and Tebo¹⁹). At these vents, microorganisms are also involved in the transformation and weathering of existing hydrothermal deposits.

WORK IN HAWAII AND ICELAND

In both Hawaii and Iceland, secondary carbonate minerals develop as weathering products from Ca and Mg silicates in fractures, cracks, pores, and in large sea caves of basaltic rock. Carbonate minerals identified by XRD include calcite (CaCO₃) (see fig. 1) aragonite (CaCO₃), magnesite (MgCO₃), hydromagnesite (Mg₅(CO₃(OH)₂ · 4H₂O) and dolomite ((Ca,Mg)CO₃). Other minerals such as clays and silica were also identified as weathering products.

Carbonate minerals were found in association with extensively fractured basaltic lava rocks in Iceland. These minerals occur in thin crusts on weathered basalt and their formation was shown to be mediated by microorganisms (Ferris et al.⁷). Calcite forming in a hot spring microbial mat in Iceland has also been shown to be influenced by microorganisms, in particular cyanobacteria (Tazaki et al.⁹).

In Hawaii, carbonate minerals appear to precipitate from meteoric waters trickling down the interior surfaces of large sea caves. The meteoric waters in the caves are most likely rich in organics as the exterior surface is densely vegetated. The carbonates occur in thin coatings (< ~5 mm) on the interior surface of the caves and in the near-surface pores, cracks and vesicles of the basalt 'host rock'. Our preliminary calculations show that a significant part of the missing carbon dioxide of the carbon cycle could be explained by such processes.

REFERENCES

1. Moore, B.; Braswell, B.H. *Ambio* 1994, 23, 4-12.
2. Pedersen, K. *Earth Sci. Rev.* 1993, 34, 243-260.
3. IEA. 1994. Carbon disposal from power stations. International Energy Agency Greenhouse Gas R&D Programme, Gloucestershire, U.K.
4. Seifritz, W. *Nature*, 1977, 345, 486.

5. Dunsmore, H.E. *Energy Conversion & Management*, **1992**, 33, 565-572.
6. Lackner, S.; Wendt, C.H.; Butt, D.P.; Joyce, E.L.Jr.; Sharpt, D.H. *Energy*, **1995**, 20, 1153-1170.
7. Fyfe, W.S.; Zang, W.; Chen, Y.; Léveillé, R. *Chemical and Engineering News*, **1996**, April 8, 5.
8. Ferris, F.G.; Weise, R.G.; Fyfe, W.S. *Geomicrobiology Journal* **1994**, 12, 1-13.
9. Tazaki, K.; Ishida, H.; Fyfe, W.S. Clays controlling the environment. **1995**, 30-37.
10. Hiebert, F.K.; Bennet, P.C. *Science*, **1992**, 258, 278-281.
11. Bachu, S.; Gunter, W.D.; Perkins, E.H. *Energy Conservation and Management*, **1994**, 35, 269-279.
12. Harrison, W.J.; Wendlandt, R.F.; Sloan, E.D. *Applied Geochemistry*, **1995**, 10, 461-475.
13. Edwards, C. *Microbiology of extreme environments*, Open University Press, **1990**.
14. Gold, T. *Proceedings of the National Academy of Science, USA*, **1992**, 89, 6045-6049.
15. Childress, J.J.; Lee, R.W.; Sanders, N.K.; Felbeck, H.; Oros, D.R.; Toulmond, A.; Desbruyeres, D.; Kennicutt, M.C.; Brooks, J. *Nature*, **1993**, 362, 147-149.
16. Szewzyk, U.; Szewzyk, R.; Stenstrom, T.-A. *Proceedings of the national Academy of Science, USA*, **1994**, 91, 1810-1813.
17. L'Haridon, S.; Reysenbach, A.-C.; Gleinat, P.; Prieur, D.; Jeanthon, C. *Nature*, **1995**, 377, 223-224.
18. Jones, B; Renault, R.W. *Canadian Journal of Earth Sciences*, **1996**, 33, 72-83.
19. Juniper, S.K.; Tebo, B.M. *The microbiology of deep-sea hydrothermal vents*, CRC Press. **1995**, 219-253.

Figures

Fig. 1. SEM image showing filamentous microorganisms on mineral surfaces of Hawaii basalt. The arrow points to CaCO₃ crystals.



A

MODELING THE OCEANIC STORAGE OF FOSSIL FUEL EMISSIONS

Arturo A. Keller, Charles J. Werth
Department of Civil Engineering, Stanford University, Stanford, CA 94305

and
Robert A. Goldstein
Electric Power Research Institute, Palo Alto, CA 94303

KEYWORDS: global carbon cycle, ocean disposal, fossil fuel emissions

ABSTRACT

We use the GLOCO model to analyze the potential for oceanic storage of carbon dioxide emissions from fossil fuel combustion, as well as the effect on atmospheric CO_2 (pCO_2) concentration. From a sensitivity analysis of the global carbon cycle, we find that the rate of transport of carbon to the deepest oceanic layers is rather insensitive to the atmosphere-ocean surface gas exchange coefficient, but to a larger extent on the upwelling velocity. The location of the carbon emissions, whether they are released in the atmosphere or in the middle of the oceanic thermocline, has a significant impact on the maximum pCO_2 subsequently reached, suggesting that oceanic burial of a significant fraction of carbon emissions (e.g. via clathrate hydrides) may be an important management option for limiting pCO_2 buildup. The effectiveness of ocean burial decreases asymptotically below about 1000 m depth, considering a one-dimensional ocean model, i.e. perfect mixing at the various ocean levels where the carbon is injected. With a constant emissions scenario (at 1990 levels), pCO_2 rises to 501 ppmv by the year 2100 if all the emissions go to the atmosphere. With ocean burial of 50% of the fossil fuel emissions at a depth of 1000 m, pCO_2 rises only to 422 ppmv. An alternative scenario looks at stabilizing pCO_2 at 450 ppmv; with no ocean burial of fossil fuel emissions, the rate of emissions has to be cut drastically after the year 2010, whereas oceanic burial of 2 GtC/yr allows for a smoother transition to alternative energy sources.

INTRODUCTION

Capturing carbon dioxide emissions at the smokestack and injecting them into the ocean has been proposed by Marchetti (1977), Hoffert *et al.* (1979), Liro *et al.* (1992), Golomb *et al.* (1992), Kheshgi *et al.* (1994) and others. These previous studies have relied on simple oceanic box models, and have mostly been used to analyze the response of a pulse injection rather than the projected ramp increases in anthropogenic carbon dioxide emissions due to fossil fuel combustion, and neglecting the impact of carbon storage in terrestrial biomes in both the transient and equilibrium carbon cycle response.

For this analysis, we use the GLOCO model (Hudson *et al.*, 1994), a global carbon cycle model with a mechanistic description of physical and biogeochemical processes in the terrestrial biomes and oceans. The model considers eight terrestrial biomes, two oceans (high and low latitude, each broken further into surface and deep layers) and one well-mixed atmosphere. Complete atmospheric mixing is assumed since the model's time step is one year. The model allows the input of different anthropogenic carbon emissions (CO_2 and CH_4), from industrial as well as agricultural and forestry activities (including land-use changes). Temperature of each biome or ocean can be independently modeled as a function of atmospheric CO_2 concentration.

The oceanic carbon cycle model used in GLOCO is based on the HILDA model (Siegenthaler and Joos, 1992), an outcrop-diffusion model. In addition to discerning between high and low latitude oceans, the model has a significant spatial resolution in the vertical direction, with 68 layers of deep low-latitude ocean. Chemical equilibrium controls the final distribution of carbon. GLOCO considers the dissociation of water, carbonic, boric and dissolved organic carbon-based acids, as well as the assimilation of carbon to particulate organic carbon (POC) and dissolved organic carbon (DOC), deposition of calcium carbonate in sediments and remineralization of POC and DOC. Each layer is considered to reach equilibrium rapidly, but due to transport limitations, the system as a whole can take thousands of years to achieve equilibrium once it is perturbed. The non-linear chemical equilibrium is coupled with convection-diffusion processes. Carbon is also transported downward to the deep ocean by the oceanic "biological pump".

The terrestrial biome models are based on a generic biome module describing photosynthesis, respiration and growth by vegetation, and microbial decomposition of plant litter and soil organic matter, with parameter values for each biome: temperate, boreal and tropical forests, grasslands, woodlands, tundra, deserts and agriculture. Carbon and nitrogen are cycled within the biome; these nutrients are allocated to the various plant tissues, and the fluxes of carbon and nitrogen in and out of the biome are considered. The rates of the biological processes are temperature dependent, to incorporate the effect of potential temperature rise in the coming centuries.

We assume that the carbon dioxide from fossil fuel combustion would be injected as a clathrate hydrate, which has been shown (Sakai *et al.*, 1990; Saji *et al.*, 1992) to form a stable phase at the pressure, temperature and salinity of the deep ocean (>500 m). Our analysis has two major assumptions. First, we assume that the injected clathrate dissolves and mixes completely and instantaneously at the depth it is injected in the low-latitude ocean. In fact, the clathrate should sink, due to the higher density of the clathrate hydrate relative to the surrounding water, and the clathrate phase should be even more stable at greater depths. Our second simplification is to neglect calcite dissolution in the bottom waters of the ocean which is expected to result in additional long term storage of carbon (Hoffert *et al.*, 1979; De Baar, 1992). Our simplifications are overall conservative and would tend to underestimate the additional storage of carbon in the deep ocean. The assumption that mixing at the injection depth is instantaneous may be conservative or not depending on the local water transport, i.e. upwelling or downwelling.

SENSITIVITY OF OCEAN TRANSPORT PARAMETERS

Considering that most of the carbon emitted to the atmosphere will eventually end up in the oceans (Keller and Goldstein, 1994), and that the approach to equilibrium is constrained mostly by oceanic physical transport, we sought to determine how important was the choice of ocean transport parameter values to reaching equilibrium. For example, there are a number of studies on the atmosphere-ocean gas-exchange coefficient (Robertson and Watson, 1992; Broecker and Maier-Reimer, 1992; Stanton, 1991; Volk and Bacastow, 1989), and its spatial and temporal variability (Etcheto *et al.*, 1991; Erickson, 1989). Values of the gas-exchange coefficient vary by more than an order of magnitude. How significant is this in terms of our analysis?

Another important parameter is the upwelling velocity of deep water in lower latitudes. Upwelling brings cold, nutrient rich water to the surface, and thus a larger upwelling velocity may increase the rate of oceanic net primary productivity, increasing the flux of carbon to DOC and sediment pools (Bacastow and Maier-Reimer, 1991; Baes and Killough, 1986) resulting in a larger carbon storage. In addition, from a mass balance on water, a larger upwelling velocity would result in a larger downward water flux at higher latitudes, carrying carbon-enriched surface waters to greater depth.

The parameter values used in the calibration of the GLOCO model correspond to those in the oceanic HILDA model, which has been used to study the distribution of radioactive tracers, matching the measured concentration profiles adequately. Given the variability in the published values of these two transport parameters, we studied the effect of increasing or decreasing them by an order of magnitude, which covers more than the published variability in parameter values. A pulse of 594 Gt C is instantaneously released in the atmosphere, to simulate a doubling of the atmospheric CO_2 (pCO_2) from its preindustrial value, and then the system is allowed to relax to a new equilibrium situation. The effect on pCO_2 is presented in Figure 1. The base case considers the calibration parameter values for GLOCO.

Increasing or decreasing the gas-exchange coefficient by a factor of 10 has very little impact on the rate at which equilibrium is reached. If the gas-exchange rate is increased by a factor of 10, there is virtually no change in the pCO_2 profile, when compared with the base case. Analyzing the profiles of dissolved inorganic carbon (DIC) in the ocean, we observe that only the top ocean layers, above the thermocline, are affected, and only by a small amount. Reducing the resistance of gas transfer to the surface of the ocean does not significantly increase the overall rate of carbon storage in the ocean because it is limited by downward transport. And the additional carbon in the surface waters does not result in additional uptake as DOC or POC, since carbon is not the limiting nutrient. The atmospheric response is slightly larger for the case where the gas-exchange coefficient is reduced by a factor of 10. In this case, the resistance to gas transfer does result in slightly larger atmospheric concentrations, in particular at early times. As expected, the equilibrium atmospheric concentration is the same for all cases.

If our current estimate of the upwelling velocity was off by a factor of 10, the impact on our predictions of future pCO_2 would be important only in the case of much greater upwelling velocities. If the upwelling velocity was $1/10^{\text{th}}$ of our current estimate, the effect would be minimal in terms of our pCO_2 predictions. However, an actual upwelling velocity ten times larger than our current estimates would result in significant increase in carbon storage both in DOC and sediments. Given that oceanic carbon storage would increase, the equilibrium would shift and less carbon would then be stored in the terrestrial biomes, as well as in the atmosphere. The net reduction in total carbon stored in the atmosphere is on the order of 35 Gt C. The impact is greatest at larger times (>200 years).

OCEAN BURIAL OF CARBON FROM FOSSIL FUEL COMBUSTION

If the same 594 Gt C pulse is injected into the ocean at a depth of 500 m as DIC, considering the calibration transport parameter values, the global carbon cycle approaches equilibrium relatively fast, redistributing carbon in the ocean, and releasing carbon to the atmosphere (Figure 1). In less than two hundred years, pCO_2 practically reaches its equilibrium value. There is no change in DOC or oceanic carbon sedimentation rates, and the approach to equilibrium is actually only delayed by the terrestrial biome uptake of the incremental atmospheric carbon. In effect, we have "bought" a delay of about 200 years in the maximum pCO_2 by burying the fossil fuel emissions at a depth of 500 m. What is the effect of burying the emissions at different depths? Can we have a bigger impact by injecting at deeper levels? And at what point does this approach become less effective?

Considering the same pulse (a 2x carbon pulse, based on the preindustrial atmospheric concentration), we studied the effect on pCO_2 of injecting at deeper ocean levels (Figure 2). All the atmospheric CO_2 profiles approach the same equilibrium value of around 325 ppmv after 750 years. However, the maximum pCO_2 is reached much later depending on the injection depth. And the maximum pCO_2 is lower as we increase the injection depth (Figure 3). We can continue to inject at lower and lower depths, but this analysis suggests that going deeper than 1500 m is not effective in terms of reducing the maximum pCO_2 , since we reach an asymptotic value. In fact, it may be argued that the difference in the maximum pCO_2 between injecting at 1000 m and injecting at 1500 m, of less than 8 ppmv, does not justify the larger expense of injecting the carbon 500 m deeper.

Studying the response of the global carbon cycle to a pulse injection is useful because it is easier to compare among models, without the added complexity of varying scenarios. However, the real perturbation to the global carbon cycle is not an instantaneous pulse but rather a continuous increase in anthropogenic carbon emissions to the atmosphere. Currently the system has already been perturbed significantly from its preindustrial levels, so that if we suddenly stopped all anthropogenic emissions to the atmosphere, the system would relax to a new equilibrium position. We studied three potential carbon emissions scenarios. The first involves achieving the current target of voluntarily limiting carbon emissions to their 1990 levels for all nations. The second carbon emissions scenario is the IPCC 92a scenario (Business as Usual). The third scenario looks at limiting carbon emissions such that pCO_2 stabilizes at 450 ppmv. To achieve the stabilization goal, carbon emissions from fossil fuel combustion and land use changes have to be drastically reduced in the next century. Whether we can make the transition to this lower rate of emissions is not entirely clear. Ocean burial of some of the emissions would make the transition easier, by providing some additional time for all nations to switch to either renewable or non-fossil fuel based energy sources.

In Figure 4 we present the result of the first scenario, i.e. carbon emissions at constant 1990 levels. Even with this lofty goal, pCO_2 rises from 354 ppmv in 1990 to 525 ppmv by the year 2100, or 48%. As we increase the fraction of the emissions that is buried in the ocean at a depth of 1000 m, beginning in the year 2000, the maximum pCO_2 by the year 2100 drops significantly. The technology for ocean burial is not in place to begin capturing, transporting and injecting carbon into the ocean by the year 2000, and significant additional modeling with a three-dimensional ocean model must be done before we know where the injection points may be, but this analysis indicates that there may be considerable reduction in the growth of pCO_2 in the future, by burying a fraction of the emissions directly in the ocean.

What if there is no action to reduce carbon emissions, and they grow as projected by the Business as Usual scenario of the IPCC? GLOCO projects a doubling of pCO_2 by the year 2100, to more than 700 ppmv (Figures 5a, 5b). If we followed the same emissions trajectory, but then decided that we should put an arbitrary cap on the maximum pCO_2 of 450 ppmv, as suggested by the 1994 IPCC modeling exercise (Enting et al., 1994) how long could we continue on the Business as Usual trajectory? And what would have to be the needed reduction in carbon emissions to reach the 450 ppmv cap? In Figure 5a we present the fossil fuel emissions trajectory obtained by inverting the GLOCO model. We could maintain the Business as Usual trajectory until the year 2010, at which time we would have to drastically reduce emissions from 8 GtC/yr to around 1 GtC/yr by 2060. The resulting

pCO₂ profile is shown in Figure 5b. If by the year 2010 we had implemented the technologies needed for burying 2 GtC/yr directly into the ocean at a depth of 1000 m, then we could add this level of fossil fuel emissions (2 GtC/yr) to the drastic carbon emissions trajectory, buying some time for the implementation of other energy sources, and making a wiser use of our fossil fuels (Figure 5a and 5b).

CONCLUSIONS

We have analyzed the sensitivity of the GLOCO model, a global carbon cycle model, to two major oceanic transport parameters. The actual value of the globally averaged gas-exchange coefficient is not well known, but our analysis suggests that in terms of the rate of carbon storage in the ocean, the model is rather insensitive to the value of this parameter, even if our calibration value is off by a factor of 10. The transport of carbon into the deep ocean is not controlled by the air-sea gas exchange.

If the upwelling velocity was much lower than our current estimates, it would also have only a minor effect on the global carbon cycle. However, if the actual value was 10 times larger than the current estimate, then the equilibrium would shift, due to upwelling of nutrients to the surface, resulting in a larger DOC pool and greater rates of sedimentation. The larger carbon storage in the ocean would be offset by a reduction in carbon in both the terrestrial biomes and the atmosphere. This indicates that further research should be directed towards understanding the globally-averaged value of the upwelling velocity.

Using the GLOCO model, we studied the effect of disposing some of the anthropogenic carbon emissions directly into the ocean, possibly as clathrate hydrides. Injection of carbon into the deep ocean becomes less and less effective, in terms of the maximum atmospheric CO₂ observed, suggesting that the optimal depth is somewhere around 1000 m.

If we take no action to reduce fossil fuel emissions (IPCC 92a case), then pCO₂ will more than double by the end of the next century. Even if we constrain emissions to their 1990 levels for the next 110 years, we can expect a rise of around 48% in pCO₂ levels. Burying a fraction of the emissions deep in the ocean would reduce the rate of increase in pCO₂ and thus the potential for an increased greenhouse effect and its implications. Public pressure, as well as political pressure from interested parties (e. g. insurance companies) may result in capping pCO₂ to a fixed level, for example 450 ppmv. This would result in significant reductions in combustion of fossil fuel in a relatively short amount of time. Burying a fraction of the emissions would provide some relief, and would allow for a smoother transition to alternative energies.

REFERENCES

- Bacastow, R. and Maier-Reimer, E.: 1991, 'Dissolved Organic Carbon in Modeling Oceanic New Production', *Global Biogeochemical Cycles*, 5: 71-85.
- Baes, C. F. and Killough, G. G. : 1986, 'Chemical and Biological Processes in CO₂-Ocean Models', in *The Changing Carbon Cycle, A Global Analysis*, ed. J. R. Trabalka and D. E. Reiche, Springer-Verlag, New York.
- Broecker, W. S. and Maier-Reimer, E.: 1992, 'The Influence of Air and Sea Exchange on The Carbon Isotope Distribution in the Sea', *Global Biogeochemical Cycles*, 6: 315-320.
- De Baar, H. J. W.: 1992, 'Options for Enhancing the Storage of Carbon Dioxide in the Oceans: A Review', *Energy Conversion and Management*, 33(5-8): 635-642.
- Enting, I. G., T. M. L. Wigley and M. Heimann, 1994, 'Future Emissions and Concentrations of Carbon Dioxide: Key Ocean/Atmosphere/Land Analyses', *CSIRO Technical Paper 31*, CSIRO, Australia
- Erickson, D. J.: 1989, 'Variations in the Global Air-Sea Transfer Velocity Field of CO₂', *Global Biogeochemical Cycles*, 3: 37-41.
- Etcheto, J., Boutin, J. and Merlivat, L.: 1991, 'Seasonal Variation of the CO₂ Exchange Coefficient over the Global Ocean using Satellite Wind Speed Measurements', *Tellus*, 43B: 247-255.
- Golomb, D. S., Zemba, S. G., Dacey, J. W. H. and Michaels, A. F.: 1992, 'The Fate of CO₂ Sequesters in the Deep Ocean', *Energy Conversion and Management*, 33(5-8): 675-683.
- Hoffert, M. I., Wey, Y. C., Callegari, A. J. and Broecker, W. S.: 1979, 'Atmospheric Response to Deep-Sea Injections of Fossil-Fuel Carbon Dioxide', *Climatic Change*, 2: 53-68.
- Hudson, R. J. M., Gherini, S. and Goldstein, R. A.: 1994, 'Modeling the Global Carbon Cycle: Nitrogen Fertilization of the Terrestrial Biosphere and the "Missing" CO₂ Sink', *Glob. Biogeochem. Cycles*, 8:3, 307-333
- IPCC: 1992, 'Climate Change 1992: The Supplementary Report to the IPCC Scientific Assessment', ed. J. T. Houghton, B. A. Callender and S. K. Varney, Cambridge University Press, UK.
- Keller, A. A. and Goldstein, R. A.: 1994, 'The Human Effect on the Global Carbon Cycle: Response Functions to Analyze Management Strategies', *World Resource Review*, 6: 63-87
- Kheshgi, H. S., Flannery, B. P., Hoffert, M. I. and Lapenis, A. G.: 1994, 'The Effectiveness of Marine CO₂ Disposal', *Energy*, 19(9): 967-974
- Liro, C. R., Adams, E. E. and Herzog, H. J.: 1992, 'Modeling the Release of CO₂ in the Deep Ocean', *Energy Conversion and Management*, 33(5-8): 667-674
- Marchetti, C.: 1977, 'On Geoengineering and the CO₂ Problem', *Climatic Change*, 1: 59-68
- Robertson, J. E. and Watson, A. J.: 1992, 'Thermal Skin Effect of the Surface Ocean and its Implications for CO₂ uptake', *Nature*, 358: 738-740.
- Saji, A., Yoshida, H., Sakai, M., Tani, T., Kamata, T., and Kitamura, H. : 1992, 'Fixation of Carbon Dioxide by Clathrate-Hydrate', *Energy Conversion and Management*, 33(5-8): 643-649.
- Sakai, H., Gamo, T., Kim, E. S., Tsutsumi, M., Tanaka, T., Ishibashi, J., Wakita, H., Yamano, M. and Oomori, T.: 1990, 'Venting of carbon dioxide-rich fluid and hydrate formation in mid-Okinawa Trough Backarc Basin', *Science*, 248: 1093-1096.
- Siegenthaler, U. and Joos, F. : 1992, 'Use of a Simple Model for Studying Oceanic Tracer Distributions and the Global Carbon Cycle', *Tellus*, 44B: 186-207.
- Stanton, B. R.: 1991, 'Ocean Circulation and Ocean-Atmosphere Exchanges', *Climatic Change*, 18: 175-194.
- Volk, T. and Bacastow, R.: 1989 'The Changing Patterns of ΔpCO₂ between Ocean and Atmosphere', *Global Biogeochemical Cycles*, 3: 179-189.

Figure 1. Time dependent atmospheric carbon response due to an instantaneous pulse of 594 GtC, for various oceanic transport parameter values, compared to the base case (calibration values and pulse in the atmosphere).

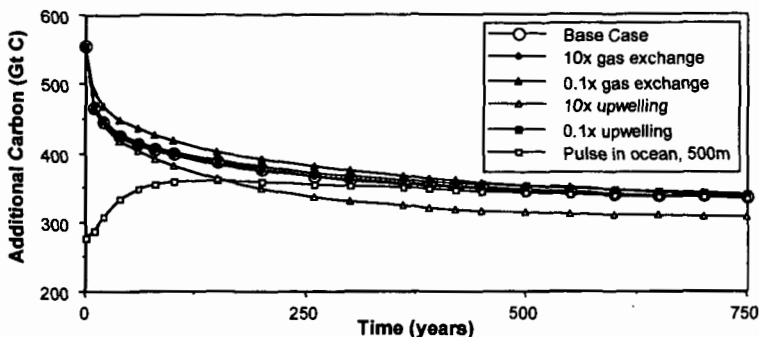


Figure 2. Atmospheric concentration (pCO_2) profiles after the injection of an instantaneous pulse of 594 Gt C directly to the atmosphere (base case) or at various depths in the low-latitude ocean.

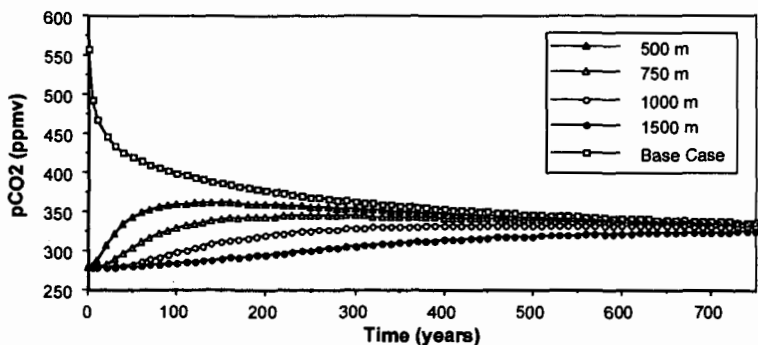


Figure 3. Maximum pCO_2 predicted during the 750 years of simulation as a function of low-latitude ocean burial depth.

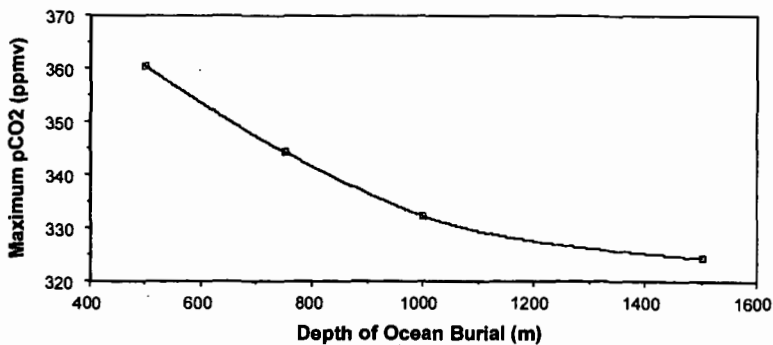


Figure 4. Atmospheric concentration (pCO_2) profiles for a constant emissions scenario at 1990 levels, considering direct emission to the atmosphere or increasing oceanic burial.

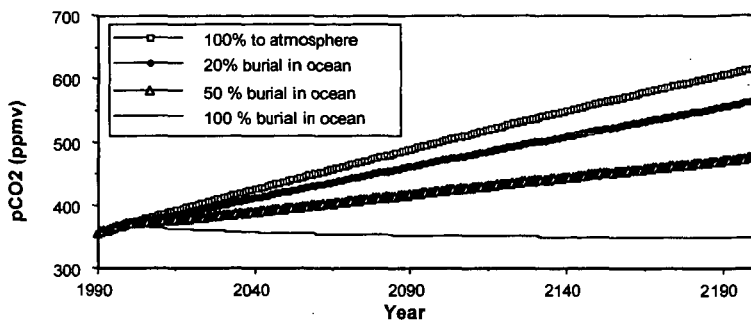


Figure 5a. Carbon emissions from combustion of fossil fuels considering the IPCC 92a Business as Usual scenario and two control scenarios aimed at achieving a stable pCO_2 of 450ppmv with and without ocean burial of emissions.

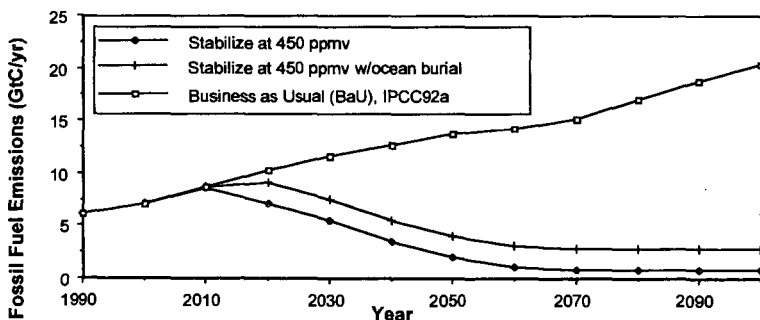
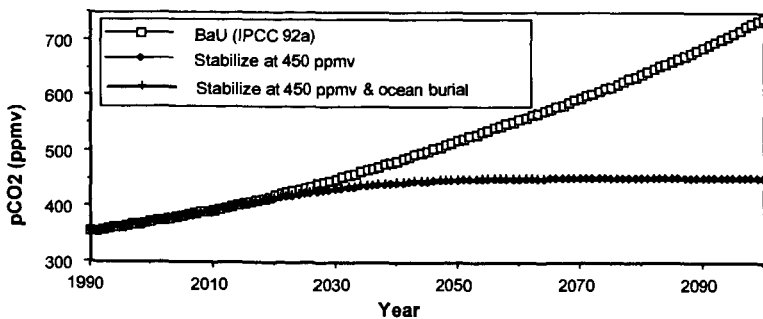


Figure 5b. Atmospheric concentration (pCO_2) profiles for the Business as Usual scenario and the two control scenarios targeting a maximum pCO_2 of 450 ppmv.



HIGHLY EFFICIENT DISPOSAL OF CO₂ INTO THE OCEAN BY GAS-LIFT METHOD (BASIC CHARACTERISTICS OF GLAD SYSTEM)

Takayuki Saito

National Institute for Resources and Environment
16-3, Onogawa, Tsukuba, Ibaraki 305, Japan

Takeo Kajishima

Department of Mechanical Engineering, Osaka University
2-1, Yamadaoka, Suita, Osaka 565, Japan

Ryuichi Nagaosa

National Institute for Resources and Environment
16-3, Onogawa, Tsukuba, Ibaraki 305, Japan

Keywords: Carbon dioxide, Gas-lift method, Ocean disposal

INTRODUCTION

7.1 ± 1.1 GtC/y of CO₂ was discharged into the atmosphere due to the human activities of energy production and its consumption in 1992 (1). Since its discharged rate is quite large in such a matter and CO₂ discharge is continued as long as fossil fuel is consumed, the global warming problem brought by CO₂ is very difficult to solve. Many kind of methods and ideas have been proposed for the problem, however, it is very hard to find out methods to be effective and realized within an early stage.

The mass transfer rate of CO₂ from the atmosphere to the ocean is low (2). The ocean has an enough capacity to absorb the whole of CO₂ which is emitted by the consumption of total fossil fuel of 7 × 10¹² tonC (3). Therefore, CO₂ disposal into the ocean is a reasonable and hopeful option to reduce the global warming. The ocean disposal is not an ultimate technology to avoid the global warming, but emergency measures for the rapid increase of CO₂ concentration in the atmosphere. The ocean disposal is required to be low cost and energy saving as well as possible. The deeper releasing can isolate CO₂ for longer period. Therefore, the deep-sea releasing might be most reliable from a viewpoint of long period isolation of CO₂. However, the liquefaction and transportation of it to the great depth consume a large amount of extra energy and cost (4). Thus, we must solve these two contradictory matters; namely reliability and cost.

We propose the GLAD (Gas-Lift Advanced Dissolution) system for CO₂ release into deep-sea as the answer to above-mentioned problems. The GALD system is significantly efficient comparing with previous ideas. In the present paper, the principle of the GLAD system is described and its characteristics is estimated based on recent numerical and experimental results.

SOME PROBLEMS ON PREVIOUS IDEAS FOR CO₂ DISPOSAL

The previous ideas of CO₂ disposal into the ocean are classified into the following categories: the first one is storage of liquid CO₂ on the deep-sea floor deeper than about 3000m. In this case, the surface of the CO₂ pond is expected to be covered by CO₂-hydrate. However, the behavior of CO₂-hydrate in the actual ocean floor is not completely understood (5). The second one is direct release of liquid CO₂ into deep water of 1000-3000m in depth (6). The released liquid CO₂ should be immediately dissolved and diffused into sea-water to reduce environmental impacts. In these case, the liquefaction of CO₂ and its transportation to great depths consume a large amount of energy and have high cost. Besides, the compressed energy of liquid CO₂ is also disposed in the ocean without work.

The third one is shallow injection of CO₂ gas and gravity current. Haugan and Drange proposed the idea which was direct release of CO₂ gas into the sea-water at the depth of 200-400m and expecting sink of CO₂ enriched solution to deep-sea by the density difference between the solution and ambient sea-water (7). Adams et al. improved the CO₂ release system, which was a large vessel fixed on the floor of continental slope at a depth of about 200m (8). These ideas are superior to the first and second ones from a viewpoint of energy and cost saving. However, there are uncertain matters from a viewpoint of fluid dynamics in these ideas, such as 1) the upward plume generated by the bubbles, 2) the horizontal turbulence diffusion before the solution reaching at enough depths to be sequestered for long period and 3) existence of density and/or temperature stratified layer in the ocean (9). In addition, considering that biological activities are very high in the area shallower than 200m depth, more deeper release of CO₂ solution without consuming extra energy is quite better. Thus, the uncertainty in the technology and the secondary environmental impact of the previous ideas should be solved simultaneously.

PRINCIPLE OF THE GLAD SYSTEM

The concept of the GLAD system is illustrated in Figure 1 (9, 10). The GLAD is an inverse J shape pipeline settled in shallow to deep water. CO₂ gas is injected into the shorter leg (hereafter, called dissolution pipe) of the GLAD at the depth of about 200-400m. Injecting CO₂ bubbles into the dissolution pipe, a gas-liquid bubbly flow is formed and a pumping action is generated by gas-lift effect. The buoyant plume rises in the dissolution pipe, and the bubbles dissolve in sea-water in some ascent. Fresh sea-water flows into the dissolution pipe at its bottom. As a result, the bubble dissolution and the transportation of the CO₂ enriched sea-water to great depth are accelerated by these effects. On the other hand, the longer leg (hereafter, called drain pipe) is used as a transportation and drain pipe for the CO₂ enriched sea-water to the area deeper than 1000m. The density of the solution is larger than that of ambient sea-water. An additional driving force to downward current is promoted by the density difference. Accordingly, the dense solution is released from the end of the drain pipe into deep water very efficiently.

NUMERICAL MODELING AND EXPERIMENTAL APPARATUS

Numerical modeling The numerical models for the gas-liquid two-phase flow in a vertical pipe of inner diameter D were developed (10). In the present paper, the outline of the numerical method is described. The basic equations, namely conservation law of mass and momentum, are employed. Defining the density and momentum of the gas-liquid mixture as $\rho = \alpha\rho_G + (1-\alpha)\rho_L$ and $\rho v = \alpha\rho_G v_G + (1-\alpha)\rho_L v_L$ respectively, the equations are as follows:

$$\frac{\partial \rho}{\partial t} + \frac{\partial(\rho v)}{\partial z} = Q_G, \quad (1)$$

$$\frac{\partial(\rho v)}{\partial t} + \frac{\partial(\alpha\rho_G v_G^2)}{\partial z} + \frac{\partial[1-\alpha]\rho_L v_L^2}{\partial z} = -\frac{\partial p}{\partial z} - \rho g - \frac{4\tau_w}{D}, \quad (2)$$

where α is the void fraction, ρ the density, v the velocity, and the subscripts G and L denote gas and liquid phase, respectively. The vertical direction is represented by z , Q_G is the gas injection rate, p the static pressure, and τ_w the shear friction at the pipe wall, respectively. The void fraction is evaluated by the mass conservation of gas phase

$$\frac{\partial(\alpha\rho_G)}{\partial t} + \frac{\partial(\alpha\rho_G v_G)}{\partial z} = Q_G + \Gamma_G, \quad (3)$$

where Γ_G denotes the gas dissolution rate. In addition, gas equation is employed. As the temperature is assumed to be constant, the energy equation is not needed. To close these equations, the drift flux model which determines the velocity of each phase is applied. Assuming mass transfer coefficient k is constant, Γ_G is evaluated as

$$\Gamma_G = 5.24\rho_G k (\alpha^2/D^2 \Delta_z)^{1/3}, \quad (4)$$

where Δ_z is the length of the computational cell (10).

The finite difference method is applied to discretized the basic equations. The implicit time marching scheme for density and pressure is adopted to deal with the high compressibility of the gas phase (11). The method was applied to a conventional air-lift pump of 200m long, and the numerical results showed reasonable agreement with the experimental data (12).

Experimental apparatus The experimental apparatus for the GLAD system is illustrated in Figure 2. Stainless steel pipes ⑨ and ⑩ (100mm in inner diameter and 8190mm in length) are connected to the GLAD dissolution pipe. They allow us to simulate the pressure conditions from the atmospheric to the 200m depth. The dissolution pipe ① is an acrylic pipe of 25mm in inner diameter and 7690mm in total length. At 840mm from the pipe bottom, CO₂ gas is injected by the gas injector ②, which is made of 108 19G needles. This injector can form almost uniform bubble diameter for any flow rate of CO₂ gas within the range of the present work.

4 double-optical-fiber probes ② (13) shown in Figure 3 are attached to the dissolution pipe in order to measure both of the bubble chord length and the bubble velocity. Each probe can be placed at any radius in the pipe. The optical signals from the probes are detected by the photo-multipliers, and the outputs from the multipliers are converted and recorded in a personal computer. The probability density function obtained by analyzing the probe signal is different from that of the bubble-water two-phase system (14), however there is some relationship between these probability density functions. In order to obtain the probability density function of the two-phase system by means of image analysis, a high-speed video camera (200 frames/sec at 20μsec shutter speed) ④ was employed (15).

RESULTS AND DISCUSSIONS ON GLAD SYSTEM

Numerical results The numerical results for the same dimensions as those of the experimental apparatus are shown in Figures 4 and 5. To compare the influence of k , two kinds of values, $k=1 \times 10^{-4}$ m/s, 2×10^{-4} m/s, are provided. The initial diameter of the bubbles was given as $r_0=3.6 \times$

10^{-3}m (which is obtained by our experiments). CO_2 injection rate was inputted as $q_{in} = 0.0164, 0.0328, 0.0656, 0.1312$ and 0.2624g/s . Figure 4 compares the effect of CO_2 injection rate on the void fraction at the top of the dissolution pipe (α_{exit}) and recirculation water velocity (J_L). In the case of $k=2 \times 10^{-4}$, the bubbles dissolve completely for $q_{in} < 10^{-3}\text{g/s}$, and positive J_L indicates a gas-lift effect takes place. The results fulfill the aim of the GLAD system successfully. In another case, they do not dissolve completely, however, mass flow rate of the CO_2 gas at the top of the dissolution pipe is negligible. Figure 5 shows the vertical profile of the void fraction for above-mentioned q_{in} . Near the gas injection point, the bubbles dissolve very rapidly, and in downstream of this region, the dissolution rate decreases for the both case of k .

Experimental results Comparisons of the experimental results with the numerical ones on both of the void fraction and the recirculation water velocity are shown in Figure 6. In the experiment, the void fraction is determined by taking account of bubble shape given by analyzing the video images. Strictly speaking, the definitions of the void fractions are different. Experimental data mean time void fraction, on the other hand, the numerical ones mean spatial void fraction (16). We think, however, the agreement between the experimental and the numerical data is reasonable. In addition, the numerical J_L shows good agreement with the experimental one. In conclusion, the accuracy of our numerical method and modeling is confirmed. In this experiment, a longer pipe is needed for CO_2 to dissolve in water completely. The authors reported, for example, the flow control is effective for complete dissolution of CO_2 bubbles (9). The feasibility of the GLAD system has been confirmed by the experiments. Considering the agreement between the experimental results and the numerical ones, the numerical simulation method for a scale-up plant of the GALD system is established.

Model plant and cost estimate In this section, a result of cost estimate for the model plant listed in Table 1 is discussed. (See (17) for the detail.) In our estimate, it is assumed that the exhausted rate of CO_2 is 100kg/s and 90 units of the GALD system are employed. The construction charge for both of the GLAD systems and the gas transportation system is about US\$ 590 million. If the period of durability is more than 15 years, the operation charge per year, which include the electric power rates, labor costs and the maintenance cost, is about US\$ 59 million. Note that the cost for CO_2 capture and separation from the exhausted gas is not included. As a result, the approximate cost of CO_2 disposal into deep-sea from a 1000MW fired power plant by the GALD system is US\$ 100 million per year. This corresponds to 1 cent/kWh. The comparison of the cost of the GLAD system with previous ideas is summarized in Table 2. Still more, the model plant requires only 4% of the generated electricity from the power plant. Note that the cost estimate for CO_2 capture and separation by DOE includes compression to over 100bars. If this compression energy is used effectively for the GLAD system, the cost for it can be rather less than 1 cent/kWh. The GLAD is most competitive to previous methods for deep-sea disposal of CO_2 from an economical point of view.

CONCLUSIONS

The basic characteristics of the GLAD system is examined experimentally. The accuracy of our numerical method is confirmed by the experimental data. Based on these results, the availability of the GLAD system to dispose CO_2 into deep-sea is confirmed from a standpoint of cost and energy. We can conclude the GLAD is the most competitive with previous ideas for CO_2 disposal into the ocean. We are grateful to Dr. Kosugi of Sumitomo Metal Industries, Ltd. for his contribution to the cost estimate and useful discussions.

REFERENCES

- 1 IPCC, *Climate Change 1994*, Cambridge University Press, (1995).
- 2 Watanabe, Y., et al., *J. Geophys. Res.*, Vol.99, pp.195-213 (1994).
- 3 Hoffert, M.I., et al., *Climate Change*, Vol.2, pp.53-68, (1979).
- 4 DOE Report, DOE/ER-30194, Vol.1, pp35-37, (1993).
- 5 Ohsumi, T., *Energy Convers. Mgmt.*, Vol.34, pp.1059-1064, (1993).
- 6 Liro, C.R., Adams, E.E. and Herzog, H.J., *Energy Convers. Mgmt.*, Vol.33, No.5-8, pp.1059-1064, (1992).
- 7 Haugan, P. M. and Drange, H., *Nature*, 357, pp.318-320, (1992).
- 8 Adams, E. E., et al., *Proc. 2nd US/Japan Workshop on Global Change*, Honolulu, (1993).
- 9 Saito, T., Kajishima, T. and Nagaosa, R., *Proc. Int. Conf. Technol. for Marine Env. Preservation*, Tokyo, pp.875-881, (1995).
- 10 Kajishima, T., Saito, T., Nagaosa, R. and Hatano, H., *Energy Convers. Mgmt.*, Vol.36, No.6, pp.467-470, (1995).
- 11 Kajishima, T. and Saito, T., to be published in *Int. J. Japan Soc. Mech. Engrs.*, (1996).
- 12 Saito, T., et al., *Proc. Oceans '89, IEEE-No.89CH27805-5*, pp.48-53, (1989).
- 13 Hatano, H., Khattab, I.A.H., Nakamura, K. and Ishida, M., *J. Chem. Eng. Japan*, Vol.19, No.5, pp.425-430, (1986).
- 14 Liu, W. and Clark, N.N., *Int. J. Multiphase Flow*, Vol.21, No.6, pp.1073-1089, (1995).
- 15 Saito, T., Kajishima, T., Kiyono, F. and Masuyama, T., *ASME, FED-Vol.209*, pp.107-113, (1995).
- 16 Welle, R., *Int. J. Multiphase Flow*, Vol.11, No.3, pp.317-345, (1985).
- 17 Kajishima, T., Saito, T., Nagaosa, R. and Kosugi, S., to be published in *Energy, Int. J.*, (1996).

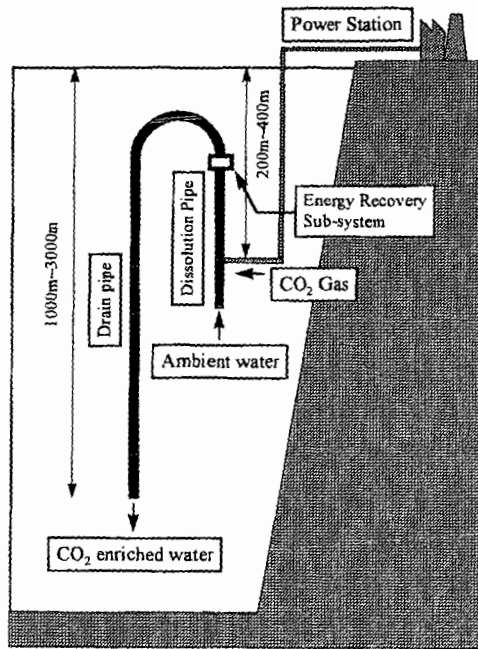


Figure 1. Concept of the GLAD system.

The dissolution and the drain pipes are about 100-200m and about 1000-3000m in length, respectively. CO₂ gas is pumped by a compressor and transported by a pipeline from a fired power plant to the GLAD. In the case that the water recirculation velocity is too high for complete dissolution of the bubbles, a resistance such as a turbine will be equipped near the top of the dissolution pipe. This suggests that excess momentum energy can be recovered. The GLAD system and the disposal method were applied for US and Japanese patent by T. Saito and T. Kajishima (1994, 1995).

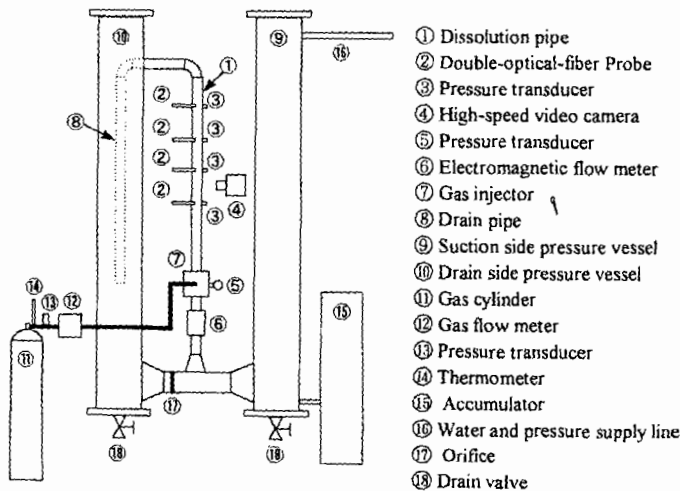


Figure 2. Outline of the Experimental Apparatus for the GLAD System

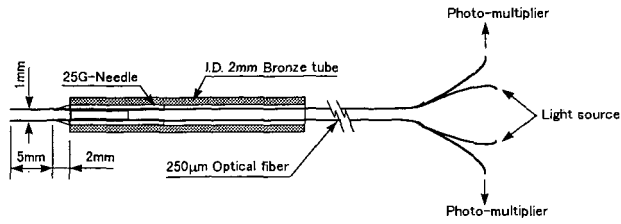


Figure 3. Structure of the double-optical-fiber probe

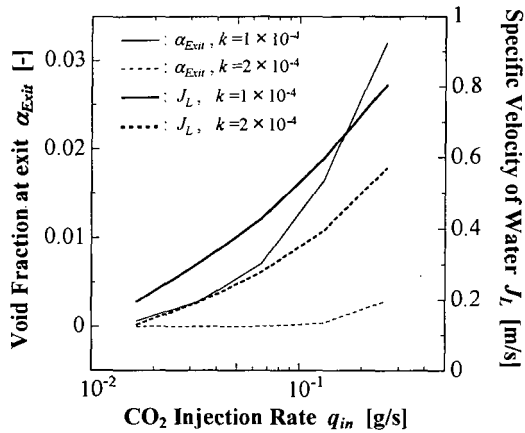


Figure 4. Recirculation velocity of water (J_L) and the Void fraction of CO_2 (α_{Exit}) at the top of the dissolution pipe.

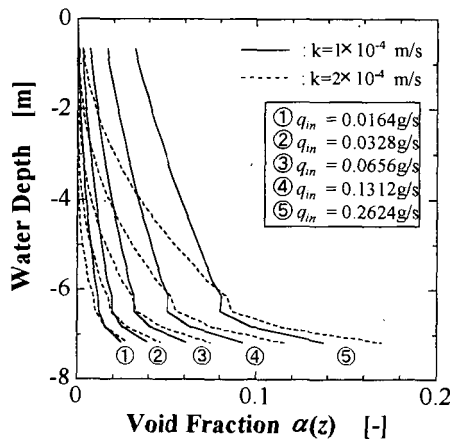


Figure 5. Profile of void fraction of CO_2 gas in the dissolution pipe.

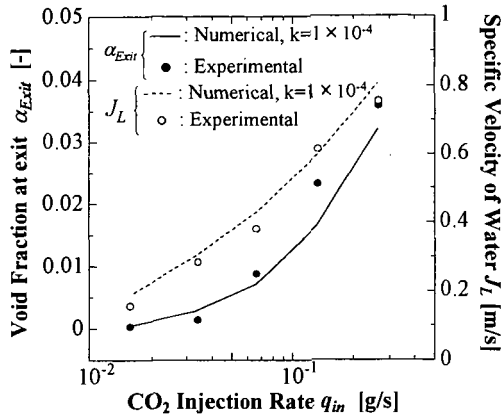


Figure 6. Comparison of the experimental results with the numerical ones.

Table 1. Dimensions of the model plant

GLAD system (fixed by tension-legs)	CO ₂ gas transportation system	Power plant (fossil fuel fired)
Steel pipe : I.D.=0.5m, L=300m Inlet depth = 400m Injection depth=390m Drain pipe : I.D.=1.0m, L=10km spirally reinforced FEP	Compressor : 7Mpa, 55m ³ /s 412000kW Pipeline : I.D.=0.5m, L=100km	Output power=1000MW CO ₂ exhausted rate=100kg/s

Table 2. Comparison of both of previous ideas and the GLAD system

Method	Cost of capture and separation ^{1),3)} [cent]	Cost of disposal ²⁾ [cent]
Previous ³⁾	1.1 ~ 4.9 ³⁾	0.6 ~ 6.7 ³⁾
GLAD	1.1 ~ 4.9 ³⁾	< 1

1) Includes costs for compression (to over 100bars) and dehydration

2) Includes transportation costs

3) DOE Report, DOE/ER-30194(1993)

THE EFFECT OF HYDRATE FORMATION ON CO₂ JET INSTABILITY

H. Teng¹, S.M. Masutani², C.M. Kinoshita², and G.C. Nihous³

¹National Institute of Materials and Chemical Research
1-1 Higashi, Tsukuba, Ibaraki 305 JAPAN

²University of Hawaii, Hawaii Natural Energy Institute
2540 Dole Street, Holmes 246, Honolulu, Hawaii 96822 USA

³Pacific International Center for High Technology Research
2800 Woodlawn Drive, Suite 180, Honolulu, Hawaii 96822 USA

Keywords: hydrate; carbon dioxide; jet instability

Abstract—Disposal of captured CO₂ in the deep ocean or in underground aquifers currently is being considered as a means to control atmospheric levels of this greenhouse gas. Long-term sequestration demands that CO₂ be released at depths where water temperatures and pressures foster the formation of a solid hydrate phase. Previous theoretical and experimental studies have demonstrated that the kinetics of formation of the CO₂ hydrate can proceed rapidly, with characteristic times of the order of a second. Under certain liquid CO₂ jet discharge scenarios, hydrate formation may have important implications related to jet instability. An analysis was performed to assess the nature and magnitude of these effects. It was determined that hydrate formation may pose problems under certain discharge conditions.

1. INTRODUCTION

Efforts to stabilize greenhouse gas emissions are underway in many industrialized nations. Carbon dioxide (CO₂) currently is the most important of these gas species, due to the preponderant quantities being released into the atmosphere by anthropogenic sources—largely through the combustion of fossil fuels. While CO₂ emissions from combustors may be reduced through fuel switching and efficiency improvements, direct control technologies also are being investigated which extract CO₂ from flue gases for reuse or disposal in the deep ocean or underground.

Modeling studies [1] have suggested that captured CO₂ must be discharged at depths greater than 500 m in the ocean in order adequately to forestall return to the atmosphere. Two primary disposal scenarios have been proposed wherein liquefied CO₂ is transported from the surface via a submerged conduit and released either at intermediate depths (typically between 500 and 1,500 m) or in the abyssal zone below 3,000 m. The former scenario acknowledges the current depth limitations of undersea pipeline deployment and maintenance. Disposal in the very deep ocean was conceived as a means to avoid potential problems related to buoyancy of the liquid CO₂ effluent at depths above 3,000 m (i.e., the CO₂ will rise toward the surface as it slowly dissolves).

Since CO₂ is a non-polar substance and water is strongly polar, liquid CO₂ is only slightly soluble in seawater; consequently, CO₂ released from a submerged pipeline (typically as jets issuing through discharge orifices) is hydrodynamically unstable and will break up into a dispersed droplet phase. The dynamics of this instability determine the distribution of droplet sizes which, in turn, can impact subsequent dissolution, coalescence (or agglomeration), and transport phenomena.

Although jet instability has been investigated extensively, earlier studies do not adequately address one important aspect of the liquid CO₂-seawater system: at conditions representative of the proposed marine disposal scenarios (i.e., pressures greater than 44.5 bar and temperatures less than 283 K), a solid hydrate phase will form at the CO₂-seawater interface. The effect of hydrate formation on discharge jet instability is poorly understood. The present theoretical study was undertaken as a response to this deficiency.

Naturally occurring CO₂ hydrates in the ocean were detected in a submersible study of a hydrothermal field in the Okinawa trough [2]. A CO₂ hydrate layer was observed to form rapidly at the interface between CO₂-rich fluid (containing approximately 86% CO₂), secreted from the seafloor at depths of 1,335-1,550 m, and the surrounding 3.8° C seawater. The solid tubes which resulted were fragile and easily fractured by hydrodynamic forces, resulting in a cylindrical pattern of break up. This study demonstrated that hydrate formation can influence jet instability—in some cases precluding droplet formation.

Laboratory investigations [3,4,5] of liquid CO₂ jets in high-pressure and low-temperature water report three patterns of jet break up corresponding to different degrees of influence by the hydrate phase. At very low jet velocity, droplets form at the discharge orifice and are immediately covered with a hydrate film. These droplets easily agglomerate (but do not coalesce) at the orifice if they are not removed quickly. Higher velocities result in a cylindrical jet. Hydrate formation on the surface of this jet may proceed rapidly enough to produce a tube-like solid structure. Further increase in jet velocity leads to normal break up into droplets. These droplets will be encased by a hydrate film that can assume a snow-like quality under certain conditions [3].

Conventional instability theory and related data predict that a liquid jet discharging into another dissimilar liquid will break up into a dispersed droplet phase. Observations made in the ocean and in the laboratory, however, suggest that other break up modes are possible and may be induced by a solid hydrate phase. This study investigates the phenomena of CO₂ jet break up in the deep

ocean and attempts to provide a theoretical basis to identify situations where jet instability may be affected by hydrate formation.

2. LIQUID CO₂ JET BREAK UP IN SEAWATER

When liquid CO₂ effluent is discharged through an orifice into seawater, droplets will form as a result of interfacial instability [6]. This instability arises from interfacial tension and/or differences in the velocities of the two fluids. At low jet velocities, break up always leads to a train of uniformly-sized droplets [4,5,7]. At high jet velocities, break up produces multiple non-uniformly-sized droplets [3,4].

The present study restricts its focus to the laminar instability flow regime [6] that is characterized by jet break up leading to a uniformly-sized droplet train. For these flows, closed form relationships can be derived for important instability parameters. Although turbulent jets are clearly relevant to the marine disposal problem, the associated mathematics are prohibitively complex and will not be pursued directly here.

For laminar flow, Rayleigh's maximum-instability theory [8] applies: break up is induced by the most unstable of numerous waves that can form on the jet surface from an initial disturbance. This "most-unstable wave" is identified by a maximum-growth-rate in amplitude. Jet instability can then be characterized by a break up time, t_b , which represents the induction period experienced by a quantity of jet fluid between discharge from the orifice and the formation of droplets.

Consider a liquid CO₂ jet in seawater. In the absence of a hydrate phase, jet instability is described by the following characteristic equation [6]:

$$\left[1 + \frac{\rho_{\text{seawater}} \eta}{2\rho_{\text{CO}_2}} \frac{K_0(\eta)}{K_1(\eta)} \right] \beta^2 + 2Z\eta^2 \beta = \eta^2 (1 - \eta^2) + \frac{1}{2} W_e \eta^3 \frac{K_0(\eta)}{K_1(\eta)} - N_s \eta^2. \quad (1)$$

Here, ρ_i is the density of fluid i ($i = \text{CO}_2$ or seawater); $\eta \equiv k r_0$ is the dimensionless disturbance wavenumber with k the dimensional disturbance wave number and r_0 the orifice radius; K_0 and K_1 are zeroth- and first-order modified Bessel functions of the second kind; $\beta \equiv \omega (2\rho_{\text{CO}_2} r_0^3 / \sigma)^{1/2}$ is the dimensionless growth rate in disturbance amplitude with ω the dimensional growth rate in the disturbance amplitude and σ the interfacial tension; $Z \equiv (3\mu_{\text{CO}_2} + \mu_{\text{seawater}}) / (2r_0 \rho_{\text{CO}_2} \sigma)^{1/2}$ is a modified Ohnesorge number with μ_i the viscosity of fluid i ; $W_e \equiv 2r_0 \rho_{\text{seawater}} U^2 / \sigma$ is the Weber number with U the jet velocity; and $N_s \equiv (C_s / \sigma) (d\sigma / dC)$ is an interfacial tension number with C_s and C , respectively, the solubility and concentration of CO₂ in seawater. Based on Rayleigh's maximum-instability theory, a relationship may be derived for the jet break up time [6]:

$$t_b = [1/r_0 \alpha_0] (2\rho_{\text{CO}_2} r_0^3 / \sigma)^{1/2} / \beta_m, \quad (2)$$

where α_0 is the amplitude of the initial disturbance and β_m is the dimensionless maximum-growth rate of the disturbance amplitude, which may be determined from equation (1).

Examination of equations (1) and (2) indicates that jet instability is affected by the discharge parameters, U and r_0 , and by fluid properties, ρ_i , μ_i , σ , C_s , and C . Over the range of depths being considered for liquid CO₂ disposal, fluid properties do not vary greatly. It is reasonable, therefore, to estimate the magnitude to t_b by adopting representative property values for substitution into (1) and (2). At a depth of 500 m, seawater temperature at most locations outside of major currents is about 279 K. Corresponding densities of seawater and CO₂ are approximately 1030 and 895 kg/m³, respectively. The interfacial tension number, N_s may be estimated as

$$N_s = \left(\frac{d\sigma}{dC} \right) \frac{C_s}{\sigma} \approx \frac{\sigma_m - \sigma}{C_s} \frac{C_s}{\sigma},$$

where σ_m and σ are, respectively, values of interfacial tension with and without mass transfer (between the jet and the seawater). Thermodynamic theory can be applied to estimate interfacial tension [6]. At 279 K, $\sigma = 71.23 \times 10^{-3}$ N/m and $\sigma_m = 70.09 \times 10^{-3}$ N/m. Hence, $N_s = -0.016$, indicating that the system is tension-decreasing. For jets discharging from moderately-sized orifices (say, with diameters > 1 mm), the modified Ohnesorge number, Z , is of the order 10^{-3} , which implies that the damping term in (1) (i.e., the second term on the LHS of the equation) may be neglected. With this simplification, and assuming conditions at 500 m, (1) becomes

$$\beta^2 = \eta^2 \frac{1.016 - \eta^2 + 0.5W_e \eta K_0(\eta) / K_1(\eta)}{1 + 0.577 \eta K_0(\eta) / K_1(\eta)}. \quad (3)$$

Equation (3) indicates that $\beta_m = \beta_m(\eta, W_e)$. In general, β_m increases with W_e (and, hence, with increasing jet velocity, U , and orifice size, r_0). From experiments reported in literature [6], it is

estimated that, for the CO₂/seawater system, $\ln(r_0/\alpha_0) = 10.7$. Employing this value in (2), a representative jet break up time is given by $t_b \cong (1.7 \times 10^3)(r_0)^{1.5}/\beta_m$.

The preceding developments are predicated on the assumption that the formation of an interfacial, solid hydrate phase during the induction (i.e., pre-break up) period of the jet exercises a negligible influence on the amplification of surface disturbances. While, in reality, this must not be true under certain flow conditions (otherwise the unconventional break up modes noted in the preceding section could not occur), it is acceptable for the purpose of this study which, as discussed below, seeks to compare characteristic times of (unimpeded) jet break up and hydrate formation to establish regimes where the hydrate effect may be neglected or may be significant.

3. HYDRATE FORMATION AT THE CO₂-SEAWATER INTERFACE

The CO₂ hydrate is a clathrate compound having a body-centered structure formed by linkage of 46 water molecules. The clathrate has two pentagonal-dodecahedral cavities and six tetrakaidecahedral cavities. When all cavities are occupied by CO₂ molecules, the hydrate has a chemical formula of 8CO₂ + 46H₂O or CO₂ • 5.75H₂O. In reality, all cavities cannot be occupied [9], so the hydrate always contains fewer than the stoichiometric number of CO₂ molecules [10].

Hydrate formation is a physicochemical process. During this process, water molecules form a hydrogen-bonded framework (i.e., the clathrate) and CO₂ molecules enter the cavities of the clathrate as "guests." The hydrate framework is formed with geometric distortions and, therefore, the clathrate is unstable unless a large percentage of the cavities are filled with CO₂ molecules [10]. Hydrate formation at the CO₂-seawater interface can be expressed as



where n is the hydrate number ($n = 5.75$ at stoichiometric conditions). The kinetics of interfacial CO₂ hydrate formation have been investigated in previous modeling studies [11,12]. It was concluded that hydrates would form rapidly at conditions representative of the deep ocean and that the resulting solid layer would be very thin. These predictions agree reasonably well with the limited experimental results reported in the literature.

The CO₂-seawater hydrate kinetics may be characterized by a formation time, t_f , which corresponds to the period required for a solid layer to develop after a liquid CO₂ phase and seawater phase are brought into contact. The theoretical expression for the hydrate formation time is [12]

$$t_f = 6.9 \left(\rho_h M_h^{-1} \right) / (\kappa C_s), \quad (5)$$

where κ is the effective rate constant of the formation reaction and ρ_h and M_h are, respectively, the CO₂ hydrate density and molar mass. It can be argued that, under the near-isothermal conditions of the deep ocean, the parameters in (5) remain essentially constant [6,12]. An estimate of t_f that can be compared with t_b can then be obtained utilizing representative values of these parameters: for $C_s = 0.91$ kmol/m³ [13], $\kappa = 30$ s⁻¹, $\rho_h = 1.112 \times 10^3$ kg/m³, and $M_h = 147.5$ kg/kmol [11], the hydrate formation time in the deep ocean is $t_f = 1.91$ s.

4. HYDRATE EFFECTS

Expressions for the characteristic times of jet instability, i.e., break up, and surface hydrate formation were obtained in the preceding sections. It is proposed that the relative magnitudes of these characteristic times can be utilized to indicate whether hydrate formation will exercise an effect on liquid CO₂ jet instability. The physical reasoning is as follows: if t_b is much shorter than t_f , then hydrates will not form in significant quantity on the jet surface prior to break up and, hence, jet instability will be unaffected; if, on the other hand, t_b is much longer than t_f (or of comparable magnitude), then a thin, solid hydrate layer will encase the jet, inhibiting the surface deformation required to induce jet break up. These two regimes are considered below.

4.1 Pre-Jet-Breakup Effects

The structure of the CO₂ jet will be affected when significant quantities of surface hydrates form prior to break up. Since hydrate formation time in the deep ocean is essentially constant, jet break up time becomes the relevant parameter. To be conservative, only maximum predicted values of this parameter, $t_{b,max}$, will be considered here; hence, low jet velocity cases are of interest (i.e., $W_e \rightarrow 0$). Employing the expression $t_b \cong (1.7 \times 10^3)(r_0)^{1.5}/\beta_m$ and solving (3) to determine β_m when $W_e \rightarrow 0$ [6], it can be shown that $t_{b,max} \geq t_f = 1.91$ s when $r_0 \geq 6.7$ mm. This implies that the pre-jet-breakup hydrate effects may become non-negligible when discharge orifice size exceeds a critical value, here, about 14 mm diameter.

If $t_f \ll t_{b,max}$, then rapid hydrate formation will establish a solid layer on the surface of the jet at the early stage of instability. This layer will inhibit surface deformation; thus, the jet remains stable and a solid tube can grow to encase the jet. Since the hydrate tube is very thin and fragile [2], it is easily broken by hydrodynamic forces. The breaking of hydrate tubes results in the cylindrical instability mode observed in the ocean at hydrothermal fields [2].

In reality, jet velocities are finite and, therefore, $t_b < t_{b,max}$. Figure 1 presents a comparison of t_r and t_b calculated for a range of jet velocities and discharge orifice diameters under deep ocean conditions. From this figure, it is observed that jet break up time increases with increasing orifice diameter and decreases with increasing jet velocity. The results imply that, for a given orifice diameter, interference by hydrates can be avoided by appropriate selection of jet velocity. To minimize pre-jet-break up effects, relatively small values of orifice diameter should be selected and/or velocities should be maintained at moderately high values.

4.2 Post-Jet-Breakup Effects

If $t_b \approx t_r$, then hydrate formation effects only are significant during the latter stages of jet instability, i.e., near to the end of the jet. Here, break up produces droplets covered with a hydrate layer. If $t_b \ll t_r$, then a conventional droplet break up pattern will be observed; however, the rapid kinetics of formation ensure that these droplets also will quickly be encased by a hydrate film.

Although hydrate formation does not significantly affect jet instability when $t_b < t_r$, it can impact the subsequent dissolution and dispersion of the droplet phase. The hydrate layer on the droplet surface is chemically stable [10] and will remain on the droplet (albeit undergoing cycles of collapse and regeneration) as it dissolves and is transported in space by buoyancy, currents, or turbulence [3,12]. Since water molecules at the hydrate surface have broken hydrogen bonds (note that each water molecule can form four hydrogen bonds) arranged toward the seawater phase [10,14], they will rapidly establish a bond when encountering a similar hydrate surface. Hence, CO_2 droplets brought in contact by hydrodynamic forces will easily agglomerate to form a droplet cluster [5,6,7,9,15]. The hydrate interphase, however, prevents the liquid CO_2 of the individual droplets from contacting and, therefore, inhibits coalescence into a single, larger droplet. This agglomeration phenomena has been observed in the laboratory.

5. CONCLUSIONS

A study was conducted to assess the effects of hydrate formation on the stability and break up of jets of CO_2 effluent released in the deep ocean. Within the laminar instability flow regime, a relationship was obtained for a characteristic jet break up time that could be applied for comparison with a hydrate formation time. It was proposed that two regimes exist which are defined by the relative magnitudes of t_b and t_r . When $t_b \ll t_r$, instability phenomena occur much faster than hydrate formation and jet break up is determined purely by hydrodynamics. When $t_b \gg t_r$, a thin hydrate layer forms on the jet surface at the early stage of instability. Since this layer separates the CO_2 and seawater phases, surface deformation of the jet is impeded and, thus, the jet remains stable. The resulting tube-like hydrate structure is fragile and easily fractured by fluid forces, producing the cylindrical mode of jet break up observed near hydrothermal vents in the ocean.

Hydrate formation effects on jet instability are believed not to be significant when $t_b \approx t_r$ or $t_b \ll t_r$; in this regime, jet break up produces a train of droplets. Rapid formation kinetics ensure that these droplets will quickly be encased by a thin hydrate shell. This hydrate phase is chemically stable and will remain on the droplets, inhibiting dissolution and promoting agglomeration.

Since, over the range of depths proposed for marine CO_2 disposal, t_r is predicted to vary only slightly, the sole determining parameter to assess the importance of hydrate formation on instability is t_b . It was shown that jet break up time depends on fluid properties, jet velocity, and orifice diameter. Large orifices result in long break up times, which increase the probability that hydrate formation will induce non-conventional instability phenomena. Low jet velocities tend to produce the same effect. Although the present results do not consider the important category of turbulent flows, they can be applied to evaluate a range of discharge conditions relevant to the ocean disposal concept.

ACKNOWLEDGMENTS

Partial funding for this study was provided by U.S. Department of Energy Grant No. DE-FG22-95PC95206. This support does not constitute an endorsement by the Department of Energy of the views expressed herein.

REFERENCES

1. Nihous, G.C., Masutani, S.M., Vega, L.A., and Kinoshita, C.M., *Climatic Change* **27**, 225 (1994).
2. Sakai, H., Gamo, T., Kim, E.S., Tsutsumi, M., Tanaka, T., Ishibashi, J., Wakita, H., Yamamoto, M., and Oomori, T., *Science* **248**, 1093 (1990).
3. Aya, I. and Yamane, K., *HTD-Vol. 215*, 17 (1993).
4. Masutani, S.M., Kinoshita, C.M., Nihous, G.C., Teng, H., and Vega, L.A., *Energy Convers. Mgmt* **34**, 865 (1993).
5. Hirai, S., Okazaki, K., Araki, N., Yoshimoto, K., Ito, H., and Hijikata, K., *Energy Convers. Mgmt* **36**, 471 (1995).
6. H. Teng, Ph.D. Thesis, University of Hawaii at Manoa (1994).
7. Nishikawa, N., Ishibashi, M., Ohta, H., Akutsu, N., Tajika, M., Sugitani, T., Hiraoka, R., Kimuro, H., and Shiota, T., *Energy Convers. Mgmt* **36**, 489 (1995).
8. Rayleigh, Lord, *Theory of Sound*, Dover, N.Y. (1945).
9. Teng, H., to appear in *Int. J. Chem. Kinetics*, **28** (1996).
10. Teng, H., Yamasaki, A., and Shindo, Y., to appear in *Chem. Eng. Sci.*, **81** (1996).

11. Shindo, Y., Lund, P.C., Fujioka, Y., and Komiyama, H., *Int. J. Chem. Kinetics* **23**, 777 (1993).
12. Teng, H., Kinoshita, C.M., and Masutani, S.M., *Chem. Eng. Sci.* **50**, 559 (1995).
13. Liro, C.R., Adams, E.E., and Herzog, H.J., *Energ. Convers. Mgmt* **33**, 667 (1992).
14. Teng, H., Yamasaki, A., and Shindo, Y., to appear in *Energy: The International Journal* **21** (1996).
15. Fujioka, Y., personal communication, March 29, 1996.

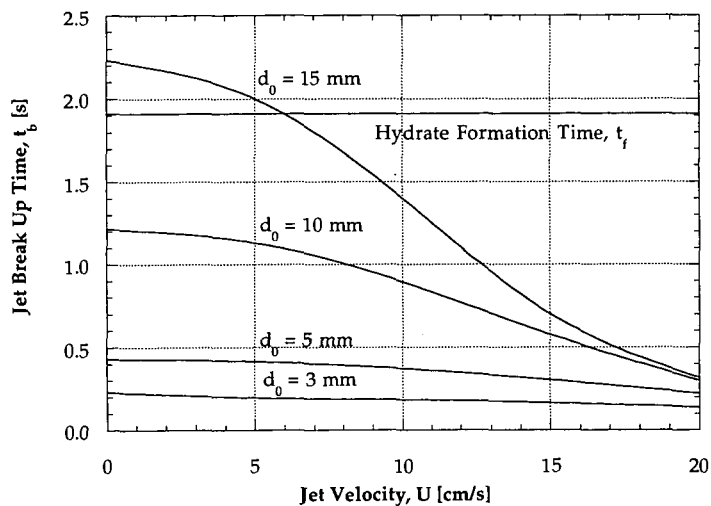


Figure 1. Comparison of hydrate formation times, t_f , and liquid CO₂ jet break up times, t_b , calculated for different discharge orifice diameters, d_0 , under deep ocean (500 m) conditions.

FORMATION AND GROWTH OF CO₂ CLATHRATE HYDRATE SHELLS AROUND GAS BUBBLES OR LIQUID DROPS.

Gerald D. Holder¹ and Robert P. Warzinski

U.S. Department of Energy, Pittsburgh Energy Technology Center, Pittsburgh, PA 15236

¹University of Pittsburgh, School of Engineering, Pittsburgh, PA 15261

Keywords: Carbon dioxide disposal, clathrate hydrates, mathematical model

INTRODUCTION

Deep ocean disposal of CO₂ may be required to mitigate rises in its atmospheric levels if other measures are ineffective and the worst global warming scenarios begin to occur. Work at PETC is directed at evaluating the technical feasibility of this option for long-term disposal.

At the pressures and temperatures associated with the depths required for effective sequestration of CO₂ (> 500 m), the crystalline CO₂ clathrate hydrate (CO₂ · nH₂O, 6 < n < 8) can form (1). Clathrate hydrates are a special type of inclusion compound in which small molecules, such as CO₂, are held in cavities formed by hydrogen-bonded H₂O molecules by van der Waals forces (1,2). The formation of the CO₂ clathrate hydrate can either facilitate or complicate the sequestration of CO₂ in the ocean (3). Sequestration would be facilitated if the clathrate hydrates form as solid crystals dense enough to sink and thus increase the residence time of the CO₂ in the ocean. The formation can complicate sequestration if a thin coating of the hydrate forms on the surface of injected bubbles or drops of CO₂. This complication would hinder dissolution of the CO₂ and permit its rise to unacceptably shallower depths and thus its premature return to the atmosphere. Being able to predict the fate of CO₂ hinges on our understanding of these phenomena and their likely occurrence in ocean disposal scenarios.

In this report, experimental and theoretical results concerning the formation of hydrate shells on gas bubbles and liquid drops of CO₂ are presented. The experimental observations show that, in the presence of hydrate crystals, a thin hydrate shell forms from a nucleus at one point on the surface of the bubble or drop and then rapidly spreads out along this surface. A model was developed to estimate both the thickness of the initially formed shell and bounds on the ultimate thicknesses of shells in saturated and unsaturated environments. The model assumes that the ultimate thickness of the shell is governed by the diffusion of the CO₂ through the hydrate shell and diffusion or convection of dissolved CO₂ away from the hydrate-covered particle.

EXPERIMENTAL

All of the experimental observations were made in a high-pressure, variable-volume view cell of 10 to 40 cm³ capacity. The view cell was enclosed in a chamber where the temperature could be maintained in the region of interest (0 to 10°C). The formation of hydrates was observed by injecting CO₂ (99+ % purity) into water treated by reverse osmosis. More complete descriptions of the view cell and the basic experimental procedures have been published (3,4).

RESULTS AND DISCUSSION

Much of the research on the impact of hydrate formation on ocean disposal of CO₂ has focused on the rates of hydrate formation and growth around a gaseous bubble or liquid drop of CO₂ injected into a large body of water (5,6,7). Teng, et al. have assumed that the CO₂ hydrate shell grows uniformly from 'hydrate clusters' that exist in the water around an initially hydrate-free drop (5). They also assume that the growth of hydrates is limited by the kinetics of the process and that the hydrate clusters can exist in water with local CO₂ concentrations lower than would exist if in equilibrium with hydrates. The values they get for hydrate formation time and thickness depend on the value they use for their rate constant, but there is no rational way of estimating its value.

Experiments have been performed at PETC in a high-pressure, variable-volume view cell in which the formation, dissolution, and relative densities of CO₂ hydrates have been studied (7). In the course of these experiments, several observations have been made of hydrate shells forming on either freshly injected gaseous bubbles or liquid drops of CO₂ in water already containing hydrate crystals. In all such cases, the hydrate shell grew from a nuclei at the point on the surface in contact with crystalline hydrate and then rapidly spread out along the drop or bubble surface. Others have also reported similar phenomenon (8). These observations do not support the view that a hydrate shell forms gradually from a uniform dispersion of nascent hydrate clusters on the surface of the drop. Two specific examples from our experimental work are described below.

In one experiment, four individual drops of liquid CO₂ were sequentially injected into the view cell that contained water and hydrate crystals which had earlier formed in the experiment around the injection port. The fate of each individual drop was monitored before the next drop was introduced. The temperature in the cell was 8.3°C and the pressure in the cell ranged from 16.0 to 18.0 MPa during the injection sequence. The drops were approximately 0.5 to 1.0 cm in diameter. Immediately upon injection, a thin hydrate coating began to form at the point of contact between the drop and the hydrate mass on the injection port. The hydrate shell grew from this point and completely enveloped the drop in 1 to 2 s.

In another experiment, several individual gaseous bubbles of CO₂ formed from a hydrate mass in the view cell when the pressure was decreased below the CO₂ vapor/liquid equilibrium point. The cell was at 5.6°C. The vapor/liquid equilibrium point at this temperature is near 3.5 MPa. The gaseous bubbles were between 0.3 and 0.5 cm in diameter. A hydrate coating immediately began to form, again starting at the point of contact between the bubble and the hydrate mass. The bubbles were completely covered in about 1 s.

Based upon the experimental observations, we propose a model assuming that a hydrate shell rapidly forms around the bubble of gas or drop of liquid CO₂. Instead of depending on the kinetics of the hydrate formation process to determine the thickness of the hydrate shell, we assume that the rate of thickening or thinning of the shell is determined by the diffusion of CO₂ through the shell and diffusion or convection of the dissolved CO₂ away from the hydrate-covered bubble or drop. Based on this assumption, we are able to put bounds on the thickness of the initially formed shell and on the thicknesses of shells in environments saturated and unsaturated with respect to CO₂. The specific case discussed below in presenting the model refers to liquid CO₂ drops in water, although the technique would be applicable to any gaseous or liquid molecule capable of forming hydrates.

Initial Shell Thickness

If a spherical drop of CO₂ is introduced into a large body of water, the CO₂ will dissolve in the water at the interface and diffuse away. Hydrates can only form if the pressure of the drop, P , is greater than the pressure required for hydrate formation at the temperature of the system, P_H . For steady-state diffusion from the drop into an infinite reservoir, the concentration profile is given by

$$C = C_0 + \frac{R_0}{r} \quad (1)$$

where C_0 is the concentration of the CO₂ at the interface of the drop of radius R_0 and C is the CO₂ concentration at any position $r > R_0$.

Our observations and the observations of others (8) indicate that drops of CO₂ or other molecules capable of forming hydrates can exist in water for long periods of time (hours to days) without the formation of hydrates even though their formation is thermodynamically possible. This delay is thought to be due to the absence of primary nucleation events that must occur prior to crystallization of the hydrate (8). Under such conditions, C_0 can exceed the concentration of CO₂ that would be possible with hydrates present, which is the saturated concentration, C_H , at P_H .

Figure 1 illustrates the basic premise of the model by showing possible concentration profiles around a CO₂ drop both in the absence and presence of a hydrate shell. The saturation concentration at the hydrate equilibrium pressure is 0.01 g/ml. The saturation concentration at the system pressure in the absence of hydrates is 0.02 g/ml. The conditions which lead to these concentrations are not unique, but such concentrations might pertain, for example, if the CO₂ were injected into the ocean at 2000 meters and hydrates were stable at 1000 meters. If no hydrates formed for a period of time, the upper concentration profile would develop. Once hydrates formed, all the CO₂ in excess of 0.01 g/cc could contribute to the formation of the hydrate shell. This excess would all be in the first 0.5 cm of water surrounding the bubble. It is also assumed that none of the gas in the drop can diffuse through the hydrate fast enough to be incorporated into the initial hydrate shell. As soon as a molecularly thick hydrate shell forms, the only CO₂ available for initial hydrate formation is the excess dissolved CO₂.

If the concentration difference is integrated from R_0 to the value of $r = r_H$ (radius where the CO₂ concentration in the absence of hydrates is equal to the CO₂ concentration in the presence of hydrates at the edge of the shell, i.e., 1.0 cm in Figure 1), the amount of CO₂ available for initially forming a hydrate shell can be determined as shown below.

$$\begin{aligned} \text{Excess hydrate former} = m_{ex} &= \int_{R_0}^{r_H} (C_0 - C_H) 4\pi r^2 dr \\ &= 4\pi R_0^3 C_H [(C_0/C_H)/2 + ((C_0/C_H)^2 - 1) - .333 * ((C_0/C_H)^3 - 1)] \end{aligned} \quad (2)$$

The ratio, C_0/C_H , can be approximated by the ratio P/P_H even though solubilities (concentrations at equilibrium) are not necessarily linear with pressure. Using the composition of hydrates (6.15 mol water/mol CO_2) and the specific volume of hydrate (22.4 mL/mol H_2O) allows the thickness of the hydrate shell, Δr , to be calculated as follows (9).

$$\Delta r = \frac{\frac{m_{ex}}{44.01} * 6.15 * 22.4}{4\pi R_0^2} \quad (3)$$

Table 1 shows typical shell thicknesses for CO_2 hydrate shells formed at oceanic temperatures for drops of various size at different CO_2 concentrations. The values in the first three columns were selected to illustrate the effects of drop size (R_0), hydrate equilibrium concentration (C_H , which is a function of temperature and pressure), and the amount of excess CO_2 over that required for hydrate formation (C_0/C_H). The fourth column was calculated using Equation 2 and assumes that all of the excess CO_2 (m_{ex}) forms hydrates of uniform thickness. The fifth column represents the maximum hydrate thickness under these scenarios and was calculated using Equation 3. The final column represents the ratio of hydrate shell thickness to the size of the initial hydrate-free drop.

Table 1. Thickness of Initial Hydrate Shells formed from CO_2 Droplets injected into the Ocean at 0-15 C and Depths of 0-3000 meters.

R_0 , cm	C_H g/mL	C_0/C_H	Mass of CO_2 in Hydrate, g	Δr , cm	$(\Delta r)/R_0$
0.1	0.01	1.5	0.000018	0.00045	0.0045
0.5	0.01	1.5	0.002291	0.00224	0.0045
1.0	0.01	1.5	0.018326	0.00448	0.0045
1.0	0.02	1.5	0.036652	0.00897	0.0090
1.0	0.03	1.5	0.054978	0.01345	0.0134
1.0	0.03	2.0	0.251327	0.06150	0.0615
1.0	0.02	2.0	0.167551	0.04100	0.0410
0.5	0.06	1.2	0.002011	0.00197	0.0039
0.5	0.06	2.0	0.062832	0.06150	0.1230

Note that in the cases shown in Table 1 the shell is always less than 0.1 cm in thickness. Thicker shells could result if the value of C_0/C_H were higher, but such values are unlikely unless the injection depth was very great (i.e., 3000 meters). In cases where the equilibrium concentrations greatly exceed the hydrate equilibrium concentrations (large C_0/C_H), it is less likely that steady-state, diffusion-controlled concentration profiles would be developed for the liquid CO_2 prior to hydrate formation. The maximum excess CO_2 is dissolved when this steady state is reached, so the formation of the hydrate shell from excess dissolved CO_2 , which is less than the maximum, will result in a thinner hydrate shell. Also, in cases where the CO_2 is dispersed more quickly than occurs with steady diffusion, there would be less excess CO_2 and the shell would be thinner than given in these estimates. Thus, this analysis gives an estimate of the upper limit of the initial hydrate shell thickness which would be less than 0.1 cm.

Steady-State Shell Model

Once the hydrate shell forms around a body of CO_2 , its thickness can either increase or decrease. If the drop is in a reservoir which is unsaturated with CO_2 , then the shell thickness will reach some steady-state value. The shell remains at constant thickness and the CO_2 diffuses through the shell, causing the drop to shrink. For this to occur, the flux away from the drop must equal the flux through the shell. This is expressed in the equation below.

$$D_H \frac{C_0 - C_H}{\Delta r} 4\pi R_i^2 = -D_w \left(\frac{\partial C}{\partial r} \right)_0 4\pi R_0^2 \quad (4)$$

In this equation, D_H and D_w are the diffusivities of CO_2 in the hydrate and water, respectively, C_0 and C_H are the equilibrium concentrations of CO_2 in water at the system pressure and the hydrate equilibrium pressure, respectively, and R_0 and R_i are the outer and inner radius of the shell, respectively. $(\partial C/\partial r)_0$ is the concentration gradient of CO_2 in the water phase at the outside of the hydrate shell. Note that the inside of the hydrate shell is pure CO_2 , but C_0 represents the true driving force since at this concentration in water the chemical potential is equal to the chemical potential of the pure CO_2 .

The thickness of the hydrate shell, Δr , can be determined using the following equation obtained by rearrangement of Equation 4.

$$\Delta r = \frac{-\frac{D_H}{D_w}(C_0 - C_H)}{(\partial C/\partial r)_0 (R_0^2/R_i^2)} \quad (5)$$

At pseudo-steady state, the thickness is constant as determined by the above equation. For a thin shell, the ratio of radii will be nearly 1.0 and can be eliminated. The concentration gradient at the surface of the hydrate can be determined by a steady- or unsteady-state diffusion model.

Steady-State Infinite Reservoir

Further approximation can be made by assuming that CO_2 is diffusing away from the drop at steady state into a water phase that is very large in extent. The only mathematical requirement is that diffusion be radially symmetric and that the concentration decreases to zero far from the drop. In this case, the concentration gradient at R_0 is represented by $-C_H/R_0$. Replacing the concentration gradient term in Equation 4 with this latter term and rearranging gives the following equation.

$$\frac{\Delta r}{R_i} = \frac{\frac{D_H}{D_w} \left[\frac{C_0}{C_H} - 1 \right]}{\left(\frac{R_0}{R_i} \right)} \quad (6)$$

As before, the ratio of the inside and outside radii will be near unity in most cases. Since the ratio of concentrations of CO_2 will range between 1 and 2 for typical ocean injections, the relative thickness of the hydrate is determined by the ratio of diffusivities in the hydrate and water phases.

It might be useful to compare diffusivities in polymers versus melts to estimate relative values. Diffusivities in liquids are about 10^{-4} to 10^{-5} cm^2/sec and diffusivities in solids are about 10^{-10} cm^2/sec (10). Using Equation 6, the estimated relative thickness would be in the range of 10^{-6} to 10^{-5} cm. This indicates that the thin layer of hydrates that initially forms on the outside of the drop should get thinner, although the absolute thickness of the hydrate depends on the drop radius.

Because of changing drop size as the CO_2 dissolves, tiny fissures or cracks may develop in the hydrate shell that may increase the effective diffusivity in the hydrate layer allowing a thicker hydrate shell. However, hydrate formation should be accelerated in these fissures because of the better contact between CO_2 and water. Such fissures would rapidly heal which means that the overall model should be reasonable. This has been observed in our laboratory.

If no hydrates are present, the gradient at the edge of the drop will increase by the factor C_0/C_H , assuming that diffusion is limiting. The absence of a shell will increase the dissolution rate by this same factor. For example, at 7.7°C , the equilibrium hydrate pressure is approximately 3.3 MPa. If solubility is linearly proportional to pressure (Henry's Law), CO_2 injected at 10 MPa (approximately 1000 m depth) would dissolve three times slower with the hydrate shell than without it. The time required will depend on the extent to which the equilibrium concentration of CO_2 at the system pressure exceeds the equilibrium CO_2 concentration in the presence of hydrates (the solubility of CO_2 in water at the hydrate equilibrium pressure). Simply put, the CO_2 dissolution rate will decrease by a factor of C_0/C_H due to hydrate formation.

The thickness of the shell is such a small fraction of the drop diameter that the buoyancy of the drop will not be affected by the hydrate, although the drag coefficient may be affected since the hydrate-covered drop may be somewhat more rigid.

Steady-State Saturated Reservoir

The main assumption in the steady-state infinite reservoir model is that the CO_2 concentration decreases with distance from the drop. A drop injected into CO_2 -saturated water cannot dissolve but can form a layer of hydrates. Since hydrates are present, the water would be saturated at the hydrate equilibrium pressure and the CO_2 , which is at a higher (hydrostatic) pressure, would still diffuse through the hydrate shell. However, the net flux would have to contribute entirely to the growth of the hydrate shell thickness at the hydrate-water interface. The growth of the hydrate caused by this flux can be determined from the following equation.

$$\frac{d\Delta r}{dt} = D_H \frac{C_0 - C_H}{\rho_H \Delta r} \quad (7)$$

where ρ_H is the density of the hydrate phase in moles of CO_2 hydrate per unit volume.

Based upon a solid-phase diffusivity of 10^{10} cm^2/sec , and a hydrate thickness of 10^{-4} cm, the hydrate would thicken at the rate of 10^3 to 10^4 cm/hr . This equation can be integrated to give the thickness as a function of time as shown below.

$$\Delta r = \left[\Delta r_0^2 + D_H \frac{C_P - C_H t}{\rho_H} \right]^{1/2} \quad (8)$$

In this equation, t is the time and Δr_0 is the initial hydrate thickness which is not known but is likely to be small. As the shell thickens, the hydrate growth rate will decrease, but for typical rise times for CO_2 injected into the ocean (10-100 hrs), a hydrate thickness of greater than 10^2 to 10^1 cm would not be expected. Since the thickness has a square root dependency on the solid-state diffusivity of CO_2 , uncertainties in this value are less critical in estimating the thickness of the hydrate shell.

No definitive experiments have been performed to demonstrate that the hydrate layer continues to thicken in CO_2 saturated water as predicted by Equation 8. It is difficult to perform such experiments because saturated water will form multiple hydrate nucleation sites. However, one could inject a CO_2 drop into saturated water and see if it is completely converted to hydrate.

CONCLUSION

It has been demonstrated that a very thin hydrate shell should form around drops of injected CO_2 . If injected into unsaturated water, a stable hydrate thickness on the order of 10^2 to 10^4 times the radius of the drop will form. The hydrates can significantly retard the dissolution of the CO_2 .

If injected into saturated water, the hydrate will form a thicker shell, possibly approaching 10^1 cm in thickness for growth periods in excess of 100 hours. Since the water is saturated with respect to hydrate-forming conditions, the hydrate shell serves only to slow the diffusion of CO_2 and thus prevent the formation of additional hydrate from the injected CO_2 . Saturated conditions could occur in the vicinity of the injection. Under this scenario, additional hydrates could form on the hydrate-covered drop from the CO_2 dissolved in the water. This was the subject of an earlier paper (7).

In summary, in all cases addressed in this paper, the modeling results predict that a hydrate shell on a CO_2 drop will remain thin and the drop will disappear more slowly than predicted by conventional models that do not consider hydrate formation. The stabilization of the drop by the thin shell will make it more likely that the injected CO_2 will rise to unacceptably shallower depths before dissolution. Injection strategies that avoid or limit this phenomena will be required for effective sequestration. Such options have been previously discussed (7).

In salt water, a further complication exists. As hydrates form, dissolved salts are excluded from the solid and their concentration in the water builds up. Since the salinity of the water affects the hydrate equilibrium pressure and the solubility of CO_2 , this effect should be accounted for. At steady state, there is no net hydrate formation and this effect can be neglected. However, if the shell is changing in thickness, the effect of salinity could be important.

DISCLAIMER

Reference in this report to any specific product, process, or service is to facilitate understanding and does not imply its endorsement or favoring by the United States Department of Energy.

REFERENCES

1. A Research Needs Assessment for the Capture, Utilization and Disposal of Carbon Dioxide from Fossil Fuel-Fired Power Plants, DOE Report DOE/ER-30194, July 1993 (available NTIS).
2. P. Englezos *Ind. Eng. Chem. Res.* 1993, **32**, 1251-1274.
3. R.P. Warzinski; A.V. Cugini; G.D. Holder *Proc. Int. Conf. Coal Sci.* 1995, **2**, 1931-1934.
4. R.P. Warzinski; C.-H. Lee; G.D. Holder *J. Supercrit. Fluids* 1992, **5**, 60-71.
5. H. Teng; C.M. Kinoshita; S.M. Masutani *Chem. Eng. Sci.* 1995, **50**(4), 559-564.
6. N. Nishikawa; M. Ishibashi; H. Ohta; N. Akutsu; M. Tajika; T. Sugitani; H. Kimuro *Book of Abstracts*, Second International Conference on Carbon Dioxide Removal, Kyoto, Japan; 1994, p 46.
7. G.D. Holder; A.V. Cugini; R.P. Warzinski *Environ. Sci. Tech.* 1995, **29**, 276-278.
8. Burruss as reported by E.D. Sloan, Jr. in *International Conference on Natural Gas Hydrates*; E.D. Sloan, Jr.; J. Happel; M.A. Hnatow, Eds.; Annals of the New York Academy of Sciences; Vol. 715; p 17.
9. G.D. Holder; S.P. Zetts; N. Pradhan *Reviews in Chem. Eng.* 1988, **5**(1), 1-70.
10. *Perry's Chemical Engineers' Handbook*, 6th ed.; R.H. Perry; D.W. Green; J.O. Maloney Eds.; McGraw Hill, New York, 1984; p 16-23 and p 3-258.

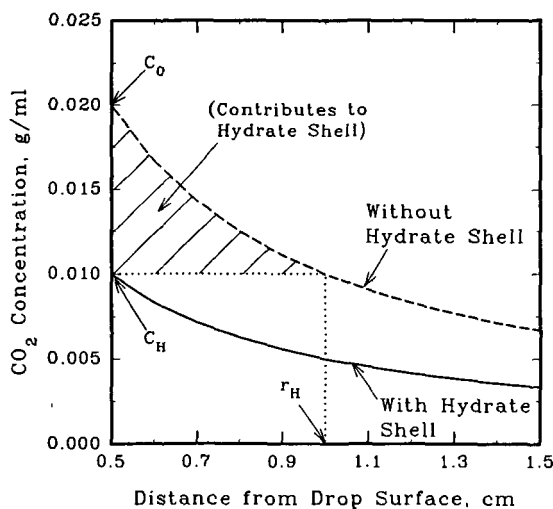


Figure 1. Concentration profiles around a CO_2 drop (0.5-cm radius) in the presence and absence of a hydrate shell in an infinite reservoir (arbitrary example).